

Determination of the Dissolution Behavior of Celecoxib-Eudragit E 100-Nanoparticles using Cross-Flow Filtration

Dissertation
zur Erlangung des Grades

“Doktor der Naturwissenschaften”

im Promotionsfach Pharmazie

im Fachbereich Chemie, Pharmazie und Geowissenschaften
der Johannes Gutenberg-Universität Mainz

Julian Schichtel

geb. in Saarbrücken

Mainz, 2016

Dekan:

1. Berichterstatter:

2. Berichterstatter:

Tag der mündlichen Prüfung: 15.12.2016

Abstract

This study deals with the development of a dissolution test method for nanoparticulate dosage forms. Thereto, nanoparticles (NPs) consisting of celecoxib as model drug and Eudragit E 100 were prepared by emulsification-diffusion and nanoprecipitation using a bench-top approach and MicroJetReactor (MJR). MJR is an enhanced impinging jet technology, which, besides the jets for solvent- and non-solvent phase, implements the use of a third jet carrying inert gas to facilitate fast depletion of the organic solvent. NPs were characterized using photon correlation spectroscopy (size, -distribution and zeta potential), scanning electron and atomic force microscopy (size and shape), HPLC and UV-Vis spectroscopy (API content) as well as differential scanning calorimetry and infrared spectroscopy (NP structure). Hence, almost spherical NPs of narrow size distribution with Z-Average of 200–450 nm, zeta potential of 40–50 mV and entrapment efficiency of 70–90 % were obtained. Dissolution tests were conducted using cross-flow filtration (CF); a new approach in pharmaceutical dissolution testing. This method, contrary to dead-end filtration, excludes the risk of filter clogging which is an important issue if NPs are present. Compared to in-situ approaches it is more robust and less expensive. Prior to investigations, the applicability of CF modules was successfully tested. Thereto, comparative photon correlation- and UV-spectroscopic measurements of nanosuspension and filtrate were performed. Different media were examined towards their suitability to achieve at least 85 % dissolution in 60 min. Hence, a medium, phosphate buffer pH 2.0 including 0.3 % cetrimide was found to be most suitable since both dissolution of Eudragit E (due to acidic pH) and sink conditions for celecoxib are given. Different filters were compared, while it was found that pore size must be sufficiently high to enable micelles including solubilized analyte to pass. Finally, the dissolution behavior of NPs of different size was compared, while there was no statistically significant difference.

Kurzzusammenfassung

Diese Arbeit beschäftigt sich mit der Entwicklung einer Freisetzungsmethode für Arzneiformen auf nanopartikulärer Basis. Als Modellpartikel dienten Celecoxib-Eudragit E 100-Nanopartikel (NP), welche durch Emulgierung-Diffusion und Nanopräzipitation mittels Bench-Top- und Mikrojetreaktor (MJR) hergestellt wurden. Der MJR ist eine Weiterentwicklung der Prallstromtechnologie, welcher, neben den Kanälen für die flüssigen Phasen, einen dritten für Inertgas zur schnellen Verdampfung des organischen Lösungsmittels beinhaltet. Charakterisiert wurden die NP mittels Photonenkorrelationsspektroskopie (Größe, -verteilung und Zetapotenzial), Rasterelektronen- und Rasterkraftmikroskopie (Größe und -verteilung), HPLC und UV-Vis-Spektroskopie (Wirkstoffgehalt) sowie Differentialthermoanalyse und IR-Spektroskopie (NP-Struktur). Dabei wurden annähernd sphärische NP mit naher Größenverteilung von 200–450 nm (Z-Average), Zetapotenzial von 40–50 mV und Einschlusseffizienz von 70–90 % erhalten. In den Freisetzungsuntersuchungen wurde Querstromfiltration (QF) verwendet, was eine Neuerung in der pharmazeutischen Freisetzungsprüfung ist. Diese Methode beinhaltet, im Gegensatz zur Tiefenfiltration, nicht das Risiko der Filterverstopfung, was in Anwesenheit von NP häufig auftritt. Weiterhin ist die Methode im Vergleich zu in situ-Verfahren robuster und kostengünstiger. Die Eignung der QF-Module NP zurückzuhalten wurde durch Photonenkorrelations- und UV-Vis-Messungen von Nanosuspension und Filtrat belegt. Verschiedene Medien wurden hinsichtlich ihrer Eignung mindestens 85 % Wirkstofffreisetzung in 60 min zu erreichen untersucht, wobei Phosphatpuffer pH 2,0 mit 0,3 % Cetrimid sich als das geeignetste erwiesen hat, da sich sowohl Eudragit E durch den sauren pH auflösen lässt, als auch Sink-Bedingungen für Celecoxib vorliegen. Verschiedene Filter wurden verglichen, wobei sich herausstellte, dass deren Porengröße ausreichend hoch sein muss um die Passage von Mizellen mit eingeschlossenem Wirkstoff zu ermöglichen. Schließlich wurde das Freisetzungsverhalten verschieden großer NP verglichen, wobei kein statistisch signifikanter Unterschied auftrat.

Table of Contents

Abstract.....	III
Kurzzusammenfassung	IV
Table of Contents.....	V
List of Abbreviations.....	VIII
1 Introduction.....	1
1.1 Nanoparticle properties.....	1
1.2 Active pharmaceutical ingredient and excipients	5
1.3 Nanoparticle production	9
1.3.1 Overview of nanoparticle production methods.....	9
1.3.1.1 Top-down	10
1.3.1.2 Bottom-up	11
1.3.2 MicroJetReactor technology	15
1.4 Nanoparticle characterization.....	20
1.4.1 Dynamic light scattering.....	20
1.4.2 Zeta potential.....	22
1.4.3 Differential scanning calorimetry.....	24
1.4.4 Infrared spectroscopy	27
1.4.5 Scanning electron microscopy	28
1.4.6 Atomic force microscopy.....	33
1.5 Dissolution testing of nanoparticulate pharmaceutical dosage forms.....	35
1.5.1 Historical development of pharmaceutical dissolution testing..	35
1.5.2 Challenges in dissolution testing of nanoparticulate dosage forms.....	39
1.5.3 Filtration of nanosuspensions	44
1.6 Aim of the study	49
2 Materials and methods	50
2.1 Materials	50
2.2 Methods	55
2.2.1 Nanoparticle preparation	55
2.2.1.1 Bench-top	55
2.2.1.2 MicroJetReactor	56
2.2.2 Nanoparticle characterization	58
2.2.2.1 Dynamic light scattering	58
2.2.2.2 Entrapment efficiency.....	58
2.2.2.3 Differential scanning calorimetry	60
2.2.2.4 Infrared spectroscopy.....	60

2.2.2.5	Scanning electron microscopy	60
2.2.2.6	Atomic force microscopy	61
2.2.3	Dissolution tests	62
2.2.3.1	Verification of cross-flow filtration.....	62
2.2.3.2	Dissolution test methodology	68
2.2.3.3	Dead-end filtration.....	70
2.2.3.4	Flow properties	70
2.2.3.5	API quantification	72
2.2.3.6	Statistical evaluation of dissolution profile equivalence.....	73
3	Results	74
3.1	Nanoparticle preparation	74
3.1.1	Bench-top.....	74
3.1.1.1	Influence of type of co-stabilizer, solvent : non-solvent ratio and drug : polymer ratio.....	74
3.1.1.2	Influence of Poloxamer 407 (co-stabilizer) concentration .	78
3.1.1.3	Increase of celecoxib and excipients quantity	81
3.1.1.4	Stability study.....	84
3.1.2	MicroJetReactor	91
3.1.2.1	Emulsification-diffusion	91
3.1.2.2	Nanoprecipitation	95
3.2	Nanoparticle characterization	98
3.2.1	Differential scanning calorimetry	98
3.2.2	Infrared spectroscopy.....	100
3.2.3	Scanning electron microscopy	104
3.2.4	Atomic force microscopy	111
3.3	Dissolution testing	113
3.3.1	Evaluation of a suitable dissolution medium for the API release of celecoxib-Eudragit E 100-NPs.....	113
3.3.1.1	Dissolution test in diluted HCl (pH 1.2)	113
3.3.1.2	Dissolution test in diluted HCl (pH 1.2) containing NaCl .	116
3.3.1.3	Dissolution tests in diluted HCl (pH 1.2) containing cetrimide	117
3.3.1.4	Dissolution tests in diluted HCl (pH 1.2) containing cetrimide using cross-flow- and dead-end filtration.....	119
3.3.1.5	Dissolution tests in phosphate buffers of different pH containing 0.3 % cetrimide.....	122
3.3.2	Comparison of the dissolution behavior of nanoparticles of different size and unprocessed celecoxib particles	124
4	Discussion.....	131
4.1	Nanoparticle preparation	131
4.2	Dissolution testing	142

5	Summary	151
6	Zusammenfassung	155
	Appendix	159
	References	178
	List of Tables	189
	List of Figures	194
	List of Equations	201
	Acknowledgement	202
	Curriculum vitae	204

List of Abbreviations

AFM	Atomic force microscopy
API	Active pharmaceutical ingredient
ATR	Attenuated total reflection
BCS	Biopharmaceutics classification system
BT	Bench-top
CAS	Chemical abstracts service registry number
CF	Cross-flow filtration
CMC	Critical micelle concentration
DLS	Dynamic light scattering
DLVO	Derjaguin Landau Verwey Overbeek
DoE	Design of experiments
DSC	Differential scanning calorimetry
EE	Entrapment efficiency
FaSSIF	Fasted state simulated intestinal fluid
FDA	US Food and Drug Administration
FeSSIF	Fed state simulated intestinal fluid
HPLC	High performance liquid chromatography
IR	Infrared spectroscopy
ISO	International Organization for Standardization
MJR	MicroJetReactor
MW	Molecular weight
MWCO	Molecular weight cut off
n/a	Not available
NSAR	Non-steroidal anti rheumatic drug
NP	Nanoparticle
PEG	Polyethylene glycol
PDI	Polydispersity index
PVA	Polyvinyl alcohol
RC	Regenerated cellulose
RPM	Revolutions per minute
RT	Room temperature

SD	Standard deviation
SDS	Sodium dodecyl sulfate
SEM	Scanning electron microscopy
STM	Scanning tunneling microscopy
TEM	Transmission electron microscopy
UK	United Kingdom of Great Britain and Northern Ireland
US	United States of America
USP	United States Pharmacopeia
UV-Vis	Ultraviolet-visible spectroscopy
ZP	Zeta potential

1 Introduction

1.1 Nanoparticle properties

According to Patel et al. (2008) „NPs exist widely in the natural world, for example as the products of photochemical by plants and algae. They have also been created for thousands of years as products of combustion and food cooking, and more recently from vehicle exhausts” [109].

Nowadays our daily routine is not imaginable without nanomaterials: they increase safety and ecological benefit of our cars and provide a high potential for climate and resources protection. Furthermore, they make mobile phones and laptops smaller and more effective and increase performance and safety of drugs [17].

In pharmaceutical science currently exists a considerable need for vehicles with the ability to carry drugs efficiently to their site of action. These vehicles can for instance be capable to provide an exactly defined in vivo drug release over a defined time span [16,125,167]. Moreover they can protect the API on the way to its site of action [155]. This comprises inter alia protection against metabolism [57,123] or phagocytosis [24,106]. Besides the possibility to protect the API against physiological degradation, nanotechnology can help to reduce its toxicological effects [85]. On the APIs route through the body it can, depending on its individual properties, interact with many structures where an effect is not desired or even harmful. It has even been demonstrated yet, that NP can serve as a kind of antidote in the example of mercury intoxication [63]. In this context, the NP contained a covalently linked aptamer to intercept the mercury. Finally, nanosizing can increase the bioavailability of orally administered drugs [96,98]. Three special features of nanoscale particles towards coarse-particles facilitate that:

First, NPs exhibit a higher dissolution velocity [33,97]. The Nernst-Brunner equation (1) [32], which describes the dissolution process, highlights the crucial importance of the surface area for the dissolution process.

$$\frac{dc}{dt} = \frac{DS}{Vh}(c_s - c) \quad (1)$$

In this equation dc/dt represents the dissolution rate, D the diffusion coefficient, S the surface area, V the volume of the dissolution medium, h the thickness of the diffusion layer, c the instantaneous concentration and c_s the saturation concentration. Accordingly, a particle size reduction from micrometer to nanometer range is attended by a thousand fold increase of the dissolution rate. Second, the saturation solubility c_s of a substance is not exclusively a function of its molecular properties, but also of size and curvature of its particles [97].

The Ostwald-Freundlich equation (2) [91,105],

$$\frac{RT}{V_m} \ln \frac{S}{S_0} = \frac{2\gamma}{r} \quad (2)$$

where S is the solubility of small particles of size r , S_0 the equilibrium solubility, R the universal gas constant, T the temperature, V_m the molar volume, and γ the surface tension, describes the relationship between particle size and solubility. This equation shows that not only the dissolution rate but also the solubility depends on the particle size. However, there exist two major limitations to that relationship:

First, the equation only refers to almost spherical particles. However, it was already discovered at the beginning of the 20th century that the solubility of non-spherical particles may differ from the prediction made by Ostwald-Freundlich equation [68]. Second, Knapp [78] discovered that solubility does not increase infinitely with decreasing particle size, but exhibits a maximum corresponding to a certain value of particle size, the so-called Lewis critical radius. This circumstance is due to different definitions concerning, density, radius of curvature and surface tension of NPs towards macroparticles [15]. Nevertheless, the right particle shape and size provided, nanosizing can increase the solubility as well as the dissolution rate.

Finally, as a result of the increased contact area, the adhesiveness of nanoscale particles is relatively higher in comparison to larger particles [97].

E.g. 125000 nanocrystals of 200 nm diameter can occupy the same spot as one microcrystal of 10 μm [97]. This intensive raise of contact area at absorption sites, like the gastrointestinal mucosa, is accompanied by an increased absorption rate. The absorption is, besides the solubility, one determining factor of the bioavailability.

In addition to the important influence on the bioavailability it has already been shown that nanosizing of drugs can also improve dose proportionality and reduce fed/fasted state and inter-subject variability [38,95,130].

A review article from Cooper (2010) [26] summarizes the benefits of NP dispersions of poorly soluble drugs for oral delivery as stated in Table 1.

Table 1: Advantages of nanoparticulate towards coarsely-dispersed API for oral administration of drugs.

Parameter	Effect
bioavailability	higher (over an order of magnitude increase not uncommon)
fed/fasted state variability	lower (variability of 6-fold could be reduced to 1.2-fold)
absorption rate	higher (t_{max} for naproxen in the fed state in humans could be reduced from 3 h to 20 min)
absorption of higher doses	higher (dose at which absorption dramatically declined could be increased)

Particulate drug carriers are, besides NPs, liposomes, micelles and microparticles. Except for larger microparticle populations they are all of colloidal size range. In all these dosage forms the API is incorporated in an excipient in a characteristic manner.

In the broader sense NPs are colloidal solid systems consisting of drug and polymer with a diameter between 50 and 500 nm. They can be further distinguished in nanocapsules and nanospheres. Nanocapsules consist of a core with the solubilized API and a certain kind of envelope. This envelope can be a solid excipient which on one hand facilitates dissolution under physiological conditions and, on the other hand, can control API release (enveloped solid system). In the case of a nanoemulsion, nanoscale droplets, containing the API dissolved in a lipophilic solvent, are surrounded by

surfactant molecules. The surfactant enhances water-solubility. These micelles can be hardened by a drying process to result in hardened micellar systems. In the case of nanospheres or nanopellets, the API is embedded in a matrix of an excipient. Depending on the dissolution properties of this excipient in certain physiological liquids, the degradation of nanospheres and therefore the API release is determined [13]. Figure 1 shows a schematic of the above described NP variations. Besides polymers also detergent like excipients and lipids are used for NP production. Solid lipid NPs are made from a solid lipid only, while nanostructured lipid carriers consist of a blend of a solid and a liquid lipid (oil) [97].

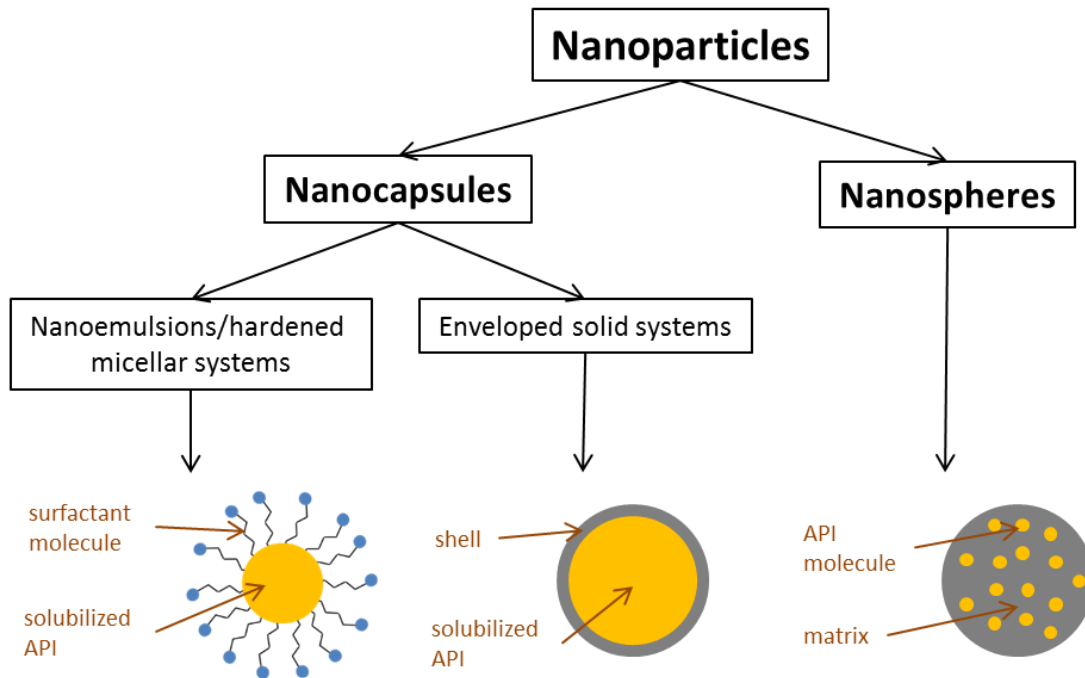


Figure 1: Classification scheme of NPs. Differentiation between nanospheres and nanocapsules and among them between nanoemulsions and enveloped solid systems (based on [3]).

1.2 Active pharmaceutical ingredient and excipients

Celecoxib, which was used as model drug in the present study, belongs to the pharmacological class of non-steroidal antirheumatic drugs (NSAR). Through inhibition of cyclooxygenases (COX-1 and COX-2) they reduce the formation of prostaglandins. Since prostaglandins are, inter alia, mediators of inflammation processes NSAR have an anti-inflammatory effect. Though, unlike other NSARs, celecoxib selectively inhibits COX-2. As COX-1 plays an important role in synthesis of gastro-protective prostaglandins, this can prevent acute or chronic damage to the gastrointestinal tract [99]. Primary indications of celecoxib are the therapy of rheumatic arthrosis and osteoarthritis. Further indications are acute pain and dysmenorrhea [126]. On the United States market Celebrex capsules are available in four dosage strengths: 50 mg, 100 mg, 200 mg and 400 mg. Currently, 400 mg are the maximum daily dose [46]. In Germany, only 100 mg and 200 mg dosage strengths are to obtain [126].

Celecoxib is a weakly acidic substance (pK_a 11.1) [33], due to a sulfone amide function in the molecule (see Figure 2). It disposes a very low water-solubility (5 $\mu\text{g/mL}$) [18] and a $\log P$ value of 3.5 [55]. Celecoxib is a BCS class 2 substance [33], i.e. it has good permeation properties across the gastrointestinal mucosa but low water-solubility. The absorption of BCS class 2 substances is controlled by their solubility and dissolution rate [6]. It has already been shown that the oral bioavailability of celecoxib can be significantly increased by nanotechnology [88].

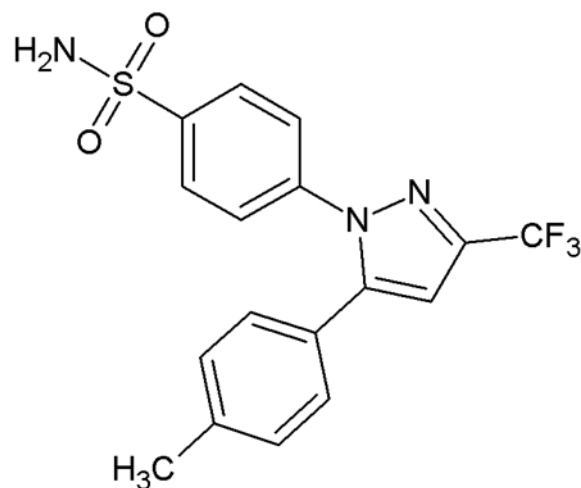


Figure 2: Structure of celecoxib.

Eudragits are cationic polymers based on dimethylaminoethyl methacrylate and other neutral methacrylic acid esters with usually molecular weights of approximately 250,000 Da. They are mainly used in peroral solid formulations as film-coating agents [162]. In pharmaceutical nanotechnology they have been widely used, for example in the preparation of amphotericin-B-loaded NPs for ocular delivery [29]. By using different subtypes various solubility characteristics can be obtained. For instance Eudragits have been employed to prepare pH-sensitive NPs releasing the API specifically at the desired physiological site of action [160,165].

Eudragit E is soluble in gastric fluid as well as in weakly acidic buffer solutions (\leq pH 5) [162]. This is due to a tertiary amino function (pK_a : 6.3 [6]) in the molecule which is protonated at acidic pH values (see Figure 3). Therefore, Eudragit E can act as an electrostatic stabilizer. Additionally, it is well-soluble in many organic solvents like acetone, alcohols, dichloromethane and ethyl acetate {Wise 2000 #9: 528. Thus, it can be added together with the API to the solvent phase. The used Eudragit E 100 (see Table 7) has a molecular weight of approximately 47,000 Da. In consideration of a monomer mass of approximately 400 Da this corresponds to circa 117 monomers (n in Figure 3) per molecule. Eudragit E is available as Eudragit E 100 (colorless to yellow tinged granules) and Eudragit E PO (white powder).

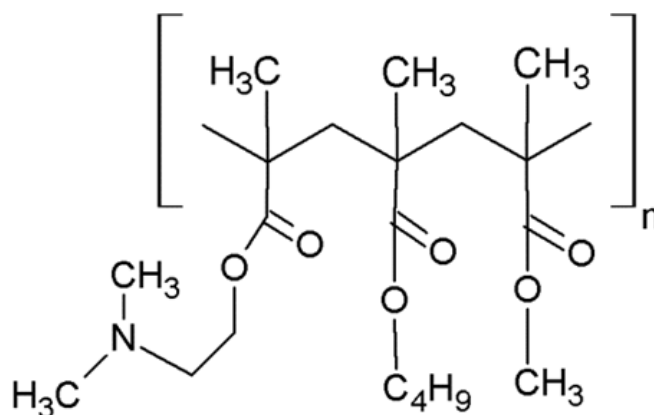


Figure 3: Structure of Eudragit E.

SDS is an anionic surfactant with a wide field of applications in non-parenteral pharmaceutical formulations and cosmetics. It is weakly alkaline and freely water-soluble [162]. Due to the negative charge of the deprotonated sulfonic acid function (see Figure 4) it is used as electrostatic stabilizer for many different formulations like, for instance, metallic or polymeric NPs [58,147].

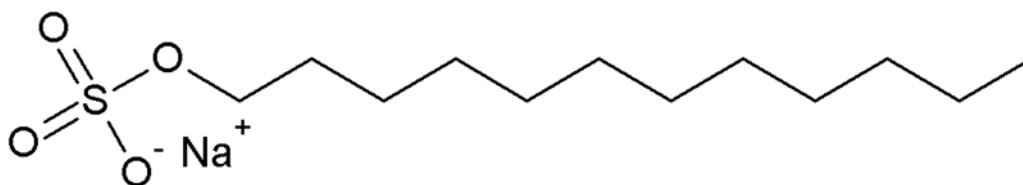


Figure 4: Structure of SDS.

„PVA is a water-soluble synthetic polymer represented by the molecular formula $(C_2H_4O)_n$. The value of n lies for commercially available materials between 500 and 5000 corresponding to an approximate molecular weight range between 20,000 and 200,000“ [162]. Its main fields of application are, for instance, ophthalmology where it can contribute to increase viscosity formulations or act as a lubricant in artificial tears and contact lens solutions. Furthermore, it is employed in sustained-release formulations for oral administration, transdermal patches or as emulsion stabilizer in topical formulations [162]. Additionally, it is a common steric stabilizer for NP suspensions [7,42]. The structure of PVA is given in Figure 5.

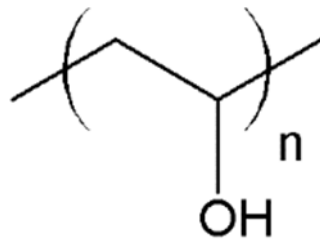


Figure 5: Structure of PVA.

„Poloxamers are nonionic polyoxyethylene–polyoxypropylene [block-]copolymers used primarily in pharmaceutical formulations as emulsifying or solubilizing agents” [162] (chemical structure given in Figure 6). Poloxamer 407, which was used in the present study, has an average molecular weight of 12,600 Da and a water-solubility of more than 10 % (m/v). Due to their emulsifying properties Poloxamers are used in intravenous fat emulsions. Furthermore, they can, in their function as solubilizing and stabilizing agents maintain the clarity of elixirs and syrups. Various semi-solid formulations contain Poloxamers as wetting agents, while they can be added as tablet binders or coating ingredients to solid dosage forms [162]. In pharmaceutical nanotechnology, they can, besides their stabilizing properties, prevent phagocytosis (stealth effect) leading to prolonged circulation when administered in vivo [64].

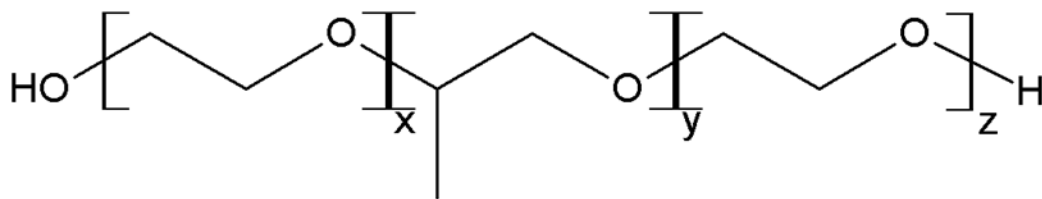


Figure 6: Structure of Poloxamers (Poloxamer 407: x=101 y=56 z=101 [166]).

1.3 Nanoparticle production

1.3.1 Overview of nanoparticle production methods

The targeted delivery of drugs to particular organs or tissues necessitates primary particles of defined size and narrow size distribution. One common type of NPs are the so-called nanocrystals: „...crystals with a size in the nanometer range, which means [...] nanoparticles with a crystalline character.” [70]. These nanocrystals are produced from the drug itself, while surfactants or polymeric stabilizers can be used as excipients. Depending on the exact formulation the API content of these NPs can theoretically reach 100 %. Further advantages of nanocrystals are the ease of production and scaling-up, which facilitates the transfer to industry [11,70]. Pharmaceutical purposes like extended release and taste masking or manufacturing issues concerning the chemical properties of the API may necessitate a more complex formulation of NPs. Thereto, the API can, for instance, be embedded in a polymer (polymeric NPs, e.g. celecoxib-Eudragit E 100-NPs) or lipid matrix (solid lipid NPs or nanostructured lipid carriers).

Generally, there exist two approaches for the manufacture of nanocrystals: bottom-up and top-down [145,157]. The first comprises the so-called bottom-up techniques which start from a, mainly organic, solution of the API that can additionally contain a dissolved polymer. Thereafter, precipitation of the API is provoked by contact with a so-called non-solvent. This non-solvent (typically water) is miscible with the solvent but does not dissolve the API leading to its precipitation. To ascertain long-term stability of the produced nanosuspension, it can be necessary to add a stabilizer to the non-solvent. Bottom-up approaches involve various techniques of controlled precipitation. Primarily, there exist two regimes: solvent evaporation and controlled evaporation of droplets [124]. Techniques of controlled evaporation are spray drying, aerosol flow reactor or electrospraying. Techniques of solvent precipitation encompass hydrosol production by anti-solvent precipitation, high-gravity controlled precipitation, flash nanoprecipitation (confined liquid impinging jets and multi-inlet vortex mixer), employment of supercritical fluids and sonoprecipitation [124].

1.3.1.1 Top-down

Top-down techniques (see Figure 7) implement the diminution of macro-particulate API, usually based on a suspension of crystalline or amorphous API particles. The suspension can contain a dissolved stabilizer. The two basic size reduction methods in pharmaceutical formulation are wet milling and high-pressure homogenization. Moreover, for industrial purposes, complex methods involving microfluidics and lithography are used [124]. To alleviate the diminution step API particles can be micronized prior to nanosizing [127]. Finally, the achieved nanocrystals can be transferred to conventional pharmaceutical dosage forms like tablets or hard gelatin capsules. Disadvantages of top-down towards bottom-up approaches are, first, increased time and energy consumption. Furthermore, potential phase transitions of the API may impact the in-vivo performance. Additionally, if wet milling is applied, there is a risk of contamination due to the erosion of milling beads [145].

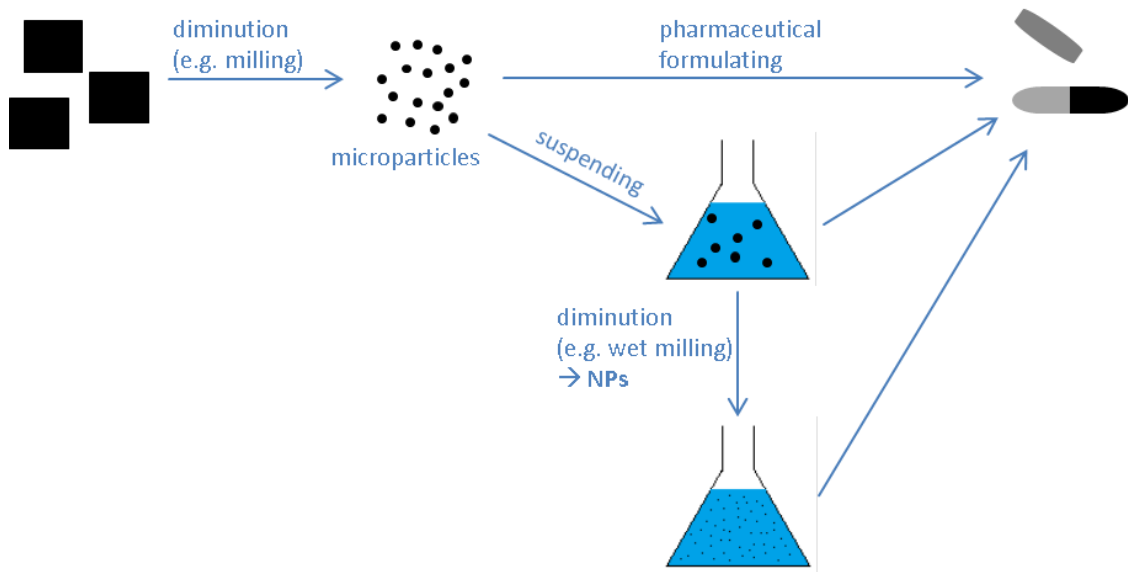


Figure 7: Schematic of pharmaceutical top-down production techniques. From diminution steps like milling microparticles are obtained. These can either be directly transferred to dosage forms or further diminished (e.g. through wet milling) to yield NPs.

1.3.1.2 Bottom-up

There exist two main categories for the bottom-up preparation of NPs; either those involving a polymerization reaction or those directly starting from preformed synthetic or preformed polymers followed by desolvation of the macromolecules [116]. Regarding the desolvation of macromolecules there primarily exist six different production methods: Nanoprecipitation, emulsification-diffusion, emulsification-coacervation, double emulsification, polymer-coating and layer by layer [92].

Nanoprecipitation was described by Fessi et al. [43,44]. It is a straightforward technique with many advantages: As a one-step method it can be performed rapidly and without major effort. Furthermore, it manages without toxic organic solvents and, in some cases, even without surfactants to stabilize the final nanoparticle suspensions. Finally, it often yields nanoparticles of small size (100–300 nm) and high uniformity [14]. The conventional performance of this method comprises a dropwise injection of a non-solvent phase (usually aqueous), containing a stabilizer, to the solvent phase under moderate stirring. The so-called Marangoni effect, which is due to interfacial turbulences at the interface of solvent and non-solvent, results in the rapid

formation of a colloidal suspension [118]. The solvent phase (usually organic) contains the drug, the polymer matrix and, if necessary in case of nanocapsule production, an oil to solubilize the drug [92]. The process of NP formation consists of three stages, which are evoked by supersaturation: nucleation, growth and aggregation. The rate of each step determines the particle size. Separation between the nucleation and the growth stages is essential for the formation of uniform NPs [86,144]. The key variables of this procedure are organic phase injection rate, aqueous phase agitation rate, the method of organic phase addition and the organic phase/aqueous phase ratio [92].

The technical procedure of the emulsification-diffusion (solvent diffusion) method resembles the nanoprecipitation. However, in contrast to nanoprecipitation, this method utilizes a partially water-miscible solvent instead of a water-miscible solvent. Hence, the production process consists of an organic phase emulsification in the aqueous phase under vigorous mixing. The subsequent addition of a larger amount of water to the system causes the diffusion of the solvent into the external phase, which results in the formation of NPs [92,119]. Besides a partially water-miscible solvent this method necessitates a very poor water-soluble drug and appropriate stabilizers [79]. A schematic of this production technique is depicted in Figure 8.

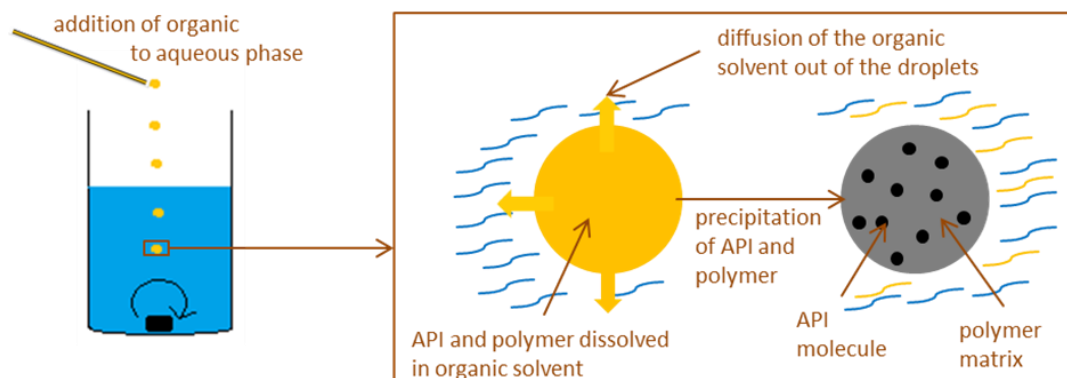


Figure 8: Schematic of the production of polymeric NPs with emulsification/solvent-diffusion technique.

For the bench-top NP preparation (see chapter 2.2.1.1), a technique was chosen combining the principles of both nanoprecipitation and emulsification-diffusion. This method has already been successfully applied, e.g. for the preparation of biodegradable cyclosporine nanoparticles [65]. It starts from intensive emulsification, usually under usage of a high-speed homogenizing device, of a solvent in an aqueous solution of a surfactant. This can contribute to the formation of homogeneous NPs. Thus, the first step of the method is analogous to emulsification-diffusion. This solvent can be partially water-soluble or even insoluble in water. Often followed by further homogenization steps the organic solvent is finally evaporated. This can, for instance, be done by simple stirring at ambient conditions. Alternatively, a rotary evaporator can be used, which is regarded to be advantageous since the precipitation process is finished in less time. This solvent removal stage, which causes supersaturation and therefore precipitation, resembles the nanoprecipitation technique.

Double emulsification is likewise a combination of nanoprecipitation and emulsion-diffusion. It starts from the formation of a w/o emulsion, whereby the inner aqueous phase contains the hydrophilic drug and the outer organic phase the polymer and a w/o surfactant. Subsequently, a second aqueous phase, containing an o/w surfactant, is added which results in the formation of a w/o/w emulsion. Here, particle hardening is obtained both through solvent diffusion (diffusion of water out of the oil droplets) and polymer precipitation. Thereafter, water is frequently added to the emulsion to achieve

full solvent diffusion [92]. While the above described methods result in the formation of NPs or -capsules, the following methods yield nanocapsules.

Emulsification-coacervation comprises the emulsification of an organic phase, containing the API, in an aqueous polymer solution. Then, a coacervation process is performed by addition of a dehydration agent [81] or by changing physicochemical parameters like temperature [89] or salt strength [83]. Finally, cross-linking steps are performed to obtain rigid nanocapsule shells [92].

The method of polymer-coating comprises the evaporation of the organic solvent after the o/w emulsification process, while nanoscale oil droplets containing the surfactant and the dissolved drug remain. These droplets are subsequently coated by incubation of a polymer solution. The coating can for instance be achieved by using a polymer which is oppositely charged to the surfactant [92].

Layer-by-layer technique usually starts from an o/w emulsion, too. It comprises the step-wise adsorption of oppositely charged polymers followed by a homogenization step [92]. This technique also allows the surface coating of metal NPs with different polymers [128].

Each of the above described methods is continued by a purification process, e.g. through washing or filtration steps. Finally, the particles can be stabilized through spray-drying [49,66] or lyophilisation [3,73].

1.3.2 MicroJetReactor technology

The MicroJetReactor technology [112] belongs to bottom-up approaches. More detailed, it is an impinging jet method. Below, the special features of this technique are stated in detail.

The main steps of a precipitation process are: chemical reaction (leading to supersaturation), nucleation, solute diffusion and particle growth [21]. In solutions there is a balance between monomers and clusters of the solute. The formation of clusters results in release of free energy. Though, beyond a certain point, further growth of the cluster leads to a decrease in free energy. Then, spontaneous nucleation can occur. The probability of formation of these so-called critical nuclei now depends on the height of the free energy barrier, which is lower at higher degree of supersaturation [54].

The nucleation rate dN/dt can be described as follows (4) [21]:

$$\frac{dN}{dt} = K_n (c_i - c)^a \quad (3)$$

where K_n is the solute nucleation constant, c_i the monomer concentration and c the saturation concentration (saturation equilibrium). The parameter a is a temperature-dependent constant, that usually lies between 5 and 18 (dimensionless). In other words, the nucleation rate is the rate at which clusters of solute molecules exceed the critical size to form crystals [54].

The particle growth rate (i.e. the rate of further growth of the freshly formed nuclei/crystals) d/dt can be described as follows (4) [21]:

$$\frac{d}{dt} = K_g (c_i - c)^b \quad (4)$$

where K_g is the solute nucleation constant, c_i the solute concentration on the particle surface and c the saturation concentration. The value of b increases with temperature and usually lies between 1 and 3. The above described circumstances are schematically depicted in Figure 9.

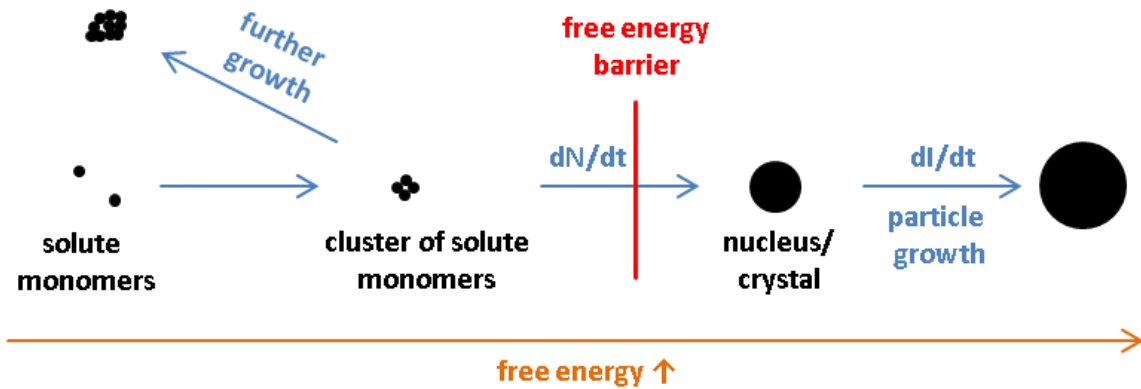


Figure 9: Schematic of steps of precipitation process.

Insufficient mixing leads to different c_i values and, therefore, to inhomogeneous particle growth. The crucial advantage of impinging jets is that they afford vigorous micromixing. Thus, the c_i value can be kept constant for all creating nuclei in the liquid and the particles grow consistently. The decisive time parameters for precipitation processes in general are nucleation induction time τ and micromixing time t_m . τ represents the required time to establish a steady-state nucleation rate while t_m exhibits the required time to achieve uniform molecular mixing. If homogeneous mixing is achieved in less than the formation time of nuclei, one yields uniform particles. The controlled precipitation methods which are described in chapter 1.3.1.2 provide this.

MJR technology uses two opposed high velocity linear jets. One jet conveys the solvent with the API, the other jet the non-solvent. Optionally, the solvent can contain a polymer and the non-solvent a stabilizer. Pumps accelerate the jets to a final velocity of up to 100 m/s. The vigorous converging of the jets evokes the rapid formation of solvent : non-solvent interface and the diffusion of solvent into non-solvent results in the precipitation of NPs [13]. „The strong mixing in the impingement zone leads to a rapid development of a monomodal probability density function [i.e. the formation of uniform particles]” [135]. Figure 10 shows a schematic of the assembly with enlarged image details to illustrate the NP formation process.

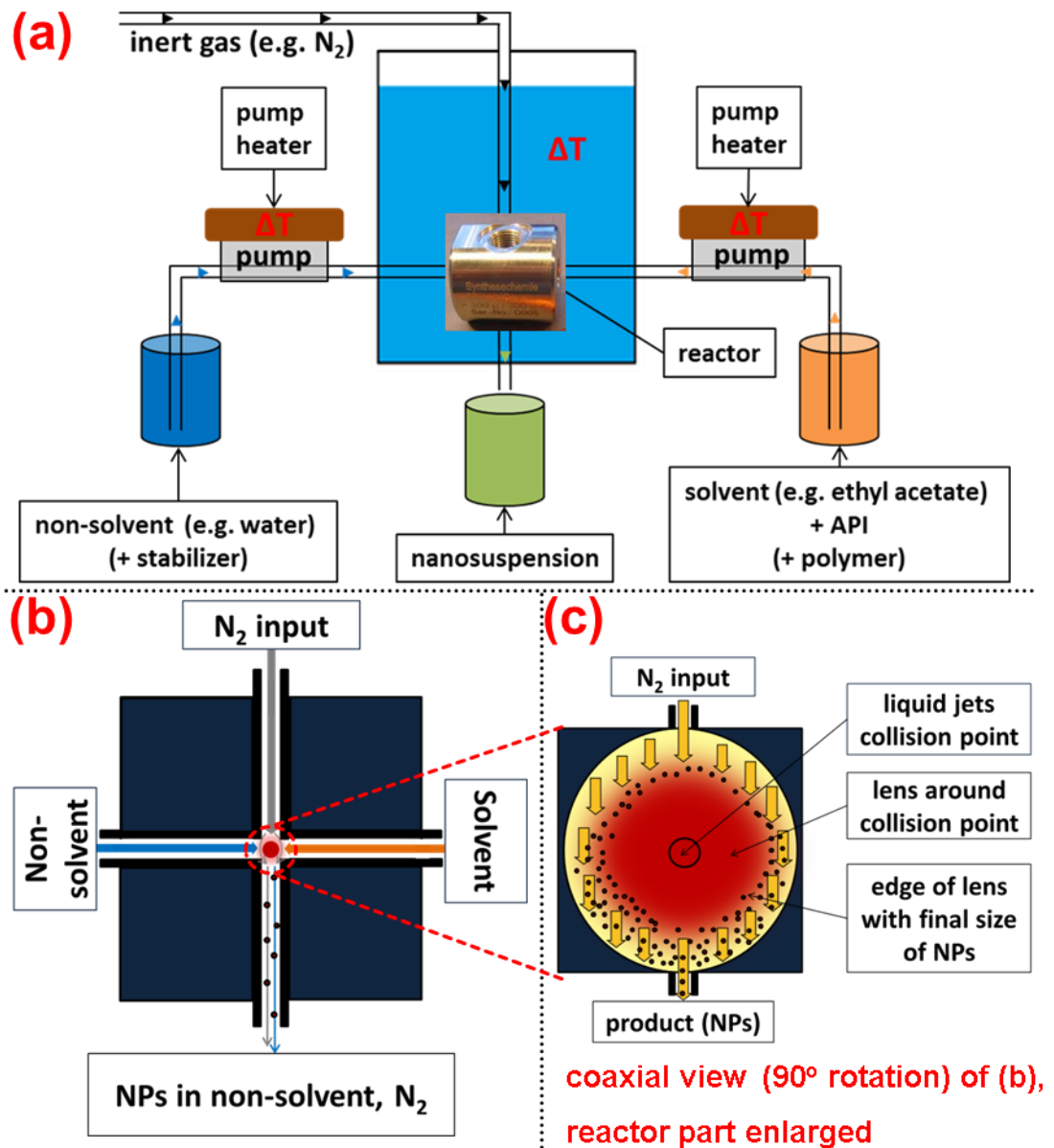


Figure 10: Functional principle of MicroJetReactor. (a) Schematic of MJR (mode of operation): Two opposed high velocity linear jets collide in reactor chamber (shown as original photograph). The left stream carries the non-solvent (alone or with co-stabilizer), the right stream the solvent containing API (nanocrystal production) or API and polymer (polymeric NP production). The third access (on the top) leads inert gas (usually nitrogen N_2) to the reactor chamber. The resulting nanosuspension leaves the outlet (on the bottom). **(b) Enlargement (side view) of reactor part (jets collision in the middle).** The solvent is evaporated by increased temperature (water bath + pump heaters), while the non-solvent containing the NPs (nanosuspension) leaves the outlet together with the inert gas. **(c) Enlargement of jets collision and NP formation process (coaxial view→ liquid jets come from below and above the visual plane).** The red circle exhibits mixing of solvent and non-solvent. NPs grow consistently from the collision point on the way to the edge of the lens. The gas stream limits the liquid jets collision to the center of the reactor.

A typical value for the nucleation induction time τ in aqueous solutions is approximately 1 ms [152]. In the case of a conventional bench-top (stirred tank) NP production micromixing time t_m is in the range of 5-50 ms, i.e. larger than the nucleation induction time [152]. This leads to inhomogeneous particle formation (see above). In contrast, in MJR setup, t_m is below 0.1 ms, i.e. lower than nucleation induction time [152]. Thus, this assembly facilitates the production of particles of narrow size distribution as well as the opportunity to scale-up the process.

A limitation of common confined liquid impinging jet technology, as a single pass process, is that mixing can only occur once. If depletion of the solvent is not completed after mixing, further precipitation may occur. Hence, the problem is that this precipitation occurs in an uncontrolled manner leading to the formation of agglomerates. In summary, this implicates that compound precipitation must complete soon after mixing [21]. To counter this problem, MJR assembly implements a third access to the reactor chamber carrying an inert gas like nitrogen. Inert gases bear the advantage that they will not affect the chemical properties of the API or excipients. The gas, which is previously warmed in a water bath, provokes fast depletion of the organic solvent in the reactor chamber. Consequently, the time scale of NP formation can be kept within the residence time in the reactor to yield uniform particles. The major advantage of the gas jet component or the MJR in general, is the precise converging of the liquid jets. In detail, the pressure of the gas stream limits the liquid jets collision to the center of the reactor (see Figure 10 (b) and (c)). In contrast to a common T-type assembly [21,156], which does not dispose a gas jet, this arrangement prevents uncontrolled distribution of the liquids in the reactor chamber and NPs grow consistently from the collision point on the way to the edge of the lens.

Further advantages of the MJR technology, as a one-step-reaction, are the high ease of manufacturing and scaling-up. Only one reactor affords a production capacity of up to 600 L/h and parallel set-up of equal reactors for more throughput is possible. Additionally, there is no exposure of the samples to intensive mechanical stress or temperature protecting the API from degradation. Finally, the process equipment only causes negligible

contaminations, aseptic production is possible and the jets can be simply cleaned with suitable solvents. This minimizes work expense for purification [152].

1.4 Nanoparticle characterization

1.4.1 Dynamic light scattering

Particles in a liquid undergo Brownian motion. This motion is induced by collisions with solvent molecules that move themselves due to their thermal energy. If the particles or molecules are illuminated with a laser, the intensity of the scattered light fluctuates by interference phenomena at a rate which depends on the particle size. Smaller particles move more rapidly than larger ones. Analysis of these intensity fluctuations in time yields the diffusion coefficient of the Brownian motion. If temperature and viscosity of the dispersion medium are known it is possible to calculate the particle size. This calculation is performed according to Stokes-Einstein relationship (5),

$$D = \frac{k_B T}{3\pi\eta d} \quad (5)$$

where η is the viscosity of the dispersion medium (in $\text{kg}\cdot\text{m}^{-1}\cdot\text{s}^{-1}$), T the temperature (in K), D the diffusion coefficient (in m^2/s), k_B the Boltzmann constant ($1.3807\cdot 10^{-23}$ J/K) and d the particle diameter (in m).

Light scattering methods like DLS do not measure the real particle diameter but the so-called hydrodynamic diameter which refers to the diffusion behavior of a particle within a liquid. This diameter is that of a sphere including the liquid shell surrounding the particle. Hence, the determined particle size is usually larger than the actual size and likewise larger compared to the determination by microscopy methods [90]. In the present study, the particle diameter is given as Z-Average. In ISO 22412 this value is defined as the „harmonic intensity averaged particle diameter” [108]. This has, amongst others, been described by Berne and Pecora (1976) [4].

The particle size distribution can be described by the following equation (6),

$$G(D) = \frac{1}{\sqrt{2\pi} D \ln(\sigma)} e^{-\frac{[\ln(D) - (D_0)]^2}{2[\ln(\sigma)]^2}} \quad (6)$$

where $G(D)$ is the distribution function, D the particle diameter, D_0 the median of the diameter and $\ln(\sigma)$ the geometric standard deviation. The geometric standard deviation is related to the polydispersity of the system. A σ value approaching one (or a $\log(\sigma)$ approaching zero) yields a delta function, which is a feature of monodisperse particles. The size distribution can serve as a surrogate for the degree of agglomeration where a σ value between 1 and 2 characterizes a well-dispersed system with a low degree of agglomeration [117]. The used DLS instrument (see Table 6) uses the decimal logarithm of σ leading to a value between 0 and 1, the so-called polydispersity index (PDI).

The particle size distribution and the mean particle diameter can be weighted by the number, the surface or the volume of the particles. These distributions can easily be transferred to each other if the particles are of spherical (or regular) shape. If the shape is irregular (e.g. needles or cubic) detailed knowledge of the shape is necessary for transformation of the size distributions. The volume-weighted distribution is most convenient to describe pharmaceutical materials (standard in pharmaceutical compendia) [12]. This is due to strong overweighting of large particles in the intensity-weighted raw data compared to volume- (or mass) weighted particle size distributions [100]. Therefore, the DLS particle size distributions are graphically depicted as volume-weighted distributions in this study. This distribution C_{m3} can be calculated due to equation (7) [100],

$$C_{m3} = \frac{S(r)}{r^3} \quad (7)$$

where $S(r)$ is the non-weighted size distribution and r the radius of solid particles or micelles. For hollow particles like liposomes the volume-weighted distribution is proportional to the second power of the radius (the membrane thickness is constant) [100].

The Z-average size, however, is the intensity weighted harmonic mean size [7]. Though, according to ISO 22412 (Dynamic Light Scattering), this size is the accepted norm for presenting particle sizing results by DLS. This is due to the fact that the Z-Average can easily be obtained. Furthermore, the

average size of a particle size distribution can be measured reliably (it increases as the particle size increases) [80].

1.4.2 Zeta potential

Zeta potential (ZP) is the electrostatic potential that exists at the shear plane of a particle, which is some small distance from the surface (see Figure 11). Colloidal particles being dispersed in a solution can be electrically charged due to their ionic characteristics and dipolar attributes. The development of a charge at the particle surface affects the distribution of ions in the neighbouring interfacial region, which results in an increased concentration of counter ions, i.e. ions of a charge opposite to that of the particles, close to the surface. Thus, each particle dispersed in a solution is surrounded by oppositely charged ions, which is called fixed layer. Outside the fixed layer, there are varying compositions of ions with opposite polarities, forming a cloud-like area. Thus, an electrostatic double layer is formed in the region of the particle-liquid interface. This double layer, in principle, consists of two parts: an inner region including ions bound relatively strong to the surface (e.g. polymer molecules as part of the NP matrix) and an outer, or diffuse, region in which the ion distribution is determined by a balance of electrostatic forces and thermal motion. The potential in this region, therefore, decreases with increasing distance from the surface, until a certain point (ideally ad infinitum it becomes zero). ZP is a function of the surface charge of a particle, any adsorbed layer at the interface and the nature and composition of the surrounding medium in which the particle is suspended. To measure ZP a controlled electric field is applied via electrodes immersed in a sample suspension. This field causes the charged particles to move towards the electrode of opposite polarity. Viscous forces acting upon the moving particles tend to oppose their motion and equilibrium is rapidly established between the effects of the electrostatic attraction and the viscosity drag. The particles therefore reach a constant terminal velocity [90]. This principle can be considered as DLS measurement under implementation of electric charge.

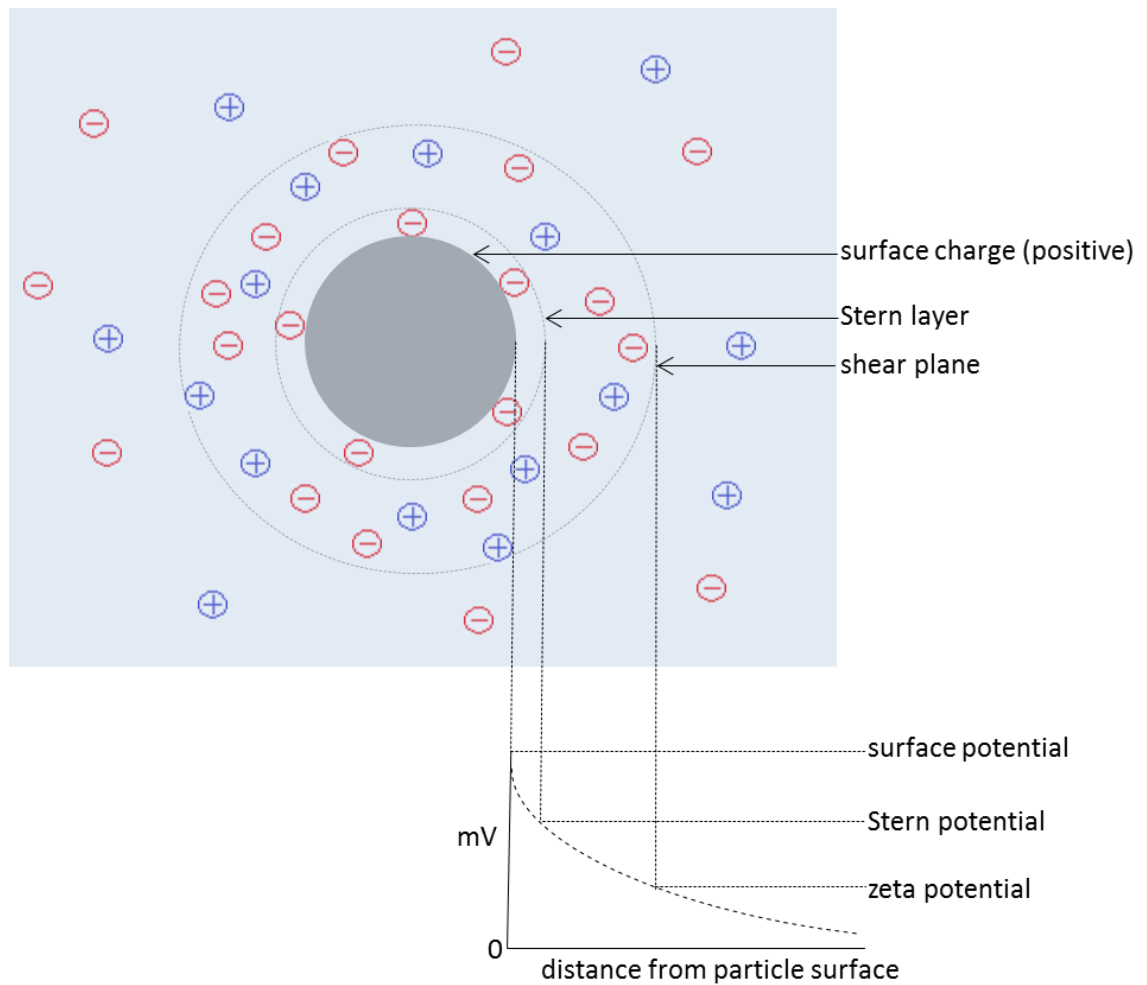


Figure 11: Schematic of zeta potential.

ZP can be calculated from Smoluchowski formula (8):

$$\zeta = 4\pi \frac{\eta\mu}{D} \quad (8)$$

where η is the viscosity of the suspension and D the dielectric constant of the solution respectively at 25 °C, while μ is the electrophoretic mobility of particles (in $\mu\text{m}\cdot\text{s}^{-1}\cdot\text{V}^{-1}\cdot\text{cm}^{-1}$) [8].

1.4.3 Differential scanning calorimetry

Differential scanning calorimetry (DSC) is a method of thermal analysis. It measures the specific heat of a sample in relation to the temperature. Physical and chemical transformations of substances either consume or release energy. Generally, processes increasing the state of order, i.e. enhancing the arrangement of particles like atoms, ions or molecules, release energy. An example for this is crystallization. However, processes decreasing the state of order consume energy. These would be, for instance, melting or glass transition [50].

DSC determines the temperature difference between sample and reference, while both pass a defined temperature-time-program with constant heating rate. The specific thermal heat capacity c_p (in $\text{J}/\text{kg}\cdot\text{K}^{-1}$) of a material is the amount of heat transferred to raise a unit mass of a material one-degree (1 K) in temperature if the pressure is kept constant. It can be expressed by the following equation (9),

$$c_p = \frac{\Delta Q}{\Delta T m} \quad (9)$$

where Q is the heat quantity (in J), T the temperature (in K or °C) and m the mass of the sample (in kg) [50].

In practice, not the thermal capacity but rather the specific heat flow over time \dot{q} might be of interest as the behavior of the sample over a certain temperature range shall be investigated. Given that the temperature increase is constant, which is standard of a DSC measurement, it follows equation (10),

$$\dot{q} = \frac{\dot{Q}}{m} \quad (10)$$

where \dot{Q} is the heat flow and m the sample mass.

Since the heat quantity is difficult to measure in practice, DSC instruments usually record the electrical output (in W) as quantity being proportional to the heat flow [50].

The schematic set-up of a DSC apparatus is depicted in Figure 12. In general, it contains the following components:

- a measuring cell consisting of
 - an oven with a well heat-conductive metal disc,
 - positions for sample and reference and
 - temperature sensors being integrated in the discs and
- a gas access to the measuring cell which grants a defined atmosphere. If an inert atmosphere is desired, one often uses nitrogen. If oxidation processes shall be examined the cell can be flushed with air or oxygen.

The sample and the reference are brought into two pans, which are usually made of aluminium, and symmetrically placed on their positions. Typically, an empty or solvent-containing pan serves as reference. During the examination both pans are simultaneously heated and the respective temperatures continuously measured. If the respective heat flows from sample and reference are equal, there results no temperature difference between the two positions. If the sample undergoes a physicochemical process, the heat flows, and therefore the measured temperatures, will be different. For evaluation the energy difference between sample and reference is usually plotted against the temperature and/or the time [50].

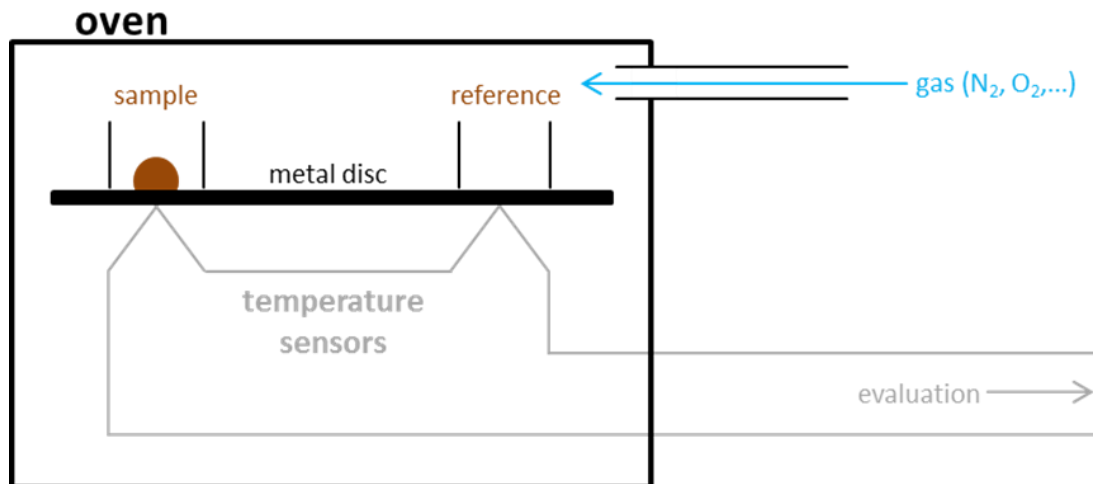


Figure 12: Schematic of DSC measuring cell.

Figure 13 shows a typical DSC curve including some basic transitions that are found during the analysis of many materials. At the melting point T_m there is a balance between the solid and the melt. Above the melting point a crystalline substance turns from the solid to the liquid state. This abrupt transition is due to the release of atoms out of the crystal lattice. As this transition leads to a lower state of order, i.e. a higher energy level, it is an endothermic process.

Conversely, crystallization means the transition from the disordered amorphous to the ordered crystalline state. Thus, it is an exothermic process.

The glass transition T_g is the temperature where a polymer turns from the glassy to the elastic state. Since the molecular motion of amorphous substances increases in several steps with rising temperature, glass transition is a range and not a sharply defined point. It can be taken from the curve as the temperature value of the intersection of the centerline between the extrapolated baselines before and after the glass transition with the curve. These values are derived from the curve as the temperature values of the maxima or minima of the respective events.

Decomposition means the destruction of the molecular structure of the substance at relatively high supply of energy resulting in smaller molecules or even atoms. In contrast, to the above described processes decomposition is irreversible [50,90].

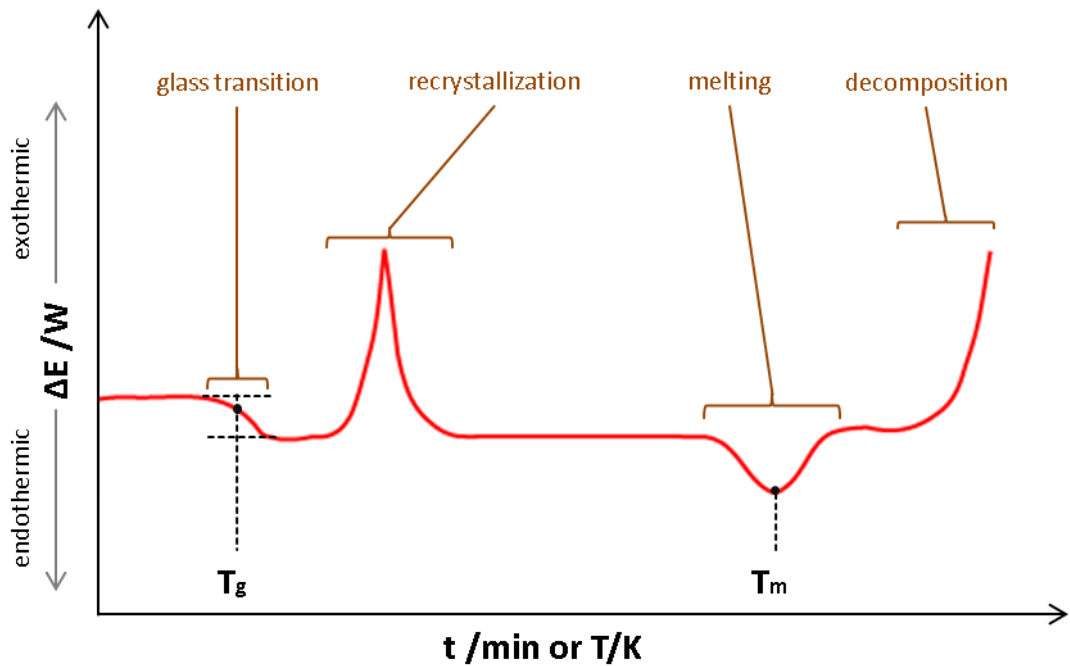


Figure 13: Schematic of a typical DSC heating-up curve.

1.4.4 Infrared spectroscopy

Infrared spectroscopy (IR) is an analytical method which detects molecular vibrations caused by infrared radiation. This is the range of electromagnetic spectrum between wavelengths of 800 nm and 500 μm . Though, for historical reasons the unit of radiation energy is not expressed as wavelength but as wave number, which is the reciprocal value of the wavelength (unit: cm^{-1}). This relationship is depicted in equation (11),

$$\tilde{\nu} = \frac{1}{\lambda} = \frac{\nu}{c} \quad (11)$$

where $\tilde{\nu}$ is the wave number and λ the wavelength. Furthermore, the wave number is equal to the quotient of frequency and vacuum velocity of light. The energy, which is required for excitation of molecular vibrations both depends on the strengths of bonding between the atoms and weight of the atoms. Since some typical vibrations can be attributed to certain functional groups IR can be used to identify substances and is part of many compendial monographs. Moreover, binding properties between different substances can

be examined, as the regarding IR spectrum may change due to chemical interactions between functional groups of these substances [34].

The schematic structure of an IR instrument is shown in Figure 14. To generate infrared light a so-called Nernst filament is typically used, which is heated until it glows to emit the desired radiation. The next part is a monochromator (e.g. potassium bromide prisms or optical grids) to select single wavelengths. However, virtually all modern instruments instead implement an interferometer, consisting of beam splitter and mirrors, to facilitate simultaneous detection of the whole wavelength range. Later a Fourier transform is done to yield the spectrum. The main advantage of Fourier transform-IR is the significantly reduced measuring time. Prior to the measurement, solid samples can be embedded in infrared-permeable material like potassium bromide. Alternatively, they can be placed on a thin infrared-permeable plate, while the light partially penetrates the sample and is reflected to detector. This is a thermocouple with a strongly temperature-dependent electrical resistance allowing conversion of infrared radiation to an electrical signal, which can be enhanced and registered [34].

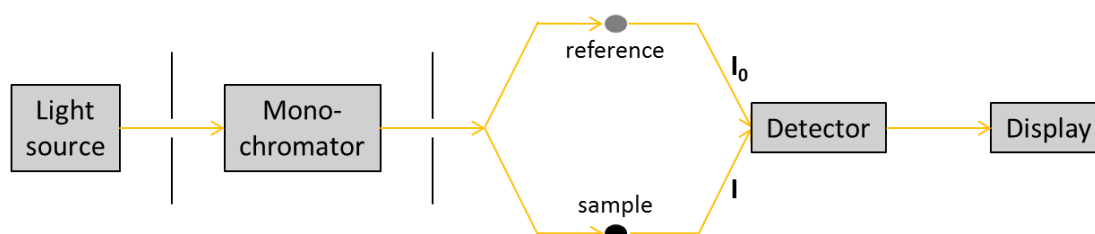


Figure 14: Schematic of an IR instrument (double-beam system).

1.4.5 Scanning electron microscopy

Basically, electron microscopes operate on similar principles as light microscopes with the exception that they use electrons instead of light to visualize an object. Electrons and photons show both properties of particles and of waves, which is called the wave-particle dualism. However, the wavelength of electrons lies after acceleration to 100 keV within a range of a few pm (10^{-12} m), depending on their kinetic energy. In contrast, the wavelength of visible light is much higher, ranging from 400 (violet light) to 800 nm (red light), respectively 4 to $8 \cdot 10^{-7}$ m. The image of a point created

by a perfect lens and monochromatic radiation of a certain wavelength is a small circle surrounded by rings of declining intensity, the so-called Airy disc (see Figure 15) [25].

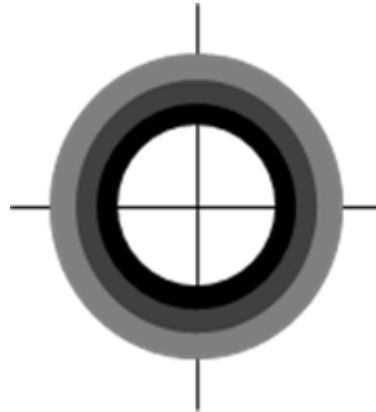


Figure 15: Schematic of the Airy disc.

The diameter of the Airy disc is given by equation (12),

$$d = 1.22 * \frac{\lambda}{\alpha'} \quad (12)$$

where λ is the radiation wavelength and α' the half angle between the observed point and the lens (see Figure 16) [25].

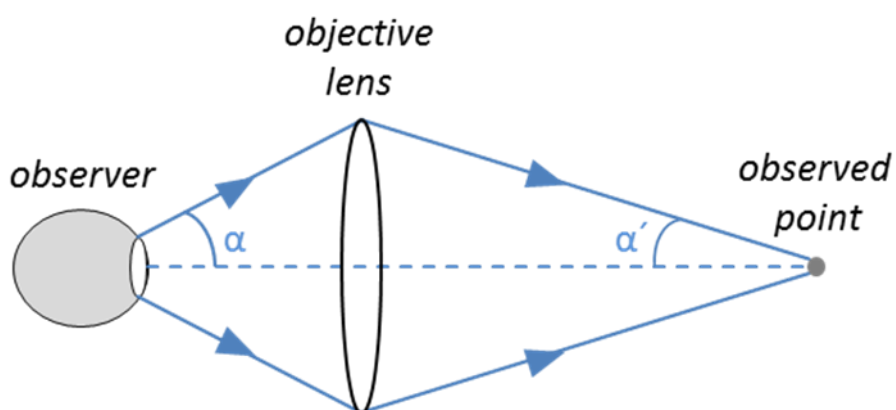


Figure 16: Beam path in a light microscope (simplified).

It can be deduced from Figure 16 that α increases with declining size of the observed point. If a short focal lens shall be used (for 100-fold magnification

or more) α must be replaced by the numeric aperture, which is described by equation (13),

$$O_n = n \cdot \sin \alpha \quad (13)$$

where n is the refractive index of the medium in which the object is immersed. The largest numeric apertures of light microscopes have values of circa 1.3 resulting in a d value of $0.56 \mu\text{m}$ [25].

The resolution s is defined as the distance between two points that can be observed separately and described by equation (14):

$$s = 0.61 \cdot \frac{\lambda}{O_n} \quad (14)$$

Since both numeric aperture and wavelength of visible light are limited, the resolution which an optical microscope can provide is likewise limited and the advantage of electron microscopes becomes evident. The electrons probing the sample inherit a much lower wavelength and a resolution a thousand times better (smaller distance of resolution) [25].

Though, the practical resolution of electron microscopes is much lower (i.e. higher than the wavelength of electrons) as source, optical elements, sample and detector move thermally [134]. A further limitation is the radiation damage of the sample by the electrons. These damages are merely acceptable for massive samples but not for biological samples (e.g. virions or ribosomes) [149]. The applied electron energy of $\sim 100 \text{ keV}$ is equivalent to some hundreds of chemical bonds (like C-C). Thus, usual electron microscopes have a resolution of 0.5 to 2 nm.

Electron microscopes can be divided into different classes according to two criteria. First, it is possible to detect either a reflection or a transmission signal. The decision for one of these methods depends on the sample properties. Hence, for compact samples, the reflection geometry of their surface will be of interest and for samples with thin layers one will measure the transmission. The second criterion concerns the type of instrument. While

conventional microscopes use the same principle as light microscopes, scanning microscopes screen the object point by point. In summary, there result four types of electron microscopy techniques which are stated in Table 2. These types are all used in practice except of reflection electron microscopy [25].

Table 2: Classification of electron microscopy techniques according to type of detection and instrument (according to Colliex and Kohl, 2008 [25]).

		Type of instrument	
		Conventional	Scanning
Type of detection	Reflection	Reflection electron microscopy (REM)	Scanning electron microscopy (SEM)
	Transmission	Transmission electron microscopy (TEM)	Scanning transmission electron microscopy (STEM)

Despite their variations electron microscopes have the following common elements:

- a pump to create a vacuum in the chamber and the particle beam,
- an electron-optical column consisting of
 - an electron source,
 - electron lenses and
 - one or more detectors,
- a sample chamber, which allows moving of the sample during observation and
- electrical power supply and computer system [25].

In the following, the design of a SEM like the one used in this study (see Table 6) is illustrated (see Figure 17).

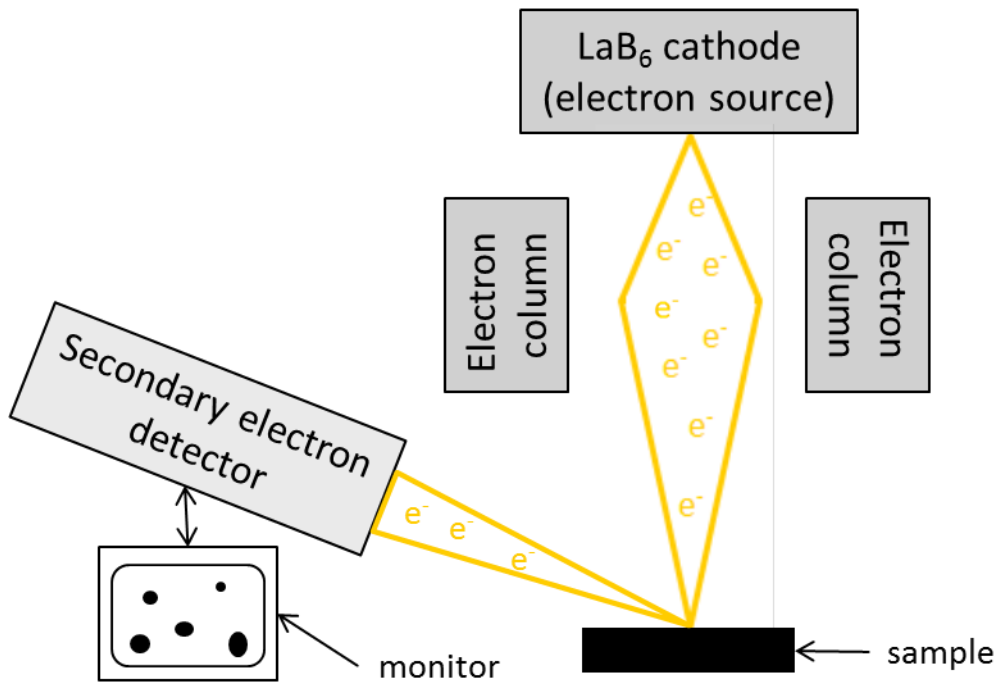


Figure 17: Schematic of a SEM with secondary electron detection (based on Zeiss Evo Series product in-formation [20]).

First, the sample has to be diluted and dried prior to transfer to the instrument. Then, a lanthanum hexaboride (LaB₆) or tungsten cathode is heated to emit electrons (thermionic cathode), which are accelerated in an electric field of ~100 keV. A high vacuum ($< 10^{-6}$ mbar) is applied to avoid collision of electrons with gas molecules. Conventionally, focusing of the electron beam on sample surface is achieved with magnetic coils. The used instrument (see Table 6) implements additional electrodes shaping the emission from the filament to form a virtual source, exhibiting a reduced source diameter and producing higher resolution. The focused electron beam scans the sample facilitating different interactions whose detection delivers information about the object. If non-conductive samples shall be visualized it is necessary that they are previously sputtered with a thin metal layer [161]. The primary electrons from the beam force electrons out of the outer layer of the sample. These are detected by a secondary electron detector which, after processing by software, facilitates visualization of surface topography.

1.4.6 Atomic force microscopy

Atomic force microscopy (AFM) was invented by Binnig, Quate and Gerber in 1986 [15] and belongs to the so-called scanning probing techniques. Contrary to light and electron microscopes scanning microscopes visualize the specimen indirectly by recording the movements of a sharp probe (the radius of curvature at the probe tip is in the order of nanometers) along its surface. Thereto, the scanning tunneling microscope (STM) monitors a tunneling current between the probe and a sample surface which bears the disadvantage that only conductive material can be investigated. Conversely, the probe of AFMs acts as a spring and, therefore, this method can be applied to unprocessed material. Generally, these techniques provide images in a resolution of even less than one nanometer together with data on the interactive forces between molecules. Thus, scanning microscopes are used for many applications, for instance to examine structures that might be useful in drug-delivery systems [37]. Further, AFM is an important analytical tool for the investigation of natural and manufactured NPs [9].

Basically, an AFM consists of the following components (see Figure 18):

- piezoelectric scanner,
- flexible cantilever containing a sharp probe,
- laser,
- photodiode detector and
- feedback electronics.

During the examination the cantilever with the atomically sharp probe moves over the sample surface. Alternatively, the sample can also be moved along the probe. The deflection of the cantilever is due to physical interaction with the sample and depends on the sample topography. These movements can be monitored by irradiation of the backside of the cantilever with a laser. The backside has a reflective surface which forwards the laser beam to a photodiode array detector. This detector records the changes in deflection of the laser [131].

There exist several methods to scan the sample. First the probe can directly be in touch with the sample (contact mode). However, new generations of

atomic force microscopes like the one used in this study (see Table 6) also use a so-called tapping mode. This mode uses a pre-defined drive of the tip. Alterations in the relevant parameters height baseline, frequency and amplitude are a function of the sample topography and allow the computer to obtain a pseudo-three-dimensional image of the sample surface. Using this method damage of samples can be minimized and the resolution enhanced [131].

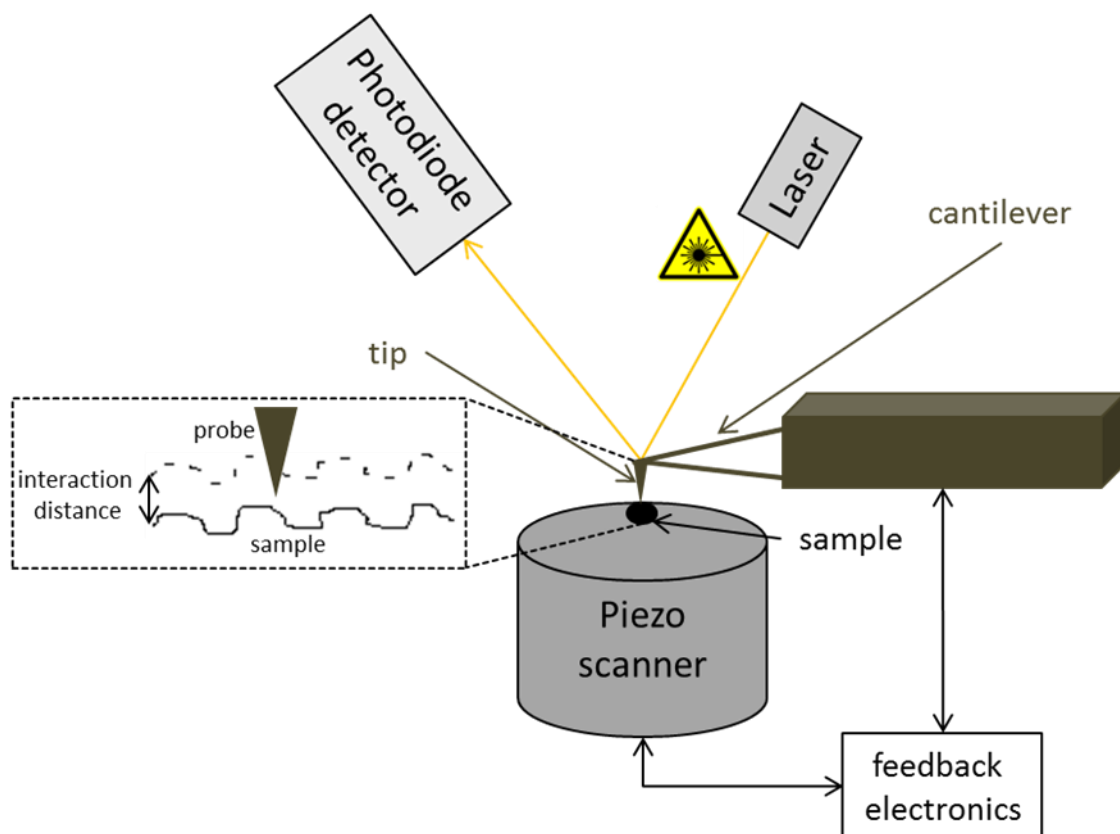


Figure 18: Schematic of an AFM including an image detail of the sample scanning operation.

1.5 Dissolution testing of nanoparticulate pharmaceutical dosage forms

1.5.1 Historical development of pharmaceutical dissolution testing

In pharmaceutical technology, orally administered solid dosage forms played the most prominent role for almost a century. At the end of the 19th century, physical chemists studied the dissolution process. In this field, however, pharmaceutical and physical science was not in touch for further 50 years. In the 1950s pharmacists started for the first time to recognize the immense dependence of the dissolution behavior of drugs on their physiological availability [32]. In past many mathematical models have been developed to predict the dissolution behavior of different substances. In 1897, Noyes and Whitney [104] studied the rate of solution of benzoic acid and lead chloride. Thereto, they let the melted substances adhere to glass rods. Then, they put these rods in glass cylinders together with distilled water and let them rotate in a thermostat at 25 °C. This was done to ascertain that the surface-area of the adhered substances did not significantly change while the experiment was performed. After a defined time span they removed the rods and immediately determined the concentration of the respective substance in the water by titration. They presumed that a thin film of saturated solution, which is kept homogeneous through the stirring, surrounds the substance, adhered to the stick. On that condition the dissolution rate would, in accordance with the law of diffusion, be proportional to the alteration of the concentration of the substance in the liquid towards its concentration in a saturated solution or, otherwise expressed, its solubility. Their assumption can be mathematically formulated by Noyes-Whitney equation (15):

$$\frac{dc}{dt} = k(c_s - c) \quad (15)$$

where dc/dt represents the rate of dissolution, c the instantaneous concentration, c_s the saturation concentration and k a constant [32].

Contrary to Noyes-Whitney equation, Nernst-Brunner equation (1) from 1904 implements all primary factors which are, to this day, known to be relevant for

the dissolution process. Over 50 years after Nernst and Brunner had formulated their equation the pharmaceutical science regarded the disintegration process of solid dosage forms by far more important than the dissolution process and so the research completely excluded the investigation of the dissolution of drugs during that time [32].

In the 1950s pharmaceutical scientists started to develop relationships between dissolution and bioavailability [36,101]. In the 1970s, research groups [87,141] discovered, using the example of cardiac glycosides, that even minor changes in the drug formulation can have an essential impact on the bioavailability.

Intensive dissolution studies initiated by the FDA [48,142] confirmed this and articulately emphasized the need for official dissolution tests. At first, the basket-stirred-flask test (USP apparatus 1) was adopted in USP for, initially, six monographs. The rapidly augmenting demand for dissolution tests led to the development of further official test methods and the implementation of a general chapter on drug release beginning with USP 21 (1985) [32]. In Table 3 the compendial dissolution tests, which are described in USP 34 [150] (Chapter 711), are summarized with year of adoption and scope of application.

Table 3: Compendial dissolution tests (USP) [138,150].

USP apparatus	Year of adoption	Description	Scope of application
1	1970	Basket Apparatus	capsules and dosage forms that tend to float or disintegrate slowly
2	1978	Paddle Apparatus	most widely used apparatus; primarily for tablets; usage of a sinker can prevent floating
3	1991	Reciprocating Cylinder	primarily designed for the release testing of extended-release products; well-appropriate for chewable tablets due to mechanical agitation; suitable if different pH-values shall be tested sequent ("Bio-Dis.")
4	1995	Flow-Through Cell	modified-release dosage forms containing APIs with very limited solubility; easy maintenance of sink conditions possible; if fresh medium is used (open system) the dissolution rate at any moment may be obtained unlike the other methods monitoring a cumulative result

In addition to the methods mentioned in Table 3, which are mainly destined for testing of oral dosage forms, there are methods to simulate drug release behavior of dosage forms intended for other routes of administration. For instance, USP comprises the apparatus 5 to 7, which can be used to examine transdermal therapeutic systems [168]. Gajendran et al. (2012) proposed a drug release methodology to predict the in vivo performance of medicated chewing gums [51].

A realistic in vitro simulation of the drug behavior in vivo does not only require a suitable dissolution testing apparatus (physical simulation) but also an appropriate dissolution medium (chemical/physicochemical simulation). This is of crucial importance for poorly-soluble drugs according to Biopharmaceutics Classification System (BCS). The BCS has been proposed by Amidon et al. in 1995 [6]. Hence the solubility of a drug is considered high if the highest dosage strength is soluble in 250 mL (~ one glass) of aqueous media over the pH range from 1 to 7.5. The drug is considered highly permeable if at least 90 % of the administered dose is absorbed compared to intravenous application. This boundary is based on measurement of the

permeation across human intestinal membrane. The properties of the single BCS classes are listed in Table 4.

Table 4: Biopharmaceutics Classification System (BCS) according to Amidon et al. [6].

BCS class	Solubility	Permeability	Examples [163]
1	high	high	Caffeine, Metoprolol
2	low	high	Celecoxib , Ritonavir
3	high	low	Cetirizine, Penicillins
4	low	low	Amphotericin B, Neomycin

Until present, the compendial monographs prescribe the usage of aqueous buffer solutions with a (synthetic) surfactant for the quality control, i.e. routine, dissolution tests of class 2 and 4 drugs. Though, for newly-developed drugs time- and cost-intensive pharmacokinetic studies have to be performed. Thus, it is an important challenge to mimic physiological conditions *in vitro*, which can be achieved by usage of biorelevant media [100]. The composition of these media should depend on the intended site of absorption of the respective drug.

For dissolution in the stomach USP describes the simulated gastric fluid (SGF), which consists of diluted hydrochloric acid (pH 1.2) with additives of sodium chloride and pepsin (gastric digestion enzyme derived from porcine mucosa) [150]. If the intestine is the intended site of absorption simulated intestinal fluid (SIF), a phosphoric buffer (pH 6.8) containing pancreatin (a mixture of pancreatic enzymes, which is secreted in the duodenum), has to be used [150].

Though, these compendial media cannot be considered biorelevant since they do not involve natural surfactants (like bile salts). Additionally, they do not consider fed or fasted state, which is a highly significant factor for absorption in the body. To counter this issue, Dressman et al. (1998) proposed media to simulate the physiological intestinal fluid in fasted (FaSSIF) and fed state (FeSSIF) [52]. These media implement natural surfactants like lecithin and cholates to simulate the strong solubilizing effect

of bile ingredients. Thus, their ability to dissolve drugs differs decisively from the compendial media.

Many further studies focus on detailed investigation and improvement of FaSSIF and FeSSIF (Langguth, Nawroth et al.). Nawroth et al. (2011) investigated the formation of liposomes from bile salt-lipid micelles, which depends on the concentration of natural surfactants (difference between FeSSIF and FaSSIF). Since intermediate complexes of lipophilic drugs with bile and lipids and their nanostructured assemblies significantly influence the bioavailability, this underlines the high importance of the composition of a biorelevant dissolution medium [100]. Based on this knowledge, Khoshakhlagh et al. (2014) examined the effect of the formation and conversion of micelles and liposomes in different media, which simulate the passage from the entry of the bile in the middle of the duodenum to the end of this gut segment. They found that the concentration of lipidic nanoparticles strongly depends on time and dilution rate. Due to the important role of liposomes and micelles as intermediate host for resolution and uptake of lipophilic drugs these findings should be considered in development of dissolution tests of lipophilic drugs [75]. In a subsequent study Khoshakhlagh et al. (2015) added cholesterol at the same levels as in human bile to FASSIF and studied biocompatibility as well as solubilizing capacity of these media on four different lipophilic drugs. They observed that these media do not damage gut cells and that their solubilization capacity considerably varies between different drugs. Accordingly, cholesterol-containing media were recommended to be used in further release studies [74]. In summary, the discoveries of this research group may be essential for exploration of in vitro tests of lipophilic drug formulations.

In conclusion, a need for close interdisciplinary cooperation seems to be necessary to improve the scientific progress in pharmaceutical dissolution testing.

1.5.2 Challenges in dissolution testing of nanoparticulate dosage forms

For determination of the drug release behavior of nanocrystals and nanoparticulate dosage forms the paddle apparatus is primarily used

[22,33,71,159]. Abdel-Mottaleb et al. [1] described a modified USP apparatus 1. Thereto, the samples are filled in glass tubes and these tubes, similar to the basket of USP apparatus 1, attached to the shaft of a dissolution apparatus. While this method was first developed for the release test of a hydrogel, it was later adapted to nanocapsules [2]. The researchers suggested that the release properties of solid lipid NPs articulately depend on variation of the physicochemical properties like stirring. Thereto, the glass tube method was used to minimize changes in this regard. Though, in the case of nanoparticulate powder the conventional basket method has not proven to be appropriate.

Heng et al. [59], who investigated dissolution of cefuroxime axetil nanocrystals with USP apparatus 1, 2 (paddle) and 4 (flow-through cell) initially observed a faster dissolution of the nanocrystals compared to the unprocessed API. In the latter course of the experiment however, the dissolution rate of the nanocrystals even fell below that of the unprocessed form. This was found to be due to floating-up of the crystals in basket or paddle, which aggravates wetting.

Much earlier, Nicklasson et al. [103] had already described that difficulty after having performed different dissolution studies with phenacetin crystals. Both research groups demonstrated that the flow-through cell may be the most suitable alternative for dissolution testing of any particles with low wettability. This was considered to be due to increased surface area and solubility, which is provided by the constant flow of fresh medium through the cell. Additionally, Heng et al. [59] investigated the release behavior, if a dialysis bag, containing the drug suspended in dissolution medium, is introduced in vessels of the paddle apparatus. Despite the usage of a membrane with a high molecular weight cut-off (12–14 kDa) the dissolution was very slow. It was concluded that the diffusion over the membrane would rather be the rate-limiting step than the dissolution itself, which makes this method inappropriate.

When the interest in pharmaceutical dissolution research grew, many studies focused on the examination of factors having an effect on the dissolution rate. Which factors these are and the relevance they have, was already

investigated from Tolloczko, Nernst and Brunner half a century ago (mentioned above). If using nanoparticulate dosage forms one factor is of particular relevance: the particle size. The effect of the particle size on both dissolution rate and solubility is described in chapter 1.1. With respect to dissolution testing it is to consider that lowering the particle size does not necessarily improve the dissolution properties.

In 1974 Finholt [45] compared the dissolution behavior of granules containing phenacetin, phenobarbital and acetylsalicylic acid in different particle sizes. One part of the granules was prepared with gelatin as hydrophilic diluent. As expected, the dissolution rate of these granules increased with decreasing particle size. However, the contrary was observed for the other part, where no gelatin was used, but if a surfactant (Tween 80) was added to the dissolution medium, the situation was the same as with gelatin. From these observations it can be concluded that, if a hydrophobic drug is not wetted properly by the dissolution medium, a decrease in particle size impairs the dissolution behavior.

This is of high relevance since, in particular, hydrophobic APIs are candidates for nanoscaling. Under physiological conditions this should not play a major role as the intestine, which is the primary location of absorption, disposes natural surfactants, the bile salts [60]. In contrast, in vitro tests often use pure water (e.g. for the qualification of dissolution apparatus with FDA prednisone tablets [121]) or buffers of different pH values [41,53] by two means: Either one produces nanoparticulate dosage forms which, besides the API, contain excipients as wetting agents. Bile salts e.g. have already been successfully tested towards their ability to improve wetting of nanoparticulate systems [23,129]. Or, alternatively, one adds surface active agents to the dissolution medium, which is a common tool, if an API is poorly soluble in water over the physiological pH range [107].

Besides the above described physicochemical properties the choice of the dissolution medium is of crucial importance for conventional as well as for nanoparticulate dosage forms (see also chapter 1.5.1). Thereto, the route of the drug through the body with changing specific features, like pH value or presence of physiological surfactants, associated with the characteristics of

the drug is to consider. In addition to the nature of the API the properties of the excipients can have an essential impact on the release behavior. According to the FDA requirements for industrial dissolution testing of immediate release solid oral dosage forms [153], dissolution testing should preferably be carried out under physiological conditions. This, *inter alia*, implements the exclusive usage of aqueous media instead of organic ones, even for drugs like celecoxib which are nearly insoluble in water. The target is the realistic interpretation of dissolution data with regard to the *in vivo* performance of the product. This does not mean that strict adherence to the gastrointestinal environment must be given, which may also not be realistic with respect to the effort. The testing conditions should be based on physicochemical characteristics of the API and the environmental conditions the dosage form might be exposed to after oral administration. If an API is, for instance, embedded in a polymer, it is a prerequisite for its release that the polymer matrix is initially dissolved. Thus, a basic polymer, like Eudragit E 100, necessitates an acidic medium to be dissolved.

As mentioned above, one prerequisite for proper dissolution testing of NPs is the choice of the right medium. Besides that, there exists a major challenge compared to conventional dissolution tests which are performed with particles of larger size. The samples that are withdrawn for analysis at a certain timepoint must exclusively contain the dissolved analyte without any particles. The presence of undissolved particles in the sample intended for analysis will probably distort the results [61]. Further dissolution of particles, which is accompanied by an increasing concentration of dissolved API, may occur within the time span between withdrawal of the sample and measurement.

One can bypass this issue by *in-situ* measurement methods like fiber optic systems or potentiometric sensors. These two methods have already been successfully applied to dissolution tests [67,69,84,111] and bear many advantages towards the conventional method where a sample is first withdrawn, filtered and then applied to analysis. First, the work expense is much lower [111]. Additionally, these methods facilitate the record of much more data in a certain time span, increasing the reliability of dissolution

profiles. However, the in-situ methods require highly expensive and sensitive equipment.

Thus, a more economic method, which does also allow the proper determination of dissolved analyte at a certain timepoint may be preferable. Thereto, separation of a withdrawn aliquot of the dissolution medium containing the dissolved API from undissolved particles must occur without delay. This, in turn, necessitates a suitable filtration system. In conventional pharmaceutical dissolution tests the sample liquid is usually withdrawn with a syringe and filtered through a syringe filter holder to retain coarse-particles from the matrix of the dosage form [61]. This procedure has already been applied on API release testing of nanoparticulate dosage forms [33,59].

However, it must be considered that both Heng et al. and Dolenc et al. investigated dissolution of NPs of much more than 200 nm diameter, which made it feasible to use syringe filter holders of 0.2 μm . Although there exist corresponding filters with even lower pore size, filter clogging might become an important issue if smaller NPs shall be separated. In this context, the classical dead-end technique, which is often used for filtration purposes, does not seem to be appropriate. Hence, cross-flow filtration, a technique with a wide field of applications, e.g. sewage treatment [122], might be a promising alternative (see chapter 1.5.3).

1.5.3 Filtration of nanosuspensions

The characteristic property of a membrane is that it allows certain substances to pass while others are retained. Thus, membranes play an essential role in biology as every intra- and intercellular boundary is based on them [76]. The membrane filtration encompasses every process intended to separate substances from the ambient liquid with the help of permeable membranes. In contrast to traditional separation techniques like distillation or sublimation these techniques are operated without strong heating. This bears many advantages like energy saving and protection of sensitive substances. Membrane filtration is applied in nutritional (e.g. extraction of milk ingredients), pharmaceutical/ biotechnological (e.g. protein purification) and environmental/chemical (e.g. wastewater treatment) industry. The main part of the market, however, takes place in medicine. In hemodialysis membrane filters can act as artificial kidney to remove toxic substances from the body. In artificial respiration they prevent the permeation of air bubbles into blood stream [143]. The different modes of membrane filtration can be classified according to the driving force of the separation process (see Table 5). Among these methods nano-, ultra- and microfiltration have the highest relevance.

Table 5: Modes of membrane filtration according to Scheper [133].

driving force	pressure	concentration gradient	electric potential gradient	temperature gradient
techniques	microfiltration ultrafiltration nanofiltration reverse osmosis gas separation pervaporation	dialysis osmosis forward osmosis	electrodialysis membrane electrolysis electrophoresis	membrane distillation

A filtration system for dissolution testing of nanoparticulate dosage forms should both be fast and simple to operate without any detrimental influence on the API. These requirements limit the choice of a suitable method. First, separation by a concentration gradient through membranes is too time-consuming to determine dissolution rates adequately.

The usage of electric gradients necessitates on one hand burdensome equipment, on the other hand is the presence of charged species a prerequisite. For molecules like celecoxib that are neutral over a broad pH range, the implementation of a charge would be necessary. Thereto, one would have to adjust the pH of the dissolution medium, which may be contradictory to the purpose of the dissolution test.

Membrane distillation technique implements the diffusion of water vapor over a membrane being impermeable for liquid water. Thereto, a temperature gradient is used. As the API molecules remain in the liquid phase this method is also not applicable.

Hence, pressure would be the single appropriate separation driving force for the issue of a pharmaceutical dissolution test. The various techniques of membrane filtration differ concerning their separation abilities with a range from the filtration of small molecules (reverse osmosis) to objects in the size of a few micrometers like bacteria (microfiltration) [110] (see Figure 19). The retention power of dialysis membranes, which e.g. are used in clinical hemodialysis, lies between ultra- and nanofiltration to allow permeation of ions or metabolites, but to retain cells and large molecules like proteins [9].

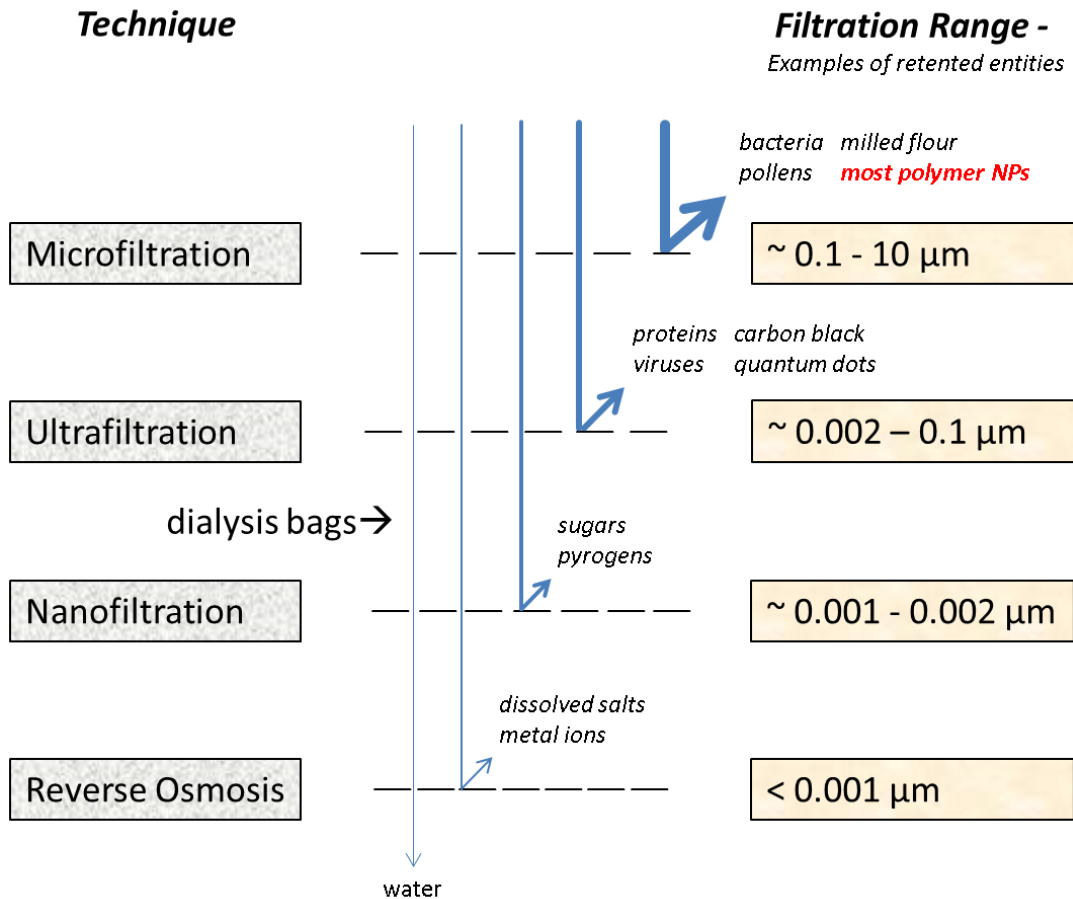


Figure 19: Classification of pressure driven filtration techniques according to filtration range.

The two main configurations of membrane filtration processes are dead-end and cross-flow (schematic shown in Figure 20). „In the dead-end configuration, the feed suspension flows perpendicular to the membrane surface, whereas in cross-flow systems, the suspension flow is tangential to the membrane [102].”

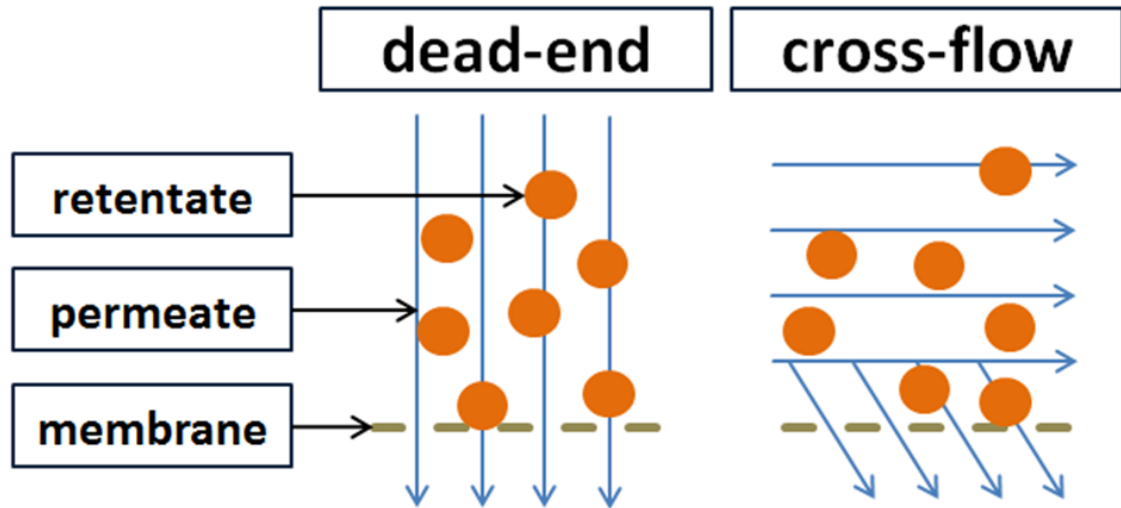


Figure 20: Schematic of dead-end- and cross-flow filtration.

Dead-end filtration is the less complex and, therefore, more cost-effective alternative of these configurations. However, especially if nanoscale particles are to filtrate, it bears the risk of filter clogging. This risk gradually increases if a filter is used repeatedly, which is usually done within pharmaceutical dissolution tests to restrict financial effort. After certain time a porous cake layer will be formed on the filter surface, whose pores will become increasingly smaller. This circumstance can be well understood if regarding Hagen-Poiseuilles law (16),

$$\dot{v} = \frac{dv}{dt} = \frac{\pi^* r^{4*} \Delta p}{8\eta^* l} \quad (16)$$

that describes the pressure decline in a newtonian fluid (i.e. fluid viscosity is directly proportional to the shear stress) flowing through a long cylindrical pipe, provided that the flow is laminar and passes a constant circular cross-section, that is substantially longer than its diameter. Hence, \dot{v} is the volumetric flow rate of the fluid, r the internal radius of the pipe, Δp the pressure difference between the two tube ends of the pipe, η the dynamic viscosity of the fluid and l the pipe length. In case of a filtration membrane the cylindrical pipe corresponds to the filter pores, while the internal pipe radius and the pipe length correspond to size and length of the pores, respectively. In this equation the pore size is in the fourth power in the numerator, which explains the immense decrease of flow rate in dead-end filtration at shrinking

pore size. Conversely, tangential flow direction can prevent filter cake formation and ascertain a constant filtration rate over the complete period of the dissolution test.

1.6 Aim of the study

In the present study polymeric NPs containing celecoxib should be produced using both a bench-top and a MicroJetReactor approach. These NPs should serve as a model to study the dissolution behavior of nanoparticulate dosage forms. Additionally, they should be suitable for utilization in solid pharmaceutical dosage forms. As production technique emulsification-diffusion was chosen, a method, which has already been successfully applied to produce celecoxib NPs [33]. Thereto, Eudragit E 100 was chosen as polymer matrix and electrostatic stabilizer, a combination which has been utilized for the preparation of celecoxib microparticles by hot-melt extrusion followed by milling [5]. Additionally, aqueous solutions of different steric stabilizing agents (Poloxamer 407, PVA and SDS) should be employed in the production as non-solvent phase. The Z-Average of the yielded NPs should be between 100 and 500 nm. Every batch should provide a narrow size distribution ($PDI \leq 0.25$) to minimize variations in dissolution and a ZP of at least ± 20 mV to ascertain adequate stability. Further, a high celecoxib concentration (≥ 2 mg/mL in nanosuspension) is favorable with regard to the amount needed for delivery of a therapeutic single dose (Celecoxib: 50–400 mg [46]). The characterization should be performed by DLS (Z-Average, PDI and ZP), HPLC-UV (EE), DSC (binding properties between celecoxib and Eudragit E 100) and AFM/SEM (NP diameter and shape). Concerning the dissolution tests a filtration system allowing fast separation of undissolved NPs from dissolved API should be developed. Furthermore, experimental conditions should be elaborated to be able to detect differences in the dissolution behavior of differently sized NPs.

2 Materials and methods

2.1 Materials

The technical equipment used for NP preparation and characterization and conduction of dissolution tests is listed in Table 6.

Table 6: Used equipment.

Device	Provider	Description
AFM – instrument	Veeco Instruments, Santa Barbara, USA	Bioscope with a Nanoscope IV controller
AFM – cantilever	Olympus, Essex, UK	OMCL-AC160TS
AFM – scanning probe	Anfatec, Oelsnitz, Germany	–
AFM – mica sheets	Plano Planet, Wetzlar, Germany	–
AFM – image analysis software	Bruker Corporation, Billerica, USA	Nanoscope SPM
Balance (0.01–10 g)	Scaltec Instruments, Heiligenstadt, Germany	SBA 31
Balance (10–100 g)	Kern, Balingen, Germany	KERN PLJ 3500-2NM
Centrifuge	Hettich Lab Technology, Tuttlingen, Germany	Universal 32R
Cross-flow filtration module (100 kDa)	Spectrum, Breda, Netherlands	MemCon Type MicroKros 100 kD (MWCO: 10 nm), housing size 3
Cross-flow filtration module (500 kDa)	Spectrum, Breda, Netherlands	MemCon Type MicroKros 500 kD (MWCO: 50 nm), housing size 3
Design of experiments software	Stat-Ease, Minneapolis, US	V7.0.0
Dissolution apparatus – magnetic bar	VWR, Darmstadt, Germany	Cylindrical Magnet Bar (length: 1.2 cm, diameter: 0.45 cm)
Dissolution apparatus – magnetic stirrer	IKA, Staufen, Germany	RCT Classic with temperature sensor VT5 S40
Dissolution apparatus – peristaltic pump	Thermo Scientific, Waltham, US	FH15
Dissolution apparatus – rubber hose	VWR, Darmstadt, Germany	Pharmed BPT Tubing SZ 25
Dissolution apparatus – syringe filter holders	Sigma Aldrich, Munich, Germany	Whatman Puradisc FP 30 0.2 µm

Table 6: Used equipment. (continued)

Device	Provider	Description
Dissolution apparatus – temperature sensor	IKA, Staufen, Germany	VT5 S40
DLS – clear disposable zeta cells	Malvern Instruments, Malvern, UK	DTS1060C
DLS – instrument	Malvern Instruments, Malvern, UK	Nano ZS90
DLS – disposable sizing cuvettes	Malvern Instruments, Malvern, UK	DTS0012
DSC – instrument	Mettler Toledo, Gießen, Germany	DSC 1 Star System
DSC – analysis software	Mettler Toledo, Gießen, Germany	Graphware
Fumehood	Waldner Laboreinrichtungen, Wangen im Allgäu, Germany	mc6
High speed homogenizer	VWR, Darmstadt, Germany	VDI 12
HPLC – vials	VWR, Darmstadt, Germany	1.0 mL, brown glass
HPLC – column	Phenomenex, Aschaffenburg, Germany	Synergi 4 μ , 150 * 4.6 mm, Fusion-RP 80 A, particle size: 4 μ m
HPLC – instrument	Hitachi, Düsseldorf, Germany	Chromaster
HPLC – software	Scientific Software, Chicago, US	EZChrom Elite
IR – instrument	Shimadzu, Duisburg, Germany	FTIR-8400S
IR – software	Shimadzu, Duisburg, Germany	IRsolution 1.60
Laser diffractometer – instrument	Sympatec GmbH, Clausthal-Zellerfeld, Germany	HELOS/BR-OM Multirange (0.1 μ m–875 μ m)
Laser diffractometer – cuvette	Sympatec GmbH, Clausthal-Zellerfeld, Germany	CUV-50ML/US
MJR assembly – HPLC pump	VWR, Darmstadt, Germany	LaPrep P110
MJR assembly – micro annular gear pump	HNP Mikrosysteme, Schwerin, Germany	mzr-7205F, 0,048–288 mL/min
MJR assembly – MicroJetReactor	Synthesechemie Dr. Penth, Lebach, Germany	Hastelloy reactor with rubin nozzle, inner diameter: 400 μ m
MJR assembly – nitrogen pressure gas bottle	Praxair, Düsseldorf, Germany	–
MJR assembly – pump heater	Enda Industrial Electronics, Istanbul, Turkey	digital thermostat ETC1311-FE-230VAC

Table 6: Used equipment. (continued)

Device	Provider	Description
MJR assembly – water bath	VWR, Darmstadt, Germany	VWB 6
pH meter	Mettler Toledo, Gießen, Germany	Seven Multi S40
Rotary evaporator	VWR, Darmstadt, Germany	IKA RV 10 digital
SEM – instrument	Carl Zeiss Microscopy, Oberkochen, Germany	EVO HD15
SEM – sputter coater	Quorum, East Grinstead, UK	Q150R ES
SEM – image analysis software	National Institutes of Health, Bethesda, US	ImageJ
Spreadsheet software	Microsoft, Redmond, US	Excel 2010
Ultrasonic bath	VWR, Darmstadt, Germany	USC300TH
UV-Vis –cuvette	Hellma Analytics, Müllheim, Germany	101-QS, 10x10 mm, quartz
UV-Vis – instrument	VWR, Darmstadt, Germany	UV/VIS-1600PC

The used chemical reagents are listed in Table 7 and were used as received.

Table 7: Chemical reagents.

Reagent	Provider	Description
Celecoxib	Fraken Biochem, Qingdao, China	CAS: 169590-42-5, MW: 381, batch: 201108054
Cetrimide	Sigma Aldrich, Munich, Germany	CAS: 9004-34-6, MW: 364, hexadecyltrimethylammonium- bromide \geq 98%, batch: SLBC8213V
Distilled water	Siemens, Munich, Germany	CAS: 7732-18-5, MW: 18, prepared with: LaboStar 3 TWF-DI/-UV
Ethyl acetate	VWR, Darmstadt, Germany	CAS: 141-78-6, MW: 88, analytical grade
Eudragit E 100	Evonik Industries, Essen, Germany	CAS: 24938-16-7, MW: \sim 47,000, poly(butyl methacrylate-co-(2- dimethylaminoethyl)methylate-co- methylmethacrylate) 1:2:1, batch: E080501129
Hydrochloric acid, 37 %	Universität des Saarlandes– Zentrales Chemikalienlager, Saarbrücken, Germany	CAS: 7647-01-0, MW: 36
Methanol	VWR, Darmstadt, Germany	CAS: 67-56-1, MW: 32, HPLC grade
Phosphoric acid	VWR, Darmstadt, Germany	CAS: 7664-38-2, MW: 98, batch: 10F240536, orthophosphoric acid 85%
Poloxamer 407	VWR, Darmstadt, Germany	CAS: 9003-11-6, MW: 1200, Pluronic F-127, polyoxypropylene polyoxyethylene co- polymer, batch: BCBC6633
Polyvinyl alcohol	Sigma Aldrich, Munich, Germany	CAS: 9002-89-5, MW: \sim 27,000, Mowiol 4-98, Lot#BCBD5639V
Potassium dihydrogen phosphate	VWR, Darmstadt, Germany	CAS: 7778-77-0, MW: 136, batch: 10H230005
Sodium chloride	VWR, Darmstadt, Germany	CAS: 7647-14-5, MW: 58, batch: 10J11040
Sodium dodecyl sulfate	VWR, Darmstadt, Germany	CAS: 151-21-3, MW: 288, batch: K41859334
Sodium hydroxide	VWR, Darmstadt, Germany	CAS: 1310-73-2 , MW: 40, batch: 13B050037

The used dissolution media are listed in Table 8.

Table 8: Dissolution media.

Dissolution medium	Preparation
HCl pH 1.2	8.00 mL of hydrochloric acid, 37 % are diluted to 1000 mL with distilled water and the pH adjusted to 1.2 ± 0.05 with hydrochloric acid, 37 %
HCl pH 1.2 + 0.15 M NaCl	8.77 g of sodium chloride are dissolved in 1000 mL of HCl pH 1.2
HCl pH 1.2 + 0.001/0.01/0.05/0.3/1.0 % cetrimide	0.010/0.10/0.50/3.0/10.0 g of cetrimide are dissolved in 1000 mL of HCl pH 1.2
0.02 M Phosphate buffer solution pH 5.2 + 0.3 % cetrimide	2.72 g of potassium dihydrogen phosphate and 3.0 g of cetrimide are dissolved in 1000 ml of distilled water. The pH of the solution is 5.2 ± 0.05
0.05 M phosphate buffer solution pH 4.5 + 0.3 % cetrimide	6.80 g of potassium dihydrogen phosphate and 3.0 g of cetrimide are dissolved in 1000 ml of distilled water. The pH of the solution is adjusted with phosphoric acid to 4.5 ± 0.05
0.5 M Phosphate buffer solution pH 3.5 + 0.3 % cetrimide	68.0 g of potassium dihydrogen phosphate and 3.0 g of cetrimide are dissolved in 1000 ml of distilled water. The pH of the solution is adjusted with phosphoric acid to 3.5 ± 0.05
0.73 M Phosphate buffer solution pH 2.5 + 0.3 % cetrimide	100.0 g of potassium dihydrogen phosphate and 3.0 g of cetrimide are dissolved in 1000 ml of distilled water. The pH of the solution is adjusted with hydrochloric acid to 2.5 ± 0.05
0.73 M Phosphate buffer solution pH 2.0 + 0.3 % cetrimide	100.0 g of potassium dihydrogen phosphate and 3.0 g of cetrimide are dissolved in 1000 ml of distilled water. The pH of the solution is adjusted with hydrochloric acid to 2.0 ± 0.05

2.2 Methods

2.2.1 Nanoparticle preparation

2.2.1.1 Bench-top

First, a solution of celecoxib (5–100 mg/mL) and Eudragit E 100 (10–200 mg/mL) in ethyl acetate (1–5 mL) was poured into 10 mL of an aqueous solution of PVA, SDS or Poloxamer 407 (0.01–5.0 % w/v). The resulting emulsion was agitated three times for 30 s each using a high speed homogenizer (see Table 6) at 30,000 rpm. Time intervals of 30 s were left after the first and the second homogenization step. Then, ethyl acetate was evaporated under vacuum. The manufacturing process is depicted schematically in Figure 21. The resulting nanosuspensions were used without further processing.

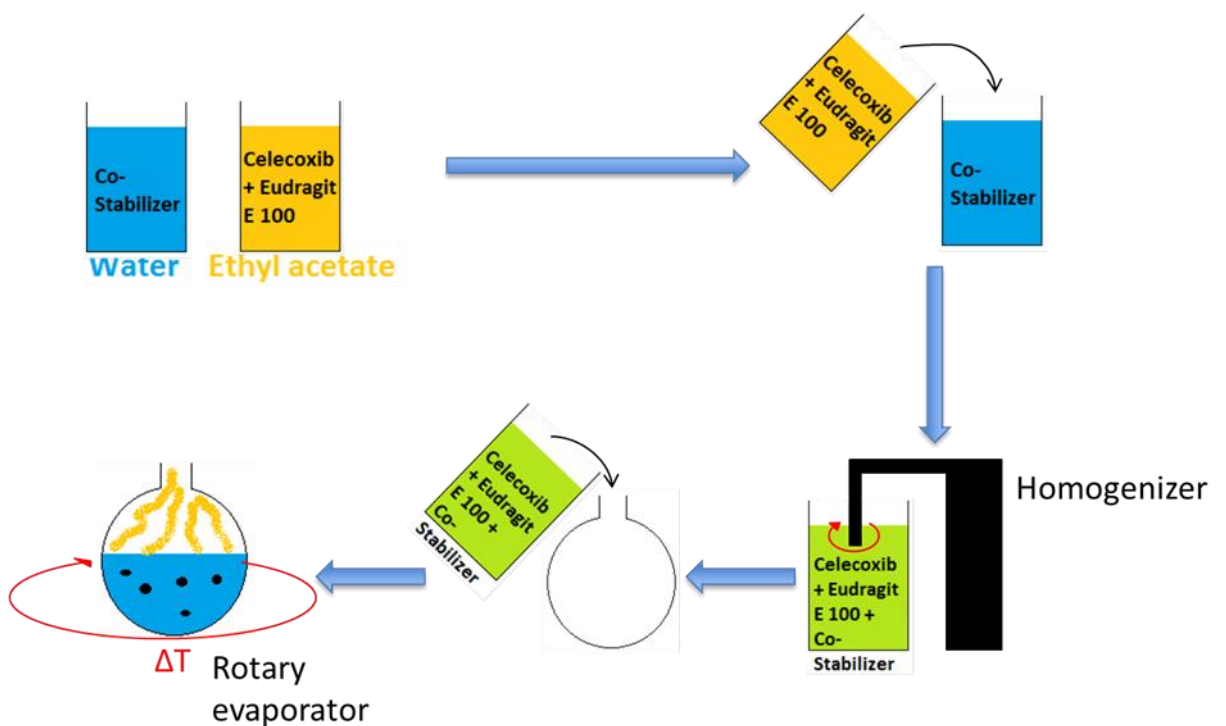


Figure 21: NP preparation procedure (bench top/emulsification-solvent evaporation).

2.2.1.2 MicroJetReactor

Celecoxib (2.5 %) and Eudragit E 100 (5.0 %) were dissolved together in ethyl acetate (emulsification-diffusion) or methanol (nanoprecipitation). Non-solvent was an aqueous solution of Poloxamer 407 (1.25 %). The solvent jet speed was varied between 100 and 1200 rpm by micro annular gear pumps, while the non-solvent jet speed was respectively five times higher. The flow rates corresponding to the respective pump rotational speed are stated in Table 9. The operation temperature (water bath and pump heaters) was chosen between 25 and 60 °C and the solutions equilibrated to the respective temperature in the water bath prior to preparation. The nitrogen flow was varied between 0 and 0.5 bar. For the setting 0 bar the nitrogen access on top of the reactor was closed to prevent liquid flow into the gas channel. The yielded suspensions were collected and remaining organic solvent evaporated at ambient conditions.

Table 9: Flow rates of MJR assembly – micro annular gear pump at selected rotational speeds (manufacturer specification).

Pump rotational speed /rpm	Flow rate /mL*min⁻¹
300	14.4
750	36
1200	57.6
1500	72
3750	180
6000	288

The previous MJR preparation methods were applied for the studies described in chapters 3.1, 3.2 (except of AFM characterization, see 3.2.4) and 3.3.2 (Dissolution behavior of differently-sized NPs). The NPs used for the dissolution studies described in chapter 3.3.1 were prepared with an alternative method. Hence, preparative HPLC pumps (without pump heaters) were used instead of micro annular gear pumps, while the remaining design, including the reactor part, complies with the MJR assembly depicted in Figure 10. This setup did not allow precise adjustment of nitrogen pressure.

The preparation technique was nanoprecipitation (solvent: methanol). A co-stabilizer (like Poloxamer 407) was not used. By this means white turbid solutions were obtained and poured in polypropylene storage tubes. To remove excessive methanol the tubes were opened and put in an operating fumehood for approximately 18 h at ambient temperature. Table 10 summarizes the preparation details. With this method small NPs of narrow size distribution can be obtained (see Table 16). Furthermore, it is not necessary to use of a co-stabilizer and the energy-consumption (heating and pumping energy) is lower. Though, this method does not facilitate the production of NPs in a larger size range. Moreover the throughput of the first method is much higher (maximum flow rates 288 mL/min versus 50 mL/min), which is a decisive advantage for transfer to industry.

Table 10: Technical parameters of MJR preparation of celecoxib-Eudragit E 100-NPs by nanoprecipitation – alternative method (without use of co-stabilizer).

Parameter	Details
Solvent	methanol
Non-solvent	water
API	celecoxib
Polymer	Eudragit E 100
API concentration in solvent	4 mg/mL
Polymer concentration in non-solvent	8 mg/mL
Solvent flow rate	50 mL/min
Non-solvent flow rate	50 mL/min
Temperature (water bath)	25 °C
Nitrogen pressure	approximately 0-0.5 bar

2.2.2 Nanoparticle characterization

2.2.2.1 Dynamic light scattering

To determine Z-Average, PDI and ZP the nanosuspensions were diluted with distilled water to a final concentration of 10^{-1} – 10^{-3} % (weight percentage of celecoxib + Eudragit E 100) and transferred to a disposable sizing cuvette or a zeta cell for measurement. This dilution factor is a compromise as, on one hand, the used instrument requires a certain dilution to be able to measure properly, whereas on the other hand, the dilution factor should be lower than 10^{-2} – 10^{-4} [148]. Prior to measurement samples were allowed to equilibrate in the apparatus for 1 min at 25 °C. ZP was calculated using the Smoluchowski equation [146]. Each measurement was performed in triplicate and the arithmetic mean calculated.

2.2.2.2 Entrapment efficiency

Entrapment efficiency of NPs was determined by HPLC. Based on a procedure from Baboota et al. [10] a HPLC method for the analysis of celecoxib in aqueous media was developed. After adaption of the eluent composition a sharp and symmetric peak was obtained at a retention time of 4.2 min. The HPLC parameters are summarized in Table 11. Linearity was evaluated through injection of five celecoxib solutions (1–50 µg/mL) in mobile phase. The correlation of the calibration curve was 0.9995.

Table 11: HPLC method parameters for the determination of celecoxib content in NPs.

Parameter	Details
Column	Synergi Fusion-RP C-12, 4 μ m, 150 * 4.6 mm
Column oven temperature	25 $^{\circ}$ C
Detector wavelength	250 nm
Elution system	isocratic
Flow rate	1 mL/min
Injection volume	20 μ L
Mobile phase	methanol : water 73 : 27 (v/v)
Standard solution	celecoxib 25 μ g/mL in mobile phase

An aliquot of the respective nanosuspension was centrifuged for 30 min at 57950 g. The supernatant was carefully removed, appropriately diluted with mobile phase and applied to HPLC. To remove excessive celecoxib and co-stabilizer the residue was washed with water, the centrifugation step repeated, the supernatant removed and the residue dried at ambient conditions. Then, methanol was given to the pellet followed by 60 min ultrasonication to ascertain complete dissolution. The obtained solution was appropriately diluted with mobile phase and applied to HPLC. The EE was calculated from equation (17),

$$EE = \frac{c_r f}{c_0} * 100 \% \quad (17)$$

where c_r is the measured celecoxib concentration in dissolved residue, c_0 the total celecoxib concentration (content of residue and supernatant) and f the dilution factor.

2.2.2.3 Differential scanning calorimetry

10 ± 0.5 mg of each sample (celecoxib: 5 ± 0.5 mg) were sealed in pierced aluminium pans of 40 µL. To obtain dry NP samples, aliquots of the respective nanosuspensions were centrifuged and washed. After removal of the supernatant they were dried for 24 h at ambient temperature. The measurements were done at a scanning speed of 10 K/min from 298 up to 463 K with 80 mL/min of nitrogen purge.

2.2.2.4 Infrared spectroscopy

Approximately 10 mg of each sample were put on the diamond ATR crystal and firmly pressed against it. For the preparation of the NP samples see chapter 2.2.2.3. Celecoxib sodium and protonated Eudragit E 100 were prepared by adding respectively 10 mL of either sodium hydroxide or hydrochloric acid solution to equimolar amounts of celecoxib and Eudragit E 100. Then, the liquid was evaporated under stirring at ambient conditions followed by two washing steps with methanol to remove excessive celecoxib or Eudragit E 100. The samples were scanned at wave numbers ranging from 600 to 4000 cm⁻¹ with a resolution of 4.0 cm⁻¹.

2.2.2.5 Scanning electron microscopy

10 µL of a 1:100 aqueous dilution of each nanosuspension was mounted onto a specimen stub and 24 h incubated at ambient conditions to evaporate the liquid. Thereafter, the samples were sputtered with gold at 20 mA for 50 s in order to prevent charging effects (layer thickness approximately 15 nm). SEM imaging was carried out under high vacuum at ambient temperature and an acceleration voltage of 10 kV. The secondary electron emission was recorded using an Everhart-Thornley detector. To determine the particle size an image analysis software (see Table 6) was used. Hereby, 20 particles were randomly selected and measured.

2.2.2.6 Atomic force microscopy

Prior to the examination the nanosuspensions were 1:10 diluted with distilled water. A drop of each of these dilutions was placed on a freshly cleaved mica sheet, respectively. Then, the mica sheet was dried for 24 h at ambient conditions to evaporate the liquid. The AFM imaging was performed under atmospheric conditions with a standard non-contact mode cantilever in tapping mode at scan rates of 0.6 Hz.

2.2.3 Dissolution tests

2.2.3.1 Verification of cross-flow filtration

Prior to the performance of dissolution tests with the nanosuspensions the suitability of the used cross-flow filtration modules (see Table 6) was verified. The modules (see Figure 22: schematic→(a), photograph→(b)) consist of a hollow shaft, which contains several hollow fibers. The shaft has two side ports, an inlet on the top and an outlet at the bottom. The inlet and the outlet are sealed, except of the openings of the hollow fibers. As these fibers have pores, which are permeable for substances below the size of 100 kDa (MWCO: 10 nm) respectively 500 kDa (MWCO: 50 nm), they represent the actual filtration system (this is depicted in the enlargement of Figure 22 (a)). The dissolution medium with undissolved NPs and the dissolved API passes the hollow fibers from the inlet to the outlet (the complete liquid circulation from the beaker over the pump to the CF-module is shown in Figure 25). Ideally, NPs shall be retained and liquid with dissolved API (filtrate) penetrates the filter pores to the cavity between the fibers and the wall of the shaft. Then, from the lower side port, filtrate can be collected and applied to analysis. For the dissolution tests the upper side port has no function and is closed with a Luer-Lok cap (this is shown in the photograph→ Figure 22 (b)). The relevant properties of the cross-flow filtration modules are listed in Table 12.

Table 12: Properties of the used cross-flow filtration modules.

Parameter	Details
MWCO	10 nm (100 kDa CF module) 50 nm (500 kDa CF module)
Fiber inner diameter	0.5 mm
Fiber material	modified polyether sulfone
Number of fibers	5-6
Filter surface area	20 cm ²
Effective length	20 cm
Total length	23 cm
Housing inner diameter	3.1 mm
Housing outer diameter	4.6 mm
Inlet/retentate inner diameter	3 mm
In/out ports	Male Luer-Lok
Side port	Female Luer-Lok

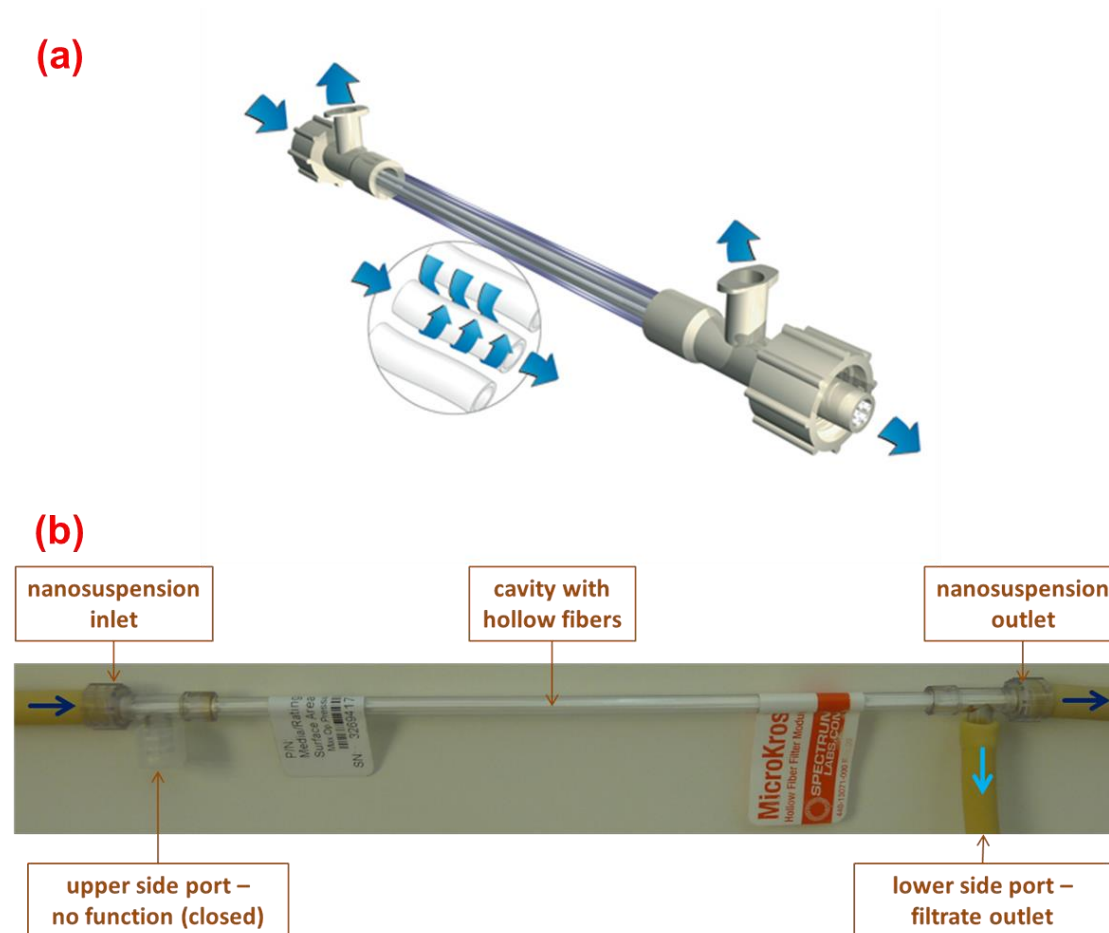


Figure 22: Cross-flow filtration module: Schematic of a MicroKros filter module (image derived from <http://eu.spectrumlabs.com/filtration/MicroKros.html?xfr=1373374033>;) with an enlargement of the hollow fibers (a) and photograph of this module as used in the dissolution apparatus (b).

As proof of principle the absence of NPs in the filtrate must be shown. Thereto, celecoxib Eudragit E 100 NPs were prepared with MJR method (alternative method, without usage of a surfactant, see chapter 2.2.1.2). The volume-weighted size distribution of these particles is depicted in Figure 23 (a) (Z-Average: 143 nm, PDI: 0.237). Approximately 20 mL of this nanosuspension passed along the hollow fibers of the filtration module using the peristaltic pump. A DLS measurement of the filtrate was done. According to the obtained result (see Figure 23 (b)) the filtrate does not contain NPs in a significant amount, although this measurement was taken without previous dilution while a 1 : 20 aqueous dilution was prepared for measurement of the unfiltered nanosuspension. The peak one (0.78 nm) in Figure 23 (b) is near to the lower measuring limit (0.3 nm) of the used DLS instrument. It can be attributed to dissolved molecules of celecoxib or Eudragit E 100. Most remarkable is the nearly complete absence of the distribution curve between approximately 40 and 1000 nm. Figure 24 shows the results of the same test, which was done with a 500 kDa CF-module. Hence, a 1 : 100 dilution of another nanosuspension was measured versus the undiluted filtrate. The result is comparable to the other experiment and reveals that > 99 % of the NPs are retained by the filter.

As second test to verify the filter function, the UV absorbance of both nanosuspension and filtrate (respectively 1 : 100 aqueous dilution) was measured ($\lambda = 252$ nm). Hence, the nanosuspension showed a strong absorbance (~ 1.8) whereas the filtrate absorbance was nearly zero (data not shown). Thus, the suitability of the cross-flow filtration module for the separation of polymer NPs was demonstrated.

The DLS verification test was successfully repeated for every CF-module (100 kDa and 500 kDa) prior to use.

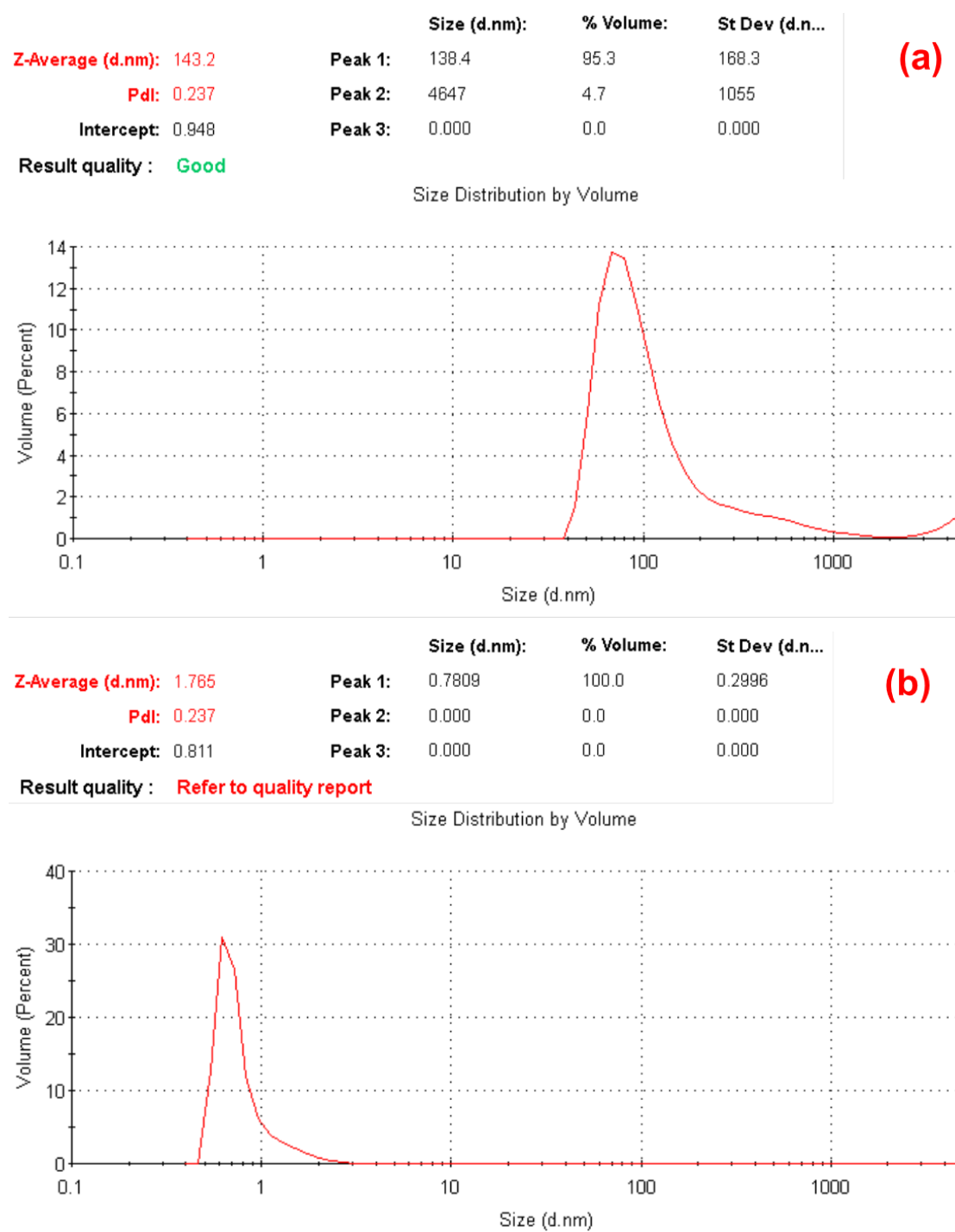
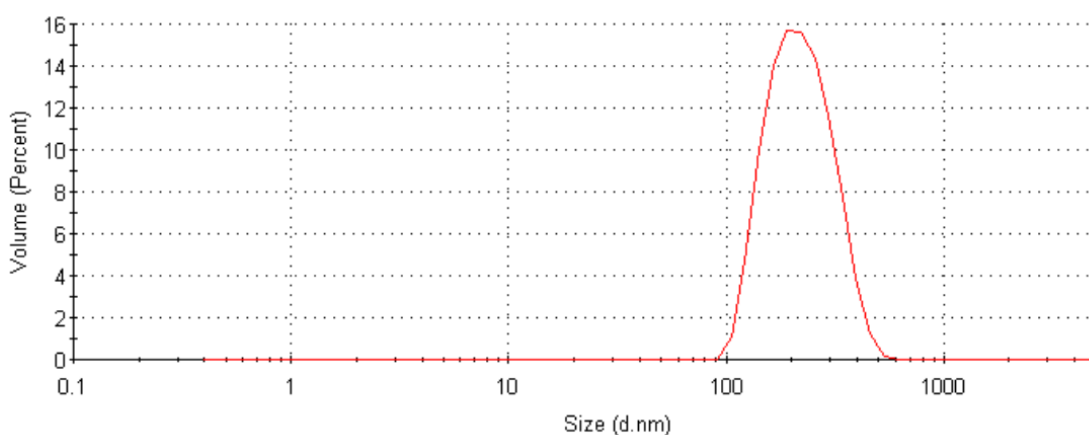


Figure 23: DLS size distribution reports (volume-weighted) of a celecoxib-Eudragit E 100 aqueous nanosuspension; NP-preparation: nanoprecipitation technique–alternative method using HPLC pumps and a non-solvent phase without surfactant (see chapter 2.2.1.2); unfiltered nanosuspension (1 : 20 dilution in water) (a) versus liquid obtained from filtration of this nanosuspension through a 100 kDa CF module (b); NP properties: 143 nm (Z-Average), 0.237 (PDI).

	Size (d.nm):	% Volume:	St Dev (d.n...	(a)
Z-Average (d.nm): 216.4	Peak 1: 227.3	100.0	75.77	
Pdl: 0.108	Peak 2: 0.000	0.0	0.000	
Intercept: 0.974	Peak 3: 0.000	0.0	0.000	

Result quality : **Refer to quality report**

Size Distribution by Volume



	Size (d.nm):	% Volume:	St Dev (d.n...	(b)
Z-Average (d.nm): 1.394	Peak 1: 0.6350	99.9	0.07258	
Pdl: 0.240	Peak 2: 7.014	0.1	1.910	
Intercept: 0.650	Peak 3: 0.000	0.0	0.000	

Result quality : **Refer to quality report**

Size Distribution by Volume

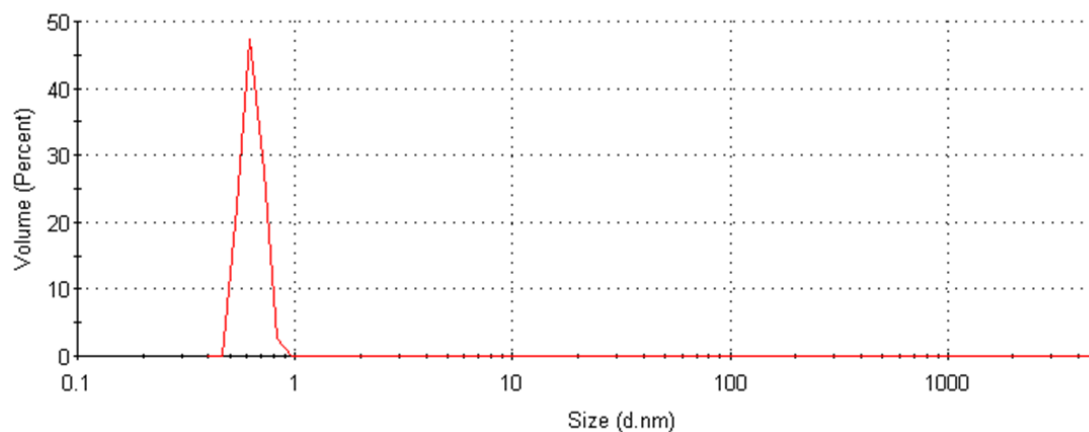


Figure 24: DLS size distribution reports (volume-weighted) of a celecoxib-Eudragit E 100 aqueous nanosuspension; NP-preparation: nanoprecipitation technique–alternative method using HPLC pumps and a non-solvent phase without surfactant (see chapter 2.2.1.2); unfiltered nanosuspension (1 : 100 dilution in water) (a) versus liquid obtained from filtration of this nanosuspension through a 500 kDa CF module (b); NP properties: 216 nm (Z-Average), 0.108 (PDI).

2.2.3.2 Dissolution test methodology

The conduction of drug release tests of nanosuspensions involving cross-flow filtration required the development of an individual experimental setup. Figure 25 shows photographs of the complete assembly (a), the filtrate outlet (b) and the sample withdrawal (c). A 150 mL-beaker, containing 99–99.75 mL of dissolution medium and a cylindrical magnetic bar (length: 1.2 cm, diameter: 0.45 cm), were put onto a magnetic stirrer. The temperature sensor of the magnetic stirrer was attached to the magnetic stirrer and dived to a depth of circa 2 cm into the dissolution medium to maintain a temperature of 37 ± 0.5 °C throughout the complete experiment. The rotational speed was set to 300 rpm. The beaker was covered with plastic paraffin film to prevent evaporation of the medium (loss of medium after 120 min at 37 °C and stirring at 300 rpm: without cover ~ 3–4 mL, with cover < 1 mL).

To start the dissolution test 0.25–1 mL of the respective nano- or API powder-suspension were given into the medium. The API powder sample was prepared by suspending celecoxib to a concentration of 4 mg/mL in water. Immediately prior to the test this suspension was ultrasonicated for 2 min followed by manual shaking for 30 s to avoid the formation of agglomerates. For sample withdrawal a rubber hose was inserted into the medium and the liquid aspirated by a peristaltic pump, which was operated throughout the complete experiment. Then, before being returned to the beaker, the medium passed the CF-module. From the lower open end at the side of the module up to 2.0 mL of filtered liquid were collected with a polypropylene reaction tube at every sampling point and applied to UV-Vis API analysis. After each sampling the collected volume was replaced with fresh medium.

After the experiment the filtration module was carefully rinsed with 0.1 M sodium hydroxide followed by distilled water. For storage the modules were emptied and the openings closed.

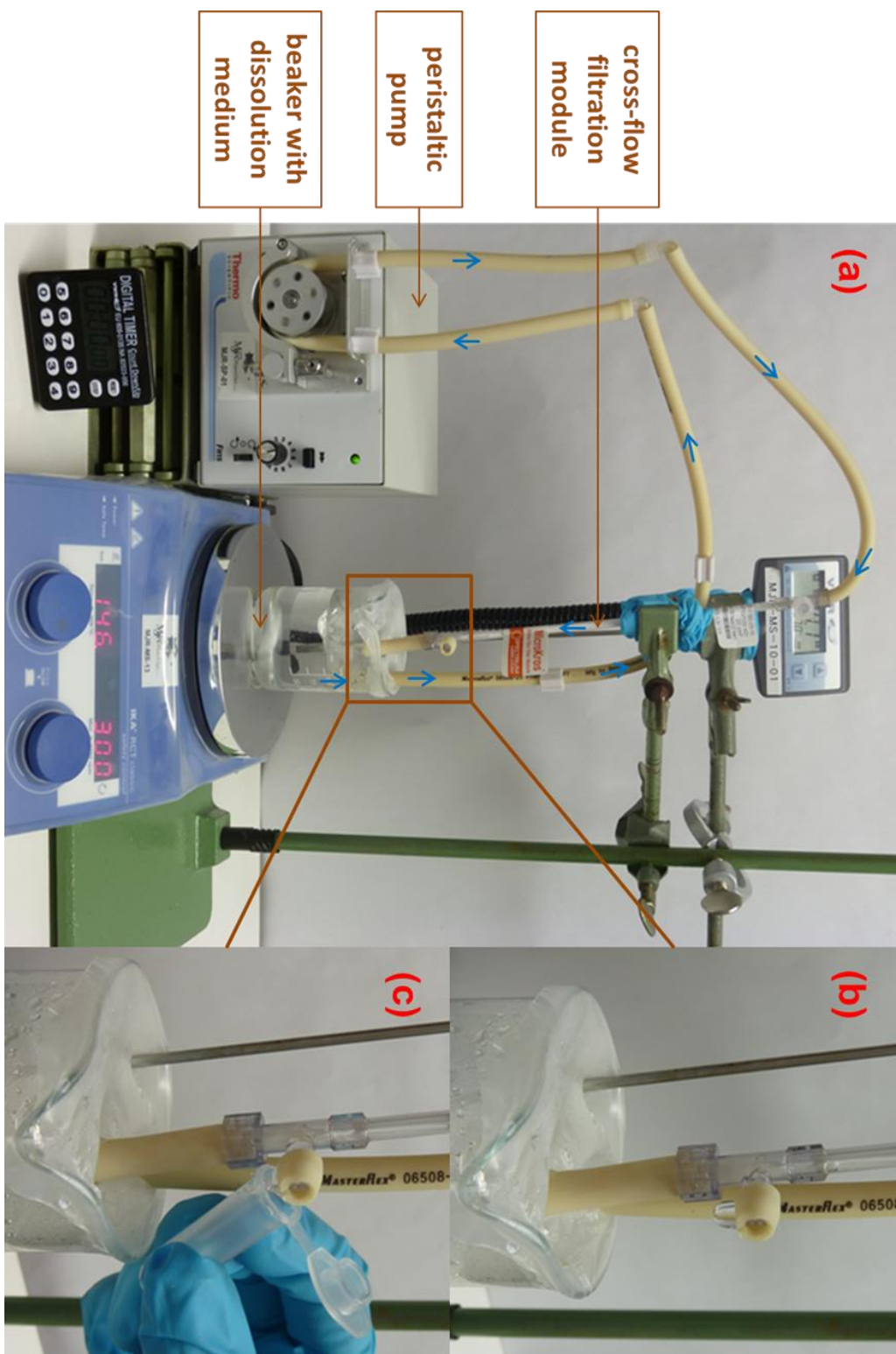


Figure 25: Photograph of the dissolution test assembly (a), with image details of the filtrate outlet (b) and the sample withdrawal (c).

2.2.3.3 Dead-end filtration

To compare the performance of the CF setup to conventional approaches implementing dead-end filters, the samples were withdrawn from the beaker using disposable syringes instead of aspiration with the peristaltic pump. Thereto, 30 s prior to the defined sampling timepoint 5 mL of dissolution medium were withdrawn and given back to the beaker immediately as washing step of the filter. At the sampling timepoint the syringe was filled again with the same volume, a 0.2 μm syringe filter holder attached and 2 mL of liquid transferred through the filter. Then, the filter was removed from the syringe, the remaining liquid given back to the beaker and the collected volume replaced with fresh medium, which was previously equilibrated to 37 °C.

2.2.3.4 Flow properties

According to the specification of the used peristaltic pump the flow rate can be varied between 0.8 and 105 mL/min. In combination with the used Pharmed BPT tubes, this corresponds to pressure values between approximately 0.01 and 2 bar. To examine the flow-through performance of the complete system (permeate and retentate flow) the arrangement was prepared as described in chapter 2.2.3.2 with the exception that a second beaker was used to collect liquid from the respective outlets. Then, the first beaker was filled with distilled water and attached to the pump, which was operated at maximum speed. The water from both outlets was collected for 60 s and the amount weighed.

A second experiment was conducted to examine the permeation rate. Hence, the water volume from the lower side outlet of the module (filtrate outlet) was collected for 10 s at maximum pump speed. Additionally, the time span between turning on of the pump and the first appearance of water at the side outlet (dead time) was determined. All trials were performed in triplicate (results listed in Table 13).

Table 13: Flow-through properties of the cross-flow filtration system (permeate plus retentate and permeate), n=3, values are mean \pm SD.

Outlet	Permeate and retentate	Permeate
Water volume collected /mL	131.7 \pm 0.9 (after 60 s)	1.75 \pm 0.035 (after 10 s)
Flow-through /mL*min⁻¹	131.7	10.5
Dead time /s	n/a	12.7 \pm 0.6

The results reveal that the flow-through rate is with a value of 131.7 mL/min even above the specification (105 mL/min). Provided that the used volume of the dissolution medium is approximately 100 mL more than the complete content of the beaker passes the CF-membrane in less than one minute.

Though, since pharmaceutical compendia demand the withdrawal of specimen within a limited time span, the more important value is the permeation rate. To gather 2 mL of filtrate for analysis circa 11.4 s are required considering the above obtained results. For instance, after 1 min this represents a deviation of 19.2 %. The USP allows a tolerance of only \pm 2 % at the stated sampling time [150].

However, it is to consider that this regulation applies to conventional withdrawal of a specimen if one uses USP Apparatus 1 (Basket) or 2 (Paddle). Hence, the specimen is withdrawn in a single drawing operation with a syringe. In detail, this means that the timepoint of withdrawal corresponds to the current status of drug release. Conversely, using the CF system, the specimen is collected over a certain period, analogously to USP Apparatus 4 (Flow-Through Cell). In this context, the sampling period will include the timepoint of interest. Thus, provided that the dissolution process is linear within the respective range, the measured concentration of dissolved API will be that of the center of the period. Under these circumstances, the filtrate collection time may exceed the compendial tolerance.

Furthermore, it was observed during conduction of the dissolution tests that the filtration rate also depends on the individual properties of the used

dissolution medium. Hence, the usage of a surfactant decelerated the filtrate flow rate by factor two to three, depending on the concentration. This was compensated through individual adaption of start and end point of sampling.

Finally, it must be stated that the experimental value of the sampling points does not correspond to the respective value since the dead time has to be added. Though, this is the same difference for each dissolution test.

2.2.3.5 API quantification

As a less time-consuming alternative compared to HPLC, UV-Vis spectroscopy was applied to quantify celecoxib in the filtrate. For verification of the method specificity, spectra of methanolic solutions of celecoxib, Eudragit E 100 and Poloxamer 407 were taken over a wavelength range from 190 to 400 nm (data not shown). Poloxamer 407 did not show UV absorbance over the investigated range. A local absorbance maximum of celecoxib, which was not significantly affected by Eudragit E 100 absorbance, was found at 252 nm.

For determination of the linearity a methanolic solution of celecoxib (without additives) was prepared ($c = 1 \text{ mg/mL}$). This solution was respectively diluted to three different concentrations with the currently used dissolution medium. These concentrations covered the range resulting from the dissolution experiments. Then, a spectrum of the highest concentrated dilution was recorded to detect the respective absorbance maximum (248–255 nm). In every case calibration yielded a correlation of 0.999 or more. Thus, UV-Vis spectroscopy was considered to be appropriate for quantification of celecoxib in presence of Eudragit E 100 and Poloxamer 407. Additionally, this is in good agreement with literature [2].

To determine the celecoxib concentration of the tested nanosuspensions corresponding to 100 % API release, six aliquots of the suspension were dissolved in methanol. These mixtures were appropriately diluted with the respective dissolution medium for measurement. Thereafter, the dilutions were applied to analysis. In the results part the degree of dissolution is given

as percentage of this concentration considering the dilution factor of the suspension in the medium.

2.2.3.6 Statistical evaluation of dissolution profile equivalence

The statistical comparison of dissolution profiles of differently-sized celecoxib-Eudragit E 100-NPs and celecoxib (API) powder was performed under application of the model independent approach according to FDA “Guidance for Industry: Dissolution Testing of Immediate Release Solid Oral Dosage Forms” [153]. This approach implements the calculation of a difference factor f_1 and a similarity factor f_2 , while the respective results confirm or deny equivalence of two curves.

The difference factor (f_1) which is a measurement of the relative error between the two curves is calculated from equation (18),

$$f_1 = \left\{ \left[\sum_{t=1}^n |R_t - T_t| \right] / \left[\sum_{t=1}^n R_t \right] \right\} \cdot 100 \quad (18)$$

where n is the number of time points and R_t and T_t are the respective dissolution values of the two compared curve at time t . In this study, the points at 20, 40 and 60 s have been used for evaluation.

The similarity factor (f_2) is a measurement of the similarity in percentage dissolution between the two curves and is calculated from equation (19).

$$f_2 = 50 \cdot \left\{ \log \left[1 + (1/n) \sum_{t=1}^n (R_t - T_t)^2 \right]^{-0,5} \cdot 100 \right\} \quad (19)$$

Two dissolution profiles were considered to be equivalent if f_1 values were between 0–15 and f_2 values between 50–100.

3 Results

3.1 Nanoparticle preparation

3.1.1 Bench-top

3.1.1.1 Influence of type of co-stabilizer, solvent : non-solvent ratio and drug : polymer ratio

To optimize the bench-top preparation of celecoxib-Eudragit E 100-NPs, type of co-stabilizer, solvent : non-solvent ratio and drug : polymer ratio were varied and the effect on Z-Average, PDI, ZP and EE investigated.

There to, three different stabilizers (Poloxamer 407, PVA and SDS) were respectively dissolved to a concentration of 0.1 % (w/v) in the non-solvent phase. Furthermore, celecoxib : Eudragit E 100 ratios (w/w) of 1 : 1 and 1 : 2 and solvent : non-solvent ratios (v/v) of 1 : 2, 1 : 5 and 1 : 10 were examined.

Hence, stabilization with Poloxamer 407 resulted in NP diameters from approximately 270 to 370 nm with PDI values in the range from 0.1 to 0.2, a ZP from circa 45 to 60 mV and an EE between 62 and 90 %. At solvent : non-solvent ratios of 1 : 5 and 1 : 10 no agglomerates appeared, neither instantaneous nor after 24 h, while slight agglomeration occurred at the 1 : 2 ratio. These results are graphically depicted in Figure 26 and the data given in Table 19. Figure 27 shows the volume-weighted DLS size distribution report of the nanosuspension prepared with 1 : 5 solvent : non-solvent ratio and 1 : 2 celecoxib : Eudragit E 100 ratio.

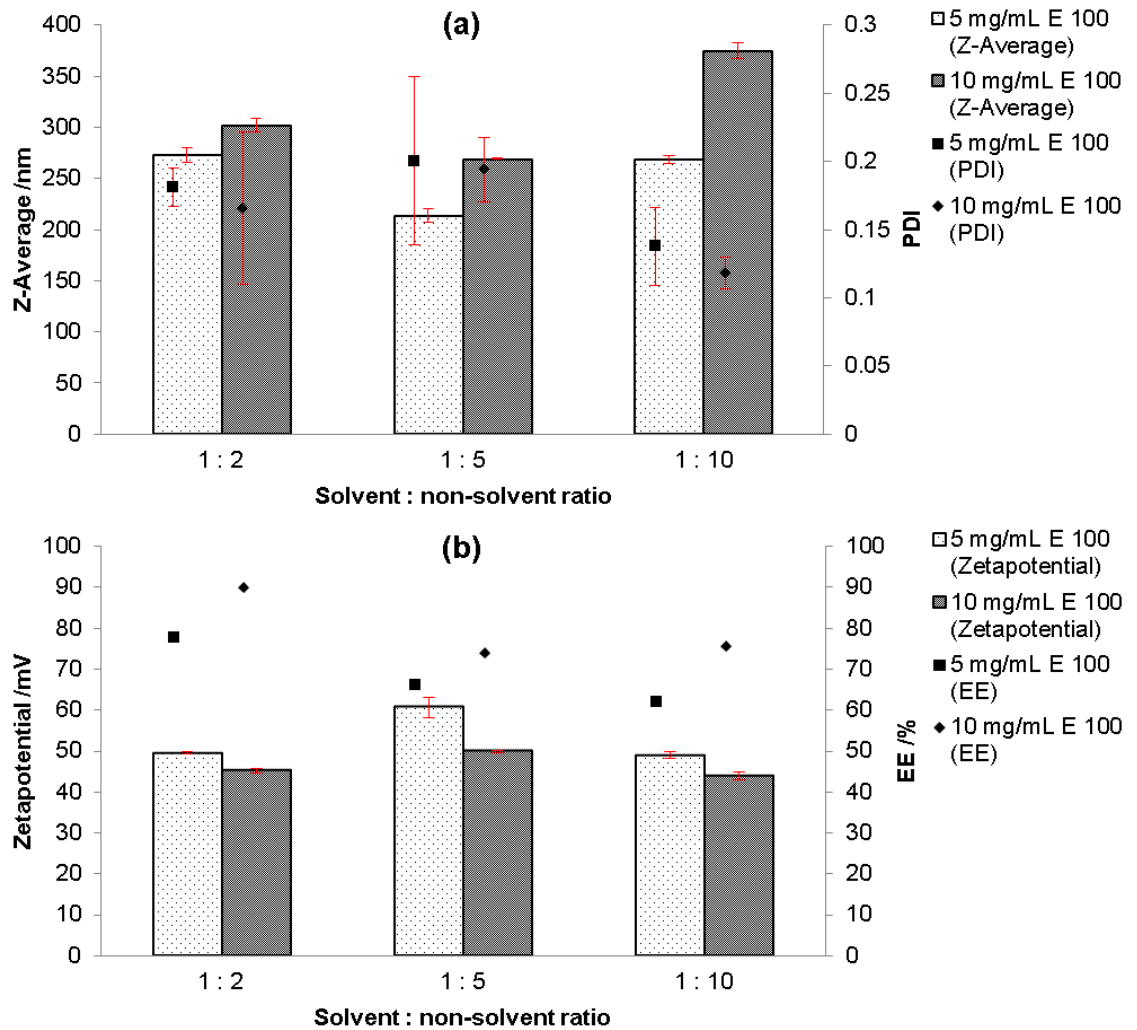


Figure 26: Bench-top preparation (emulsification-diffusion) of celecoxib-Eudragit E 100 – NPs with Poloxamer 407 as co-stabilizer, (a) Z-Average and PDI, (b) ZP and EE: Solvent phase: 5 mg/mL celecoxib and 5/10 mg/mL Eudragit E 100 in 1/2/5 mL of ethyl acetate, non-solvent phase: 1 mg/mL Poloxamer 407 in 10 mL of water, n=1, Z-Average, PDI and ZP values are mean of three measurements, EE values respectively single measurement, red lines represent SD.

	Size (d.nm):	% Volume:	St Dev (d.n...)
Z-Average (d.nm): 269.0	Peak 1: 332.8	100.0	145.4
Pdl: 0.169	Peak 2: 0.000	0.0	0.000
Intercept: 0.937	Peak 3: 0.000	0.0	0.000
Result quality : Good			

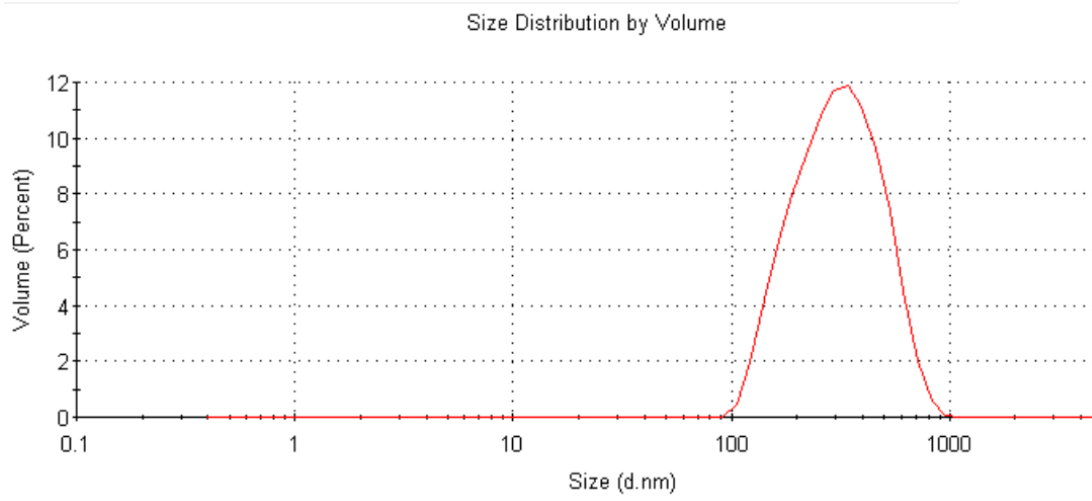


Figure 27: DLS size distribution report (volume-weighted) of celecoxib-Eudragit E 100 – NPs with Poloxamer 407 as co-stabilizer: Solvent phase: 5 mg/mL celecoxib and 10 mg/mL Eudragit E 100 in 2 mL of ethyl acetate, non-solvent phase: 1 mg/mL Poloxamer 407 in 10 mL of water; Preparation method: Bench-top (emulsification-diffusion).

Using SDS, particles between approximately 200 and 7200 nm diameter, PDI values between 0.03 and 0.67, a ZP from circa -10 to 50 mV and EEs from 55 to 90 % were obtained. In every sample of this setup agglomeration occurred directly after preparation. The particles prepared with a 1 : 2 solvent : non-solvent ratio completely agglomerated after 24 h storage at ambient temperature.

With PVA the particle diameter ranged from about 270 nm to large microparticles with PDI values between 0.5 and 1.0 and a ZP between -4 and 12 mV. The EE did not exceed 1 %. The suspensions exclusively contained agglomerates.

These results are listed in the appendix (SDS→ Table 20, PVA→ Table 21).

3.1.1.2 Influence of Poloxamer 407 (co-stabilizer) concentration

To elaborate the influence of Poloxamer 407, it was dissolved to different concentrations (0.1-10 mg/mL) in water as non-solvent phase, while the solvent phase was prepared according to the previously elaborated conditions (see chapter 3.1.1.1). The results of this experimental setup are listed in Table 22 and shown in Figure 28. Figure 29 shows the volume-weighted DLS size distribution report of one nanosuspension prepared with 2.5 mg/mL of Poloxamer 407 in non-solvent phase.

The resulting NP diameters decreased with increasing stabilizer concentration from more than 400 nm at 0.1 mg/mL to slightly more than 200 nm at 2.5 mg/mL which basically remained constant at higher concentrations. The PDI values were between 0.25 and 0.30 for 0.1 mg/mL and 0.5 mg/mL, at approximately 0.15 for 1 mg/mL and at 0.05 or slightly below at the higher concentrations. While the ZP values did not particularly differ from 0.1 mg/mL to 1 mg/mL (50 mV or slightly less), they decreased over circa 40 mV at 2.5 mg/mL to around 30 mV at 5 mg/mL and 10 mg/mL. The EE values decreased from 90 % to 50 % with increasing Poloxamer 407 concentration. Decreasing EE values were accompanied by increasing API concentrations in the supernatant. In every case white, turbid suspensions were yielded, while with 5 mg/mL and 10 mg/mL of Poloxamer 407 the color tended to slightly bluish. Using 0.1 mg/mL, 0.5 mg/mL or 1 mg/mL sediments appeared on the flask wall during evaporation.

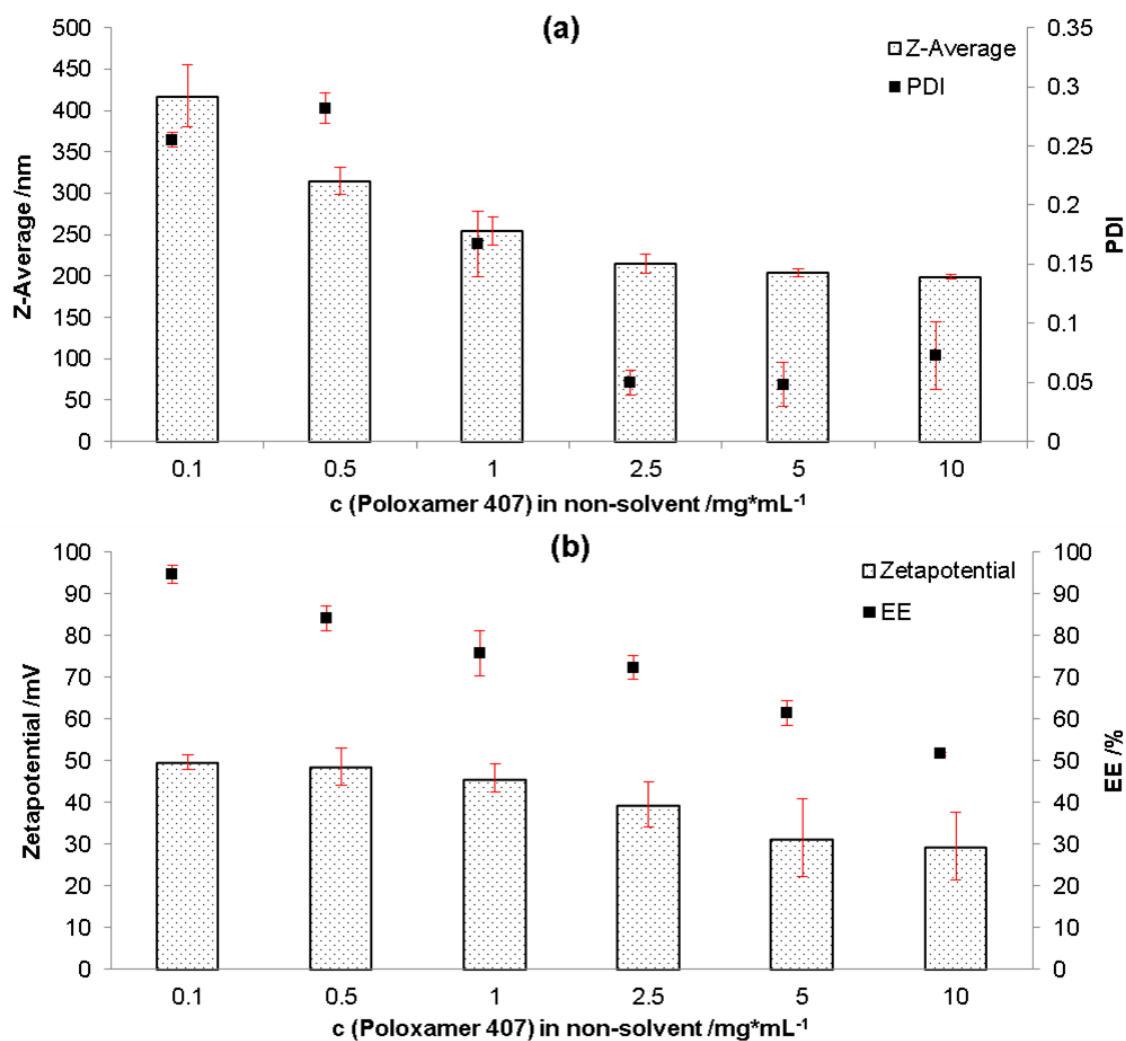


Figure 28: Bench-top preparation (emulsification-diffusion) of celecoxib Eudragit E 100 – NPs with varying amounts of Poloxamer 407, (a) Z-Average and PDI, (b) ZP and EE: Solvent phase: 5 mg/mL celecoxib and 10 mg/mL Eudragit E 100 in 2 mL of ethyl acetate, non-solvent phase: 0.1/0.5/1/2.5/5/10 mg/mL Poloxamer 407 in 10 mL of water, n=3, red lines represent SD.

	Size (d.nm):	% Volume:	St Dev (d.n...)
Z-Average (d.nm): 213.0	Peak 1: 218.2	100.0	53.44
Pdl: 0.007	Peak 2: 0.000	0.0	0.000
Intercept: 0.929	Peak 3: 0.000	0.0	0.000
Result quality : Good			

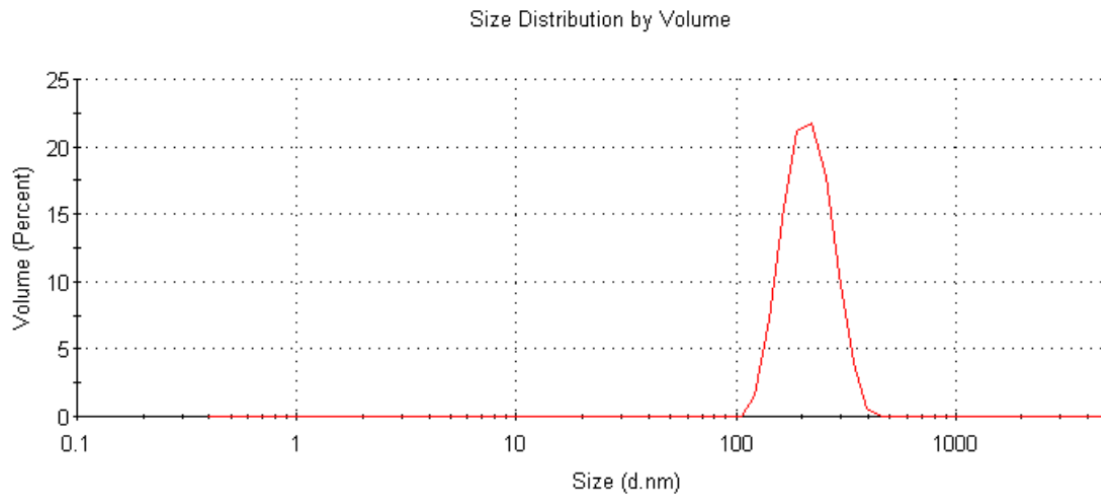


Figure 29: DLS size distribution report (volume-weighted) of celecoxib-Eudragit E 100 – NPs with Poloxamer 407 as co-stabilizer: Solvent phase: 5 mg/mL celecoxib and 10 mg/mL Eudragit E 100 in 2 mL of ethyl acetate, non-solvent phase: 2.5 mg/mL Poloxamer 407 in 10 mL of water; Preparation method: Bench-top (emulsification-diffusion).

3.1.1.3 Increase of celecoxib and excipients quantity

The celecoxib concentration in the solvent phase was increased from 5 mg/mL to 25, 50 and 100 mg/mL. Simultaneously the concentrations of Eudragit E 100 and Poloxamer 407 were increased to maintain the previously elaborated ratios. A celecoxib : Eudragit E 100 : Poloxamer 407 ratio of 1 : 2 : 0.025 was once employed to examine the influence of a very low co-stabilizer concentration at relatively high celecoxib amount. Then, the effect on NP size, PDI, ZP and EE was investigated. The results of these experiments are listed in Table 14. Both formulations produced with 100 mg celecoxib agglomerated already during the preparation process and solidified after 24 h storage at ambient conditions. With a Poloxamer 407 concentration of 2.5 mg/mL and 50 mg/mL the Z-Average was 810 ± 126 nm and 1002 ± 261 nm, the ZP 53 ± 1 mV and 34 ± 1 mV and the EE (HPLC) circa 97 % and 86 %, respectively. The PDI was 1 in both cases. The usage of 50 mg celecoxib likewise resulted in agglomeration, while the Z-Average was 579 ± 66 nm, the PDI was 1, the ZP 37 ± 1 mV and the EE (HPLC) approximately 80 %. With the lowest tested celecoxib concentration (25 mg/mL), the Z-average was around 350 nm, the PDI was slightly below 0.1, the ZP was circa 36 mV and the EE circa 85 %. Figure 30 shows a volume-weighted DLS size distribution report of this nanosuspension.

Table 14: Bench-top preparation (emulsification-diffusion) of celecoxib-Eudragit E 100 – NPs with Poloxamer 407 as co-stabilizer. Solvent phase: 25/50/100 mg/mL celecoxib and 50/100/200 mg/mL Eudragit E 100 in 2 mL ethyl acetate, non-solvent phase: 2.5/12.5/25/50 mg/mL Poloxamer 407 in 10 mL of water, 3 x 30 s homogenization at 30000 rpm, removal of ethyl acetate in rotary evaporator (5 min at 40 °C, 220 mbar and 280 rpm followed by 10 min at 40 °C, 180 mbar, and 280 rpm), n=3 (25 mg/mL celecoxib, 50 mg/mL Eudragit E 100 and 12.5 mg/mL Poloxamer 407) and n=1 (other formulations), n=1: Z-Average, PDI and ZP values are mean of three measurements \pm SD, EE values respectively single measurement, n=3: values are mean \pm SD.

c(celecoxib) ; c(Eudragit E 100) /mg*mL ⁻¹	c (Poloxamer 407) /mg*mL ⁻¹	Visual inspection	Z-Average /nm	PDI	ZP /mV	EE /%
25 ; 50	12.5	a	352 \pm 6	0.09 \pm 0	36 \pm 0.3	85.3 \pm 2.6
50 ; 100	25	b	579 \pm 66	1	37 \pm 1	79.5
100 ; 200	50	c	1002 \pm 261	1	34 \pm 1	85.7
100 ; 200	2.5	d	810 \pm 126	1	53 \pm 1	97.2

a: white, turbid liquid

b: slight agglomeration on the flask wall, white, turbid liquid

c: agglomeration on the flask wall, white, turbid liquid, sample entirely agglomerated after 24 h

d: strong agglomeration on the flask wall, white, turbid liquid, sample entirely agglomerated after 24 h

	Size (d.nm):	% Volume:	St Dev (d.n...)
Z-Average (d.nm): 351.7	Peak 1: 380.7	100.0	87.32
Pdl: 0.016	Peak 2: 0.000	0.0	0.000
Intercept: 0.883	Peak 3: 0.000	0.0	0.000
Result quality : Good			

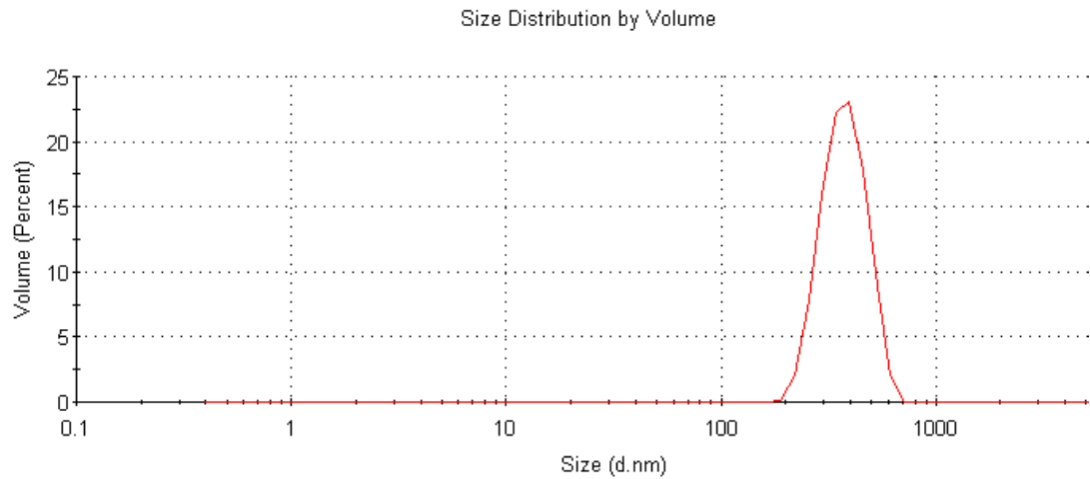


Figure 30: DLS size distribution report (volume-weighted) of celecoxib-Eudragit E 100 – NPs with Poloxamer 407 as co-stabilizer: Solvent phase: 25 mg/mL celecoxib and 50 mg/mL Eudragit E 100 in 2 mL of ethyl acetate, non-solvent phase: 12.5 mg/mL Poloxamer 407 in 10 mL of water; Preparation method: Bench-top (emulsification-diffusion).

3.1.1.4 Stability study

To choose an appropriate formulation as template for optimization with MJR technology the stability of the formulations containing 5 mg/mL (see chapter 3.1.1.2) and 25 mg/mL (see chapter 3.1.1.3) celecoxib was investigated over 28 d. Thereto, each formulation was prepared in triplicate and respectively split into two parts to be stored at ambient temperature and at 5 ± 2 °C. NP size, PDI, ZP and EE were determined on the day of preparation and after 1, 2, 3, 4, 7 and 14 d storage. After 28 d all samples had been crystallized (sharp needles on the container interior wall, clear liquid). Figure 31 shows photographs of the formulations after preparation (a), 7 d ((b) and (c)) and 28 d ((d), (e) and (f)). The results are listed in Table 23 (5 mg/mL celecoxib, storage at ambient temperature), Table 24 (5 mg/mL celecoxib, storage at 5 °C), Table 25 (25 mg/mL celecoxib, storage at ambient temperature) and Table 26 (25 mg/mL celecoxib, storage at 5 °C). The results are graphically displayed in Figure 32 (Z-Average and PDI), Figure 33 (ZP) and Figure 34 (EE). The results of the statistical evaluation (t-tests for comparison of Z-Average, PDI, ZP and EE: storage at room temperature versus storage at 5 °C and usage of 5 mg/mL versus 25 mg/mL celecoxib in solvent phase) are stated in Table 27.

On the basis of a 95 % confidence interval the storage temperature (first comparison) had no significant influence on the examined parameters. Concerning the second comparison (between the two formulations) both Z-Average and EE showed a significant difference if considering a storage period of 14 d. Hence there also was a difference in PDI for those samples being stored at room temperature.

The Z-Average after preparation was about 220 nm for the formulation with low and about 290 nm for the formulation with high celecoxib content. From days three to seven the Z-Average values increased while they were constant for the formulation with high celecoxib content, which was stored at ambient temperature.

The PDI was overall approximately 0.1 at the beginning and was likewise constant for the formulation with high celecoxib content, which was stored at ambient temperature. If this formulation was stored at 5 °C it increased to

about 0.37 after 4 d. With low celecoxib content it changed to 0.15–0.16 after 2 d of storage and further increased thereafter regardless of the storage conditions.

The ZP values were initially 39 ± 1 mV in every case. With low celecoxib content they continuously increased over the storage period to about 56 mV (RT) respectively 52 mV (5 °C). With high celecoxib content values reached approximately 45 mV.

The EE values varied between circa 70 % and 80 % (formulations with low celecoxib content) and between 80 % and 90 % (formulations with high celecoxib content) without a trend. Thus, this parameter is obviously not stability-related.

Figure 35 shows volume-weighted DLS size distribution reports of one nanosuspension prepared with the higher celecoxib concentration immediately after preparation and after 14 d of storage (RT).

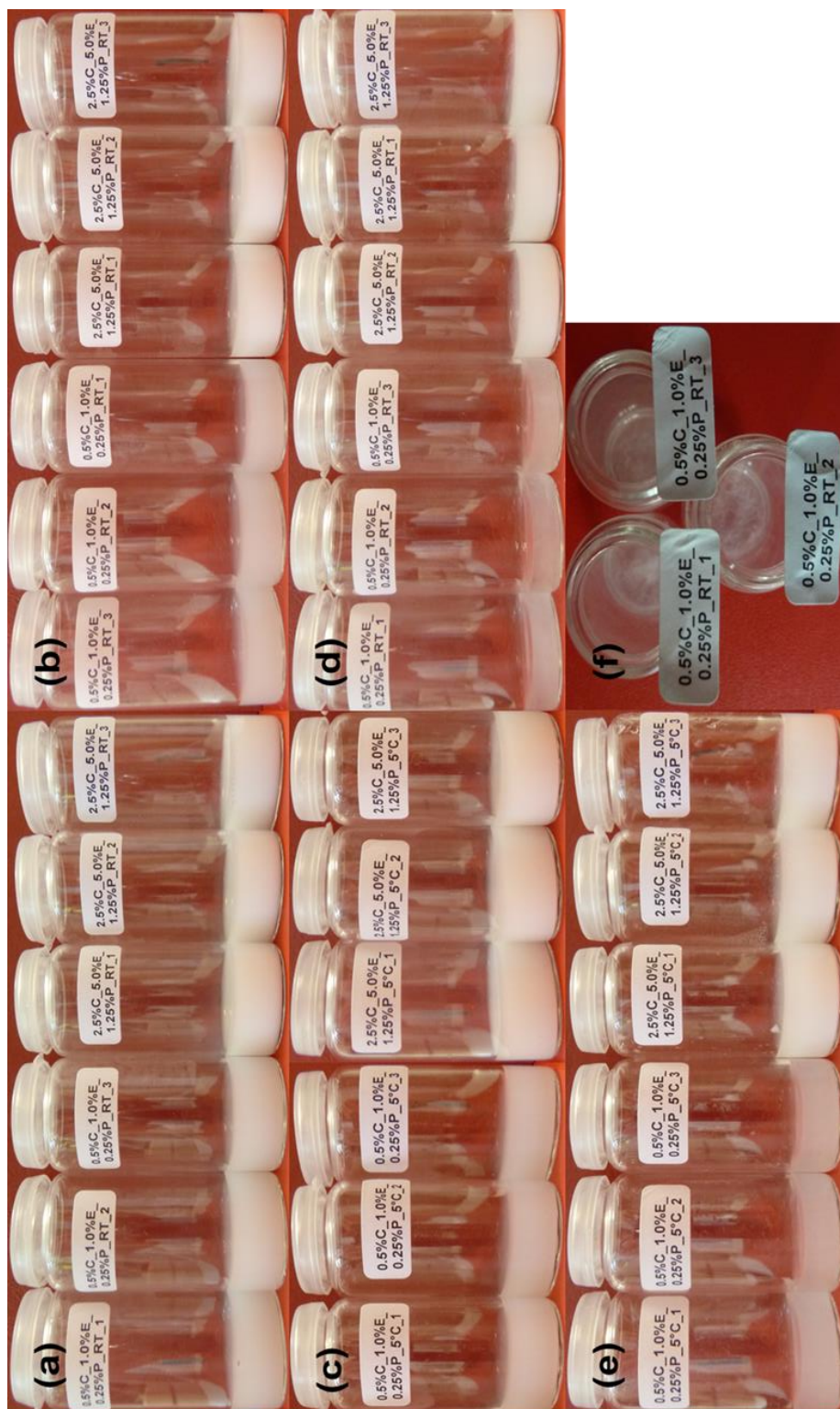


Figure 31: Photographs of celecoxib-Eudragit E 100-NPs stabilized with Poloxamer 407, after preparation (a), 7 d at ambient temperature (b), 7 d at 5 °C (c), 28 d at ambient temperature (d), 28 d at 5 °C (e) and 28 d at 5 °C (top view) (f): C = celecoxib, E = Eudragit E 100, P = Poloxamer 407, RT = room/ambient temperature.

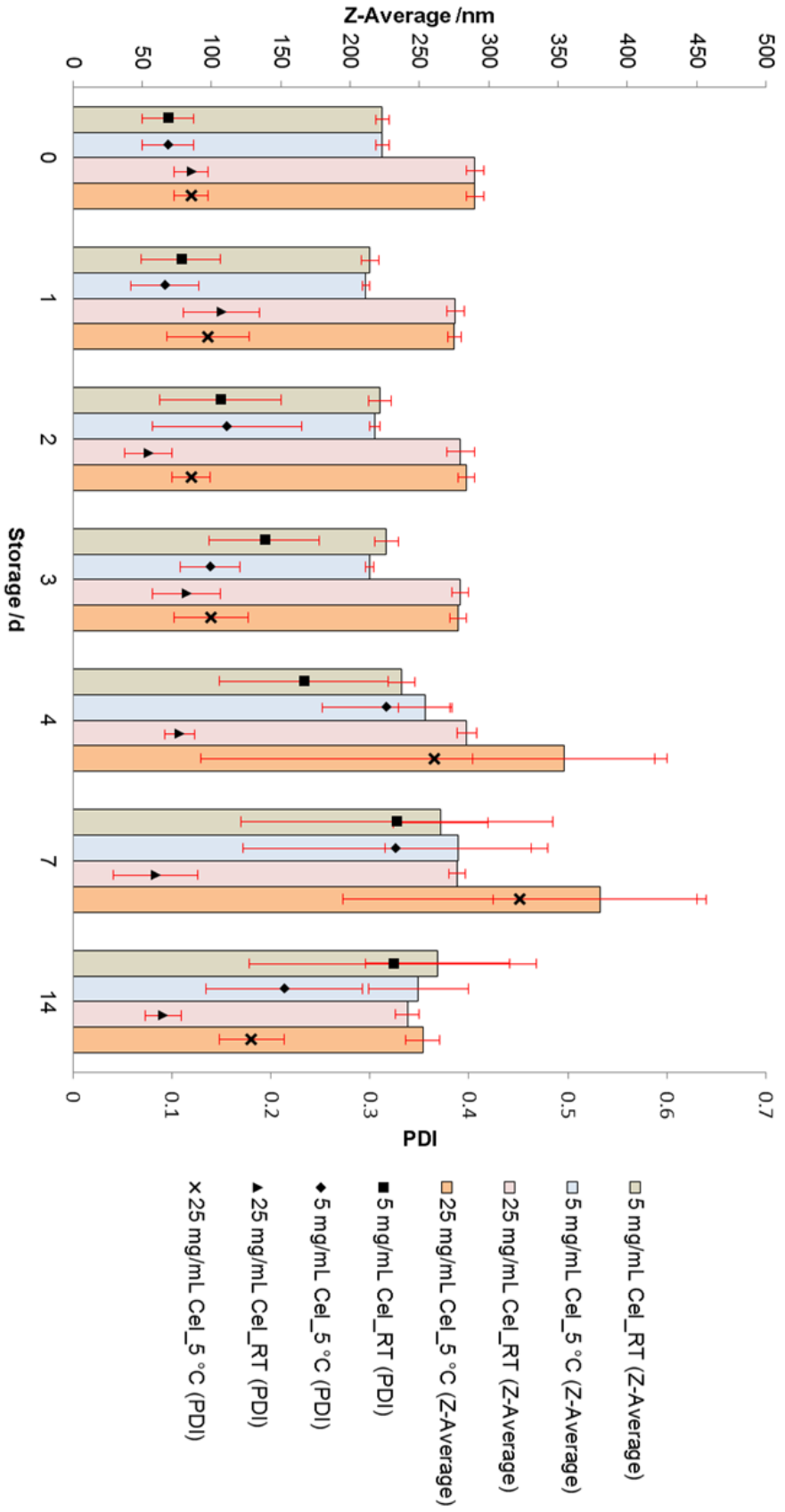


Figure 32: Stability study of celecoxib-Eudragit E 100 – NPs stabilized with Poloxamer 407 (Z-Average and PDI): Solvent phase: 5/25 mg/mL celecoxib and 10/50 mg/mL Eudragit E 100 in 2 mL ethyl acetate, non-solvent phase: 2.5/12.5 mg/mL Poloxamer 407 in 10 mL water, respectively stored at room temperature (RT) and at 5 °C, n=3, values are mean of three measurements, red lines represent SD.

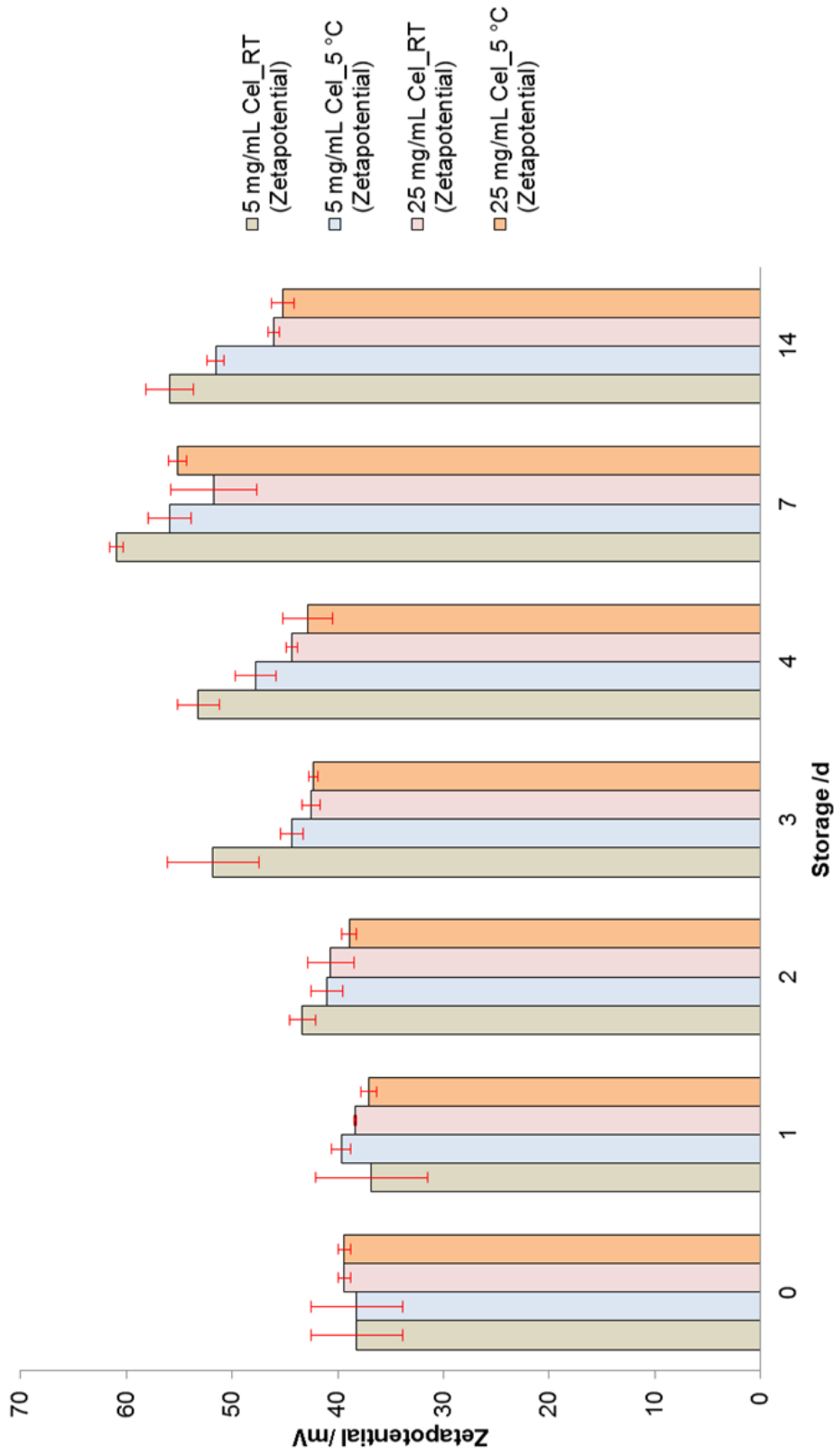


Figure 33: Stability study of celecoxib-Eudragit E 100 – NPs stabilized with Poloxamer 407 (ZP): Solvent phase: 5/25 mg/mL celecoxib and 10/50 mg/mL Eudragit E 100 in 2 mL ethyl acetate, non-solvent phase: 2.5/12.5 mg/mL Poloxamer 407 in 10 mL water, respectively stored at room temperature (RT) and at 5 °C, n=3, values are mean of three measurements, red lines represent SD.

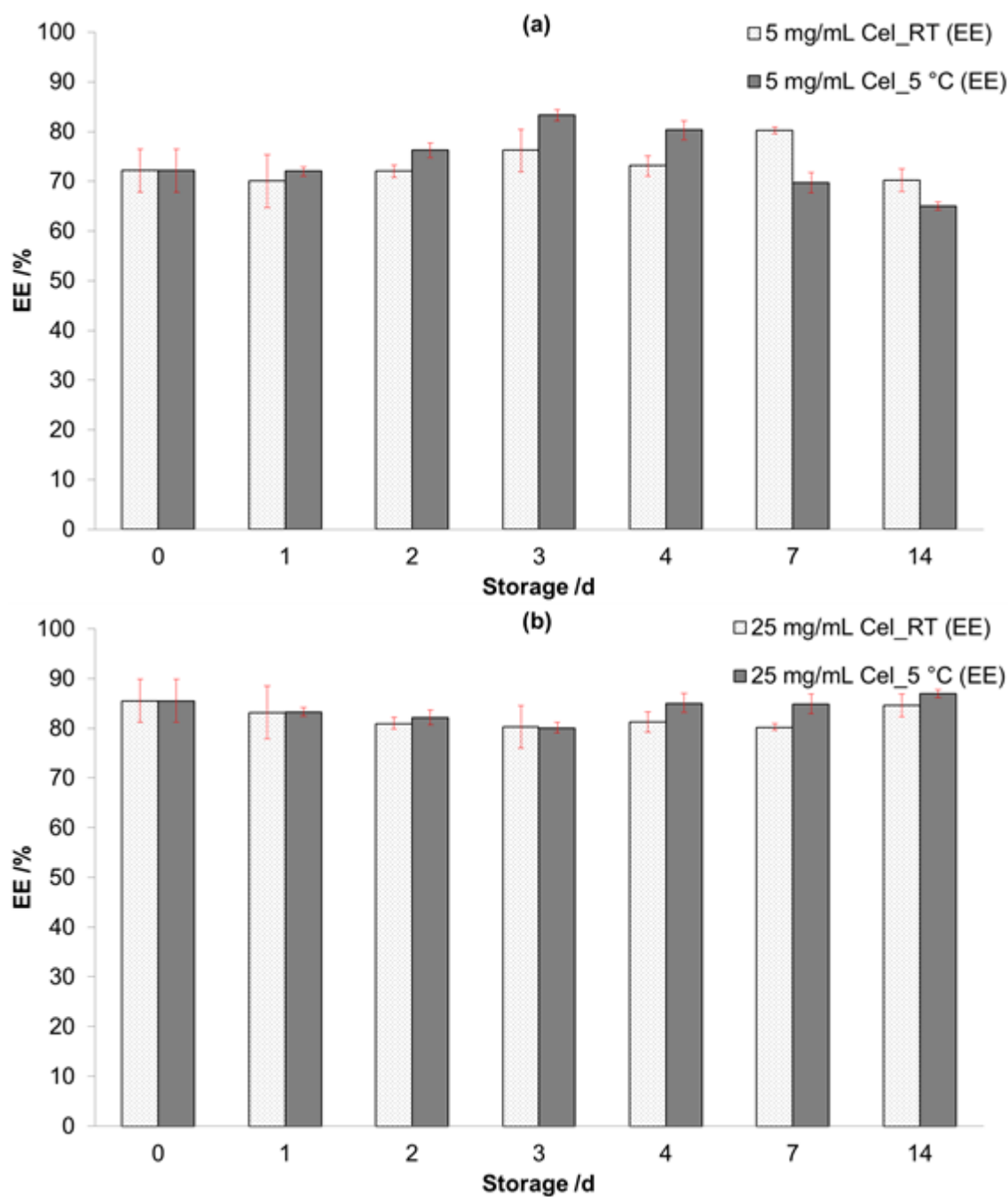
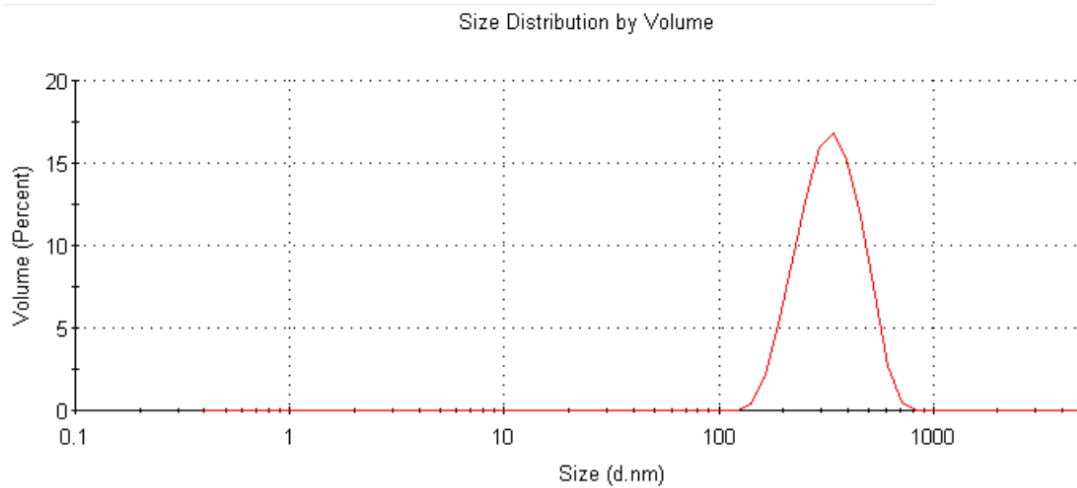


Figure 34: Stability study of celecoxib-Eudragit E 100 – NPs stabilized with Poloxamer 407 (EE), (a) 5 mg/mL celecoxib and (b) 25 mg/mL celecoxib: Solvent phase: 5/25 mg/mL celecoxib and 10/50 mg/mL Eudragit E 100 in 2 mL ethyl acetate, non-solvent phase: 2.5/12.5 mg/mL Poloxamer 407 in 10 mL water, respectively stored at room temperature (RT) and at 5 °C, n=3, single measurements, red lines represent SD.

	Size (d.nm):	% Volume:	St Dev (d.n...	
Z-Average (d.nm): 297.1	Peak 1: 343.9	100.0	109.5	(a)
Pdl: 0.093	Peak 2: 0.000	0.0	0.000	
Intercept: 0.941	Peak 3: 0.000	0.0	0.000	
Result quality : Good				



	Size (d.nm):	% Volume:	St Dev (d.n...	
Z-Average (d.nm): 250.0	Peak 1: 260.7	100.0	61.43	(b)
Pdl: 0.029	Peak 2: 0.000	0.0	0.000	
Intercept: 0.930	Peak 3: 0.000	0.0	0.000	
Result quality : Good				

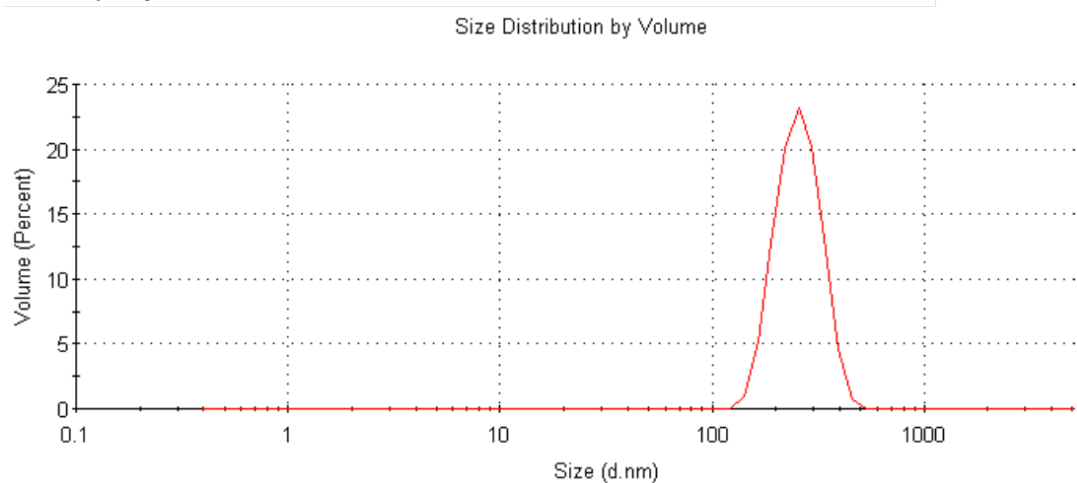


Figure 35: DLS size distribution reports (volume-weighted) of celecoxib-Eudragit E 100 – NPs with Poloxamer 407 as co-stabilizer: Solvent phase: 25 mg/mL celecoxib and 50 mg/mL Eudragit E 100 in 2 mL of ethyl acetate, non-solvent phase: 12.5 mg/mL Poloxamer 407 in 10 mL of water; immediately after preparation (day 0) (a) and after two weeks storage at ambient temperature (day 14) (b); Preparation method: Bench-top (emulsification-diffusion).

3.1.2 MicroJetReactor

3.1.2.1 Emulsification-diffusion

Since stable NPs of narrow size distribution should be prepared in three different sizes the MJR technology was applied (see chapter 2.2.1.2) based on the elaborated formulation made with 25 mg/mL celecoxib and 50 mg/mL Eudragit E 100 (see Table 28). To reduce the experimental effort DoE was used. As independent variables temperature, nitrogen pressure and pump rotational speed were chosen. Thereby, the effect on the Z-Average (dependent variable) was investigated. According to findings from pre-experiments (data not shown) the temperature was varied between 40 and 60 °C, the nitrogen pressure between 0 and 0.50 bar and the pump rotational speed between 300 : 1500 and 1200 : 6000 rpm. In this way, NPs of Z-Averages between 260 and 750 nm and of PDI values between 0.06 and 1 were yielded. The experimental setup and the corresponding results are summarized in Table 28.

For the evaluation a response surface reduced quadratic model was chosen. This model is significant due to a p-value of the fit function < 0.0001 and a Model F-value of 65.80 (Program conclusion: "There is only a 0.01% chance that a "Model F-Value" this large could occur due to noise...Values of "Prob > F" [p-values] less than 0.0500 indicate model terms are significant. Values greater than 0.1000 indicate the model terms are not significant."). The R-squared value is 0.9869. The design cube is shown in Figure 36. The model is represented by equation (20) where *A* represents the operation temperature, *B* the nitrogen pressure and *C* the rotational speed of the pump, which carries the solvent.

$$\begin{aligned}
 \text{Z-Average} = & \\
 & 310.475 + (17.35 * A) - (22.575*B) - (57.5*C) - \\
 & (91.025*AC)+(158.125*BC) - (52.725*A^2)+ \\
 & (48.725*B^2)+(130.875*C^2)
 \end{aligned}
 \tag{20}$$

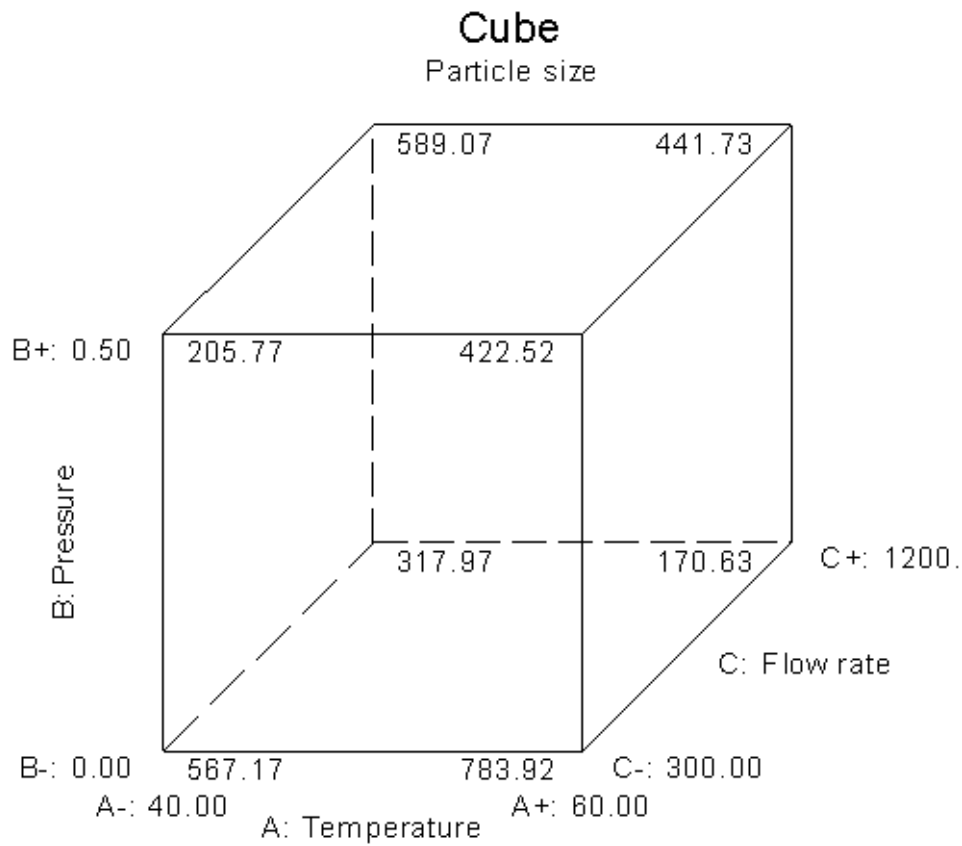


Figure 36: Design cube (particle size) of the DoE model. Values at the cube edges represent the Z-Average in nm (dependent variable). The x-axis (A) represents the temperature (in °C), the y-axis (C) the flow rate (expressed as pump rotational speed in rpm) and the z-axis (B) the nitrogen pressure (in bar).

For the validation of the previously obtained DoE model solutions of equation (20) were calculated for four different Z-Average values (300, 350, 400 and 450 nm). In addition to the Z-Average, PDI, ZP and EE were measured (results stated in Table 29). The PDI values ranged from 0.08 to 0.22, the ZP values were circa 45 ± 3 mV and the EE ranged from 81–91 %. The Z-Average values corresponded to the predicted values with deviations of less than 10 % except of one formulation (59.0 °C_0.36 bar_350 : 1750 rpm) whose Z-Average differed 12.4 % from the predicted result. The actual Z-Average values are plotted against the predicted values in Figure 37. Hence, the R-squared value is 0.8792. Figure 38 shows the volume-weighted DLS size distribution report of one nanosuspension with a predicted value of 350 nm.

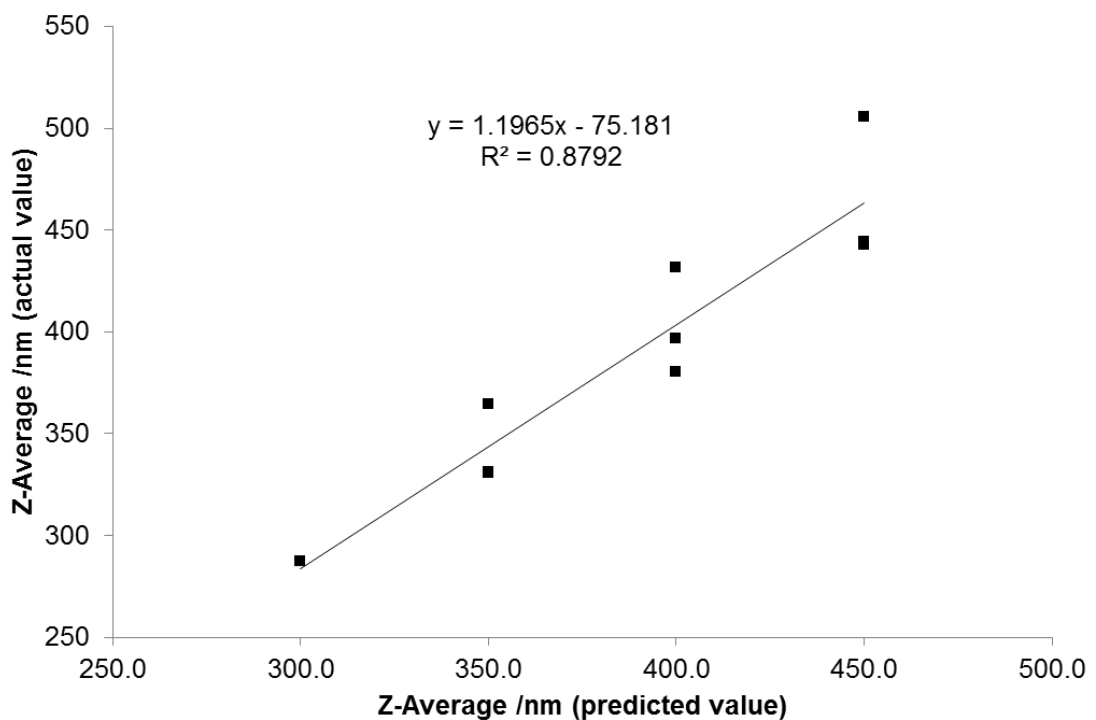


Figure 37: Design of experiments – validation: Actual Z-Average values of ten approaches in three sizes (300, 350, 400 and 450 nm) plotted against predicted values obtained from DoE equation.

	Size (d.nm):	% Volume:	St Dev (d.n...)
Z-Average (d.nm): 332.7	Peak 1: 363.9	100.0	87.59
Pdl: 0.038	Peak 2: 0.000	0.0	0.000
Intercept: 0.891	Peak 3: 0.000	0.0	0.000

Result quality : Good

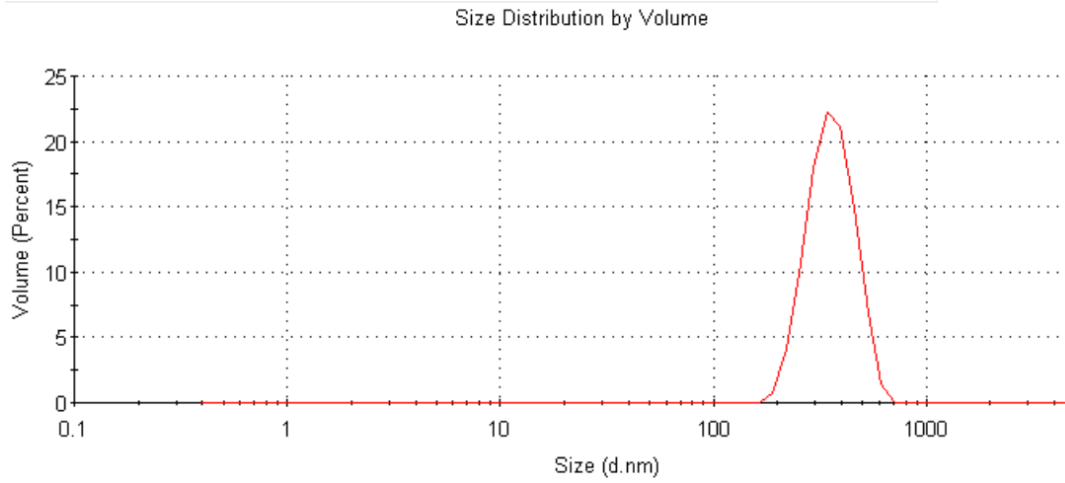


Figure 38: DLS size distribution report (volume-weighted) of celecoxib-Eudragit E 100 – NPs stabilized with Poloxamer 407, prepared with MJR (emulsification-diffusion): Solvent phase: 25 mg/mL celecoxib and 50 mg/mL Eudragit E 100 in ethyl acetate, non-solvent phase: 12.5 mg/mL Poloxamer 407 in water, operation temperature: 58.4 °C, nitrogen pressure: 0.40 bar, pump rotational speed (solvent phase : non-solvent phase) 510 : 2550 rpm; predicted Z-Average: 350 nm.

3.1.2.2 Nanoprecipitation

As an alternative to the emulsification-diffusion method nanoprecipitation was applied for the preparation of NPs. Thereto, methanol was employed as solvent instead of ethyl acetate while the NP composition and preparation were analogous to emulsification-diffusion. Concerning the MJR parameters the nitrogen pressure was varied between 0 and 0.50 bar and the pump rotational speed between 300 : 1500 and 1200 : 6000 rpm as previously (see chapter 3.1.2.1). Contrary to emulsification-diffusion the temperature was set to 30 or 50 °C since the boiling point of methanol (65 °C) is lower than that of ethyl acetate (77 °C). The results are stated in Table 15. The Z-Average values were mainly in a range between 300 and 500 nm at a PDI from 0.1 to 0.5 except of one setting (run 5) which led to strong agglomeration directly after preparation (Z-Average: ~ 960 nm, PDI: ~ 1). The ZP values were 36 ± 3 mV throughout all settings. The EE was consistently higher if the pump rotational speed was 300 : 1500 (~ 83–95 %), while using the ratio of 1200 : 6000 smaller values were obtained (~ 57–70 %) except of one setting (run 3: ~ 83 %). Figure 39 shows the volume-weighted DLS size distribution report of one of the prepared nanosuspensions.

Table 15: MJR preparation of celecoxib-Eudragit E 100-NPs stabilized with Poloxamer 407, nanoprecipitation technique: Solvent phase: 25 mg/mL celecoxib and 50 mg/mL Eudragit E 100 in methanol, non-solvent phase: 12.5 mg/mL Poloxamer 407 in water, operation temperature: 40 and 60 °C, nitrogen pressure: 0 and 0.5 bar, pump rotational speed (solvent phase : non-solvent phase) 300 : 1500 rpm and 1200 : 6000 rpm, n=1, Z-Average, PDI and ZP values are mean of three measurements \pm SD, EE values respectively single measurement.

Run	Temperature /°C	Nitrogen pressure /bar	Pump rotational speed /rpm	Z-Average /nm	PDI	ZP /mV	EE /%
1	30.0	0.50	300 : 1500	416.9 \pm 5.3	0.136 \pm 0.070	34.5 \pm 0.7	94.9
2	50.0	0.50	300 : 1500	517.7 \pm 35.8	0.178 \pm 0.155	35.3 \pm 0.252	85.7
3	30.0	0.50	1200 : 6000	384.7 \pm 17.0	0.441 \pm 0.026	33.3 \pm 1.4	83.1
4	50.0	0.50	1200 : 6000	313.7 \pm 11.5	0.339 \pm 0.084	38.2 \pm 0.7	56.9
5	30.0	0	300 : 1500	964.2 \pm 180.8	0.993 \pm 0.012	34.5 \pm 0.6	87.1
6	50.0	0	300 : 1500	335.4 \pm 9.3	0.482 \pm 0.076	37.2 \pm 0.7	83.4
7	30.0	0	1200 : 6000	313.7 \pm 10.3	0.362 \pm 0.059	34.7 \pm 0.6	70.3
8	50.0	0	1200 : 6000	321.9 \pm 7.9	0.253 \pm 0.036	40.7 \pm 0.6	64.1

	Size (d.nm):	% Volume:	St Dev (d.n...)
Z-Average (d.nm): 325.0	Peak 1: 348.5	100.0	107.1
Pdl: 0.251	Peak 2: 0.000	0.0	0.000
Intercept: 0.938	Peak 3: 0.000	0.0	0.000

Result quality : Good

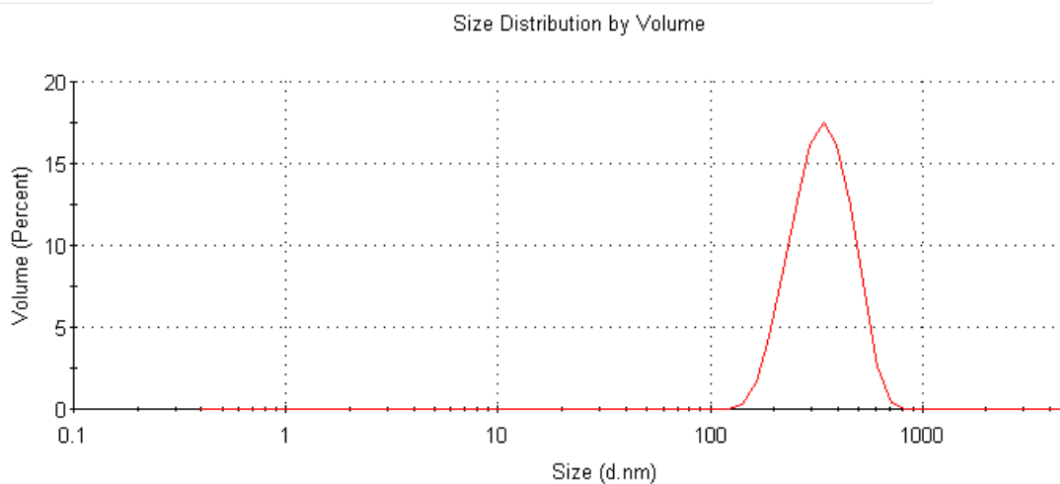


Figure 39: DLS size distribution report (volume-weighted) of celecoxib-Eudragit E 100 – NPs stabilized with Poloxamer 407, prepared with MJR (nanoprecipitation): Solvent phase: 25 mg/mL celecoxib and 50 mg/mL Eudragit E 100 in methanol, non-solvent phase: 12.5 mg/mL Poloxamer 407 in water, operation temperature: 50.0 °C, without nitrogen, pump rotational speed (solvent phase : non-solvent phase) 1200 : 6000 rpm.

3.2 Nanoparticle characterization

3.2.1 Differential scanning calorimetry

To elucidate the structure of the prepared NPs DSC measurements were performed. Figure 40 shows DSC traces of celecoxib, Eudragit E 100, a physical 1:2 mixture of celecoxib and Eudragit E 100 as well as celecoxib-Eudragit E 100-NPs prepared by emulsification-diffusion and nanoprecipitation technique.

The glass transition (T_g) of Eudragit E 100 was detected at circa 45 °C (inflection point of the decline of the Eudragit E 100 trace between 33 °C and 58 °C) followed by a negative peak indicating enthalpy relaxation at 60 °C. The celecoxib melting point (T_m) was at approximately 164 °C. In the physical mixture the Eudragit E glass transition was shifted to circa 42 °C, while the melting peak of celecoxib was bimodal with minima at 154 °C and 158 °C. The NPs, which were prepared with the emulsification-diffusion technique, showed a glass transition at 37 °C, while further distinct signals were missing. Concerning the comparison of the two NP preparation methods (nanoprecipitation and emulsification-diffusion) there was no difference in the glass transition. However, the NPs, which were prepared by nanoprecipitation, exhibited an additional broad signal from 96 °C to 160 °C, which was attributed to a melting process.

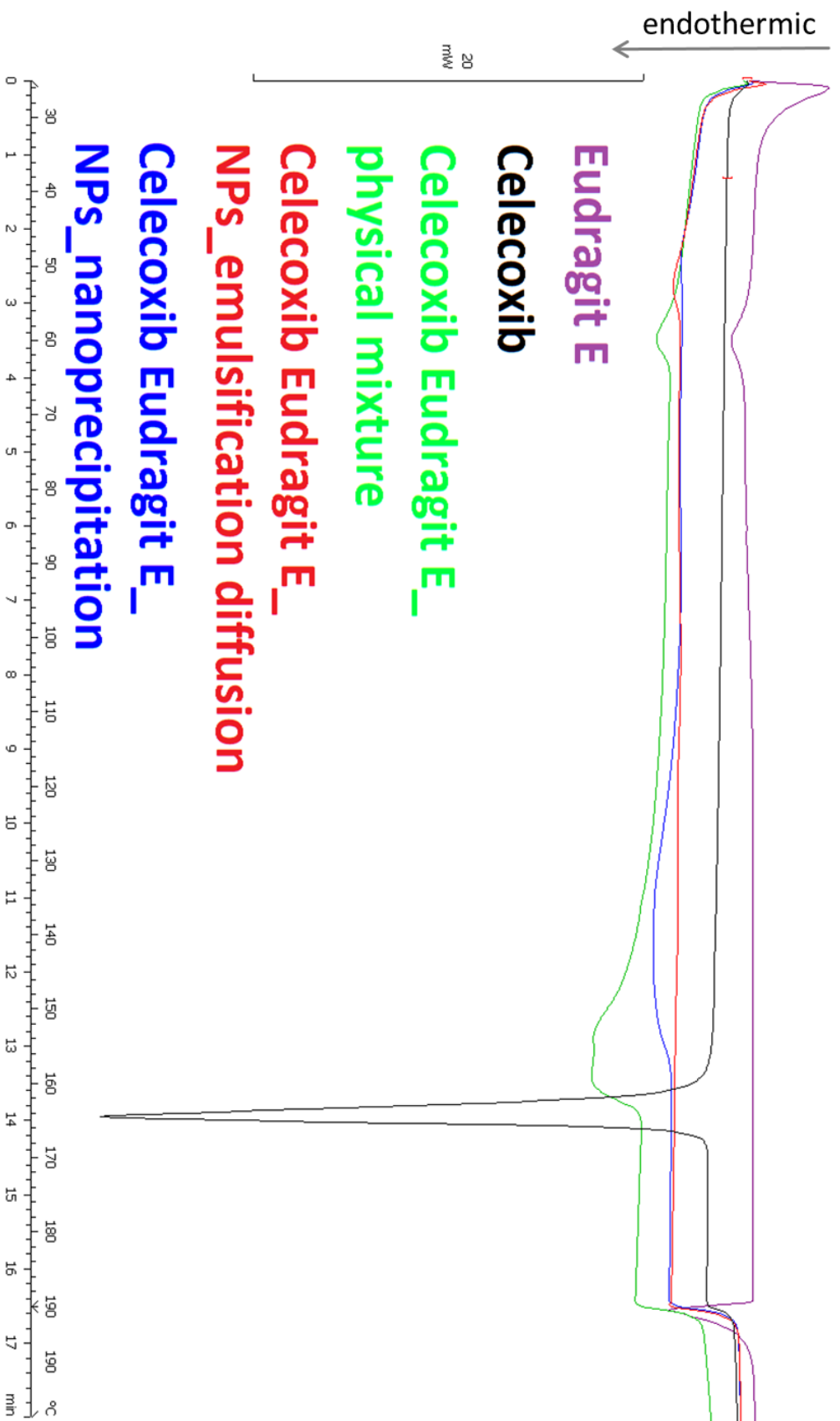


Figure 40: DSC traces of Eudragit E 100, celecoxib, a physical mixture of celecoxib and Eudragit E 100 as well as of celecoxib-Eudragit E 100-NPs prepared by MJR (emulsification-diffusion and nanoprecipitation technique).

3.2.2 Infrared spectroscopy

In order to examine chemical interactions between celecoxib and Eudragit E 100 in the NPs, IR spectra of these substances, their ionized forms (celecoxib sodium and protonated Eudragit E 100), physical 1:2 mixtures of both non-ionized and ionized forms, as well as of celecoxib-Eudragit E 100-NPs prepared by emulsification-diffusion and nanoprecipitation technique were taken.

The celecoxib spectrum (see Figure 41) inter alia exhibited doublet N–H stretching signals at approximately 3300 cm^{-1} , aromatic C–H bands slightly above 3000 cm^{-1} , C=C signals between 1400 and 1600 cm^{-1} , SO_2 band at circa 1350 cm^{-1} , multiple vibrations around 1100 cm^{-1} , due to CF_3 group and out-of-plane vibrations below 1000 cm^{-1} . In the spectrum of celecoxib sodium distinct signals disappeared except of a broad band at circa 1400 cm^{-1} and a band between 800 and 900 cm^{-1} [34].

The Eudragit E 100 (see Figure 42) spectrum mainly contained two N– CH_3 stretching bands at 3200 and 3300 cm^{-1} , a C–H stretching band at 3000 cm^{-1} , C=O vibration at approximately 1700 cm^{-1} , N– CH_3 vibration at 1500 cm^{-1} , two C–N vibrations between 1200 and 1300 cm^{-1} and ester band at 1150 cm^{-1} . At the protonated form of Eudragit E 100 the signals which are attributed to nitrogen bonds changed in the sense that doublet signals merged into one [34].

Concerning the comparison of the NP samples to the physical mixtures (see Figure 43) it can be stated that NPs prepared by emulsification-diffusion resemble more the signal pattern of the mixture of ionized substances. For instance, the N–H/N– CH_3 stretching bands at 3200 and 3300 cm^{-1} lack completely in both spectra and N–H/N– CH_3 vibrations at circa 1500 cm^{-1} are not clearly distinguished. In contrast, the patterns from NPs prepared by nanoprecipitation are similar to the mixture of non-ionized substances.

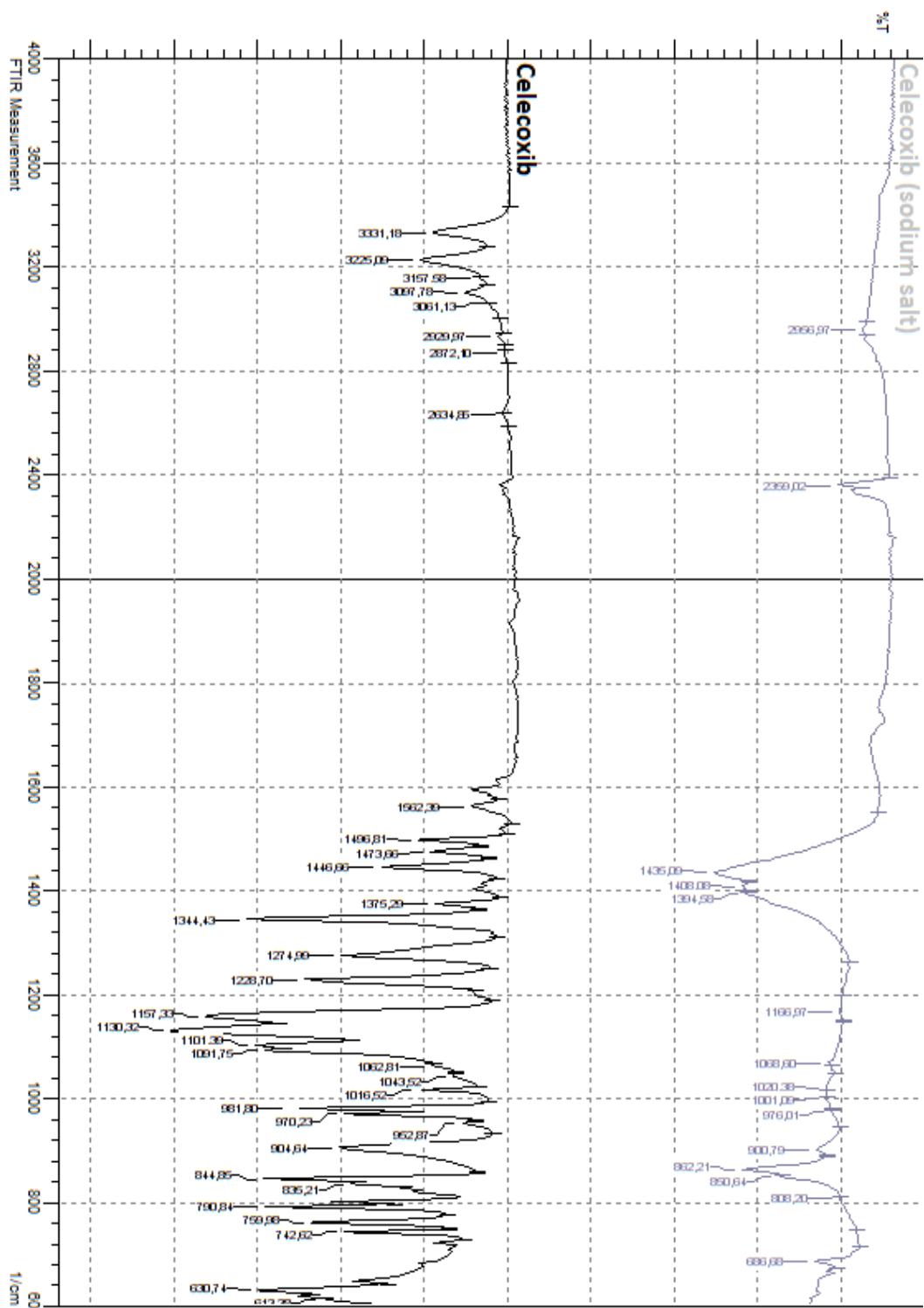


Figure 41 : FTIR spectra of celecoxib sodium salt (charged) and celecoxib (non-charged).

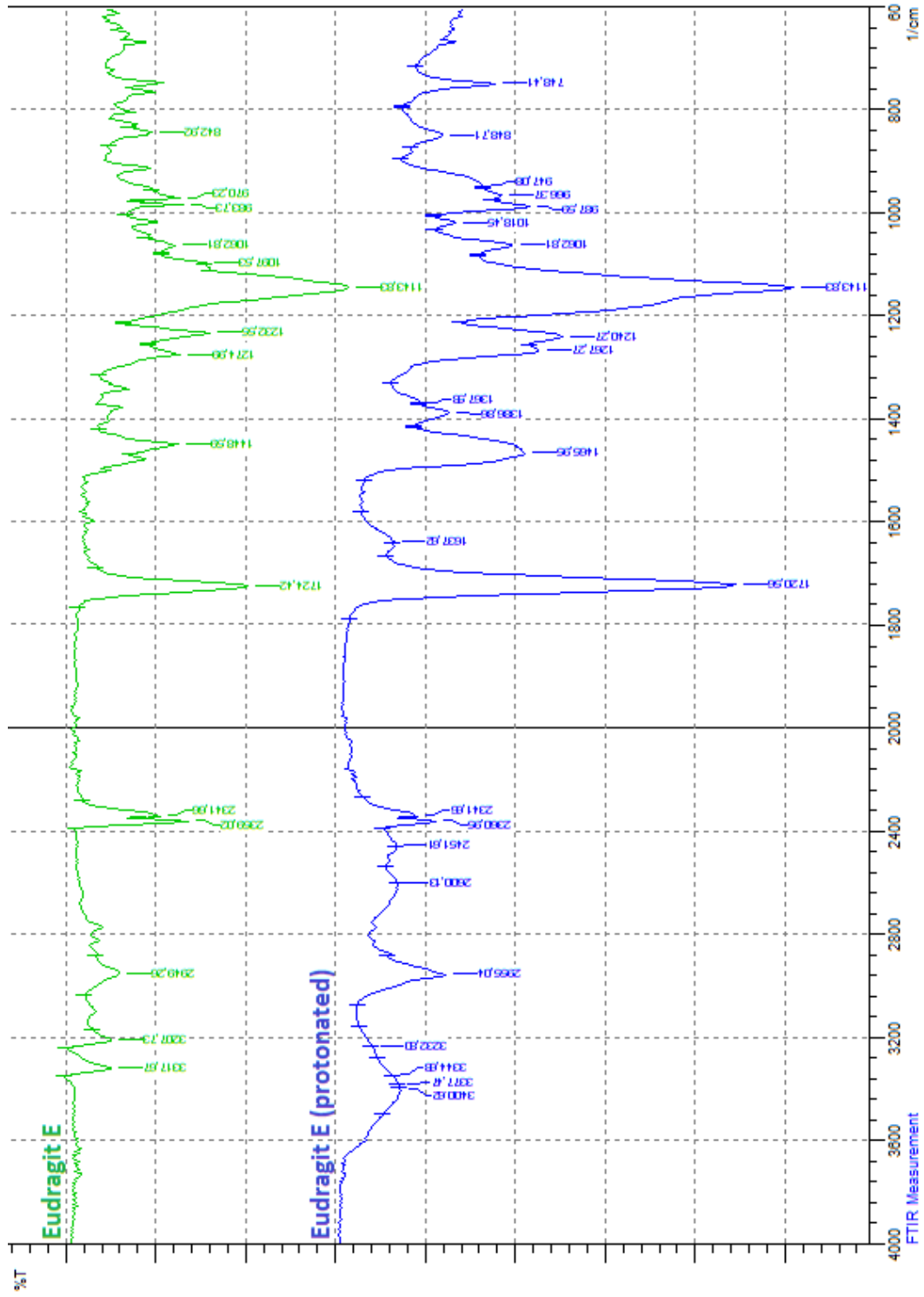


Figure 42: FTIR spectra of Eudragit E 100 (non-charged) and protonated Eudragit E (charged).

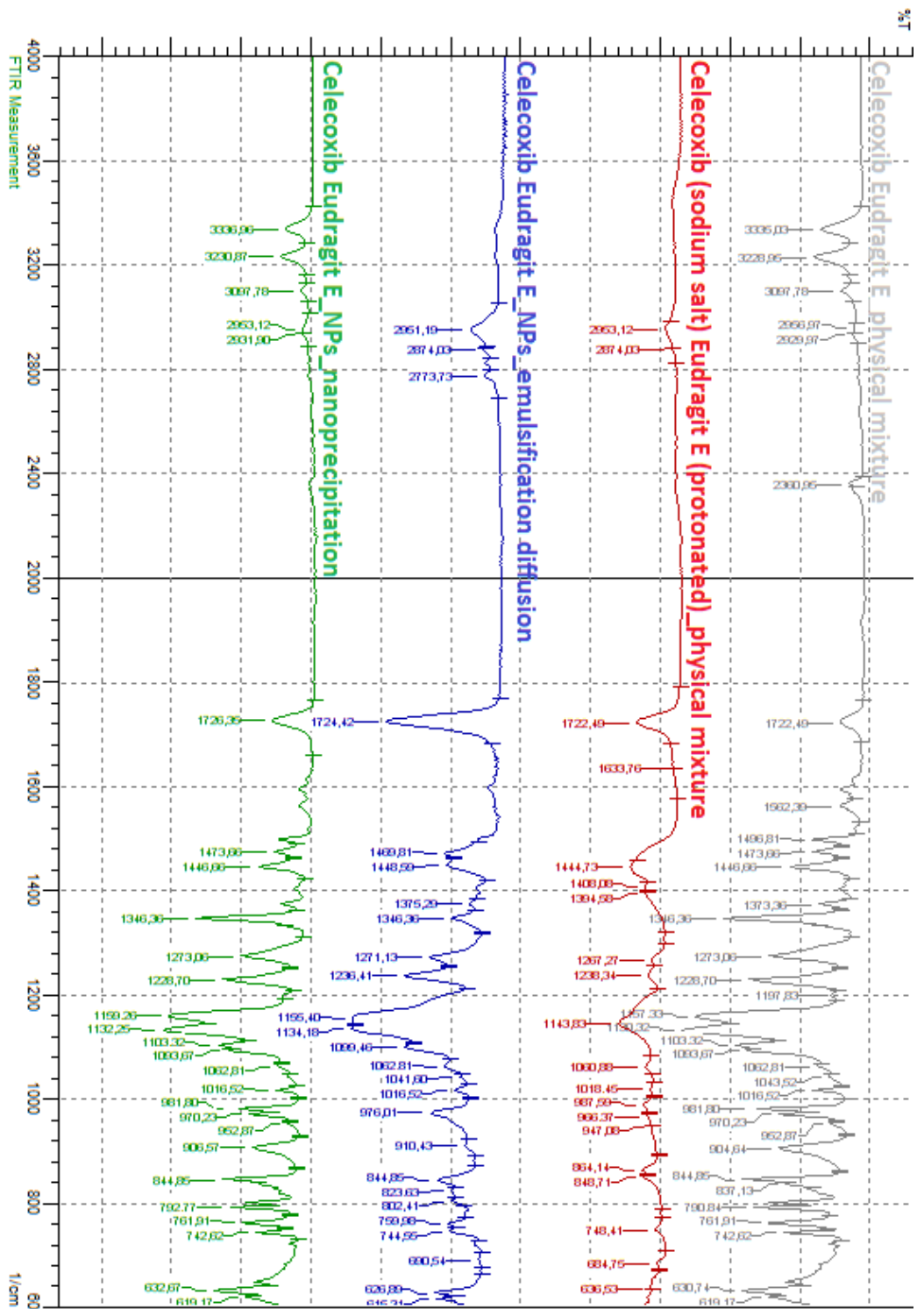


Figure 43: FTIR spectra of physical mixtures of celecoxib and Eudragit E 100 and charged celecoxib and Eudragit E 100 as well as celecoxib-of Eudragit E 100-NPs prepared by MJR (emulsification-diffusion and nanoprecipitation technique).

3.2.3 Scanning electron microscopy

To determine the shape SEM images of MJR-produced celecoxib-Eudragit E 100-NPs prepared by nanoprecipitation (see Figure 44 and Figure 45) and emulsification-diffusion (see Figure 46 and Figure 47) were taken. Hence, respectively two different parameter settings were applied in the NP preparation to obtain different sizes (see legends of Table 16). In the figures image detail (b) respectively shows the volume-weighted DLS size distribution report of the nanosuspension. In the appendix further SEM images of these particles at higher magnification are shown (Figure 64 – Figure 67).

A SEM image and the related DLS size distribution report of NPs, which were prepared by the alternative nanoprecipitation method (see chapter 2.2.1.2), is depicted in Figure 48.

The Z-Average and the PDI (measured by DLS) as well as the NP shape and diameter (determined by SEM) are summarized in Table 16. The Z-Average values, which were obtained from DLS, are approximately 30–40 nm higher compared to those determined by SEM, except of the NPs, which were prepared by the alternative method (**sample 3** in Table 16). Since the first sample, which was prepared by nanoprecipitation (**sample 1**), agglomerated, its size was only measured by DLS. The particle diameters, which were obtained from volume-weighted scaling, were higher compared to the Z-Average. Though, due to high standard deviations of the volume-weighted diameters this difference cannot be regarded as significant. In case of the NPs, which were prepared by the alternative method this value was lower than the Z-Average and equal to the diameter, which was obtained by SEM image analysis. This correlates well with the fact that larger particles are usually overweighted if the size distribution is weighted by the scattered light intensity (as it is done to obtain the Z-Average) and not by the particle volume (see also chapter 1.4.1).

Sample 2 (nanoprecipitation method) was of a spherical, slightly wrinkled shape, while the NPs, which were prepared by emulsification-diffusion (**samples 4 and 5**) and those, prepared by the alternative nanoprecipitation method, possessed a spherical shape.

Table 16: Z-Average, PDI (DLS), shape and diameter (SEM) of MJR produced celecoxib-Eudragit E 100-NPs (nanoprecipitation and emulsification-diffusion technique), values are mean of three measurements \pm SD.

Sample number (related figures)	Production technique (production details stated below the table)	Z-Average DLS /nm	Peak 1 diameter DLS, volume-weighted size distribution /nm	PDI	Shape SEM	Diameter SEM /nm
1 (Figure 44, Figure 64)	nanoprecipitation ¹	1156 \pm 11	1504 \pm 494	0.14 \pm 0.07	sample agglomerated	n/a
2 (Figure 45, Figure 65)	nanoprecipitation ²	387 \pm 10	421 \pm 125	0.29 \pm 0.06	spherical, slightly wrinkled	343 \pm 107
3 (Figure 48)	nanoprecipitation (alternative method) ³	109 \pm 40	96 \pm 32	0.13 \pm 0.01	spherical	96 \pm 14
4 (Figure 46, Figure 66)	emulsification-diffusion ¹	611 \pm 13	849 \pm 338	0.26 \pm 0.05	spherical	575 \pm 196
5 (Figure 47, Figure 67)	emulsification-diffusion ²	254 \pm 2	285 \pm 112	0.15 \pm 0.01	spherical	215 \pm 122

- 1 operation temperature: 50.0 °C, nitrogen pressure: 0.25 bar, 300 : 1500 rpm (pump rotational speed – solvent phase : non-solvent phase)
- 2 operation temperature: 50.0 °C, nitrogen pressure: 0.25 bar, 1200 : 6000 rpm (pump rotational speed – solvent phase : non-solvent phase)
- 3 operation temperature: 25.0 °C, no nitrogen, 50 mL/min (solvent : non-solvent flow rate), solvent phase composition: 0.4 % celecoxib, 0.8 % Eudragit E 100

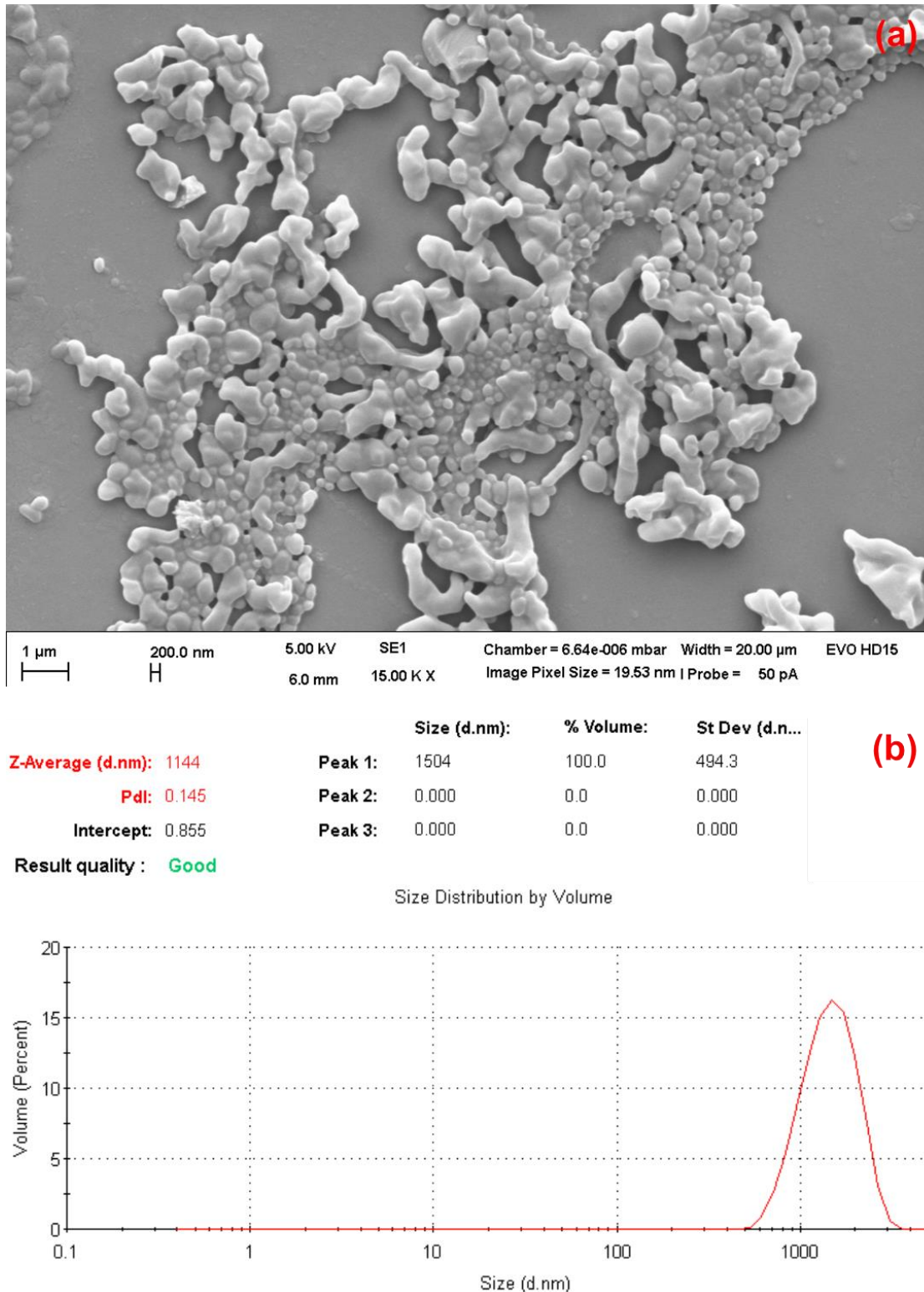


Figure 44: SEM image (a) and volume-weighted DLS size distribution report (b) of MJR produced celecoxib-Eudragit E 100-particles (nanoprecipitation technique): NP properties (determined by DLS, mean of three measurements): 1156 nm (Z-Average), 0.144 (PDI).

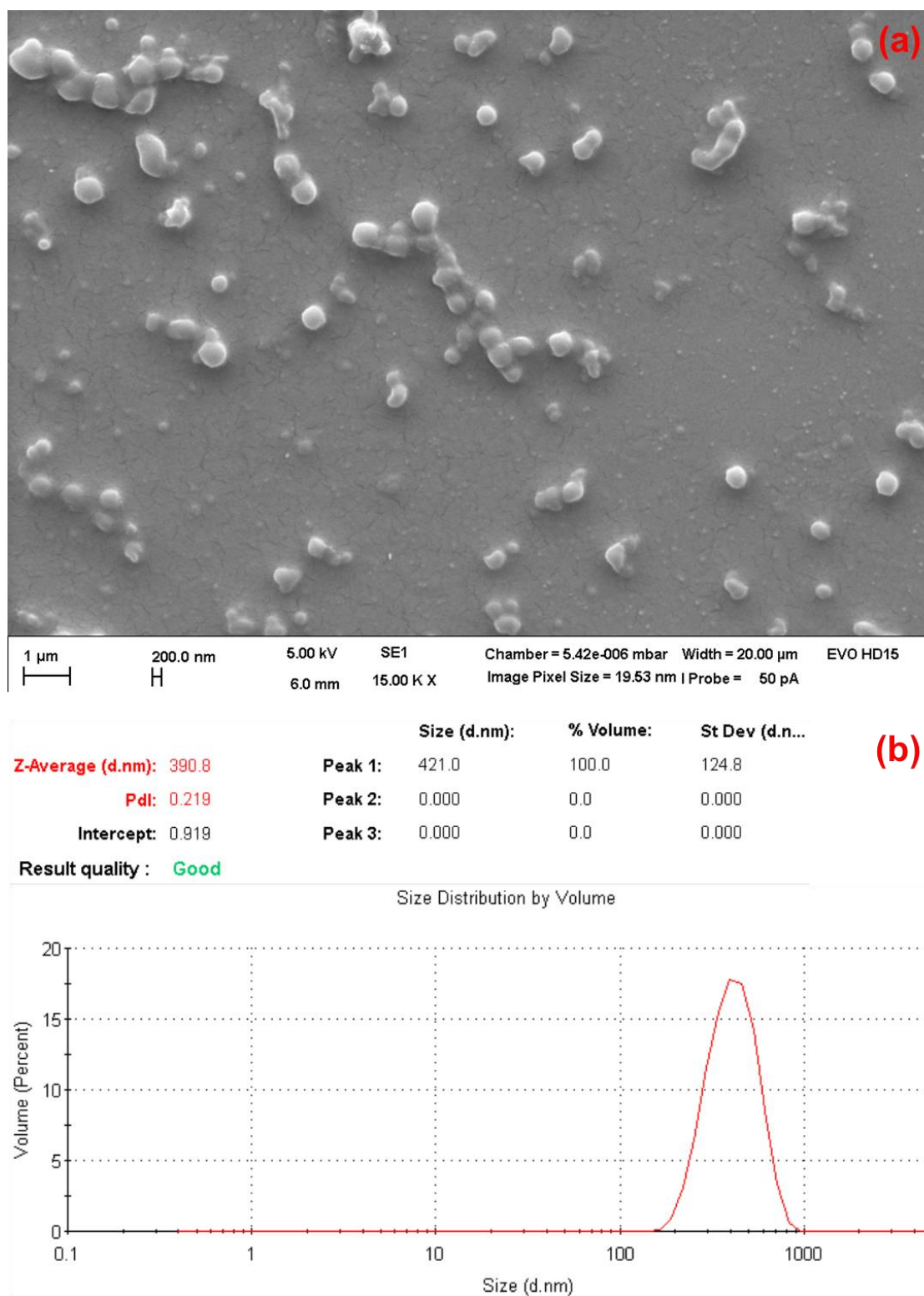


Figure 45: SEM image (a) and volume-weighted DLS size distribution report (b) of MJR produced celecoxib-Eudragit E 100-NPs (nanoprecipitation technique): NP properties (determined by DLS, mean of three measurements): 387 nm (Z-Average), 0.285 (PDI).

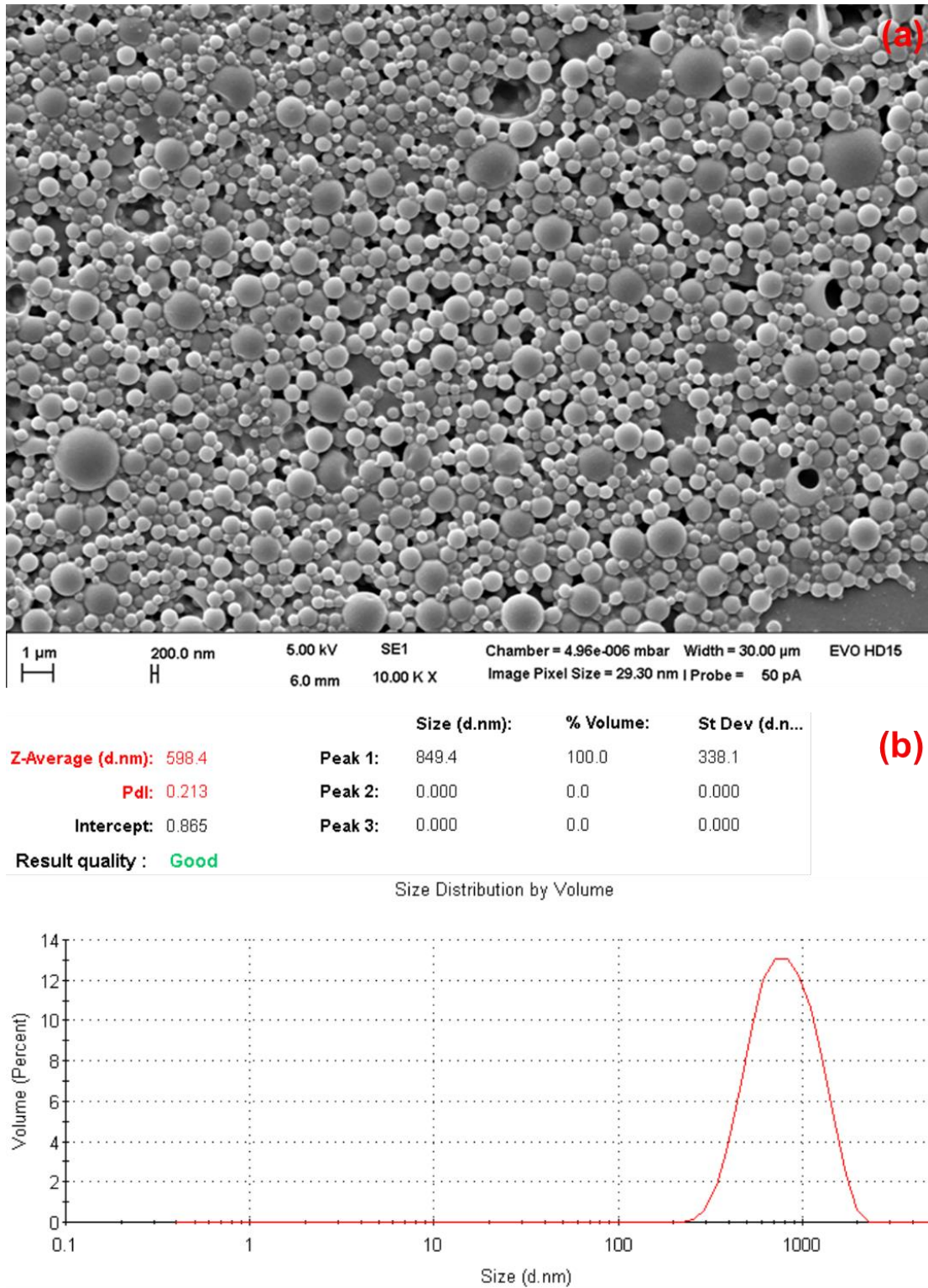


Figure 46: SEM image (a) and volume-weighted DLS size distribution report (b) of MJR produced celecoxib-Eudragit E 100-NPs (emulsification-diffusion technique): NP properties (determined by DLS, mean of three measurements): 611 nm (Z-Average), 0.258 (PDI).

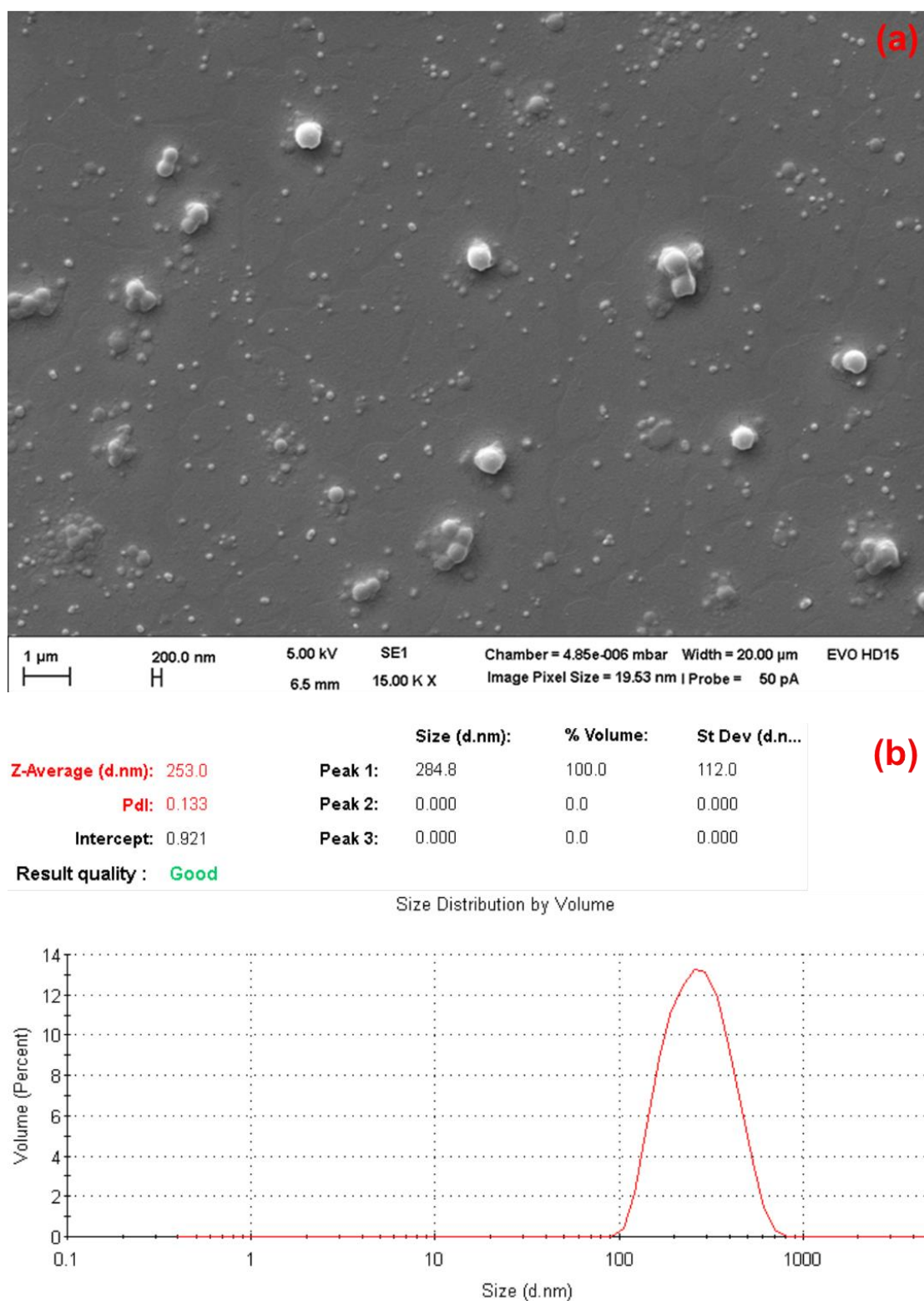
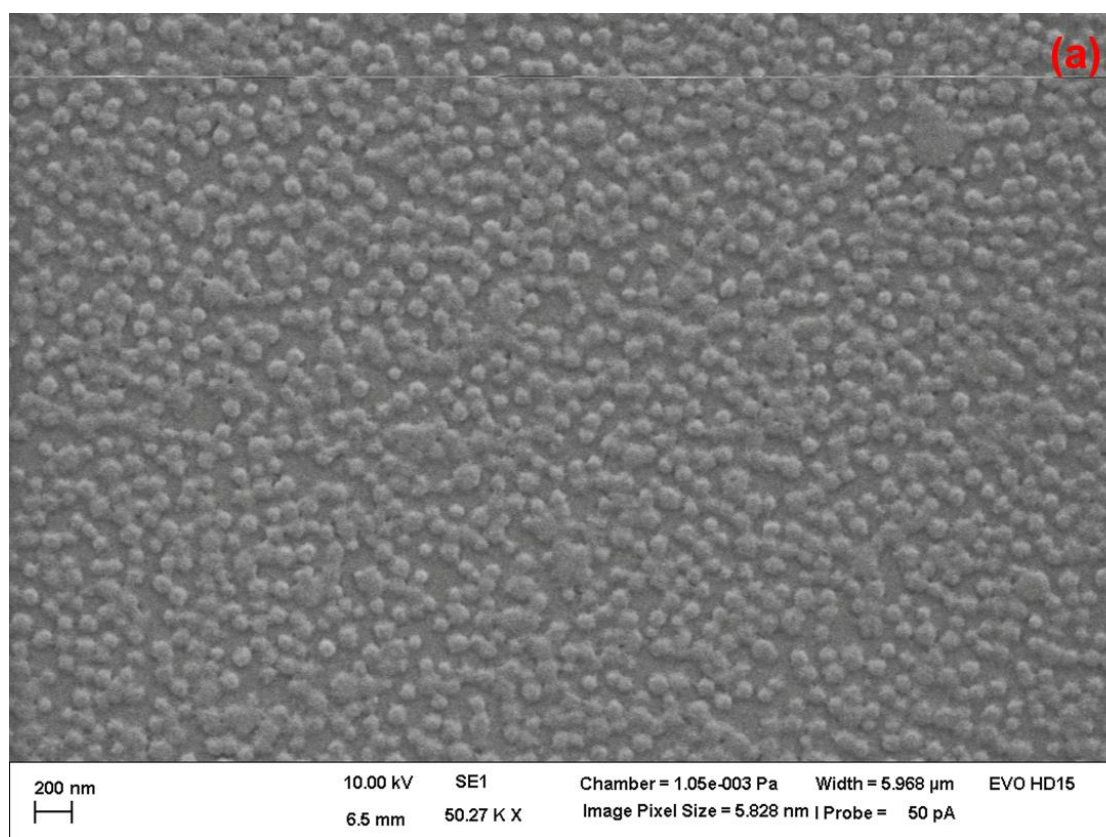


Figure 47: SEM image (a) and volume-weighted DLS size distribution report (b) of MJR produced celecoxib-Eudragit E 100-NPs (emulsification-diffusion technique): NP properties (determined by DLS, mean of three measurements): 254 nm (Z-Average), 0.148 (PDI).



	Size (d.nm):	% Volume:	St Dev (d.n...
Z-Average (d.nm): 109.8	Peak 1: 96.48	100.0	32.44
Pdl: 0.126	Peak 2: 0.000	0.0	0.000
Intercept: 0.948	Peak 3: 0.000	0.0	0.000

Result quality : Good

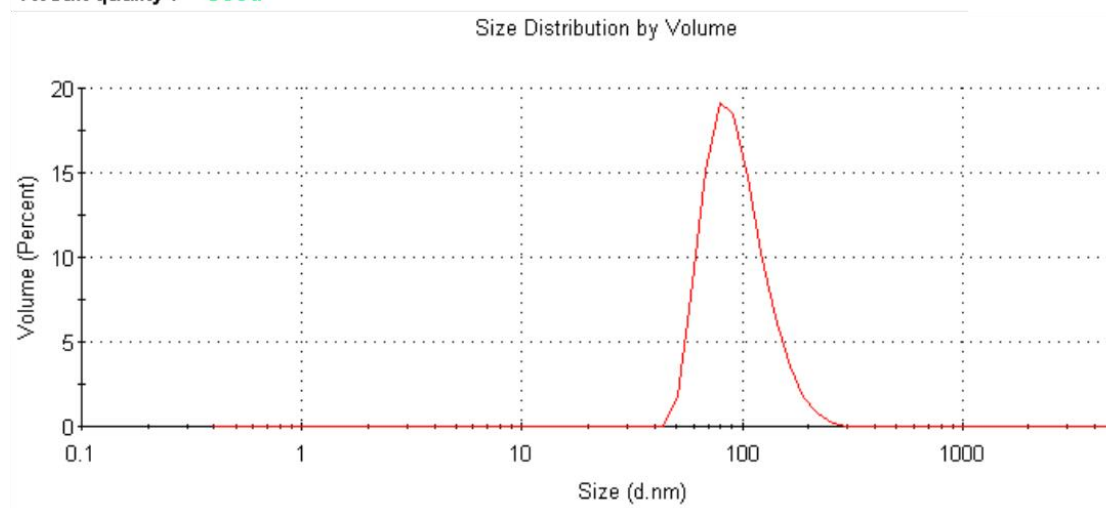


Figure 48: SEM image (a) and volume-weighted DLS size distribution report (b) of MJR produced celecoxib-Eudragit E 100-NPs (nanoprecipitation technique–alternative method using HPLC pumps and a non-solvent phase without surfactant, see chapter 2.2.1.2): NP properties (determined by DLS, mean of three measurements): 109 nm (Z-Average), 0.132 (PDI).

3.2.4 Atomic force microscopy

Figure 49 shows AFM images (two different enlargements of the same sample) of MJR produced celecoxib-Eudragit E 100-NPs. These NPs were prepared by the alternative nanoprecipitation method (see chapter 2.2.1.2 → usage of HPLC pumps instead of micro annular gear pumps and of water without surfactant as non-solvent phase). The volume-weighted size distribution report of these NPs is shown in Figure 48.

In these images length and width of the NPs can be derived from the axis below and at the side of the images. The color scale between the images indicates the height of the NPs ranging from white (≥ 150 nm) over yellow (75 nm) to black (0 nm).

The NPs exhibited a narrow size-distribution with diameter values between circa 50 to 100 nm. All particles were of spherical or almost spherical shape. This correlates well with the SEM characterization of these NPs (see the third sample in Table 16 and Figure 48).

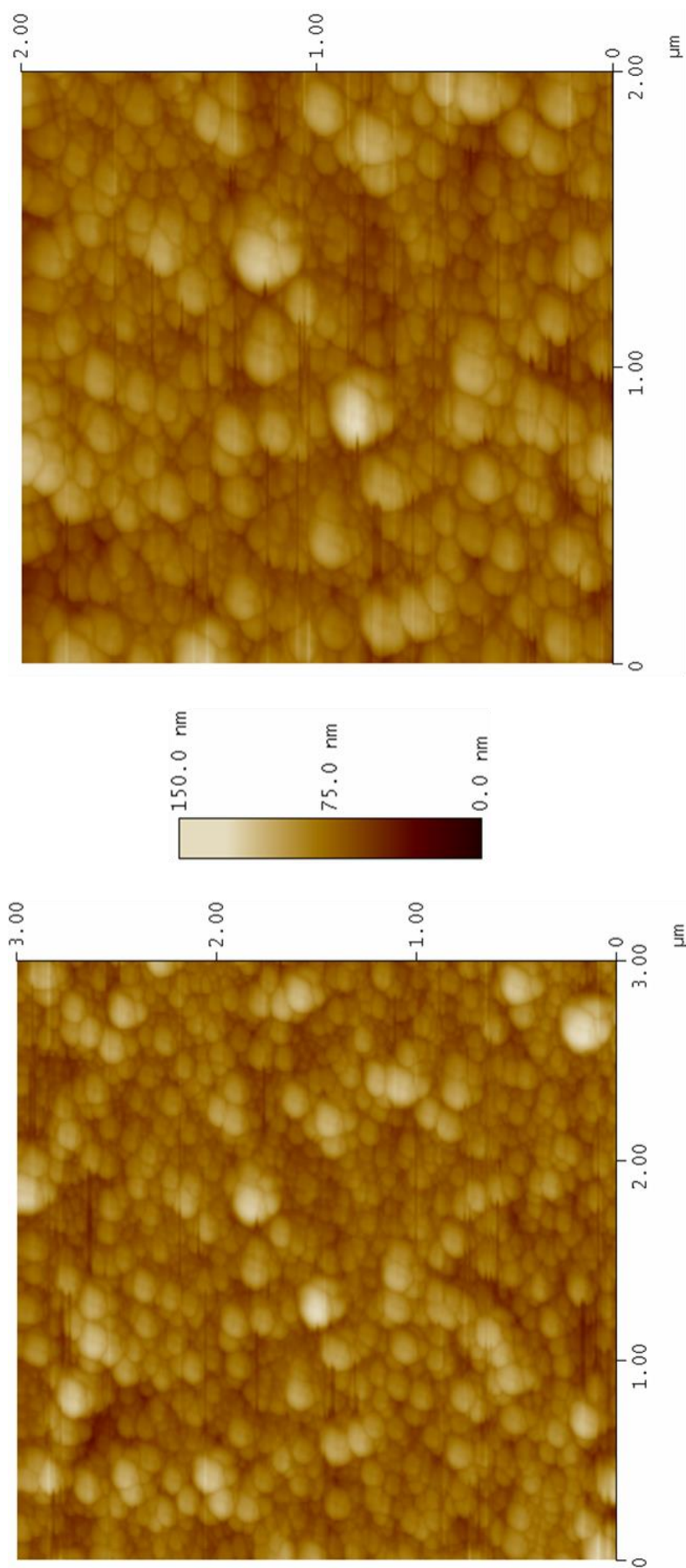


Figure 49: AFM images (two different enlargements of the same sample) of MJR produced celecoxib-Eudragit E 100-NPs (nanoprecipitation technique—alternative method using HPLC pumps and a non-solvent phase without surfactant, see chapter 2.2.1.2): NP properties (determined by DLS, mean of three measurements): 109 nm (Z-Average), 0.132 (PDI); volume-weighted DLS size distribution report shown in Figure 48 (b).

3.3 Dissolution testing

3.3.1 Evaluation of a suitable dissolution medium for the API release of celecoxib-Eudragit E 100-NPs

3.3.1.1 Dissolution test in diluted HCl (pH 1.2)

All nanosuspensions, which were used for the dissolution tests in chapter 3.3.1, were prepared by the alternative MJR nanoprecipitation method (without addition of a surfactant to the non-solvent phase, see chapter 2.2.1.2). First, a dissolution test of MJR-produced celecoxib-Eudragit E 100-NPs in diluted HCl (pH 1.2) was performed as described in chapter 2.2.3.2 (experimental set-up depicted in Figure 25). In short, 1 mL of the nanosuspension to be tested was added to a 150 mL beaker containing 99 mL of the dissolution medium. The medium was stirred, using the magnetic stirrer (for details see Table 6), at 300 rpm, and maintained at 37 ± 0.5 °C using the temperature sensor and the heating plate of the magnetic stirrer. The peristaltic pump with the attached tubes carried the medium continuously through the CF module. Respectively 2 mL of filtrate, containing the dissolved API/analyte, were withdrawn at the defined sampling points and applied to UV-Vis analysis.

The results are shown in Figure 50 and Table 30. Hence, more than 50 % drug release occurred within 9 min. Up to 12 min this value remained constant followed by a successive decline of the concentration until 34 % at 60 min.

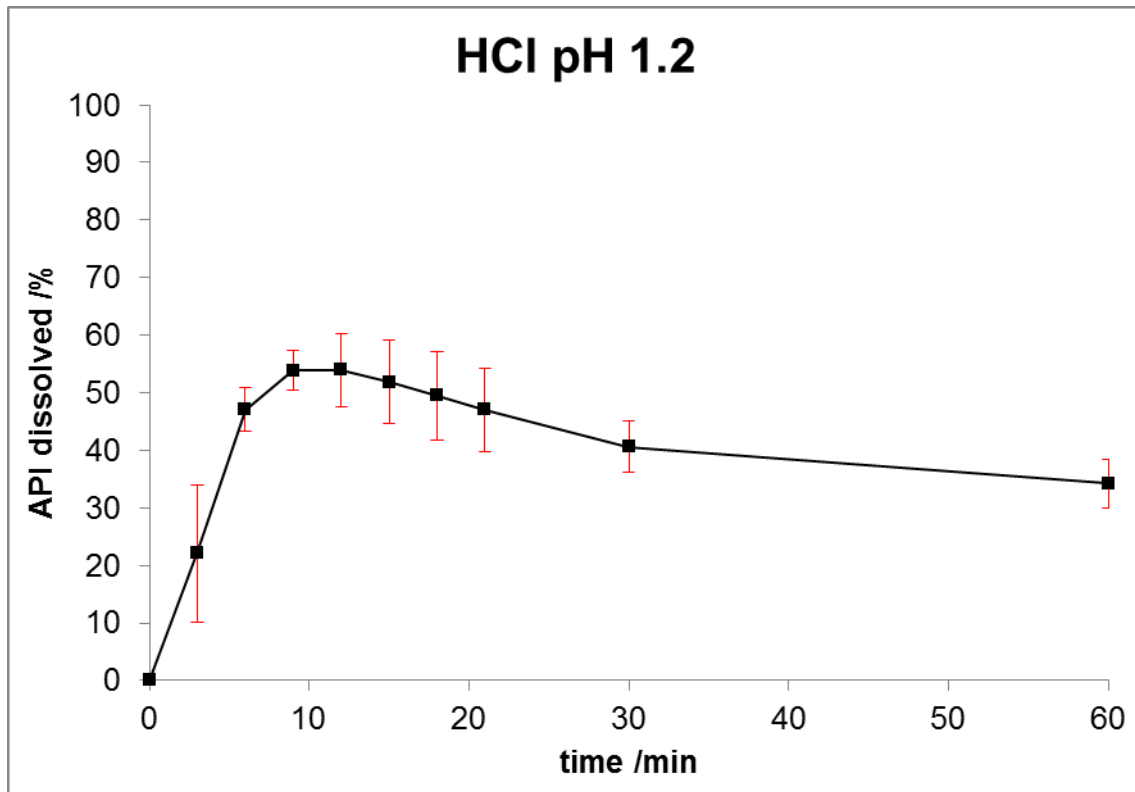


Figure 50: Dissolution of celecoxib-Eudragit E 100-NPs in HCl pH 1.2: NP properties: 80 nm (Z-Average), 0.131 (PDI) and 2.573 mg/mL (celecoxib concentration of the nanosuspension, i.e. a 2.573 mg dose of celecoxib), detection: UV-Vis (248 nm), n=3, red lines represent SD.

For the purpose of a detailed investigation of the analyte concentration decline, a SEM image of the same nanosuspension in HCl pH 1.2 was taken (see Figure 51). Thereto, a 1:100 dilution of the nanosuspension in HCl pH 1.2 (dilution factor corresponds to the dissolution experiment) was stored for 24 h at ambient temperature in a closed container. This was done to simulate the reaction of the NPs with the dissolution medium. Then, this sample was prepared for the SEM analysis without further dilution or washing as described in chapter 2.2.2.5.

Thereby, rectangular particles in a size range of a few microns appeared, while no NPs were visible.

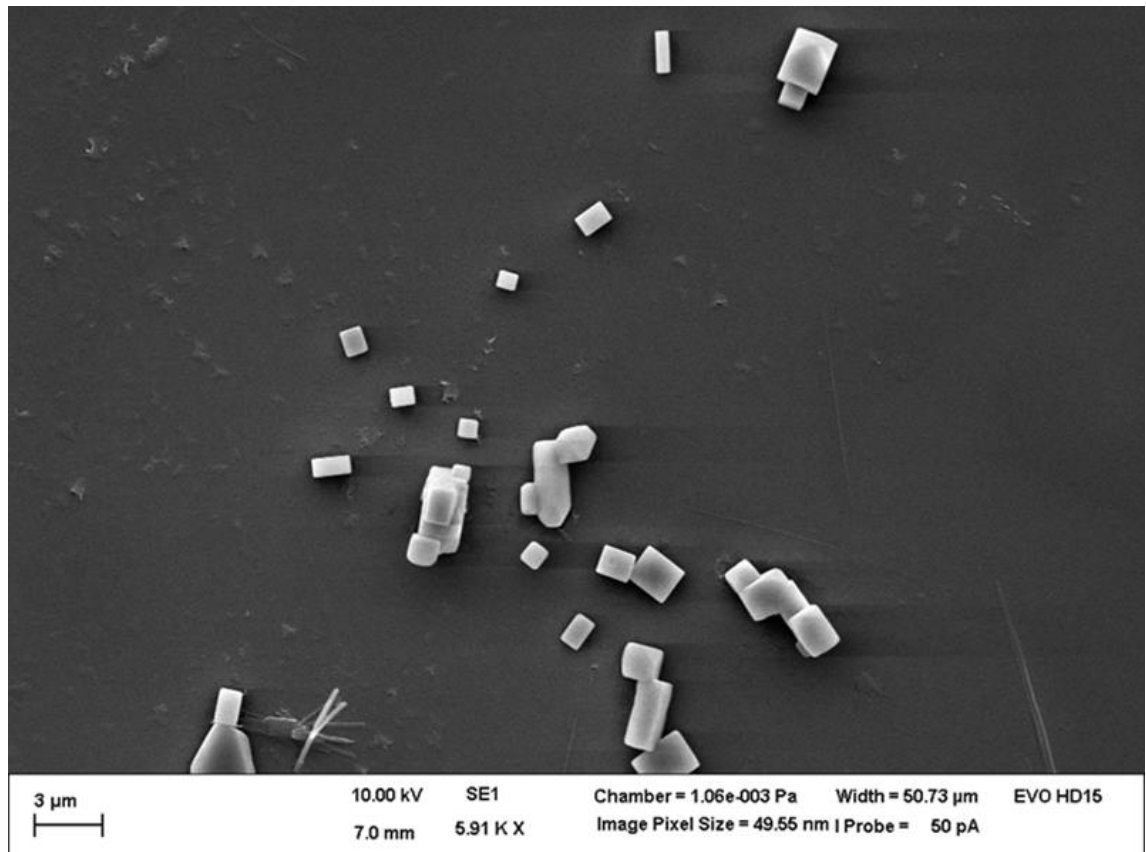


Figure 51: SEM image with precipitations of a 1:100 dilution of celecoxib-Eudragit E 100-NPs in 0.1 M HCl after 24 h storage at ambient temperature; NP preparation parameters: MJR, nanoprecipitation technique-alternative method (without usage of a surfactant).

3.3.1.2 Dissolution test in diluted HCl (pH 1.2) containing NaCl

The second dissolution test was performed with HCl pH 1.2 containing 0.15 M NaCl to examine the influence of electrolyte addition. Hence, another NP batch was used than in chapter 3.3.1.1, but the preparation method was the same and Z-Average, PDI and API concentration are similar. The test parameters were the same as in chapter 3.3.1.1. The dissolution profile is shown in Figure 52 (values stated in Table 31) together with the profile without NaCl (from Figure 50) for comparison.

Hence, the dissolution rate was, in the presence of NaCl, faster and celecoxib was completely dissolved at 12 min. Thereafter, a concentration decline again occurred up to a value corresponding to 54 % dissolution.

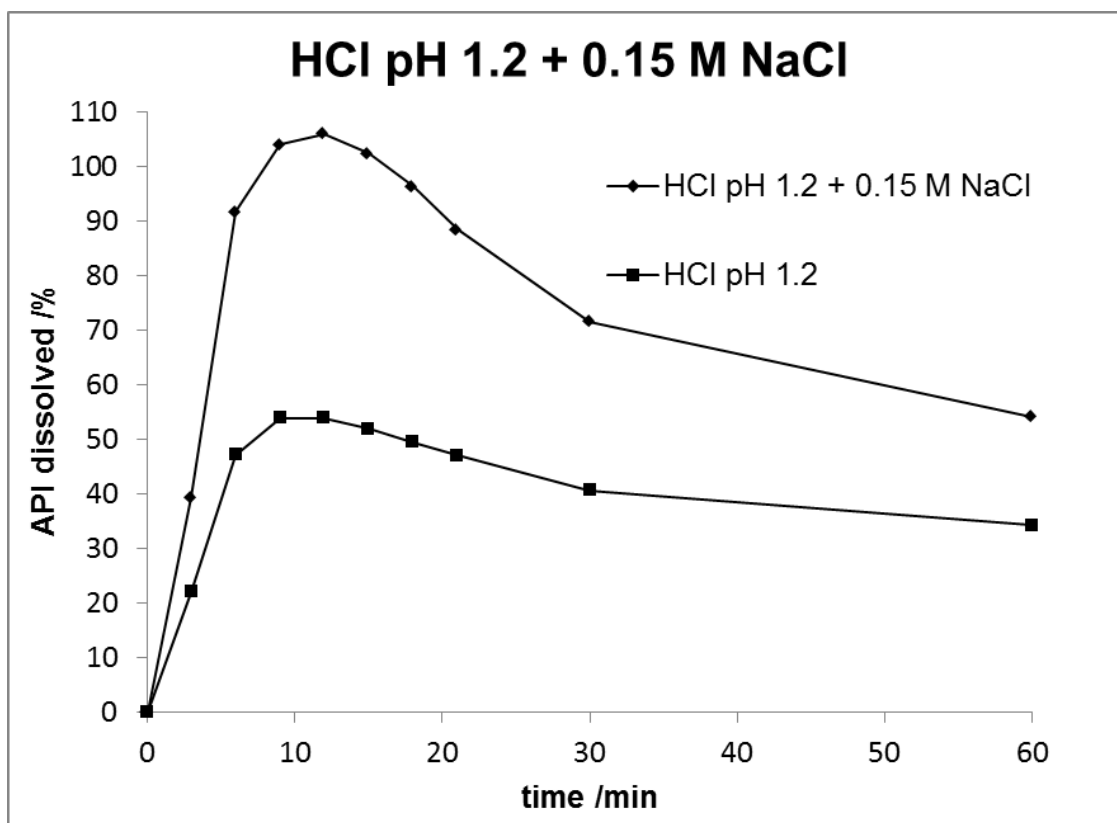


Figure 52: Dissolution of celecoxib-Eudragit E 100-NPs in HCl pH 1.2 + 0.15 M NaCl: NP properties: 100 nm (Z-Average), 0.100 (PDI) and 2.331 mg/mL (celecoxib concentration of the nanosuspension, i.e. a 2.331 mg dose of celecoxib), detection: UV-Vis (248 nm), n=1.

3.3.1.3 Dissolution tests in diluted HCl (pH 1.2) containing cetrimide

Albers et al. [5] used cetrimide to ascertain sink conditions for release testing of celecoxib-Eudragit E-extrudates. Thus, the dissolution behavior of the NPs was examined in HCl pH 1.2 including 0.001, 0.01, 0.3 and 1.0 % (see Figure 53 and Table 32). Hence, the nanosuspension and the test parameters were the same as in chapter 3.3.1.1.

Hereby, the dissolution profile obtained with 0.001 % cetrimide resembled that one of pure HCl pH 1.2 (see Figure 50) with the exception that both initial increase and following decrease were more intensive. Using 0.01 %, a maximum concentration of 34 % was reached at 21 min followed by slight decrease up to 30 % at 120 min. In contrast to these profiles a concentration decline did not occur if 0.3 % (sink conditions [2]) or 1.0 % of surfactant was used, while the slope was higher for 0.3 % than for 1.0 % with maxima at 39 % and 25 % API dissolved, respectively.

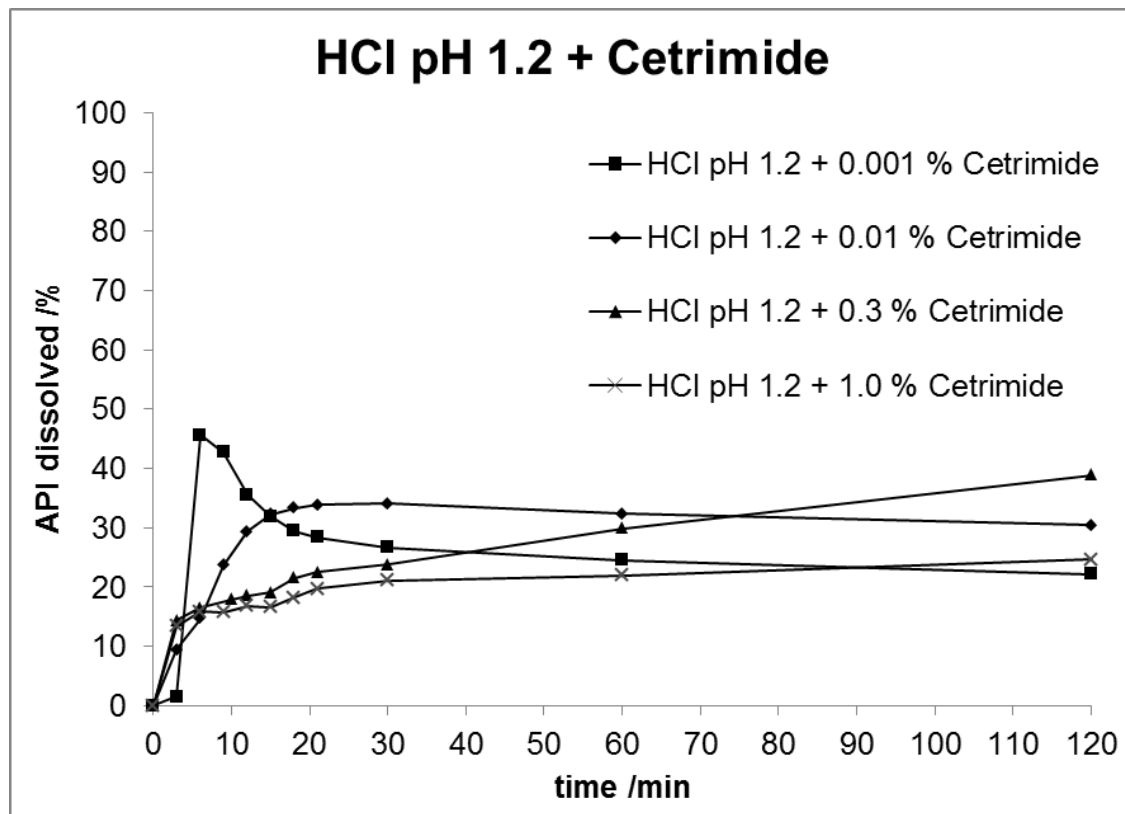


Figure 53: Dissolution of celecoxib-Eudragit E 100-NPs in HCl pH 1.2 + 0.001/0.01/0.3/1.0 % cetrимide: NP properties: 80 nm (Z-Average), 0.131 (PDI) and 2.573 mg/mL (celecoxib concentration of the nanosuspension, i.e. a 2.573 mg dose of celecoxib), detection: UV-Vis (248 nm), n=1.

3.3.1.4 Dissolution tests in diluted HCl (pH 1.2) containing cetrimide using cross-flow- and dead-end filtration

With regard to the issue that the dissolution process, even under sink conditions, was not completed after 120 min (see chapter 3.3.1.3) the effect of filter type and filter pore size were investigated. Hence, a nanosuspension was used with a Z-Average of 160 nm, a PDI of 0.094 and a celecoxib concentration of 2.388 mg/mL (same preparation method as in chapter 3.3.1.1).

These dissolution tests were performed under sink conditions (HCl pH 1.2 + 0.3 % cetrimide) using three different filters: the 100 kDa CF module (MWCO: 10 nm), which was already used in the previous dissolution tests, and a 500 kDa CF module (MWCO: 50 nm) as well as 0.2 μ m syringe filter holders to represent dead-end filtration. The sample withdrawal with the syringe filter holders was performed analogously to conventional dissolution tests and is described in chapter 2.2.3.3. The applicability of the new module to retain these NPs was proven with the same procedure, which is described in chapter 2.2.3.1. In the same way the 0.2 μ m syringe filter holders were tested successfully. The volume-weighted DLS size distribution reports of the verification of both filters are shown in the appendix (see Figure 68). Apart from the different filtration types the dissolution tests were performed as described in chapter 3.3.1.1

Figure 54 reveals a great difference between the dissolution profiles obtained with, on one hand, the 500 kDa CF module and 0.2 μ m syringe filter holders and, on the other hand, the 100 kDa CF module (values stated in Table 33). In the latter case the experimental values did not exceed 10 % of the maximum amount after 120 min. Conversely, nearly 100 % dissolution were reached after only 3 min with both the 500 kDa CF module and the 0.2 μ m syringe filter holder at slightly higher initial increase with the syringe filter holder.

To investigate whether the NPs are dissolved, 1:100 dilutions of the tested nanosuspension in both water and 0.1 M HCl + 0.3 % cetrimide were prepared. These dilutions were respectively filled without filtration in a cuvette of the DLS instrument and measured at 37 °C (dissolution test temperature).

The sample in dissolution medium was measured at several timepoints from 0–15 min (incubation time in the cuvette at 37 °C). The measurement at 15 min and the comparison in water are shown in the appendix (see Figure 69). Hence, it was observed that the NPs were completely dissolved in the dissolution medium.

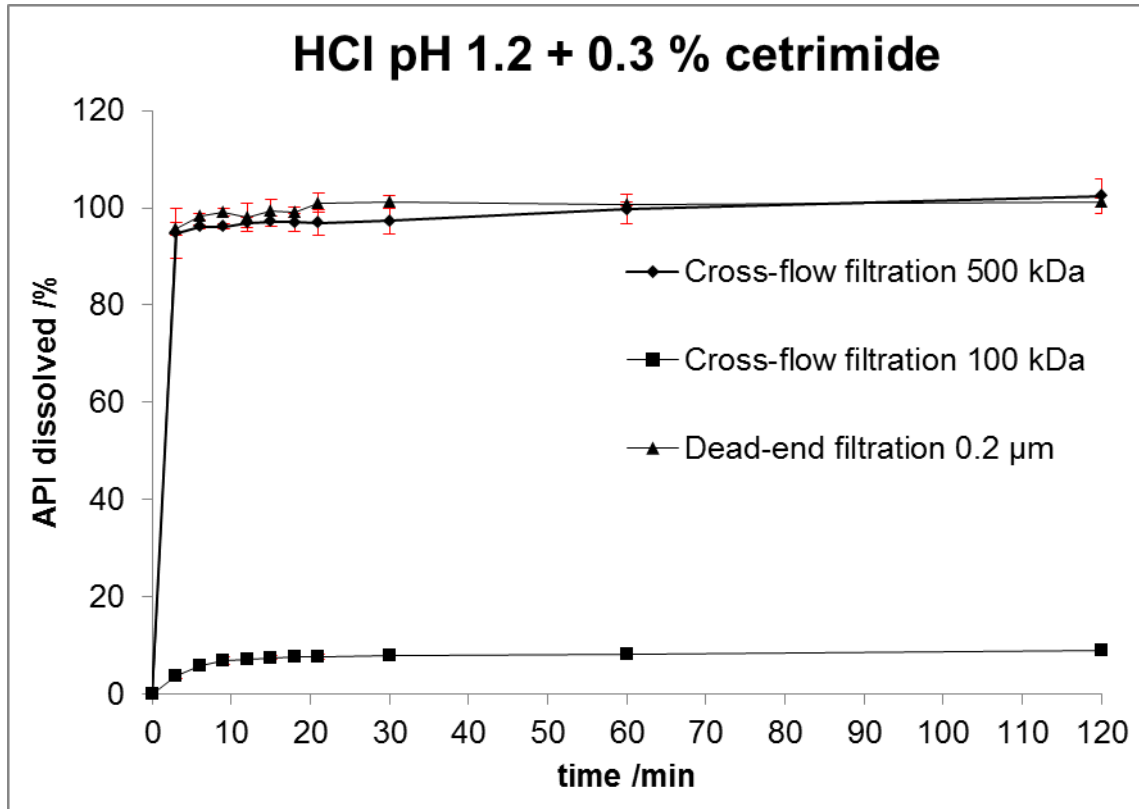


Figure 54: Dissolution of celecoxib-Eudragit E 100-NPs in diluted HCl pH 1.2 + 0.3 % cetrimide: NP properties: 160 nm (Z-Average), 0.094 (PDI) and 2.388 mg/mL (celecoxib concentration of the nanosuspension, i.e. a 2.388 mg dose of celecoxib), filters: CF modules of 100 kDa and 500 kDa and 0.2 µm syringe filter holders (dead-end), detection: UV-Vis (248 nm), n=3, red lines represent SD.

To achieve a slower dissolution rate the cetrimide concentration in the medium was decreased to 0.05 % (m/V) and the dissolution tests performed as described above. Hence, if using the 100 kDa CF modules, the maximum release increased, compared to the medium with 0.3 % cetrimide, from 9 % to 14 % maximum release (see Figure 55 and

Table 34). Concerning the 500 kDa CF module, a similar curve progression as previously was obtained with the exception that the release after 120 min did not exceed 89 %. This was similar if the 0.2 μm syringe filter holders were used, while the related profile exhibited a slower increase between 3 min and 20 min (~72 % to 84 %). This indicates insufficient solubilization of celecoxib (see chapter 4.2).

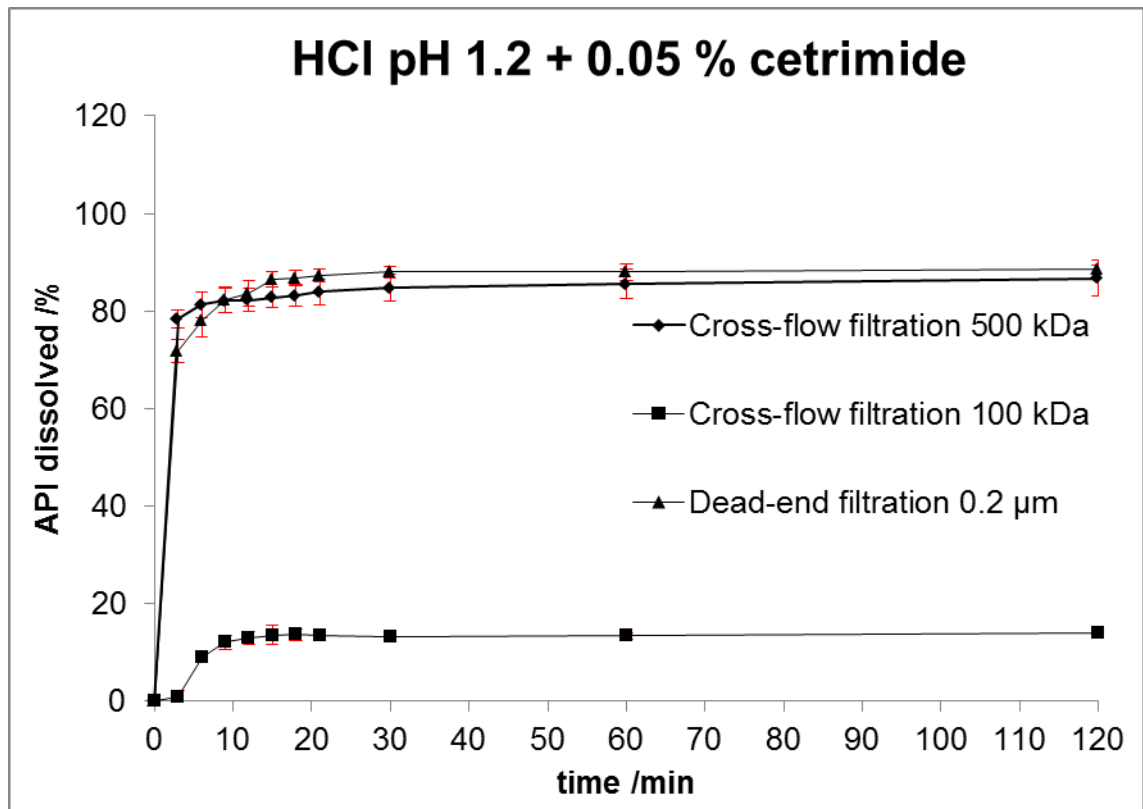


Figure 55: Dissolution of celecoxib-Eudragit E 100-NPs in diluted HCl pH 1.2 + 0.05 % cetrimide: NP properties: 160 nm (Z-Average), 0.094 (PDI) and 2.509 mg/mL (celecoxib concentration of the nanosuspension, i.e. a 2.509 mg dose of celecoxib), filters: cross-flow filtration modules of 100 and 500 kDa and 0.2 μm syringe filter holders (dead-end), detection: UV-Vis (248 nm), n=3, red lines represent SD.

3.3.1.5 Dissolution tests in phosphate buffers of different pH containing 0.3 % cetrimide

As the usage of a strongly acidic medium (HCl pH 1.2) in combination with 0.3 % cetrimide led to immediate and nearly complete release of celecoxib (see Figure 54), different phosphate buffers of higher pH values were tested towards their suitability to generate a dissolution profile, which is more suitable to compare differently-sized NP batches. Furthermore, a high degree of dissolution should be achieved. Hence, a nanosuspension was used with a Z-Average of 220 nm, a PDI of 0.086 and a celecoxib concentration of 3.666 mg/mL (same preparation method as in chapter 3.3.1.1). The test parameters were the same as in chapter 3.3.1.1 except that a 500 kDa CF module was used.

Hence, the respective values after 120 min dissolution increased from 32.4 ± 3.6 API release at pH 5.2 to 88.8 ± 1.2 API release at pH 2.0 (see Figure 56 and Table 35). The slope of the dissolution curves from the first sampling point at 3 min to 120 min became smaller with decreasing pH (~23–31 % release at pH 5.2 versus ~81–89 % at pH 2.0).

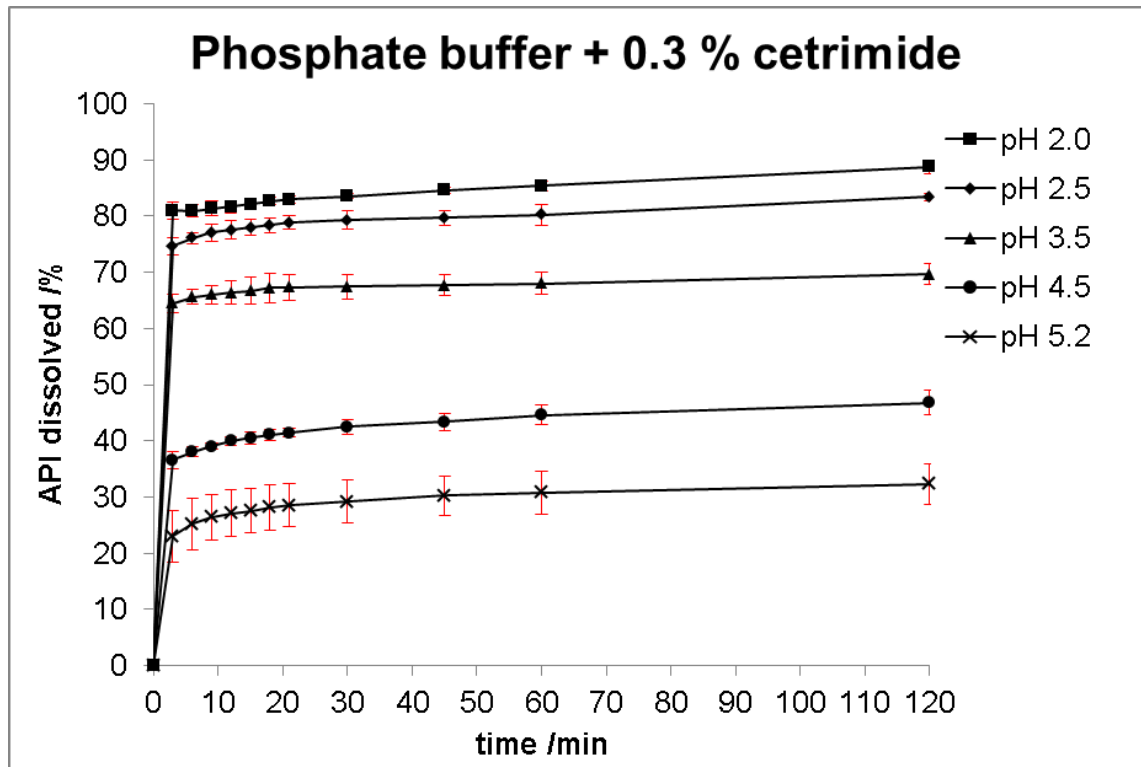


Figure 56: Dissolution of celecoxib-Eudragit E 100-NPs in phosphate buffer pH 2.0/2.5/3.5/4.5/5.2+ 0.3 % cetrimide: NP properties: 220 nm (Z-Average), 0.086 (PDI) and 3.666 mg/mL (celecoxib concentration of the nanosuspension, i.e. a 3.666 mg dose of celecoxib), filter: 500 kDa cross-flow filtration module, detection: UV-Vis (248 nm), n=3, red lines represent SD.

3.3.2 Comparison of the dissolution behavior of nanoparticles of different size and unprocessed celecoxib particles

Finally, the dissolution profiles of NPs of different size (220, 250, 300, 350 and 500 nm) and unprocessed celecoxib particles were compared in phosphate buffer pH 2.0 + 0.3 % cetrimide as medium to achieve a high degree of dissolution (see chapter 3.3.1.5). The size of the unprocessed particles was determined by laser light diffraction (volume-weighted median diameter: 22.58 μm , size distribution report shown in the appendix \rightarrow Figure 70). Thereto, API powder was suspended in water and the suspension simultaneously ultrasonicated and stirred before it was measured. The NPs of different size were prepared by MJR technology as described in chapter 3.1.2.1 (emulsification-diffusion, with usage of Poloxamer 407 in the non-solvent phase). The test parameters were the same as in chapter 3.3.1.1 except that a 500 kDa CF module was used and that 0.25 mL of each nanosuspension were used for each dissolution test.

Hence, the profiles obtained for nanosuspensions strongly resemble each other (see Figure 57). From start to 20 s they moderately increased up to circa 10 % release, followed by sharp increase between 20 and 40 s to approximately 80 % release. After 60 s circa 85 % of API were released. From 60 s to the end of the test at 120 s there was no distinct change. In contrast, the API powder samples showed nearly no release below 20 s. Only from this timepoint on there was an increase to approximately 60 % release at 120 s, while the slope of the curves slightly decreased up to this point (see Figure 57). After 60 min 84.5 ± 12.6 % of API powder was dissolved (see Table 36).

The statistical evaluation (for description see chapter 2.2.3.6), results stated in Table 17) did not reveal significant changes between any of the nanosuspension dissolution profiles with f_1 values below 15 and f_2 values from 50–100 for every comparison. Though, the dissolution behavior of the unprocessed API particles was clearly distinguished from all nanosuspensions ($f_1 > 15$ and $f_2 < 50$).

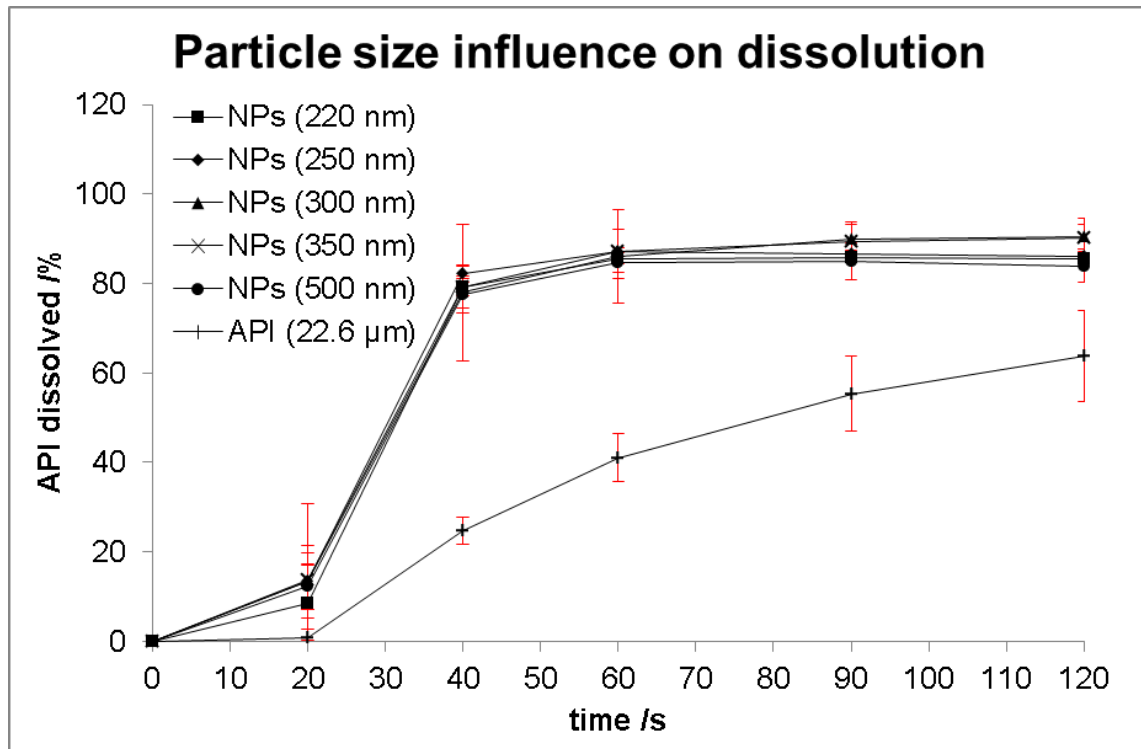


Figure 57: Dissolution of celecoxib-Eudragit E 100-NPs of different size and celecoxib (API) powder in phosphate buffer pH 2.0 + 0.3 % cetrimide: NP properties: 221/255/293/362/497 nm (Z-Average), < 0.25 (PDI) and ~ 2.650–4.850 mg/mL (celecoxib concentration of the nanosuspension, i.e. 0.663 mg-1.213 mg celecoxib dose), API powder: 2537 μg/mL (celecoxib concentration of the suspension), filter: 500 kDa cross-flow filtration module, detection: UV-Vis (248 nm), n=6, red lines represent SD.

Table 17: Statistical comparison of dissolution profiles of celecoxib-Eudragit E 100-NPs of different size and celecoxib (API) powder: Evaluation performed with model independent approach using a similarity factor according to FDA “Guidance for Industry: Dissolution Testing of Immediate Release Solid Oral Dosage Forms” [153], equivalence is given if $f_1 < 15$ (0–15) and $f_2 > 50$ (50–100).

Comparison	Difference factor f_1	similarity factor f_2	Equivalence of dissolution curves
221 nm - 255 nm	5.3	74.5	yes
221 nm - 293 nm	3.8	77.7	yes
221 nm - 362 nm	4.0	75.7	yes
221 nm - 497 nm	3.6	81.9	yes
221 nm - API powder	61.6	26.9	no
255 nm - 293 nm	2.8	81.2	yes
255 nm - 362 nm	1.6	89.6	yes
255 nm - 497 nm	3.3	76.3	yes
255 nm - API powder	61.8	26.1	no
293 nm - 362 nm	1.6	99.2	yes
293 nm - 497 nm	1.7	98.1	yes
293 nm - API powder	62.5	26.8	no
362 nm - 497 nm	3.3	84.9	yes
362 nm - API powder	61.8	26.5	no
497 nm - API powder	61.8	27.2	no

Since the performed evaluation did not reveal differences between the dissolution behavior of the differently-sized NPs a second evaluation was done. To detect the respective endpoints of dissolution the reciprocals of the release percentages were plotted against the reciprocals of dissolution time. Then, the y-intercept of the line through the last three sampling points was determined ($1/y\text{-intercept} = \text{maximum release} \rightarrow R_{\max}$). The R_{\max} -values are given in Table 18 and the graph for the NPs of ~350 nm diameter is exemplarily shown below (see Figure 58).

In the next step the natural logarithm of the release was plotted against the dissolution time. Hence, the release was corrected through division of the respective values by the above-obtained R_{\max} -values. The dissolution time was corrected by subtraction of the dead time t_d (~13 s, determined experimentally, see chapter 2.2.3.4). To compare the dissolution velocities the value k was determined as slope of the regression line through the first three sampling points. The k -values are given in Table 18 and the graph for the NPs of ~350 nm diameter is exemplarily shown below (see Figure 59).

Concerning the determined k -values there is a great difference between the API powder ($k = 0.017$) and the NPs. Additionally the k -values of the NP batches of 220 nm (0.124), 250 nm (0.138) and 500 nm (0.117) differ from those of 300 nm (0.059) and 350 nm (0.087).

Table 18: R_{\max} - and k-values of the dissolution of the differently-sized NP batches. R_{\max} values obtained as y-intercept of a line through the last three sampling points after plotting of the reciprocal of release percentage against the reciprocal of dissolution time. k-values obtained as slope of the regression line through the first three sampling points after plotting of the natural logarithm of release against dissolution time.

Particle size /nm	R_{\max}	k
221	85.5 ± 0.6	0.124 ± 0.041
255	85.4 ± 0.5	0.138 ± 0.01
293	96.0 ± 1.8	0.059 ± 0.01
362	93.6 ± 0.1	0.087 ± 0.024
497	83.8 ± 1.4	0.117 ± 0.006
22580 (API powder)	84.5 ± 0.5	0.017 ± 0

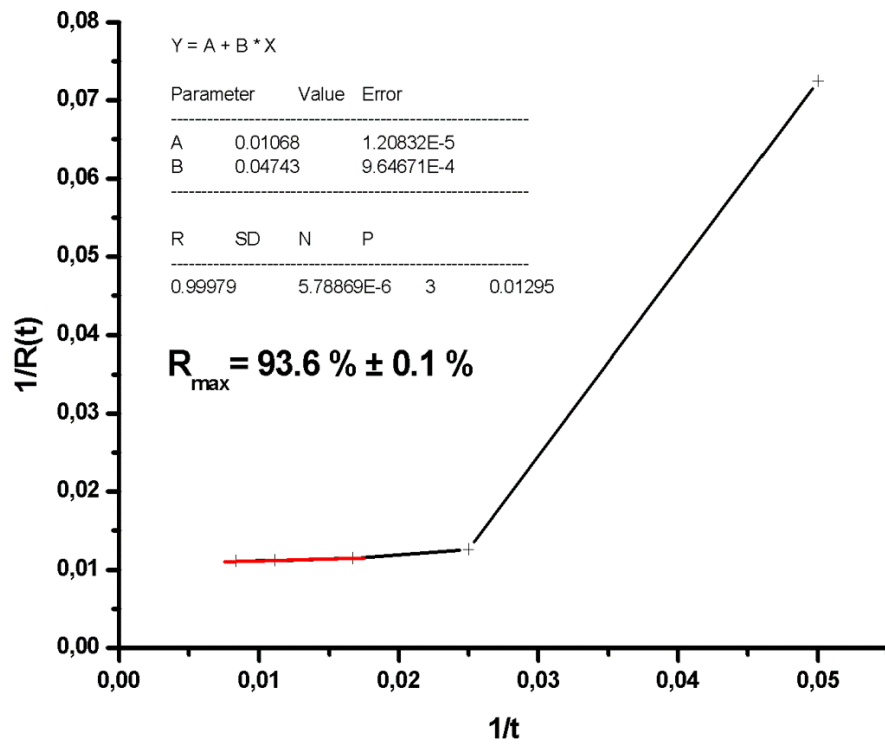


Figure 58: Plot of the reciprocal of release percentage against the reciprocal of dissolution time for the NP batch of 362 nm diameter. The R_{\max} corresponds to the reciprocal of the y-intercept of the **red line** through the last three sampling points.

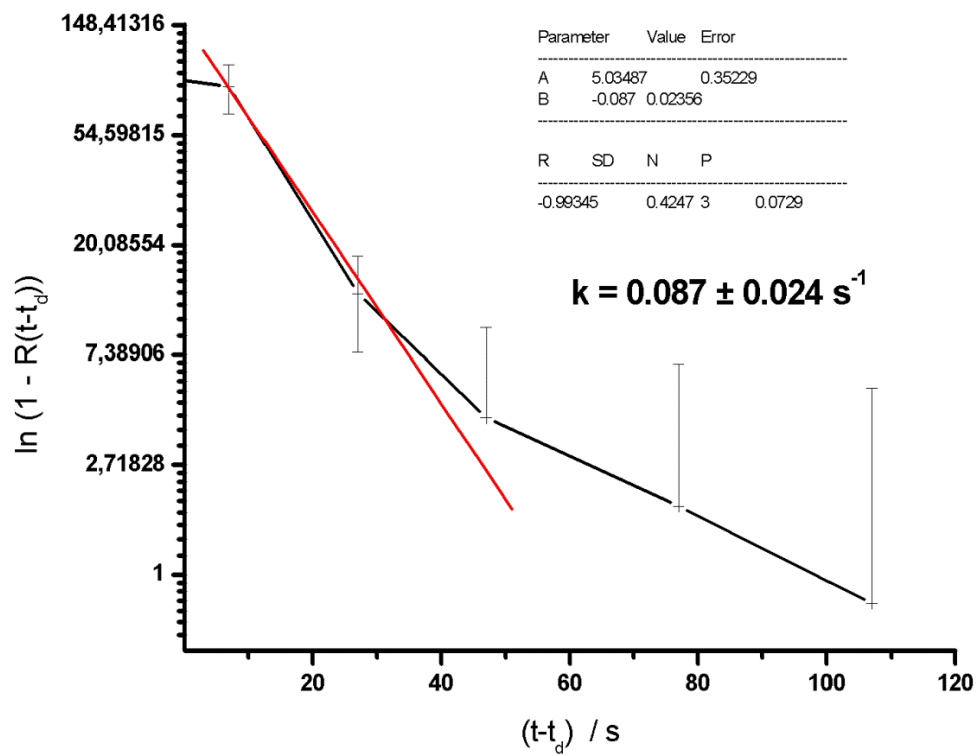


Figure 59: Plot of the natural logarithm of release against dissolution time for the NP batch of 362 nm diameter (vertical bars represent the standard deviation). The k-value corresponds to the slope of the **red regression line** through the first three sampling points.

4 Discussion

4.1 Nanoparticle preparation

The usage of the MJR technology for the production of NPs was based on the doctoral thesis of Akif Emre Türeli [13]. Türeli prepared different NP formulations using hydroxypropyl methyl cellulose phthalate (HPMCP 50), low molecular weight chitosan and Eudragit S 100 as polymers. Fenofibrate, Danazol and Gliclazide served as APIs. These formulations were gastro-resistant. Additionally, he adapted the MJR technology (Penth, 2005 [11]) to enable the custom preparation of NPs (see also 1.3.2). In the present study, NPs were manufactured that can dissolve in the stomach by using Eudragit E instead of Eudragit S. The API Celecoxib does not require a gastro-resistant formulation, as it is an NSAR without harmful effect on the gastric mucosa (see 1.2). Hence, the focus is on fast dissolution of the poorly-soluble API. The most significant difference of the present study to the thesis of Türeli is the development of a new and robust approach for dissolution testing of nanoparticulate dosage forms. Türeli used the conventional USP 2 apparatus with standard syringe filter holders to perform dissolution studies. The disadvantages of this technique were intensively discussed above (see chapters 1.5.2 and 1.5.3). Thereto, the prepared Celecoxib-Eudragit E-NPs served as a model.

The combination of celecoxib and Eudragit E proved to be suitable to produce extrudates by hot-melt extrusion [1][5]. After the extrusion the molten mass was cooled and milled to obtain powders in different size fractions up to 500 μm . This process is a top-down approach (see chapter 1.3.1.1). In the present study NPs of celecoxib and Eudragit E 100 were produced by a bottom-up approach (see chapter 1.3.1.2) either as bench-top method or by MJR technology. This study revealed that the bench-top preparation of celecoxib-Eudragit E 100-NPs with emulsification-diffusion technique requires an adequate co-stabilizer. Thereto, the applicability of three stabilizers, two steric (PVA and Poloxamer 407) and one negatively charged electrostatic stabilizer (SDS), for the NP production was tested (see

chapter 3.1.1.1). Since the system already contained a positively charged stabilizer (Eudragit E 100), the implementation of a further one was considered to be ineffective due to repulsion between them.

Of this choice only Poloxamer 407 was appropriate. Concerning SDS, aggregation with Eudragit E 100 molecules due to ionic interactions may reduce surface charge and therefore stability. In case of PVA, the arrangement with Eudragit E 100 molecules on the NP surface is obviously unfavourable leading to relatively low ZP values (see Table 21) and likewise poor stability. In contrast, the use of Poloxamer 407 resulted in significantly higher ZP values (above 40 mV). Accordingly, every PDI value did not exceed 0.25 while all values were higher for PVA stabilization. In summary, every approach with Poloxamer 407 met the desired criteria of a Z-Average between 100 and 500 nm, a PDI not more than 0.25 and a ZP of at least 20 mV while this did not apply for the most approaches with PVA or SDS. Since Poloxamer molecules both include hydrophilic and hydrophobic segments this effectively prevents aggregation due to steric hindrance [132].

Regarding the solvent : non-solvent ratio, only Poloxamer 407 at 1 : 5 and 1 : 10 ratios did not cause visible agglomeration after 24 h. A possible explanation for the instability of the 1 : 2 ratio may be that celecoxib and Eudragit E 100 precipitation continued after preparation due to delayed evaporation of remaining ethyl acetate. Without agitation this can provoke coalescence of solvent droplets leading to formation of larger particles and finally agglomeration [21]. From current literature concerning preparation of polymeric NPs, with both emulsification-diffusion and nanoprecipitation technique, it is known that the use of higher concentrations of API/polymer in smaller amounts of organic solvent is more common than vice versa and that the preparation of suitable nanosuspensions generally requires a high degree of supersaturation [28].

The smallest particles were obtained if using a 1 : 5 solvent : non-solvent ratio (see Table 19). A possible explanation is that lower amounts of organic solvent result in precipitation of API and polymer immediately after mixing. If this occurs before the formation of a homogeneous nanoemulsion, the NP size can be influenced since deposition on already existing nuclei is

thermodynamically favoured [90]. Further explanations deliver the findings from Deng et al. who prepared paclitaxel nanocrystals stabilized by Poloxamer 407 [30]. They found that, at higher concentration, Poloxamer 407 can form micelles which pull Poloxamer molecules off the NP surface and therefore lead to reduced stability and larger size. Due to the low particle size, an adequate PDI and the relatively higher API content, the 1 : 5 solvent : non-solvent ratio was used in further experiments.

Concerning the Eudragit E 100 concentration, the use of 10 instead of 5 mg/mL in the solvent phase increased the NP size (about 50 nm for the 1 : 5 solvent : non-solvent ratio) at constant PDI. Though, the EE values were consistently higher, which, according to literature, can be explained by an increase in organic phase viscosity due to higher polymer content. Higher viscosity might, in turn, reduce drug partitioning to the aqueous phase [39]. In consideration of the molar masses of celecoxib (≈ 380 Da) and Eudragit E monomers (≈ 400 Da) the higher Eudragit E : celecoxib ratio leads to a molar excess of Eudragit E. This enables the complete molecular complexation of celecoxib with Eudragit E (see Figure 60). Thus, it was given preference to a Eudragit E 100 concentration of 10 mg/mL in the solvent phase.

Type and concentration of stabilizers are known to play an essential role to inhibit crystal growth, which would cause instability of nanosuspensions [56]. Electrostatic stabilization depends on an interaction between repulsive electrostatic forces and attractive van-der-Waals forces, the so-called DLVO forces [31,158]. The charge on the particle surface provokes the formation of an electrostatic double-layer in the direct environment of the particles, which results in the zeta potential (see chapter 1.4.2). Ideally, a sufficiently high ZP avoids approximation of the particles and prevents agglomeration. The use of ionic surfactants and polymers is regarded to be the most effective way to stabilize NP dispersions [151].

Since the system of combined stabilization (Eudragit E 100 and Poloxamer 407) proved to be suitable for the production of celecoxib NPs, the influence of the stabilizer concentration was examined in the next step (see chapter 3.1.1.2). It is in good agreement with literature data that the NP diameter tends to decrease with increasing Poloxamer concentration (see

Figure 28 (a) [64]. Higher concentrations of stabilizer molecules will more effectively protect the creating nuclei from agglomeration. This likewise explains the decrease of the PDI, i.e. the higher homogeneity of the NPs.

However, an increase from 2.5 mg/mL to higher concentrations of Poloxamer 407 did not lead to further improvement of PDI or decline of size. Additionally, at these concentrations the ZP values were lower. Thus, it can be assumed that an optimal arrangement of Eudragit E 100 and Poloxamer 407 molecules on the NP surface is achieved between 1 and 2.5 mg/mL Poloxamer 407 concentration in the non-solvent phase leading to the lowest size at adequate PDI and ZP.

Figure 60 (a) depicts a schematic of the NPs according to the assumed model. Hence, the NP surface is positively charged due to the tertiary amino groups of Eudragit E 100, which are protonated at neutral or acidic pH [82]. Dissolved Poloxamer 407 molecules act as steric stabilizer. The combination of non-ionic with ionic stabilizers is regarded to be more effective than ionic or non-ionic stabilization alone. This is due to inclusion of non-ionic between ionic stabilizer molecules, which reduces self-repulsion and therefore facilitates a more suitable arrangement on the NP surface [164]. Celecoxib molecules form complexes (ionic interaction) with Eudragit E molecules. This is facilitated by the protonated tertiary amino groups of Eudragit E and the deprotonated sulfone amide groups of celecoxib (Figure 60 (b), chemical equation shown in Figure 61). Figure 60 (c) shows the aromatic (celecoxib) and aliphatic (Eudragit E and Poloxamer 407) hydrophobic domains of the molecules. Hence, hydrophobic interactions are possible between all involved molecules. These interactions are much weaker than electrostatic interactions [8]. In case of the bonding between Eudragit E and Poloxamer 407 it is the sole interaction. In-vivo the hydrophobic domain and the rigid ring structure of celecoxib advise an interaction with bile salts (solubilization in the duodenum) [10]. Further results (DSC and IR, see chapters 3.2.1 and 3.2.2 and discussion below) reinforce this model in case of the NPs prepared with emulsification-diffusion technique. However, these methods indicate different chemical interactions in the NPs, which were prepared using the nanoprecipitation technique.

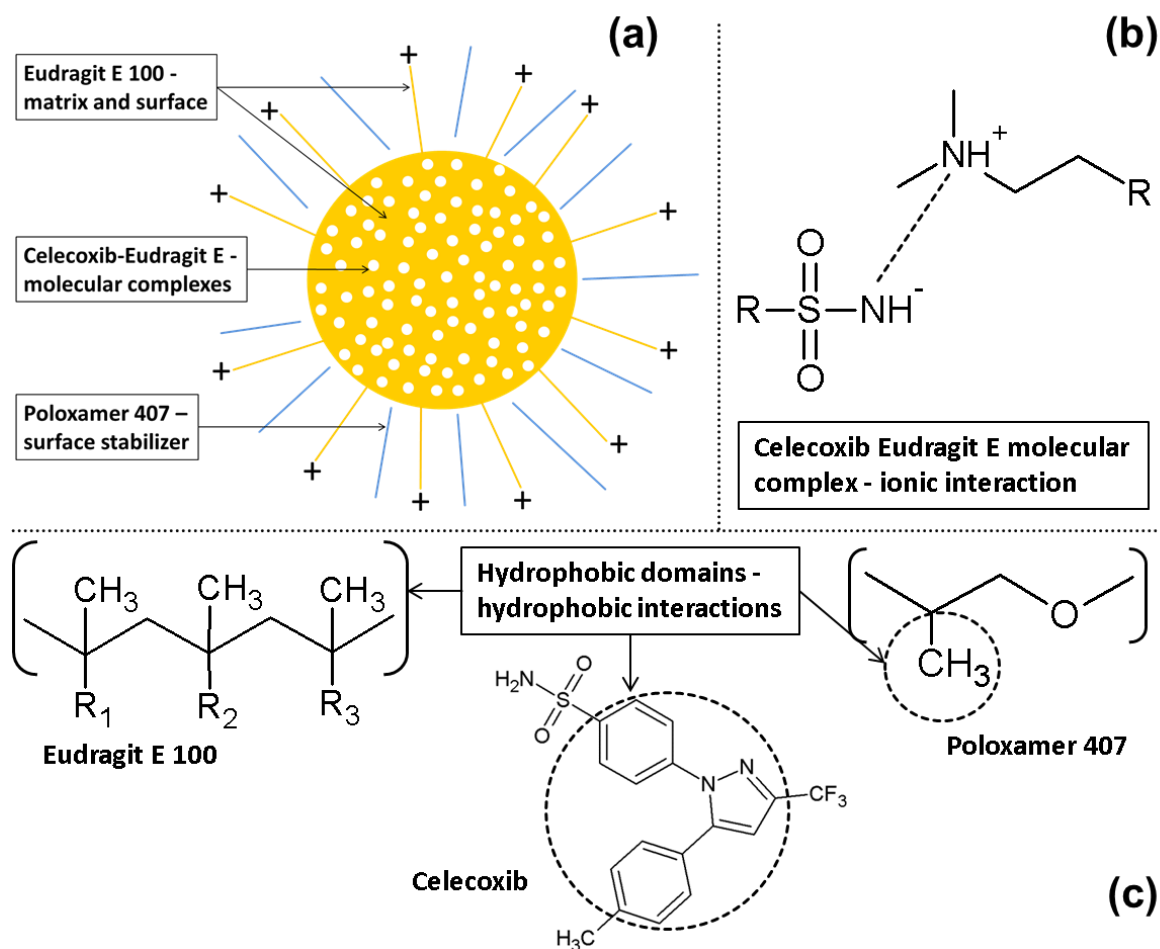


Figure 60: (a) Schematic of a celecoxib-Eudragit E 100-NP in aqueous suspension co-stabilized by Poloxamer 407: Celecoxib (white spheres) molecular complexes embedded in a matrix of Eudragit E 100 (orange sphere). Surface charge is positive due to protonated Eudragit molecules (orange lines). Poloxamer 407 (blue lines) molecules contribute to stabilization by inclusion between Eudragit molecules. (b) Molecular complex of celecoxib and Eudragit E 100, dotted line shows ionic interaction. (c) Hydrophobic domains (dotted circles) of Eudragit, Poloxamer and celecoxib molecules.

The EE values (see Figure 28 (b)) decreased over the examined range with increasing Poloxamer 407 concentration. These results show that higher Poloxamer concentrations are accompanied by higher celecoxib concentrations in the supernatant. With regard to the surface-active properties of Poloxamer this is very probably due to enhanced solubilization of celecoxib. Finally, a 2.5 mg/mL Poloxamer 407 concentration in the non-solvent phase is regarded to be optimal. Beyond this point the size and the PDI could not be improved by increasing the concentration, while the EE decreased.

The lowest therapeutic single dose of celecoxib is 50 mg [47]. An EE of 70 % provided (value of the optimized formulation, see above), circa 70 mL of the nanosuspension would be necessary to administer this amount. Thereto, NPs with higher celecoxib and Eudragit E 100 concentrations were prepared (see chapter 3.1.1.3). For each nanosuspension was the absolute value of the ZP sufficiently high (> 30 mV) to ascertain adequate stabilization. According to literature, a ZP value of at least ± 20 mV is convenient, provided that the system is, in combination, electrostatically and sterically stabilized [164].

Though, the pre-defined criteria concerning size and homogeneity (Z-Average < 500 nm and PDI < 0.25) were not met if using a celecoxib concentration in the solvent phase of 50 mg/mL or more. At higher concentrations the stabilizers were obviously not able to protect the NPs from agglomeration, why these nanosuspensions are inappropriate despite the high EE values. In conclusion, the formulations prepared with 25 mg/mL celecoxib and 50 mg/mL Eudragit E 100 in the solvent phase and 12.5 mg/mL Poloxamer 407 in the non-solvent phase were not equivalent to those prepared with 5 mg/mL celecoxib and 10 mg/mL Eudragit E 100. However, they still fulfil the required criteria regarding size and homogeneity to a particularly high degree (Z-Average ~ 350 nm versus 200 nm, ZP of ~ 36 versus 39 mV and PDI ~ 0.1 versus 0.05) and provide higher EE (85 % versus 72 %).

In a stability study two formulations, one prepared with 5 mg/mL, the other with 25 mg/mL celecoxib in solvent phase, were compared if stored at 5 °C and room temperature, respectively (see chapter 0). In this context, it emerged that the formulation with the higher celecoxib content was superior if it was stored at room temperature. First, both Z-Average and PDI remained constant over a period of 14 d (see Figure 32) while the other samples under test became inhomogeneous after three or four days storage. Analogously, the ZP values changed (see Figure 33). The EE was significantly higher over the complete storage period if more celecoxib and Eudragit E 100 were used independent on the storage temperature (see Figure 34).

Hence, it is to consider that the use of higher API and excipient concentrations in the solvent phase provokes a more intense supersaturation after contact with the non-solvent phase, which is only partially compensated by the use of more surfactant. First of all, this explains the higher EE values obtained at the higher concentration, i.e. higher amounts of celecoxib and Eudragit E 100 precipitate as NPs and smaller amounts are dissolved in the surrounding liquid (determined as concentration in the supernatant). This has two consequences: First, it is desirable to achieve high EE values to increase the yield of nanoparticulate API. Second, higher concentrations of dissolved API/excipient are accompanied by higher probability of delayed and therefore uncontrolled precipitation.

Concerning the storage conditions room temperature was more advantageous than 5 °C. While there was no significant change in the Z-Average over the complete period the PDI values of the approaches stored at 5 °C increased after day three compared to room temperature. This may be caused by crystallization, which, as an exothermic process, is enhanced at lower temperatures. After 28 d at every sample sharp needles appeared on the interior wall of the container, while the liquid was clear. This was attributed to crystallization. The storage temperature had no apparent influence on ZP and EE.

Since, as mentioned above, the highest possible API concentration is preferred and due to better stability, was the optimization of the NP preparation with MJR technology based on the higher-concentrated composition of API and excipients. Thereby, implementing DoE, NPs in size range from 300 to 450 nm of narrow size distribution ($PDI < 0.25$) could be produced. The ZP and EE values were very similar to those obtained from NPs prepared with the BT procedure. The DoE equation (20), which implements three MJR variables (temperature, nitrogen pressure and flow rate), provided a good correlation. The calibration function (see Figure 37), which was obtained by comparing the measured Z-Average values of certain NP preparations to the corresponding predicted values, likewise has a good correlation of approximately 0.88. Additionally, there was no obvious trend concerning deviation of the single values. Thus, the developed model proved

to be appropriate for the fast and controlled manufacture of celecoxib NPs in different size ranges.

As an alternative to emulsification-diffusion technique, NPs were prepared by the nanoprecipitation technique. However, these NPs were not equivalent to those prepared by emulsification-diffusion. First, their size distribution was broader being demonstrated by higher PDI values, which failed to meet the criterion to be lower than 0.25. Additionally, lower ZP values (~ 35 mV versus ~ 45 mV) indicated worse stability. Concerning the EE, equivalent values were obtained if using a pump rotational speed of 300 : 1500 rpm (solvent : non-solvent), while a 1200 : 6000 rpm ratio mainly led to significantly lower values. Thus, this setting was obviously inappropriate to generate adequate mixing conditions in the reactor chamber. Additionally, NPs were produced by the nanoprecipitation technique with an alternative method (see chapter 2.2.1.2). Hence, the non-solvent phase was water without addition of a surfactant and HPLC pumps with lower flow rates were used. With this setup NPs of diameters from approximately 80–200 nm (Z-Average), PDI values below 0.15 and ZP values from circa 40–60 mV were obtained (see chapter 3.3.1 and Figure 68 (a)). These NPs had a spherical shape, which was shown by SEM (see Figure 48) and AFM (see Figure 49). The related nanosuspensions were stable over at least one month. However, this method did not allow a reproducible production of NPs of different sizes.

In general, it is to consider that, concerning a comparison between nanoprecipitation and emulsification-diffusion method, a reliable statement cannot be made since a full experimental design was not performed. However, it can be concluded that nanoprecipitation is a suitable alternative for preparation of celecoxib-Eudragit E 100-NPs but the controlled manufacture of different sizes would require further experiments.

The obtained DSC curves (see chapter 3.2.1) provide an insight into the thermal behavior of the NP components. Furthermore, they reveal differences between the NPs and the blend of their components. Celecoxib is a crystalline substance with a defined melting point T_m . From Figure 40 this

value was determined to 164 °C as minimum of the endothermic peak, which correlates well with the literature value of 162 °C [5]).

As a polymeric substance Eudragit E has no crystalline structure and, therefore, a glass transition range instead of a defined melting point. From the Eudragit E DSC trace the glass transition temperature T_g was determined to 45 °C. This is likewise in good agreement with the literature value of 48 °C [136]. The endothermic peak, which follows the glass transition range, may be due to enthalpy relaxation. This is a typical phenomenon, which arises from the fact that amorphous substances change their structure time-dependent if they are stored below T_g to attain a thermodynamic equilibrium [113]. The respective sample was manufactured approximately three years before measurement.

In the curve of the physical mixture with Eudragit E 100 T_g was shifted to a slightly lower value (42 °C). It is known that drug molecules can impede intermolecular interactions leading to lower T_g , if they are located between polymer chains, [5]. The melting peak of celecoxib was significantly broadened indicating the presence of amorphous celecoxib, i.e. a solid dispersion [27,137].

While this peak was further broadened and appeared at lower temperature in case of the NPs prepared by nanoprecipitation it disappeared at NPs prepared by emulsification-diffusion. This indicates that, in first case, a solid dispersion with crystalline portion of celecoxib was formed while, in the second case, celecoxib mainly exists in amorphous form.

In combination with the fact that T_g of Eudragit E was circa 8 °C lower, these findings clearly indicate that, in both cases, the API molecules are embedded in a matrix of the excipient as postulated above (see Figure 60). Furthermore, the possibility to produce solid dispersions of celecoxib in Eudragit E has already been shown [5].

Concerning the IR measurements (see chapter 3.2.2) it can first be stated that ionization of celecoxib and Eudragit E 100 led to substantial changes in the spectra. At celecoxib sodium the sulfone amide is deprotonated, which is clearly recognizable from the missing SO_2 and NH signals. Additionally, the

CF₃ bands were missing and out-of-plane vibrations were significantly reduced. This may be attributed to distribution of the free electron over the π -system of the molecule.

If the tertiary amino function of Eudragit E 100 was protonated, the doublet signals being related to nitrogen bonds (N–CH₃ and C–H vibrations) coalesced. Contrary to celecoxib the molecule provides no mesomeric system and further substantial changes, especially regarding the carbonyl and ester signals, were missing.

Concerning the NP samples it was evident that those prepared with ethyl acetate (emulsification-diffusion technique) were very similar to the blend of the charged compounds while the opposite was the case for those prepared with methanol (nanoprecipitation technique). In addition to the obtained DSC results (see above) this confirms the assumption that NPs produced by emulsification-diffusion are entirely amorphous while the others are partially crystalline. This can possibly be explained by polarity differences between the two solvents. Methanol, as a protic solvent, can be a competitor to the very weak acid celecoxib as a proton donor. Consequently, less celecoxib would be ionized, which is prerequisite for dissolution in the Eudragit E 100 matrix. In contrast, ethyl acetate, as an aprotic solvent, has no influence on the acid-base reaction between celecoxib and Eudragit E 100.

Finally, SEM imaging revealed that most of the produced NPs were of spherical shape (see chapters 3.2.3 and 3.2.4). This is advantageous since the dissolution rate of spherical particles is increased towards equal-sized particles of irregular shape [94]. Furthermore, they have in solid form more favourable flow properties due to the relatively lower surface area and consequently lower cohesive forces between the particles. This, in turn, ensures more uniform packing and, therefore, increased dose uniformity [62]. Slight deviations from spherical shape appeared at NPs, which were prepared by nanoprecipitation. This is in agreement with the findings obtained from DSC and IR, which indicated a partially crystalline structure of these NPs. Furthermore, size and uniformity of spherical NPs can reliably be determined by non-imaging techniques like DLS [12]. This was corroborated

by a good correlation between the NP diameters, which were determined with DLS and SEM (see Table 16).

4.2 Dissolution testing

The FDA database of dissolution methods [154] recommends two types of media for the dissolution test of celecoxib capsules. The first is 1000 mL of a 0.04 M tribasic sodium phosphate buffer (pH 12) containing 1 % SDS as a tier 1 medium. Alternatively, a tier 2 medium can be used. Thereto, the dissolution test is started in 750 mL of simulated gastric fluid (USP) including pepsin. After 20 min 180 mL of a SDS solution is added to reach a final concentration of 1 % SDS, followed by circa 70 mL of 1.2 M NaOH to adjust the pH to 12. The sampling points are at 10, 20, 30, 45 and 60 min. The selection of these media relies on the fact that celecoxib is, as a weak acid, soluble in strong alkalis and that the usage of surfactants can enhance the solubility.

However, a basic or neutral medium is not applicable for the dissolution of celecoxib-Eudragit E 100-NPs since Eudragit E is intended to be dissolved in gastric fluid up to pH 5.0 [40]. Dissolution media of basic or neutral pH would inhibit the disintegration of the Eudragit E 100 matrix and, consequently, the release of celecoxib. Thus, the dissolution behavior in diluted HCl without any surfactant was examined first. As the stomach is the intended dissolution site for the NPs in-vivo, the pH was adjusted to 1.2. This value is recommended by the FDA to simulate gastric fluid [153].

The dissolution profile obtained with this medium showed an uncommon course (see Figure 50). Usually the API concentration reaches a maximum at a certain timepoint that either corresponds to 100 % dissolution or the saturation solubility of the analyte. Then, this value remains constant until the end of the test. A curve progression showing a maximum followed by a decline indicates that dissolved API precipitates after a certain time span. This circumstance was confirmed by taking a SEM image of the same nanosuspension after 24 h incubation in HCl pH 1.2. Thereby, microparticles of non-spherical shape appeared. The same observation has been made by Albers et al. [2].

These findings can be explained if considering the specific structure of the NPs (see Figure 60). Since the API (celecoxib) is embedded in a matrix of

the excipient (Eudragit E 100) the presence of a so-called solid dispersion can be presumed. A plethora of publications exists in this field while Craig (2002) [27] has reviewed the release mechanisms of drugs out of solid dispersions in detail. Hence, there exist two mechanisms: carrier-controlled and drug-controlled dissolution. Both mechanisms implement a layer around the particles that is rich of dissolved polymer (matrix material) and has to be passed by the drug. How this occurs in detail depends on the viscosity of the polymer-rich layer which itself is controlled by the polymer concentration. At carrier-controlled dissolution the time for the particles to be released into the medium is insufficient. Therefore, dissolution of the drug in the polymer-rich layer is provoked. Here, diffusion through this layer is the rate-determining step and can be described by the Stokes-Einstein equation (5). In contrast, at drug-controlled dissolution, the drug particles dissolve comparatively slow in the polymer layer and reach the medium mainly intact. In this case, the dissolution process is determined by the physicochemical properties of the drug like, for instance, the particle size.

Which of these mechanisms dominates in the present system cannot be postulated with utmost certainty. Dubois and Ford (1985) [35] examined the dissolution rates of ten drugs as solid dispersions in PEG 6000 using the rotating disc methodology. Their results indicate that carrier-controlled dissolution might only occur up to a certain drug-polymer ratio. On this basis one may assume that drug-controlled dissolution is the favored mechanism in the present system. However, as even the initial particle size is in nanometer range, this is not necessarily an obstacle for fast and effective release of the API.

Albers et al. (2009) [5] produced different hot-melt extrudates, also consisting of celecoxib and a polymethacrylate carrier. They, inter alia, performed dissolution experiments in 0.1 M HCl and measured for one formulation after 5 min an API release being 58-fold higher than the saturation solubility at this pH. Though, they observed thereafter a distinct decline within a few minutes. This resembles the obtained results (see Figure 50) and can be explained by the fact that the solubility of amorphous substances is higher than that of the corresponding crystalline form due to their lower thermodynamic stability.

However, when the amorphous drug gets into contact with the dissolution medium two processes start: on one hand the dissolution, but on the other hand crystallization of the API as this is the thermodynamically preferred form. Therefore, recrystallization of dissolved API can lead to a decline of the measured concentration [5].

Since 100 % dissolution was not obtained if using diluted HCl the next issue was to achieve complete dissolution of celecoxib and to inhibit recrystallization. Therefore, it is commonly recommended to provide sink conditions [153]. In USP chapter <1092> sink conditions are defined as “the volume of medium at least three times that required in order to form a saturated solution of drug substance” [150]. The used nanosuspension volume for the previous dissolution tests contained a celecoxib amount of nearly ten-fold above the saturation solubility at pH 1 (3.15 mg/L) [4].

In general, there are two approaches to counter this issue: first, one can increase the volume of dissolution medium to a level that grants sink conditions. However, it is to consider that API amounts used for dissolution tests should reflect a single therapeutic dose. Consequently this would necessitate a medium volume of at least 17 L which is hardly feasible in practice. The second approach is to add substances being able to enhance the API solubility which would allow keeping the medium volume lower.

Different research groups have shown that electrolytes can improve dissolution of complexes consisting of Eudragit E and anionic drugs [77,120]. Quinteros et al. (2008) [120] titrated several such complexes with a NaCl solution and plotted the pH value against the time. They mainly attributed the occurring pH shift to an exchange of the deprotonated acid, i.e. the API, by a chloride ion. Then, the acid withdraws the proton from Eudragit leading to an increase in pH. Taking the example of a system of celecoxib and Eudragit E this process is described in the chemical equations below (see Figure 61). Since both the chloride of Eudragit E and the sodium salt of celecoxib are well water-soluble this is favorable for dissolution.



Figure 61: Equations of the reaction of celecoxib-Eudragit E complex with NaCl leading to exchange of deprotonated celecoxib by a chloride ion (a) followed by protonation of celecoxib (b) (Cel = celecoxib and EU = Eudragit E).

Kindermann et al. (2011) [77] performed dissolution studies of hot-melt extruded complexes of naproxen and Eudragit E. As dissolution medium they added different electrolytes in various concentrations to a 0.001 % aqueous solution of polysorbate 20. After electrolyte addition the dissolution rate increased depending on type and concentration of the electrolyte, while a 0.15 M NaCl solution was found to be most suitable.

The addition of NaCl in this concentration to the medium was proven to be beneficial for both rate and degree of dissolution. Though, even if 100 % dissolution were obtained, this value could not be maintained and a concentration decline occurred, which was even more intense than with diluted HCl alone (see Figure 52). Here, it must be kept in mind that the concentration of dissolved API is at maximum about ten-fold higher than its saturation solubility. In summary, this means that electrolyte addition can be used to increase the dissolution rate of polyelectrolyte complexes but is not appropriate to improve the solubility. This meets the results obtained from Kindermann et al. who observed that the dissolution process of naproxen, even in presence of electrolytes, stopped in its saturation solubility [77].

Since electrolyte addition to the medium was not sufficient to achieve a satisfactory dissolution profile it was necessary to search for an appropriate alternative. In pharmaceutical dissolution testing, surfactants are extensively used to improve dissolution profiles of sparingly water-soluble APIs [12,139,153]. Bates et al. discussed in 1966 that addition of surfactants to the dissolution medium enhances the saturation solubility and, therefore, the dissolution rate [12]. This is due to the fact that this rate, according to the Noyes-Whitney equation (15), linearly depends on the saturation solubility. This effect is caused by two mechanisms: first, surfactants decrease the

interfacial tension between API and dissolution medium, second, the API can be solubilized within micelles. Naturally, the latter mechanism is only relevant if surfactants are used in a concentration above the CMC, i.e. the point from which micelles are formed to a significant extent. If solubilization in micelles occurs, Bates et al. consider this to play the major role [12].

The compendial dissolution method for Celebrex[®] capsules involves the usage of 1 % SDS [154], which is a wide-spread and well-suitable additive to dissolution media [139]. However, this surfactant may not be suitable for drug release out of a Eudragit E matrix as cationic Eudragit E could possibly interact with anionic SDS. Thus, a cationic or non-ionic surfactant would be recommendable. Since Albers et al. (see above) performed dissolution studies of extrudates also consisting of celecoxib and Eudragit E, it was decided to utilize cetrimide (see Figure 62). This is a cationic surfactant which was added to 0.1 M HCl to ascertain sink conditions (solubility of celecoxib in HCl pH 1.2 + 0.3 % cetrimide: 254.19 mg/L) [5].

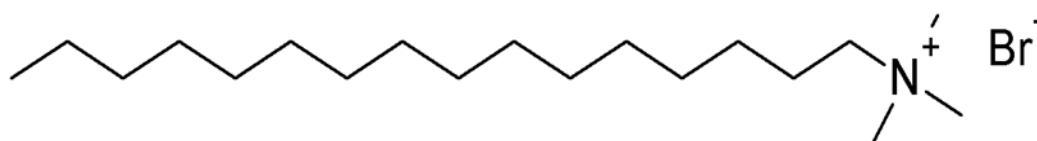


Figure 62: Structure of cetrimide.

First, the use of cetrimide did, regardless of the concentration, not have the expected effect of fast and complete dissolution of the API. If cetrimide concentration was in a range, which cannot provide sink conditions, a decline after a certain time occurred as already observed (see Figure 50 and Figure 53). This decline did not appear at higher concentrations of cetrimide where sink conditions are given. This can be explained by the fact, that solubility enhancement due to nanoscaling may not be sufficient to have a decisive influence on saturation solubility in the present case. However, it is contradictory that the dissolution rate decreases with increasing surfactant concentration. This can possibly be explained if considering the mechanisms of solubility and dissolution rate enhancement of surfactants (see above). Hence, Bates et al. consider solubilization within micelles to be of essential importance besides the reduction of interfacial tension [12].

At 30 °C cetrimide forms micelles with an aggregation number of 75-120 [19]. Shanthy et al. determined the CMC of cetrimide in water to 3.88 mM at ambient temperature [140], which corresponds to a concentration of 1.4 mg/mL respectively 0.14 % (m/V). As the formation of micelles is a thermodynamic process this value will not be the same at 37 °C, which is standard temperature in dissolution experiments of most dosage forms. Results from Perger et al., who measured micellization of different alkyl ammonium halogenides, show that CMC decreases with increasing temperature [114]. Moreover, this effect is augmented at higher alkyl chain length. However, even though a substance with a chain length of 16 C atoms like cetrimide was not included in that study, it can be assumed based on those results that the respective values for cetrimide at 25 and 37 °C will not deviate substantially from each other. In conclusion, this means that the presence of micelles can be expected at cetrimide concentrations of 0.3 % (m/V) or more. To investigate the presence of micelles two dissolution media, HCl pH 1.2 + 0.05 % cetrimide and HCl pH 1.2 + 0.3 % cetrimide, were examined by DLS. Thereby, structures of approximately 5 nm diameter (Peak 1, 100 % volume) were detected at the higher cetrimide concentration (> CMC) while this peak had a considerably smaller proportion (Peak 2, 0.7 % volume) at the lower concentration (< CMC) (see Figure 71, appendix). According to literature micelles usually have a diameter of 5–15 nm [90].

Furthermore, it is known from literature that it is feasible to separate micelles from the surrounding liquid with cross-flow filtration modules [115]. According to the specification are particles up to a size of 10 nm retained by the used 100 kDa CF module, which is an approximate value and very near to the measured micelle size. As discussed above it can be assumed that the majority of celecoxib molecules are solubilized within micelles if these are available. In this context, the unexpected slow dissolution rate obtained at higher cetrimide concentrations is probably due to retention of micelles containing the API. Since pharmaceutical dissolution tests generally implement the usage of syringe filter holders with much larger pore sizes (0.45 µm or, more rarely, 0.1 µm) this issue has no greater relevance for the current compendial methodologies.

Thus, dissolution tests were performed to compare the used CF module to one of larger pore size and to conventional syringe filter holders. The results, which were obtained using filters of higher pore size (see Figure 54), clearly indicate that micelle formation prevented the passage of celecoxib across the membrane if the dissolution medium contained higher amounts of surfactant. Additionally, in contrast to previous tests, the concentration of dissolved API did not decline throughout the complete experiment. Thus, the FDA recommendation for immediate release dosage forms to reach at least 85 % dissolution after 60 min was fulfilled [153]. However, precise comparison of different dissolution profiles requires at least two points below 85 % release [93].

With a dissolution medium containing 0.05 % cetrimide instead of 0.3 % the initial increase was slower with several sampling points below 85 % release (see Figure 55). However, it cannot be proclaimed with certainty that this is due to slower dissolution of NPs but maybe to insufficient solubilization of celecoxib. If considering, that size-dependent differences of the dissolution behavior of different NP batches shall be examined in the latter course, this may restrict the suitability of the method. Thereto, it should be searched for an alternative dissolution medium. The influence of physicochemical factors like pH, ionic strength or surfactant has been discussed above. Apart from that, physical factors like temperature and mechanical agitation likewise play a role. While it is uncommon to choose another temperature than 37 °C, the agitation rate can be matter of variation. In conventional USP apparatus 1 or 2 applications this would be the shaft rotational speed. In the present system, the agitation depends on the stirring rate of the magnetic bar and the flow rate of the peristaltic pump. However, although it is commonly known that agitation has a deep impact on drug dissolution, it is to consider that this is rather due to variation of dosage form disintegration than to API dissolution rate [72]. Since, nanosuspensions were directly applied to dissolution test without being previously converted to a dosage form like tablets or capsules, agitation is not regarded to have a decisive influence on the dissolution rate. Thus, it was decided to vary the medium pH and the effect of different phosphate buffers containing 0.3 % cetrimide was investigated.

Thereby, the dissolution rate decreased with increasing pH value. Solely at pH 2.0 85 % of API release were reached after 60 min (see Figure 56). Furthermore, this value is comparable to the pH of the stomach (fasted state between pH 1 and pH 3 [3]) as the intended in-vivo site of dissolution of the NPs. Thus, this medium was used to compare the release behavior of NPs of different size. However, since the dissolution was relatively slow from the first sampling point at 3 min to the last at 60 min it was decided to collect additional samples at earlier points, while some of the latter points can be waived.

Using the FDA model independent approach potential (see chapter 3.3.2) differences regarding the dissolution behavior of NPs of different size could not be detected using the developed methodology. Hence, it is first to consider that the analysis occurred with a delay due to the sampling procedure. In-situ techniques allow contemporary detection of the analyte concentration and can eliminate potential mistakes occurring at sampling. For instance, Sarnes et al., conducted dissolution experiments of differently sized indomethacin nanocrystals using a channel flow method with continuous UV-spectroscopic data acquisition [132]. Hence, they detected significant differences if the NP size varied in the range of a few hundred nanometers. Another explanation for the lack of discriminative power may be the choice of the medium. It is theoretically possible that the use of other surfactants would enable discrimination. Though, the difference between all nanoparticulate samples and the unprocessed API is very pronounced giving evidence of the superior release properties of the NPs.

The second evaluation (see chapter 3.3.2), which included semilogarithmic plots to obtain k-values of the dissolution process, additionally revealed slight differences between, on one hand, NPs with a diameter of approximately 220 nm ($k = 0.124 \pm 0.041$), 250 nm ($k = 0.138 \pm 0.01$) and 500 nm ($k = 0.117 \pm 0.006$) and, on the other hand, NPs of approximately 300 nm ($k = 0.059 \pm 0.01$) and 350 nm ($k = 0.087 \pm 0.024$). Hence, it seems to be contradictory that the k-value of the largest NPs is increased towards the smaller ones. This may be explained by the degradation mechanism of the NP. In Figure 60 two different possibilities of polymer NP degradation are

schematically depicted. The first is a continuous surface erosion of the NP, the second starts with a disintegration of the NP in several fragments, which is followed by surface erosion of these fragments. The second mechanism might lead to a burst release of celecoxib molecules within a low time span (<1 min), which is in good agreement with the experimental results. Structural differences of differently-sized NPs may either hinder or promote the disintegration process. Thus, the results indicate that the effective release does not linearly depend on the particle size.

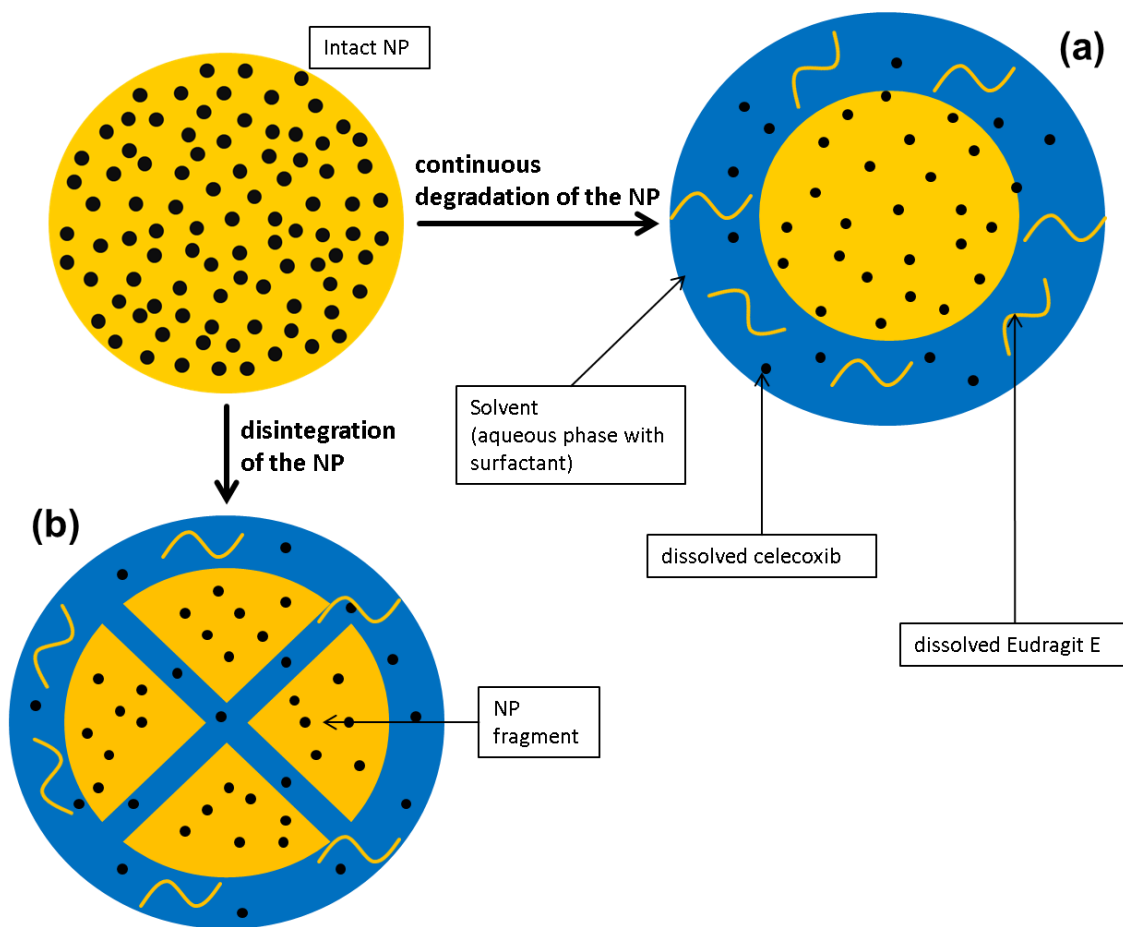


Figure 63: Schematic of two theoretical degradation pathways of celecoxib-Eudragit E 100-NPs. (a) continuous surface erosion of the NP in the dissolution liquid with release of dissolved celecoxib and Eudragit E 100 and (b) disintegration of the NP in several fragments followed by erosion of these fragments.

5 Summary

In the present study celecoxib nanoparticles (NPs) were produced using both a bench-top and a MicroJetReactor approach. They were used as a model to examine differences in the dissolution behavior of differently-sized NPs. As production technique emulsification-diffusion was chosen, a method, which has already been successfully applied to produce celecoxib NPs [33]. In preliminary studies it was first tried to produce nanocrystals, i.e. NPs consisting of the active pharmaceutical ingredient (API) and one or more stabilizing agents. Thereto, solutions of celecoxib in ethyl acetate were mixed with aqueous solutions of different stabilizers. As it was not feasible to yield stable nanosuspensions, polymeric NPs instead of nanocrystals were produced. Thereto, the polymer Eudragit E 100 was chosen as matrix and electrostatic stabilizer, a combination which has already been utilized for the preparation of microparticles by hot-melt extrusion [5]. Additionally, aqueous solutions of different steric stabilizers (Poloxamer 407, polyvinyl alcohol and sodium dodecyl sulfate) were employed in the production as non-solvent phase while Poloxamer 407 evolved to be the most suitable candidate. The Poloxamer 407 concentration was optimized and the concentration of celecoxib/Eudragit E 100 in the solvent phase increased. Hence, if using 25 mg/mL celecoxib, 50 mg/mL Eudragit E 100 in the solvent phase and a 12.5 mg/mL aqueous solution of Poloxamer 407 as non-solvent phase, NPs with a Z-Average of circa 350 ± 6 nm, a zeta potential (ZP) of 36 ± 0.3 mV, a polydispersity index (PDI) of 0.09 and an entrapment efficiency (EE) of 85.3 ± 2.6 % were yielded. This formulation was shown to be stable regarding size and -distribution, ZP and EE for 14 d at ambient temperature.

This optimized composition of API and excipients was transferred to MicroJetReactor (MJR) preparation. Design of experiments (DoE) was applied to investigate the influence of temperature, nitrogen pressure and pump rotational speed, i.e. solvent : non-solvent flow rate, on the NP size. By this means, NPs in a size range from 300 nm to 450 nm of narrow size distribution (PDI < 0.25) were produced. Additionally, the emulsification-diffusion technique was compared to the nanoprecipitation technique by

using methanol as solvent. However, these NPs were not equivalent to those prepared by emulsification-diffusion since their PDI was higher and the ZP lower.

The NP characterization was performed by dynamic light scattering (→DLS) (size, -distribution and ZP), high performance liquid chromatography with UV-Vis detection (HPLC-UV) (→EE), differential scanning calorimetry (DSC) and infrared spectroscopy (IR) (→structure) as well as scanning electron microscopy (SEM) and atomic force microscopy (AFM) (→size and shape).

To characterize the NP formulation by dissolution testing (second part of the thesis), the ability of cross-flow filtration (CF) modules to retain NPs was successfully tested by comparative DLS- and UV-Vis-measurements of both the nanosuspension and the filtrate. Further, the flow velocities in the developed dissolution apparatus were examined. Hence, the whole volume of dissolution medium passed the CF module in less than one minute and the dead time of liquid to reach the filtrate outlet was only 12.7 ± 0.6 s.

As an alternative with higher ease in performance compared to HPLC, a UV-Vis-spectroscopic method was developed which facilitates the quantification of celecoxib in the presence of Eudragit E 100 and Poloxamer 407. The next step was the screening for a suitable dissolution medium which on one hand grants complete dissolution of the NPs and on the other hand enables discriminative properties between the dissolution profiles of differently-sized NPs. As first medium hydrochloric acid of pH 1.2 was chosen due to the solubility of Eudragit E at acidic pH and the intended site of dissolution in-vivo (stomach in fasted state). Since diluted HCl without additive did not facilitate the complete dissolution, sodium chloride was added to the medium. Thereby, celecoxib was completely dissolved but precipitated again after 12 min. This concentration decline was attributed to recrystallization, which was confirmed by SEM imaging. Thus, different concentrations of a surfactant (cetrimide) were added to the medium. Though, at higher concentrations the dissolution rate decreased which can be explained by the fact that micelles containing celecoxib, are retained by the CF module. To counter this issue CF modules of different pore size and, for comparison, a dead-end filter, were examined at cetrimide concentrations of 0.05 % and

0.3 % (m/v) in the dissolution medium, respectively. Hence, if 0.3 % of cetrimide was used, more than 95 % of celecoxib were dissolved within three minutes. With 0.05 % of cetrimide, the dissolution stopped slightly below 90 %. Thus, this medium was not considered to be suitable. To be able to compare dissolution profiles of NPs of different size, the effect of phosphate buffers of different pH values containing 0.3 % cetrimide was examined. Hence, using a pH 2.0 buffer, 85 % of the API was dissolved after 60 min, while the release at the higher pH values stopped at lower values. Since a high extent of dissolution was favored and as the stomach pH (site of in-vivo-dissolution) is in fasted state between 1 and 3 [3], this medium was chosen for comparison of the different NP sizes.

In detail, the dissolution behavior of NPs of five different sizes between approximately 220 nm and 500 nm and unprocessed celecoxib particles ($\sim 22 \mu\text{m}$ \rightarrow volume-weighted median diameter determined by laser light diffraction) was investigated. The statistical evaluation, which was performed according to the FDA guideline (model independent approach) [153], did not find a significant distinction between the NP samples, while the dissolution rate of unprocessed particles was significantly slower. Though, a second evaluation, including semilogarithmic plots of the release, revealed differences between the dissolution rates of the NP samples.

In future, the prepared NPs can be part of solid dosage forms like tablets or capsules. Due to their significantly higher dissolution rate towards microscale API, an increased bioavailability can be assumed. Furthermore, the complexation of the API with the polymer positively impacts the dissolution properties, which is an advantage compared to pure API NPs. Concerning the dissolution testing, the adoption of CF can be a well-promising approach. For instance, CF modules could be installed into automatic sampling devices. To reduce the experimental effort and to obtain more detailed dissolution profiles the filtrate could be continuously measured using flow-through analytical systems. Hence, it is to consider that, if surfactants are added above their critical micellar concentration (CMC) to the medium, the filter pore size must be large enough. This may be a restriction since very small NPs could be excluded from determination by this methodology. Though, in

summary, the CF technique is a robust, less cost-intensive approach with high ease in performance that excludes the risk of filter clogging. In this context, the findings of this study can serve as a basis for the development of devices being suitable for the routine testing of nanoparticulate dosage forms.

6 Zusammenfassung

In der vorliegenden Arbeit wurden Celecoxib-NP (NP), sowohl mittels eines Bench-Top- als auch eines Mikrojetreaktorverfahrens, hergestellt. Diese dienen als ein Modell um Unterschiede im Freisetzungsverhalten verschieden großer NP zu untersuchen. Als Produktionstechnik wurde die Emulgierungsdiffusionsmethode verwendet, welche bereits erfolgreich eingesetzt wurde um Celecoxib-NP herzustellen [5]. In vorangegangenen Versuchen wurde zunächst versucht Nanokristalle herzustellen, welche aus einem pharmazeutischen Wirkstoff und einem oder mehreren Stabilisatoren bestehen. Hierzu wurden Lösungen von Celecoxib in Ethylacetat mit wässrigen Lösungen verschiedener Stabilisatoren gemischt. Da es nicht möglich war stabile Nanosuspensionen zu erhalten, wurden statt Nanokristallen Polymer-NP hergestellt. Dazu wurde das Polymer Eudragit E 100 als Matrix und elektrostatischer Stabilisator eingesetzt. Diese Kombination aus Celecoxib und Eudragit E wurde bereits für die Produktion von Mikropartikeln mittels Schmelzextrusion genutzt [2]. Zusätzlich wurden als Antisolvens wässrige Lösungen verschiedener sterischer Stabilisatoren (Poloxamer 407, Polyvinylalkohol und Natriumdodecylsulfat) verwendet, wovon Poloxamer 407 sich als der am meisten geeignete herausstellte. Die Poloxamer 407-Konzentration wurde optimiert und die Konzentration an Celecoxib/Eudragit E 100 in der Solvens-Phase erhöht. Hierbei wurden, bei Konzentrationen von 25 mg/mL celecoxib und 50 mg/mL Eudragit E 100 in der Solvens-Phase und 12,5 mg/mL Poloxamer 407 in der Antisolvens-Phase, NP mit einem Z-Average von etwa 350 ± 6 nm, einem Zetapotenzial (ZP) von $36 \pm 0,3$ mV, einem Polydispersitätsindex (PDI) von 0,09 und einer Einschlusseffizienz (EE) von $85,3 \pm 2,6$ % erhalten. Diese Formulierung erwies sich als stabil für 14 Tage hinsichtlich Größe und Größenverteilung, ZP sowie EE.

Diese optimierte Zusammensetzung von Wirkstoff und Hilfsstoffen wurde auf die Herstellung mittels Mikrojetreaktor (MJR) übertragen. Statistische Versuchsplanung wurde angewendet um den Einfluss von Temperatur, Stickstoffdruck und Pumpenumdrehungsgeschwindigkeit, also

Solvens : Antisolvens-Flussrate, auf die Größe der NP zu untersuchen. Auf diese Weise wurden NP in einem Größenbereich zwischen 300 nm und 450 nm hergestellt, welche zudem eine enge Größenverteilung ($PDI < 0,25$) aufwiesen. Zusätzlich wurde die Emulgierungsdiffusionsmethode mit der Technik der Nanopräzipitation, bei welcher Methanol als Solvens diente, verglichen. Diese NP waren jedoch, aufgrund höheren PDIs und niedrigeren ZPs, denen nicht äquivalent, welche mit der Emulgierungsdiffusionsmethode produziert wurden. Die Charakterisierung der NP erfolgte mit dynamischer Lichtstreuung (DLS) (\rightarrow Größe, Größenverteilung und ZP), Hochleistungsflüssigchromatographie mit UV-Vis-Detektion (HPLC-UV) (\rightarrow EE), Differentialthermoanalyse (DSC) und Infrarotspektroskopie (IR) (\rightarrow Struktur) sowie Rasterelektronenmikroskopie (REM) und Rasterkraftmikroskopie (RKM). (\rightarrow Größe und Gestalt).

Um die NP-Formulierung durch Untersuchung der Wirkstofffreisetzung zu charakterisieren (zweiter Teil der Arbeit), wurden Querstromfiltrations (QF)-Module, hinsichtlich ihrer Eignung NP zurückzuhalten, mit DLS- und UV-Vis-Vergleichsmessungen von Nanosuspension und Filtrat erfolgreich getestet. Des Weiteren wurden die Fließgeschwindigkeiten in dem entwickelten Freisetzungsapparat untersucht. Es zeigte sich, dass das gesamte Volumen des Freisetzungsmediums das QF-Modul in weniger als einer Minute passiert und die Totzeit bis zum Austritt von Flüssigkeit am Filtratauslass lediglich $12,7 \pm 0,6$ s beträgt.

Als eine, im Vergleich zur HPLC einfacher durchführbare, Alternative, wurde eine UV-Vis-spektroskopische Methode entwickelt, welche die Quantifizierung von Celecoxib in Gegenwart von Eudragit E 100 und Poloxamer 407 ermöglicht. Der nächste Schritt war das Screening nach einem geeigneten Freisetzungsmedium, welches zum einen in der Lage ist die NP komplett aufzulösen und es zum anderen ermöglicht Unterschiede im Freisetzungsprofil verschieden großer NP zu erkennen. Als erstes Medium wurde, aufgrund der Löslichkeit von Eudragit E im sauren Milieu sowie des beabsichtigten Ortes der in-vivo-Freisetzung (Magen im nüchternen Zustand), Salzsäure mit einem pH von 1,2 gewählt. Da die verdünnte Salzsäure ohne Zusätze keine komplette Freisetzung bewirkte, wurde

Natriumchlorid zum Medium zugegeben. Dadurch löste sich Celecoxib vollständig, fiel aber nach 12 min wieder aus. Dieses Absinken der Konzentration von gelöstem Celecoxib wurde auf Rekristallisation zurückgeführt, was durch eine REM-Aufnahme bestätigt wurde. Daher wurden dem Medium verschiedene Konzentrationen eines Tensids (Cetrimid) zugefügt. Jedoch sank bei höheren Konzentrationen die Freisetzungsrates, was dadurch erklärt werden kann, dass Mizellen, welche Celecoxib einschließen, vom QF-Modul zurückgehalten werden. Als Lösung hierfür, sowie um einen Vergleich anzustellen, wurden QF-Module mit verschiedenen Porengrößen sowie, zum Vergleich, ein Tiefenfilter, bei Cetrimidkonzentrationen von 0,05 % und 0,3 % (m/V) im Freisetzungsmedium, untersucht. Bei Verwendung von 0,3 % Cetrimid gingen mehr als 95 % des Celecoxibs innerhalb von 3 min in Lösung, während mit 0,05 % Cetrimid die Freisetzung knapp unterhalb von 90 % endete, weshalb dieses Medium als ungeeignet erachtet wurde. Um die Freisetzungsprofile verschieden großer NP miteinander vergleichen zu können, wurde der Effekt von Phosphatpuffern verschiedener pH-Werte mit einem Zusatz von jeweils 0,3 % Cetrimid untersucht. Hierbei wurden mit dem Puffer pH 2,0 85 % Wirkstofffreisetzung nach 60 min erreicht, während bei den höheren pH-Werten die Freisetzung bei niedrigeren Werten endete. Da ein hohes Ausmaß an Freisetzung favorisiert wurde und der Nüchtern-pH-Wert des Magens zwischen 1 und 3 liegt [3], wurde dieses Medium für den Vergleich der verschiedenen NP-Größen ausgewählt.

Im Detail wurde das Freisetzungsverhalten von NP in fünf verschiedenen Größen von ungefähr 220 nm bis 500 nm und unverarbeiteten Celecoxibpartikeln ($\sim 22 \mu\text{m} \rightarrow$ volumengewichteter Median des Durchmessers ermittelt mit Laserlichtbeugung) untersucht. Die statistische Bewertung, welche gemäß FDA-Richtlinie (modellunabhängiger Ansatz) [14] durchgeführt wurde, zeigte keinen signifikanten Unterschied zwischen den verschieden großen Nanopartikeln, während die Freisetzungsrates der unverarbeiteten Wirkstoffpartikel signifikant niedriger war. Eine zweite Auswertung, welche eine semilogarithmische Auftragung der Freisetzung beinhaltet, wies jedoch Unterschiede in den Freisetzungsrates der Nanopartikel auf.

Zukünftig können die hergestellten NP Bestandteil fester Arzneiformen wie Tabletten oder Kapseln sein. Aufgrund ihrer erheblich höheren Freisetzungsrates gegenüber Wirkstoffpartikeln im Mikrometerbereich, kann von einer erhöhten Bioverfügbarkeit ausgegangen werden. Auch hat die Komplexbildung des Wirkstoffs mit dem Polymer einen positiven Einfluss auf die Freisetzungseigenschaften, was einen Vorteil zu reinen Wirkstoff-NP darstellt. Hinsichtlich der Durchführung von Freisetzungsforschungen kann die Anwendung der QF ein vielversprechender Ansatz sein. Zum Beispiel könnten QF-Module in automatische Probenahmesysteme installiert werden. Um den experimentellen Aufwand zu reduzieren und um aussagekräftigere Freisetzungsprofile zu erhalten könnten kontinuierliche Messungen mit einem Durchflusssystem durchgeführt werden. Hierbei ist jedoch zu beachten, dass, falls dem Medium Tenside oberhalb der kritischen Mizellbildungskonzentration (CMC) zugefügt werden, die Porengröße des Filters ausreichend hoch sein muss. Dies könnte insofern eine Einschränkung sein, als sehr kleine NP von der Bestimmung mit dieser Methode ausgeschlossen sein könnten. Zusammenfassend lässt sich jedoch feststellen, dass die QF-Technik einen robusten, sehr leicht durchführbaren und kostengünstigen Ansatz darstellt, welcher das Risiko der Filterverstopfung ausschließt. In diesem Zusammenhang, können die in dieser Arbeit gewonnenen Erkenntnisse als Basis für die Entwicklung von Geräten dienen, welche für Routineuntersuchungen von nanopartikulären Arzneiformen geeignet sind.

Appendix

Table 19: Preparation of celecoxib-Eudragit E 100 – NPs with Poloxamer 407 as co-stabilizer. Solvent phase: 5 mg/mL celecoxib and 5/10 mg/mL Eudragit E 100 in 1/2/5 mL of ethyl acetate, non-solvent phase: 1 mg/mL Poloxamer 407 in 10 mL of water, 3 x 30 s homogenization with the high speed homogenizer at 30,000 rpm, removal of ethyl acetate in the rotary evaporator (5 min at 40 °C, 220 mbar and 280 rpm followed by 10 min at 40 °C, 180 mbar, and 280 rpm), n=1, Z-Average, PDI and ZP values are mean of three measurements \pm SD, EE values respectively single measurement.

c(Eudragit E 100) /mg*mL⁻¹	Ethyl acetate volume /mL	Visual inspection	Z-Average /nm	PDI	ZP /mV	EE /%
5	1	a	269 \pm 4	0.14 \pm 0.03	49.0 \pm 1	62.1
5	2	b	214 \pm 7	0.20 \pm 0.06	60.7 \pm 2.5	66.2
5	5	b, c	273 \pm 7	0.18 \pm 0.01	49.6 \pm 0.3	77.6
10	1	a	374 \pm 8	0.12 \pm 0.01	44.0 \pm 0.9	75.2
10	2	b	269 \pm 1	0.19 \pm 0.02	50.0 \pm 0.3	73.5
10	5	b, c	302 \pm 7	0.17 \pm 0.06	45.3 \pm 0.6	89.6

a: white, turbid liquid, no visible agglomerates

b: bluish, turbid liquid, no visible agglomerates

c: slight agglomeration after 24 h

Table 20: Preparation of celecoxib-Eudragit E 100 – NPs with SDS as co-stabilizer. Solvent phase: 5 mg/mL celecoxib and 5/10 mg/mL Eudragit E 100 in 1/2/5 mL of ethyl acetate, non-solvent phase: 1 mg/mL SDS in 10 mL of water, 3 x 30 s homogenization with the high speed homogenizer at 30,000 rpm, removal of ethyl acetate in the rotary evaporator (5 min at 40 °C, 220 mbar and 280 rpm followed by 10 min at 40 °C, 180 mbar, and 280 rpm), n=1, Z-Average, PDI and ZP values are mean of three measurements \pm SD, EE values respectively single measurement.

c(Eudragit E 100) /mg*mL ⁻¹	Ethyl acetate volume /mL	Visual inspection	Z-Average /nm	PDI	ZP /mV	EE /%
5	1	a	260 \pm 17	0.27 \pm 0.11	- 11 \pm 0.4	95.4
5	2	a	552 \pm 86	0.13 \pm 0.12	4.4 \pm 0.2	95.5
5	5	a, b	393 \pm 6	0.06 \pm 0.04	39.2 \pm 1.1	99.7
10	1	a	825 \pm 74	0.15 \pm 0.02	2.7 \pm 0.5	88.5
10	2	a	205 \pm 5	0.03 \pm 0.02	27.1 \pm 0.6	99.0
10	5	a, b	7,205 \pm 2,069	0.67 \pm 0.27	51.8 \pm 1.3	99.8

a: appearance of large agglomerates

b: crystallization after 24 h, no visible turbidity

Table 21: Preparation of celecoxib-Eudragit E 100 – NPs with PVA (MW: 27,000) as co-stabilizer. Solvent phase: 5 mg/mL celecoxib and 5/10 mg/mL Eudragit E 100 in 1/2/5 mL of ethyl acetate, non-solvent phase: 1 mg/mL PVA in 10 mL of water, 3 x 30 s homogenization with the high speed homogenizer at 30,000 rpm, removal of ethyl acetate in the rotary evaporator (5 min at 40 °C, 220 mbar and 280 rpm followed by 1 min at 40 °C, 180 mbar, and 280 rpm), n=1, Z-Average, PDI and ZP values are mean of three measurements \pm SD, EE values respectively single measurement.

c(Eudragit E 100) /mg*mL⁻¹	Ethyl acetate volume /mL	Visual inspection	Z-Average /nm	PDI	ZP /mV	EE /%
5	1	a, b	278 \pm 74	0.49 \pm 0.14	- 3.8 \pm 1.3	7.7
5	2	a, b	548 \pm 214	0.77 \pm 0.20	2.5 \pm 0.8	13.5
5	5	a, b	31,183 \pm 14,732	0.94 \pm 0.11	11.3 \pm 1.6	36.5
10	1	a, b	484 \pm 32	0.47 \pm 0.04	1.9 \pm 0.2	34.4
10	2	a, b	431 \pm 155	0.74 \pm 0.16	2.1 \pm 1.1	14.6
10	5	a, b	982 \pm 321	0.87 \pm 0.19	4.1 \pm 0.5	39.3

a: appearance of large agglomerates

b: suspension not turbid

Table 22: Preparation of celecoxib-Eudragit E 100 – NPs with varying amounts of Poloxamer 407. Solvent phase: 5 mg/mL celecoxib and 10 mg/mL Eudragit E 100 in 2 mL of ethyl acetate, non-solvent phase: 0.1/0.5/1/2.5/5/10 mg/mL Poloxamer 407 in 10 mL of water, 3 x 30 s homogenization with the high speed homogenizer at 30,000 rpm, removal of ethyl acetate in the rotary evaporator (5 min at 40 °C, 220 mbar and 280 rpm followed by 10 min at 40 °C, 180 mbar, and 280 rpm), n=3, values are mean \pm SD.

c (Poloxamer 407) /mg*mL⁻¹	Visual inspection	Z-Average /nm	PDI	ZP /mV	EE /%
0.1	a	417 \pm 38	0.26 \pm 0.01	50 \pm 3	94.6 \pm 0
0.5	a	315 \pm 17	0.28 \pm 0.01	49 \pm 1	84.0 \pm 3
1	a	254 \pm 17	0.17 \pm 0.03	46 \pm 4	75.7 \pm 3
2.5	b	215 \pm 11	0.05 \pm 0.01	39 \pm 2	72.3 \pm 5
5	c	204 \pm 5	0.05 \pm 0.02	31 \pm 1	61.4 \pm 3
10	c	199 \pm 3	0.07 \pm 0.03	29 \pm 0	51.6 \pm 2

a: white, turbid liquid, sediments on the flask wall

b: white, turbid liquid

c: white, slightly bluish, turbid liquid

Table 23: Stability study of celecoxib-Eudragit E 100 – NPs stabilized with Poloxamer 407: Solvent phase: 5 mg/mL celecoxib and 10 mg/mL Eudragit E 100 in 2 mL of ethyl acetate, non-solvent phase: 2.5 mg/mL Poloxamer 407 in 10 mL of water, 3 x 30 s homogenization with the high speed homogenizer at 30,000 rpm, removal of ethyl acetate in the rotary evaporator (5 min at 40 °C, 220 mbar and 280 rpm followed by 10 min at 40 °C, 180 mbar, and 280 rpm), stored at room temperature, n=3, values are mean \pm SD.

Storage /d	Z-Average /nm	PDI	ZP /mV	EE /%
0	223 \pm 5	0.10 \pm 0.03	38.2 \pm 4.3	72.2 \pm 3.6
1	214 \pm 6	0.11 \pm 0.04	36.8 \pm 5.3	70.0 \pm 6.6
2	222 \pm 8	0.15 \pm 0.06	43.3 \pm 1.2	72.0 \pm 11.0
3	226 \pm 9	0.19 \pm 0.06	51.8 \pm 4.3	76.2 \pm 11.6
4	237 \pm 10	0.23 \pm 0.09	53.2 \pm 2.0	73.1 \pm 6.2
7	265 \pm 34	0.33 \pm 0.16	61.0 \pm 0.7	80.2 \pm 5.5
14	263 \pm 52	0.32 \pm 0.14	55.9 \pm 2.3	70.2 \pm 8.6

Table 24: Stability study of celecoxib-Eudragit E 100 – NPs stabilized with Poloxamer 407: Solvent phase: 5 mg/mL celecoxib and 10 mg/mL Eudragit E 100 in 2 mL of ethyl acetate, non-solvent phase: 2.5 mg/mL Poloxamer 407 in 10 mL of water, 3 x 30 s homogenization with the high speed homogenizer at 30,000 rpm, removal of ethyl acetate in the rotary evaporator (5 min at 40 °C, 220 mbar and 280 rpm followed by 10 min at 40 °C, 180 mbar, and 280 rpm), stored at 5 °C, n=3, values are mean \pm SD.

Storage /d	Z-Average /nm	PDI	ZP /mV	EE /%
0	223 \pm 5	0.10 \pm 0.03	38.2 \pm 4.3	72.2 \pm 3.6
1	211 \pm 2	0.09 \pm 0.03	39.7 \pm 0.9	72.0 \pm 0.1
2	218 \pm 4	0.16 \pm 0.08	41.0 \pm 1.5	76.2 \pm 2.4
3	214 \pm 3	0.14 \pm 0.03	44.3 \pm 1.1	83.3 \pm 1.1
4	254 \pm 19	0.32 \pm 0.06	47.8 \pm 1.9	80.3 \pm 1.0
7	278 \pm 53	0.33 \pm 0.15	55.9 \pm 2.0	69.7 \pm 1.9
14	249 \pm 36	0.21 \pm 0.08	51.6 \pm 0.8	65.0 \pm 10.5

Table 25: Stability study of celecoxib-Eudragit E 100 – NPs stabilized with Poloxamer 407: Solvent phase: 25 mg/mL celecoxib and 50 mg/mL Eudragit E 100 in 2 mL of ethyl acetate, non-solvent phase: 12.5 mg/mL Poloxamer 407 in 10 mL of water, 3 x 30 s homogenization with the high speed homogenizer at 30,000 rpm, removal of ethyl acetate in the rotary evaporator (5 min at 40 °C, 220 mbar and 280 rpm followed by 10 min at 40 °C, 180 mbar, and 280 rpm), stored at room temperature, n=3, values are mean \pm SD.

Storage /d	Z-Average /nm	PDI	ZP /mV	EE /%
0	290 \pm 7	0.12 \pm 0.02	39.4 \pm 0.6	85.6 \pm 4.3
1	276 \pm 6	0.15 \pm 0.04	38.3 \pm 0.2	83.2 \pm 0.5
2	280 \pm 10	0.08 \pm 0.02	40.6 \pm 2.2	81.0 \pm 1.5
3	280 \pm 6	0.11 \pm 0.03	42.5 \pm 0.8	80.3 \pm 2.5
4	284 \pm 7	0.11 \pm 0.01	44.3 \pm 0.5	81.3 \pm 10.2
7	277 \pm 6	0.08 \pm 0.04	51.7 \pm 4.0	80.3 \pm 1.8
14	241 \pm 8	0.09 \pm 0.02	46.1 \pm 0.5	84.6 \pm 1.0

Table 26: Stability study of celecoxib-Eudragit E 100 – NPs stabilized with Poloxamer 407: Solvent phase: 25 mg/mL celecoxib and 50 mg/mL Eudragit E 100 in 2 mL of ethyl acetate, non-solvent phase: 12.5 mg/mL Poloxamer 407 in 10 mL of water, 3 x 30 s homogenization with the high speed homogenizer at 30,000 rpm, removal of ethyl acetate in the rotary evaporator (5 min at 40 °C, 220 mbar and 280 rpm followed by 10 min at 40 °C, 180 mbar, and 280 rpm), stored at 5 °C, n=3, values are mean \pm SD.

Storage /d	Z-Average /nm	PDI	ZP /mV	EE /%
0	290 \pm 7	0.12 \pm 0.02	39.4 \pm 0.6	85.6 \pm 4.3
1	275 \pm 5	0.14 \pm 0.04	37.1 \pm 0.7	83.3 \pm 3.0
2	284 \pm 6	0.12 \pm 0.02	38.9 \pm 0.7	82.2 \pm 3.4
3	278 \pm 6	0.14 \pm 0.04	42.3 \pm 0.5	80.1 \pm 3.5
4	354 \pm 66	0.37 \pm 0.24	42.9 \pm 2.4	85.1 \pm 1.4
7	380 \pm 77	0.45 \pm 0.18	55.2 \pm 0.9	84.9 \pm 0.9
14	252 \pm 12	0.18 \pm 0.03	45.2 \pm 1.1	87.0 \pm 3.3

Table 27: Stability study of celecoxib-Eudragit E 100 – NPs stabilized with Poloxamer 407: t-test for comparison of storage at room temperature versus storage at 5 °C and usage of 5 mg/mL versus 25 mg/mL celecoxib in solvent phase, data rows from days 0 to 14 are respectively compared.

Comparison	Parameter	p-value
5 mg/mL_RT versus 5 mg/mL_5 °C	Z-Average	0.9708
	PDI	0.8023
	ZP	0.4839
	EE	0.8069
25 mg/mL_RT versus 25 mg/mL_5 °C	Z-Average	0.1799
	PDI	0.0561
	ZP	0.9180
	EE	0.1800
5 mg/mL_RT versus 25 mg/mL_RT	Z-Average	0.0016
	PDI	0.0214
	ZP	0.1985
	EE	0.0001
5 mg/mL_5 °C versus 25 mg/mL_5 °C	Z-Average	0.0061
	PDI	0.7014
	ZP	0.4703
	EE	0.0021

Table 28: MJR preparation of celecoxib-Eudragit E 100 – NPs stabilized with Poloxamer 407 using DoE: Solvent phase: 25 mg/mL celecoxib and 50 mg/mL Eudragit E 100 in ethyl acetate, non-solvent phase: 12.5 mg/mL Poloxamer 407 in water, operation temperature: 40-60 °C, nitrogen pressure: 0-0.50 bar, pump rotational speed (solvent phase : non-solvent phase) 300 : 1500 rpm to 1200 : 6000 rpm, removal of remaining ethyl acetate by evaporating for 18 h in the fume hood, values are mean of three measurements.

Run	Temperature /°C	Nitrogen pressure /bar	Pump rotational speed /rpm	Z-Average /nm	PDI
1	60.0	0.25	1200 : 6000	263.6	0.157
2	60.0	0.25	300 : 1500	539.3	0.352
3	60.0	0.50	750 : 3750	297.7	0.14
4	50.0	0.50	300 : 1500	369.6	0.08
5	40.0	0.50	750 : 3750	286	0.145
6	40.0	0	750 : 3750	283.2	0.163
7	50.0	0	300 : 1500	746.9	1
8	50.0	0.25	750 : 3750	320.5	0.259
9	50.0	0.25	750 : 3750	327.4	0.249
10	50.0	0.50	1200 : 6000	549.5	0.836
11	50.0	0.25	750 : 3750	301.2	0.164
12	60.0	0	750 : 3750	359	0.101
13	40.0	0.25	1200 : 6000	420	0.46
14	40.0	0.25	300 : 1500	331.6	0.157
15	50.0	0	1200 : 6000	294.3	0.103
16	50.0	0.25	750 : 3750	292.8	0.06
17	50.0	0.25	750 : 3750	560.1	0.804

Table 29: MJR preparation of celecoxib-Eudragit E 100 – NPs stabilized with Poloxamer 407, validation of DoE model: Solvent phase: 25 mg/mL celecoxib and 50 mg/mL Eudragit E 100 in ethyl acetate, non-solvent phase: 12.5 mg/mL Poloxamer 407 in water, operation temperature: 55-59 °C, nitrogen pressure: 0.31-0.47 bar, pump rotational speed (solvent phase : non-solvent phase) 300 : 1500 rpm to 719 : 3595 rpm, removal of remaining ethyl acetate by evaporating for 18 h in the fume hood, n=1, Z-Average, PDI and ZP values are mean of three measurements \pm SD, EE values respectively single measurement.

Experimental conditions	Z-Average (predicted value) /nm	Z-Average (actual value) /nm	PDI	ZP /mV	EE /%
57.4 °C_0.39 bar_719 : 3595 rpm	300	287.5 \pm 2.4	0.156 \pm 0.045	41.9 \pm 0.3	84.3
58.4 °C_0.40 bar_510 : 2550 rpm	350	330.6 \pm 3.0	0.081 \pm 0.066	46.2 \pm 1.0	86.5
56.0 °C_0.45 bar_491 : 2455 rpm	350	331.3 \pm 26.5	0.126 \pm 0.057	44.1 \pm 1.0	88.3
55.0 °C_0.31 bar_571 : 2855 rpm	350	364.3 \pm 9.3	0.086 \pm 0.057	43.5 \pm 0.9	91.2
58.1 °C_0.32 bar_457 : 2285 rpm	400	396.7 \pm 6.6	0.219 \pm 0.077	44.4 \pm 0.2	81.0
56.2 °C_0.47 bar_349 : 1745 rpm	400	431.6 \pm 15.4	0.146 \pm 0.077	45.3 \pm 0.5	83.7
55.8 °C_0.35 bar_433 : 2165 rpm	400	380.1 \pm 11.8	0.144 \pm 0.075	47.2 \pm 2.1	90.4
55.7 °C_0.41 bar_300 : 1500 rpm	450	442.7 \pm 20.0	0.223 \pm 0.078	44.0 \pm 1.0	85.4
57.5 °C_0.40 bar_313 : 1565 rpm	450	444.3 \pm 23.4	0.168 \pm 0.092	43.7 \pm 3.4	87.7
59.0 °C_0.36 bar_350 : 1750 rpm	450	505.6 \pm 9.7	0.202 \pm 0.074	44.6 \pm 3.5	82.3

Table 30: Dissolution of celecoxib-Eudragit E 100-NPs in HCl pH 1.2: NP properties: 80 nm (Z-Average), 0.131 (PDI) and 2.573 mg/mL (celecoxib concentration of the nanosuspension), detection: UV-Vis (248 nm), n=3, values are mean \pm SD.

Sampling point /min		3	6	9	12	15	18	21	30	60	120
API dissolved /%	HCl pH 1.2	22.1	47.1	53.8	53.9	51.9	49.5	47.0	40.6	34.3	33.5
		\pm 12.0	\pm 3.8	\pm 3.4	\pm 6.3	\pm 7.3	\pm 7.7	\pm 7.3	\pm 4.4	\pm 4.2	\pm 1.7

Table 31: Dissolution of celecoxib-Eudragit E 100-NPs in diluted HCl pH 1.2 + 0.15 M NaCl: NP properties: 100 nm (Z-Average), 0.100 (PDI) and 2.331 mg/mL (celecoxib concentration of the nanosuspension), detection: UV-Vis (248 nm), n=1.

Sampling point /min		3	6	9	12	15	18	21	30	60	120
API dissolved /%	HCl pH 1.2 + 0.15 M NaCl	13.1	30.6	34.7	35.3	34.1	32.1	29.5	23.9	18.0	5.0

Table 32: Dissolution of celecoxib-Eudragit E 100-NPs in diluted HCl pH 1.2 + 0.001/0.01/0.3/1.0 % cetrimide: NP properties: 80 nm (Z-Average), 0.131 (PDI) and 2.573 mg/mL (celecoxib concentration of the nanosuspension), detection: UV-Vis (248 nm), n=1.

Sampling point /min		3	6	9	12	15	18	21	30	60	120
API dissolved /%	HCl pH 1.2 + 0.001 % cetrimide	0.5	15.2	14.2	11.8	10.6	9.8	9.5	8.9	8.2	7.4
	HCl pH 1.2 + 0.01 % cetrimide	3.2	4.9	7.9	9.8	10.7	11.1	11.3	11.3	10.8	10.1
	HCl pH 1.2 + 0.3 % cetrimide	4.8	5.5	5.9	6.2	6.4	7.2	7.5	7.9	10.0	12.9
	HCl pH 1.2 + 1.0 % cetrimide	4.5	5.3	5.2	5.6	5.5	6.1	6.6	7.0	7.3	8.2

Table 33: Dissolution of celecoxib-Eudragit E 100-NPs in diluted HCl pH 1.2 + 0.3 % cetrimide: NP properties: 160 nm (Z-Average), 0.094 (PDI) and 2.388 mg/mL (celecoxib concentration of the nanosuspension), filters: cross-flow filtration modules of 100 and 500 kDa and 0.2 µm syringe filter holders (dead-end), detection: UV-Vis (248 nm), n=3, values are mean ± SD.

Sampling point /min		3	6	9	12	15	18	21	30	60	120
API dissolved /%	100 kDa cross-flow	3.7 ± 0.6	5.9 ± 0.5	6.8 ± 0.7	7.1 ± 0.3	7.4 ± 0.4	7.7 ± 0.2	7.6 ± 0.6	7.8 ± 0.7	8.3 ± 0.7	9.0 ± 0.6
	500 kDa cross-flow	96.6 ± 5.1	95.7 ± 0.4	95.8 ± 0.5	96.3 ± 1.1	96.8 ± 1.1	96.3 ± 1.7	97.2 ± 2.6	97.4 ± 2.7	98.9 ± 3.1	101.4 ± 3.7
	0.2 µm dead-end	95.6 ± 1.3	98.2 ± 0.6	99.1 ± 0.7	98.0 ± 2.9	99.5 ± 2.4	99.1 ± 1.0	101. 0 ± 1.9	101. 3 ± 1.4	100.8 ± 0.4	101.1 ± 1.0

Table 34: Dissolution of celecoxib-Eudragit E 100-NPs in diluted HCl pH 1.2 + 0.05 % cetrimide: NP properties: 160 nm (Z-Average), 0.094 (PDI) and 2.509 mg/mL (celecoxib concentration of the nanosuspension), filters: cross-flow filtration modules of 100 and 500 kDa and 0.2 µm syringe filter holders (dead-end), detection: UV-Vis (248 nm), n=3, values are mean ± SD.

Sampling point /min		3	6	9	12	15	18	21	30	60	120
API dissolved /%	100 kDa cross-flow	1.0 ± 1.1	9.0 ± 1.1	12.1 ± 1.5	12.9 ± 1.3	13.6 ± 1.9	13.7 ± 1.3	13.4 ± 0.6	13.3 ± 1.0	13.4 ± 0.7	14.0 ± 0.4
	500 kDa cross-flow	78.4 ± 1.8	81.3 ± 2.6	82.1 ± 2.5	82.2 ± 2.3	82.8 ± 2.1	83.2 ± 2.1	83.9 ± 2.6	84.8 ± 2.7	85.5 ± 3.0	86.7 ± 3.6
	0.2 µm dead-end	71.8 ± 2.3	78.1 ± 3.4	82.2 ± 2.6	83.6 ± 2.6	86.4 ± 1.6	86.8 ± 1.5	87.3 ± 1.3	88.0 ± 1.2	88.0 ± 1.7	88.6 ± 0.8

Table 35: Dissolution of celecoxib-Eudragit E 100-NPs in phosphate buffer pH 2.0/2.5/3.5/4.5/5.2+ 0.3 % cetrimide: NP properties: 220 nm (Z-Average), 0.086 (PDI) and 3.666 mg/mL (celecoxib concentration of the nanosuspension), filter: 500 kDa cross-flow filtration module, detection: UV-Vis (248 nm), n=3, values are mean ± SD.

Sampling point /min		3	6	9	12	15	18	21	30	45	60	120
API dissolved /%	pH 2.0	81.0 ± 1.5	80.9 ± 1.1	81.4 ± 1.2	81.6 ± 1.1	82.2 ± 0.8	82.7 ± 0.6	83.0 ± 0.7	83.6 ± 0.5	84.6 ± 0.5	85.4 ± 0.9	88.8 ± 1.2
	pH 2.5	74.6 ± 1.5	76.1 ± 1.0	77.1 ± 1.5	77.5 ± 1.6	78.0 ± 1.4	78.4 ± 1.3	78.8 ± 1.2	79.3 ± 1.7	79.7 ± 1.3	80.3 ± 1.8	83.4 ± 0.7
	pH 3.5	64.5 ± 1.6	65.6 ± 1.3	66.0 ± 1.6	66.4 ± 2.2	66.7 ± 2.4	67.2 ± 2.6	67.3 ± 2.3	67.4 ± 2.2	67.7 ± 1.9	68.1 ± 2.1	69.7 ± 1.9
	pH 4.5	36.6 ± 1.5	38.1 ± 0.8	39.0 ± 0.6	40.0 ± 0.8	40.6 ± 1.1	41.1 ± 1.0	41.4 ± 0.8	42.5 ± 1.3	43.4 ± 1.5	44.6 ± 1.8	46.8 ± 2.1
	pH 5.2	23.0 ± 4.6	25.2 ± 4.6	26.5 ± 4.1	27.1 ± 4.2	27.6 ± 3.9	28.2 ± 4.1	28.6 ± 3.8	29.2 ± 3.8	30.2 ± 3.4	30.8 ± 3.8	32.4 ± 3.6

Table 36: Dissolution of celecoxib-Eudragit E 100-NPs of different size and celecoxib powder in phosphate buffer pH 2.0 + 0.3 % cetrimide: NP properties: 221/255/293/362/497 nm (Z-Average), < 0.25 (PDI) and ~ 2.650–4.850 mg/mL (celecoxib concentration of the nanosuspension), API powder: 2537 µg/mL (celecoxib concentration of the suspension), filter: 500 kDa cross-flow filtration module, detection: UV-Vis (248 nm), n=6, values are mean ± SD.

Sampling point /s		20	40	60	90	120	900	1800	3600
API dissolved /%	221 nm	8.6 ± 6.3	79.2 ± 1.8	85.5 ± 0.9	85.8 ± 0.7	85.4 ± 0.9	-	-	-
	255 nm	13.4 ± 8.3	82.1 ± 1.8	87.0 ± 1.2	86.7 ± 0.9	86.1 ± 1.1	-	-	-
	293 nm	13.4 ± 8.1	78.0 ± 15.3	86.0 ± 10.5	89.8 ± 3.4	90.4 ± 2.8	-	-	-
	362 nm	13.8 ± 17.1	79.3 ± 4.8	87.2 ± 4.8	89.3 ± 4.5	90.3 ± 4.3	-	-	-
	497 nm	12.2 ± 5.1	77.5 ± 4.2	84.6 ± 3.5	85.0 ± 4.1	83.9 ± 3.6	-	-	-
	API powder	0.8 ± 2.0	24.7 ± 3.1	41.0 ± 5.4	55.4 ± 8.5	63.7 ± 10.2	80.8 ± 13.3	82.0 ± 13.1	84.5 ± 12.6

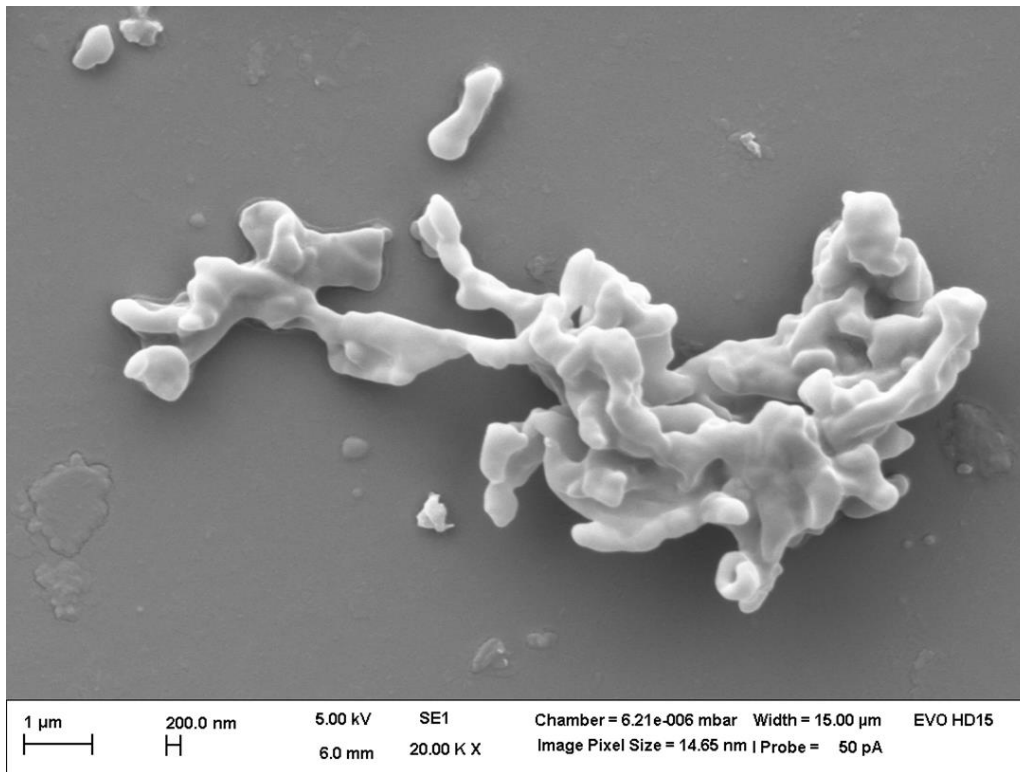


Figure 64: SEM image of MJR produced celecoxib-Eudragit E 100-particles (nanoprecipitation technique): NP properties (determined by DLS, mean of three measurements): 1156 nm (Z-Average), 0.144 (PDI).

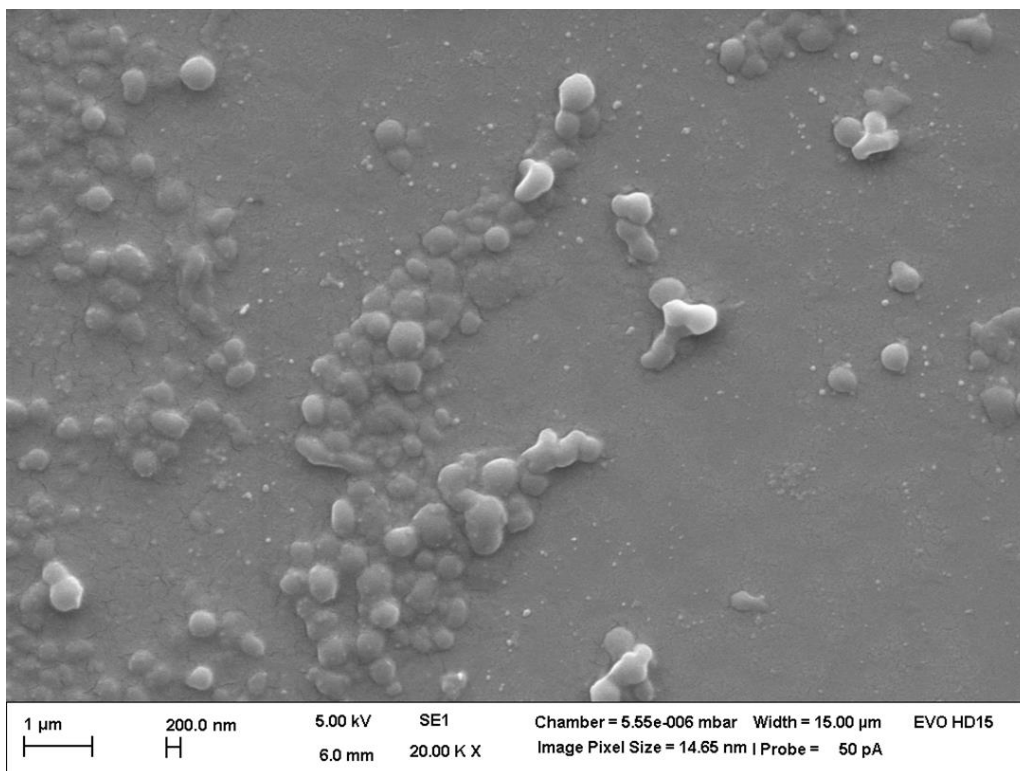


Figure 65: SEM image of MJR produced celecoxib-Eudragit E 100-NPs (nanoprecipitation technique): NP properties (determined by DLS, mean of three measurements): 387 nm (Z-Average), 0.285 (PDI).

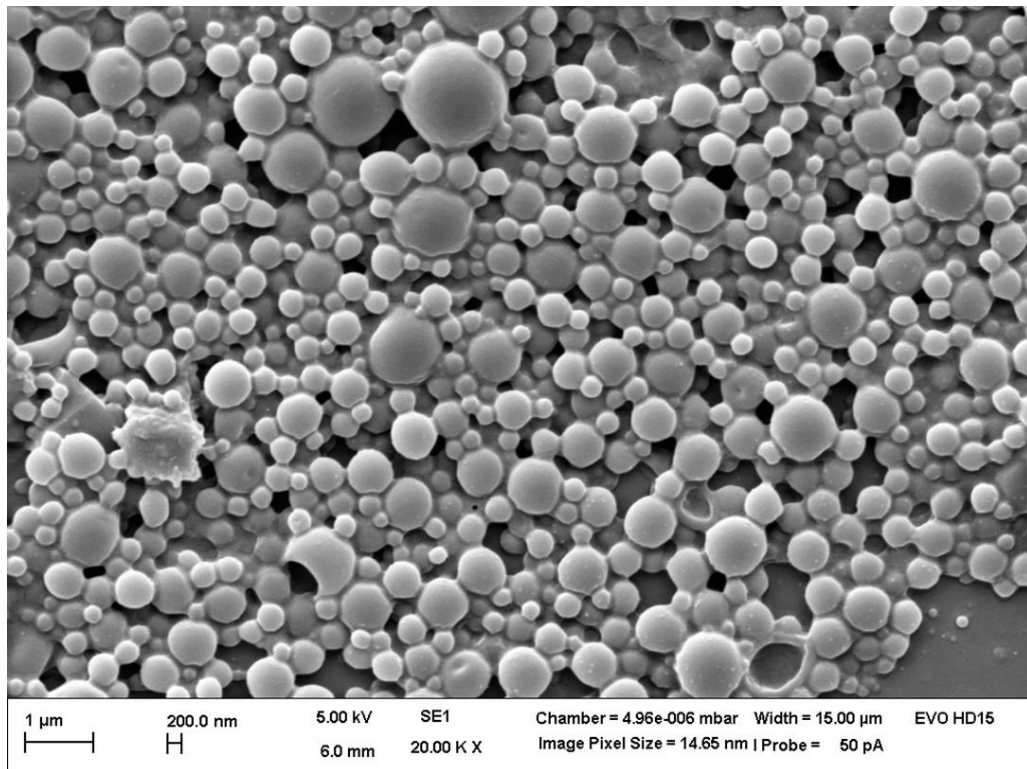


Figure 66: SEM image of MJR produced celecoxib-Eudragit E 100-NPs (emulsification-diffusion technique): NP properties (determined by DLS, mean of three measurements): 611 nm (Z-Average), 0.258 (PDI).

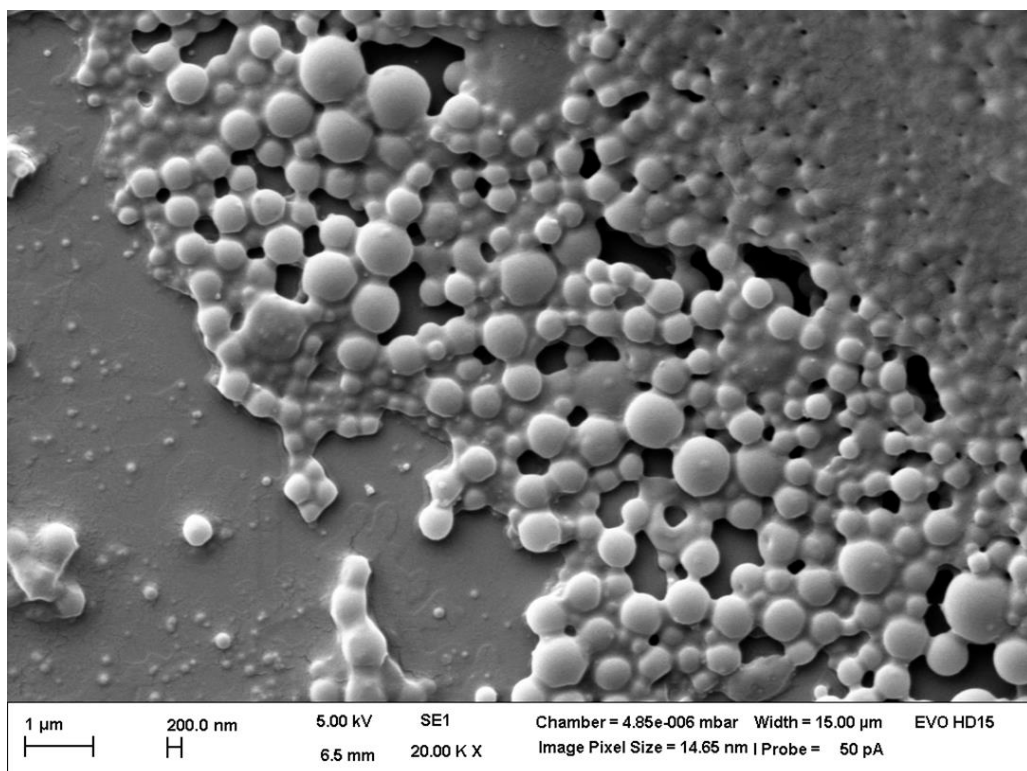


Figure 67: SEM image of MJR produced celecoxib-Eudragit E 100-NPs (emulsification-diffusion technique): NP properties (determined by DLS, mean of three measurements): 254 nm (Z-Average), 0.148 (PDI).

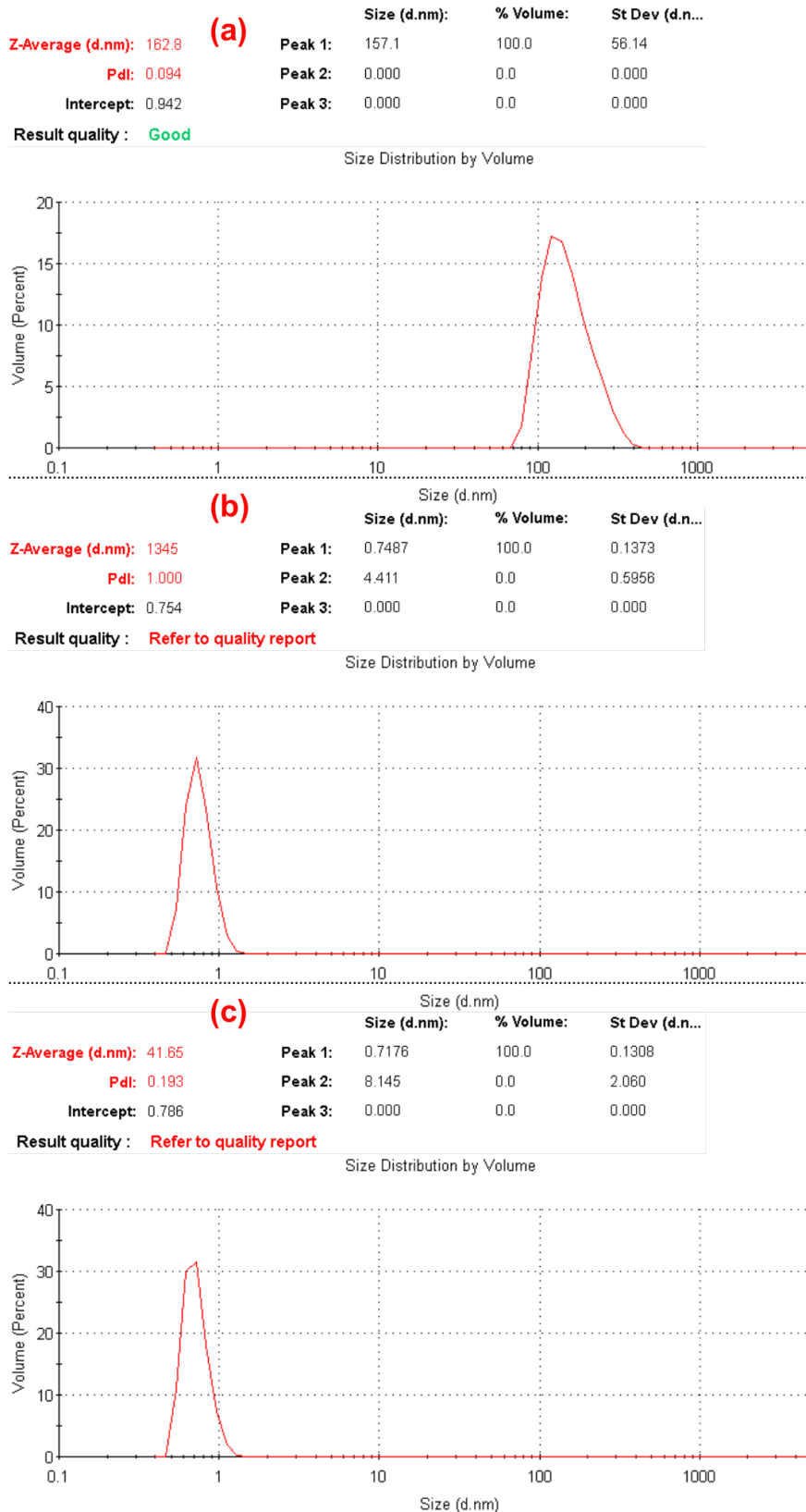
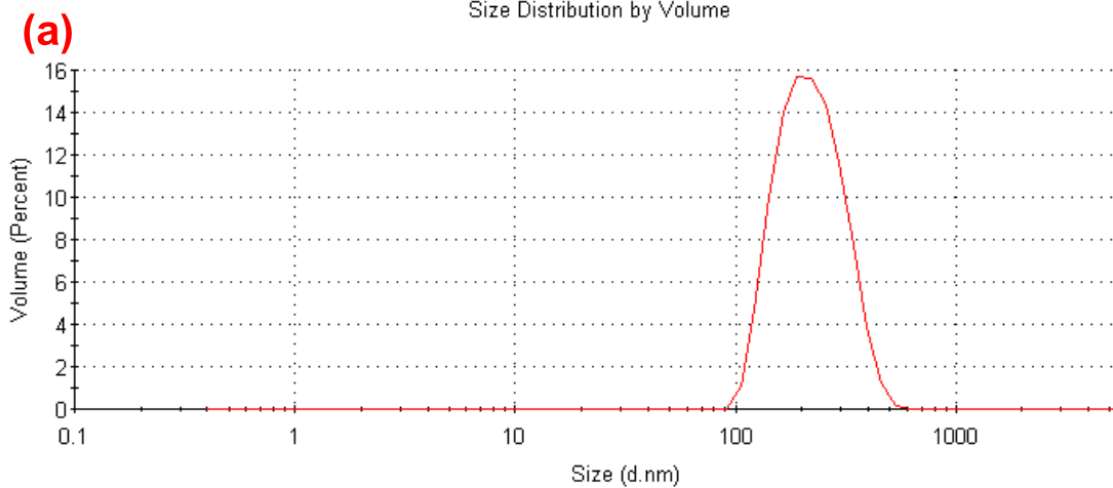


Figure 68: DLS size distribution reports (volume-weighted) of celecoxib-Eudragit E 100-NPs; NP-preparation: nanoprecipitation technique–alternative method, non-solvent phase without surfactant, see chapter 2.2.1.2; unfiltered nanosuspension (a) versus liquid obtained from filtration of this nanosuspension through a 500 kDa CF module (b) and from filtration through a syringe filter holder with 0.2 μm pore size (c); NP properties: 160 nm (Z-Average), 0.094 (PDI).

	Size (d.nm):	% Volume:	St Dev (d.n...)
Z-Average (d.nm): 216.4	Peak 1: 227.3	100.0	75.77
Pdl: 0.108	Peak 2: 0.000	0.0	0.000
Intercept: 0.974	Peak 3: 0.000	0.0	0.000

Result quality : **Refer to quality report**



	Size (d.nm):	% Volume:	St Dev (d.n...)
Z-Average (d.nm): 6.190	Peak 1: 0.7153	96.9	0.1206
Pdl: 0.294	Peak 2: 4.042	3.1	1.402
Intercept: 0.780	Peak 3: 0.000	0.0	0.000

Result quality : **Refer to quality report**

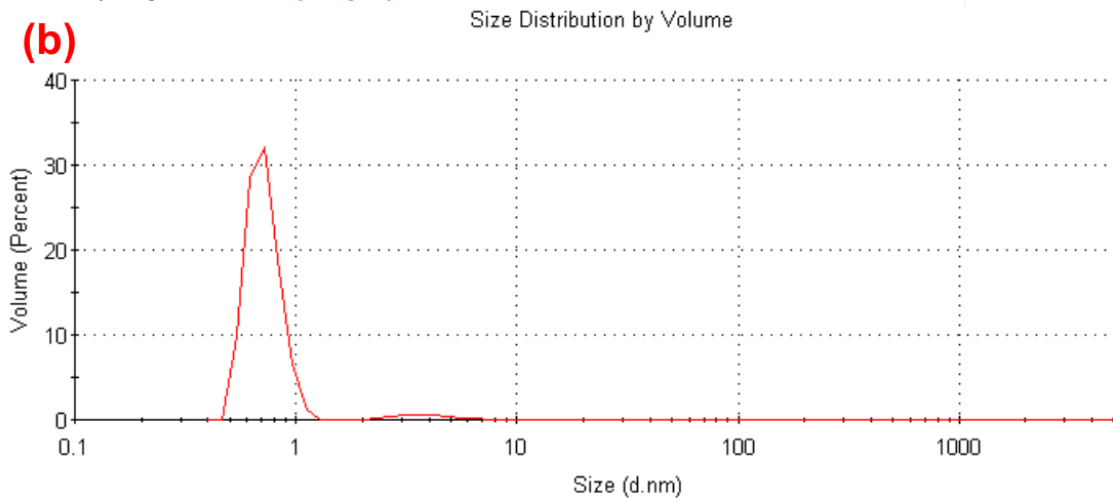


Figure 69: Simulation of the NP dissolution process in dissolution medium: DLS size distribution reports (volume-weighted) of celecoxib-Eudragit E 100-NPs; same nanosuspension as in Figure 68, but respectively measured at 37 °C (dissolution test temperature); 1:100 aqueous dilution of the nanosuspension (a) versus 1:100 dilution in 0.1 M HCl + 0.3 % cetrimide after 15 min incubation time in the cuvette of the DLS instrument (b).

HELOS (H3048) & CUVETTE, R4: 0.5/1.8...350µm

Test_monodispersity

2014-10-09, 10:42:42,757

$x_{10V} = 3,04 \mu\text{m}$ $x_{50V} = 13,48 \mu\text{m}$ $x_{90V} = 56,76 \mu\text{m}$
 $x_{16} = 4,23 \mu\text{m}$ $x_{84} = 42,18 \mu\text{m}$ $x_{99} = 112,32 \mu\text{m}$

SMD = 7,08 µm **VMD = 22,58 µm**
 $S_v = 0,85 \text{ m}^2/\text{cm}^3$ $S_w = 8471,90 \text{ cm}^2/\text{g}$

$x_{10N} = 0,66 \mu\text{m}$ $x_{50N} = 1,31 \mu\text{m}$ $x_{90N} = 2,58 \mu\text{m}$

Span vol=3,99
 CoV vol=107,87
 Spannum=1,46
 Covnum=80,66

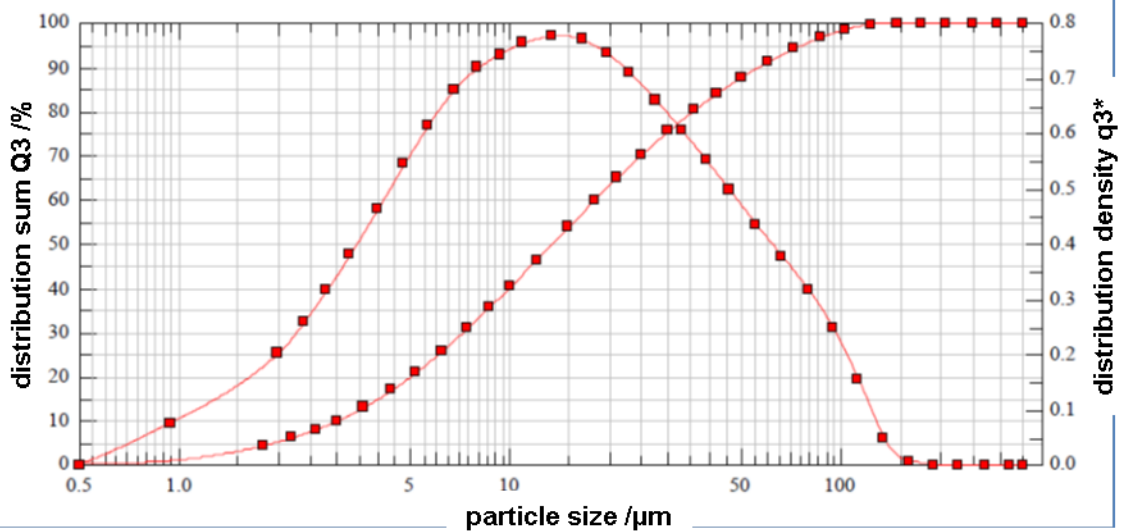
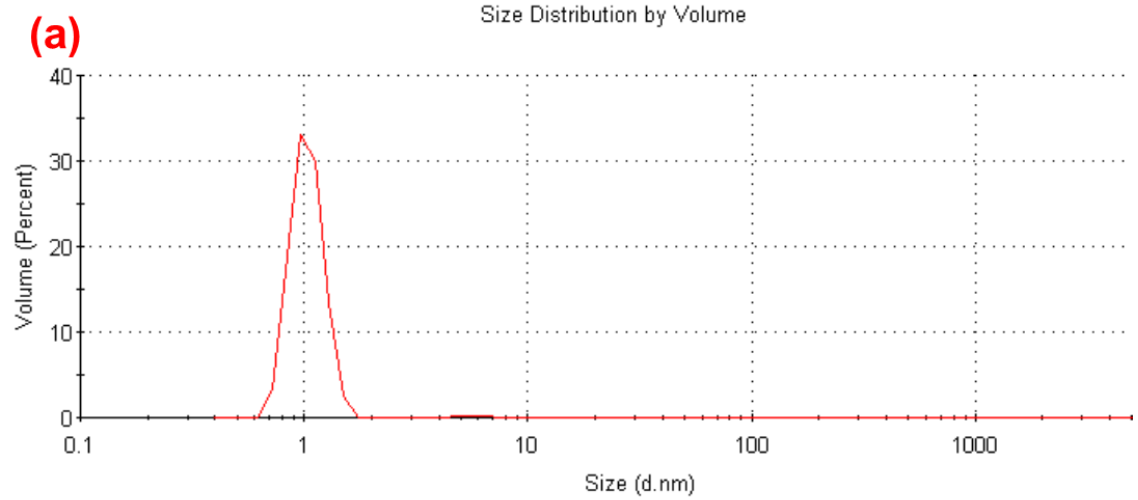


Figure 70: Laser light diffraction size distribution report of unprocessed celecoxib particles; density distribution and cumulative distribution; volume-weighted median diameter (VMD) in red rectangle.

	Size (d.nm):	% Volume:	St Dev (d.n...)
Z-Average (d.nm): 492.6	Peak 1: 1.038	99.3	0.1683
Pdl: 0.845	Peak 2: 6.095	0.7	0.8893
Intercept: 0.937	Peak 3: 0.000	0.0	0.000

Result quality : **Refer to quality report**



	Size (d.nm):	% Volume:	St Dev (d.n...)
Z-Average (d.nm): 227.9	Peak 1: 5.264	100.0	0.9789
Pdl: 0.473	Peak 2: 0.000	0.0	0.000
Intercept: 0.971	Peak 3: 0.000	0.0	0.000

Result quality : **Refer to quality report**

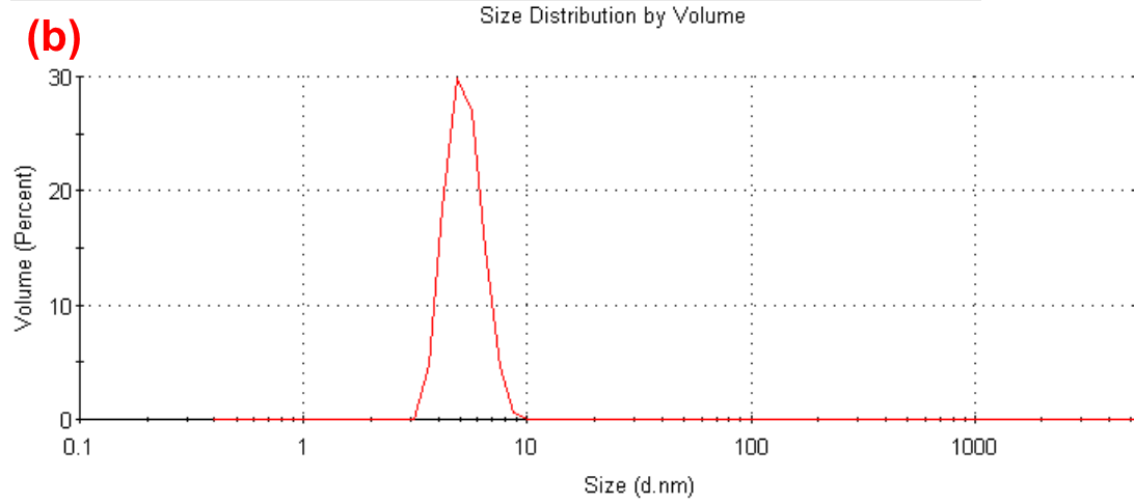


Figure 71: DLS size distribution reports (volume-weighted) of two dissolution media: HCl pH 1.2 + 0.05 % cetrimide (a) and HCl pH 1.2 + 0.3 % cetrimide (with micelles) (b).

References

- [1] M.M.A. Abdel-Mottaleb, N.D. Mortada, A.A. El-Shamy, G.A.S. Awad, Physically cross-linked polyvinyl alcohol for the topical delivery of fluconazole, *Drug Dev Ind Pharm* 35 (2009) 311–320.
- [2] M.M.A. Abdel-Mottaleb, D. Neumann, A. Lamprecht, In vitro drug release mechanism from lipid nanocapsules (LNC), *Int J Pharm* 390 (2010) 208–213.
- [3] W. Abdelwahed, G. Degobert, S. Stainmesse, H. Fessi, Freeze-drying of nanoparticles: formulation, process and storage considerations, *Adv Drug Deliver Rev* 58 (2006) 1688–1713.
- [4] J. Albers, Hot-melt extrusion with poorly soluble drugs. Ph.D. Thesis, Düsseldorf, 2008.
- [5] J. Albers, R. Alles, K. Matthée, K. Knop, J.S. Nahrup, P. Kleinebudde, Mechanism of drug release from polymethacrylate-based extrudates and milled strands prepared by hot-melt extrusion, *Eur J Pharm Biopharm* 71 (2009) 387–394.
- [6] G.L. Amidon, H. Lennernäs, V.P. Shah, J.R. Crison, A theoretical basis for a biopharmaceutic drug classification: the correlation of in vitro drug product dissolution and in vivo bioavailability, *Pharm Res* 12 (1995) 413–420.
- [7] A.N. Ananth, S.C.G.K. Daniel, T.A. Sironmani, S. Umapathi, PVA and BSA stabilized silver nanoparticles based surface-enhanced plasmon resonance probes for protein detection, *Colloid Surface B* 85 (2011) 138–144.
- [8] G. Askarieh, M. Hedhammar, K. Nordling, A. Saenz, C. Casals, A. Rising, J. Johansson, S.D. Knight, Self-assembly of spider silk proteins is controlled by a pH-sensitive relay, *Nature* 465 (2010) 236–238.
- [9] M. Baalousha, J. Lead, Characterization of natural and manufactured nanoparticles by atomic force microscopy: Effect of analysis mode, environment and sample preparation, *Colloid Surface A* 419 (2013) 238–247.
- [10] S. Baboota, S. Faiyaz, Ahuja A., Ali J., Shafiq S., S. Ahmad, Development and validation of stability-indicating HPLC method for analysis of Celecoxib (CXB) in bulk drug and microemulsion formulations, *Acta Chromatogr* (2007) 116–129.
- [11] Y. Barenholz, Doxil®-the first FDA-approved nano-drug: lessons learned, *J Control Release* 160 (2012) 117–134.
- [12] T.R. Bates, M. Gibaldi, J.L. Kanig, Rate of dissolution of griseofulvin and hexoestrol in bile salt solutions, *Nature* 210 (1966) 1331–1333.
- [13] K.H. Bauer, B.C. Lippold, H. Egermann, *Lehrbuch der Pharmazeutischen Technologie: Mit einer Einführung in die Biopharmazie ; 95 Tabellen*, 8 ed., Wissenschaftliche Verlagsgesellschaft, Stuttgart, 2006.
- [14] U. Bilati, E. Allémann, E. Doelker, Development of a nanoprecipitation method intended for the entrapment of hydrophilic drugs into nanoparticles, *Eur J Pharm Sci* 24 (2005) 67–75.
- [15] G. Binnig, C.F. Quate, C. Gerber, Atomic Force Microscope, *Phys Rev Lett* 56 (1986) 930–934.

- [16] G. Bisker, D. Yeheskely-Hayon, L. Minai, D. Yelin, Controlled release of Rituximab from gold nanoparticles for phototherapy of malignant cells, *J Control Release* 162 (2012) 303–309.
- [17] BMBF, Nanopartikel - kleine Dinge, große Wirkung, 2008, http://www.bmbf.de/pub/nanopartikel_kleine_dinge_grosse_wirkung.pdf, accessed 15 April 2013.
- [18] A. Bohr, J. Kristensen, E. Stride, M. Dyas, M. Edirisinghe, Preparation of microspheres containing low solubility drug compound by electrohydrodynamic spraying, *Int J Pharm* 412 (2011) 59–67.
- [19] C.A. Bunton, F. Nome, F.H. Quina, L.S. Romsted, Ion Binding and Reactivity at Charged Aqueous Interfaces, *Acc. Chem. Res. (Accounts of Chemical Research)* 24 (1991) 357–364.
- [20] Carl Zeiss Microscopy, ZEISS EVO Your High Definition SEM with Workflow Automation: Product Information Version 1.0, 2013, [http://applications.zeiss.com/C125792900358A3F/0/A7A32858228B4D46C1257BBB004E6E74/\\$FILE/EN_42_011_092_EVO.pdf](http://applications.zeiss.com/C125792900358A3F/0/A7A32858228B4D46C1257BBB004E6E74/$FILE/EN_42_011_092_EVO.pdf), accessed 9 October 2013.
- [21] H.-K. Chan, P.C.L. Kwok, Production methods for nanodrug particles using the bottom-up approach, *Adv Drug Deliv Rev* 63 (2011) 406–416.
- [22] X. Chen, J.M. Vaughn, M.J. Yacaman, R.O. Williams, K.P. Johnston, Rapid dissolution of high-potency danazol particles produced by evaporative precipitation into aqueous solution, *J Pharm Sci* 93 (2004) 1867–1878.
- [23] Y. Chen, Y. Lu, J. Chen, J. Lai, J. Sun, F. Hu, W. Wu, Enhanced bioavailability of the poorly water-soluble drug fenofibrate by using liposomes containing a bile salt, *Int J Pharm* 376 (2009) 153–160.
- [24] K.Y. Choi, K.H. Min, H.Y. Yoon, K. Kim, J.H. Park, I.C. Kwon, K. Choi, S.Y. Jeong, PEGylation of hyaluronic acid nanoparticles improves tumor targetability in vivo, *Biomaterials* 32 (2011) 1880–1889.
- [25] C. Colliex, H. Kohl, *Elektronenmikroskopie: Eine anwendungsbezogene Einführung*, Wiss. Verlagsges., Stuttgart, 2008.
- [26] E.R. Cooper, Nanoparticles: A personal experience for formulating poorly water soluble drugs, *J Control Release* 141 (2010) 300–302.
- [27] D.Q.M. Craig, The mechanisms of drug release from solid dispersions in water-soluble polymers, *Int J Pharm* 231 (2002) 131–144.
- [28] S.M. D'Addio, R.K. Prud'homme, Controlling drug nanoparticle formation by rapid precipitation, *Adv Drug Deliv Rev* 63 (2011) 417–426.
- [29] S. Das, P.K. Suresh, R. Desmukh, Design of Eudragit RL 100 nanoparticles by nanoprecipitation method for ocular drug delivery, *Nanomedicine* 6 (2010) 318–323.
- [30] J. Deng, L. Huang, F. Liu, Understanding the structure and stability of paclitaxel nanocrystals, *Int J Pharm* 390 (2010) 242–249.
- [31] B. Derjaguin, L. Landau, Theory of the stability of strongly charged lyophobic sols and of the adhesion of strongly charged particles in solutions of electrolytes, *Prog Surf Sci* 43 (1993) 30–59.
- [32] A. Dokoumetzidis, P. Macheras, A century of dissolution research: from Noyes and Whitney to the biopharmaceutics classification system, *Int J Pharm* 321 (2006) 1–11.
- [33] A. Dolenc, J. Kristl, S. Baumgartner, O. Planinšek, Advantages of celecoxib nanosuspension formulation and transformation into tablets, *Int J Pharm* 376 (2009) 204–212.

- [34] A. Dominik, D. Steinhilber, *Instrumentelle Analytik: Kurzlehrbuch und kommentierte Originalfragen für Pharmazeuten*, 2 ed., Dt. Apotheker-Verl., Stuttgart, 2002.
- [35] J.L. Dubois, J.L. Ford, Similarities in the release rates of different drugs from polyethylene glycol 6000 solid dispersions, *J Pharm Pharmacol* 37 (1985) 494–495.
- [36] L. Edwards, The dissolution and diffusion of aspirin in aqueous media, *Trans Faraday Soc* (1951) 1191–1210.
- [37] J.M. Edwardson, R.M. Henderson, Atomic force microscopy and drug discovery, *Drug Discov Today* 9 (2004) 64–71.
- [38] M.H. El-Shabouri, Positively charged nanoparticles for improving the oral bioavailability of cyclosporin-A, *Int J Pharm* 249 (2002) 101–108.
- [39] A.H. Elshafeey, A.O. Kamel, G.A. Awad, Ammonium methacrylate units polymer content and their effect on acyclovir colloidal nanoparticles properties and bioavailability in human volunteers, *Colloid Surface B* 75 (2010) 398–404.
- [40] Evonik Industries AG, Eudragit E 100 Product Information, <http://eudragit.evonik.com/product/eudragit/en/products-services/eudragit-products/protective-formulations/e-100/Pages/default.aspx>, accessed 31 May 2014.
- [41] H.M. Fadda, H.A. Merchant, B.T. Arafat, A.W. Basit, Physiological bicarbonate buffers: stabilisation and use as dissolution media for modified release systems, *Int J Pharm* 382 (2009) 56–60.
- [42] T. Feczko, J. Tóth, G. Dósa, J. Gyenis, Influence of process conditions on the mean size of PLGA nanoparticles, *Chem Eng Process* 50 (2011) 846–853.
- [43] H. Fessi, J.-P. Devissaguet, F. Puisieux, C. Thies, Process for the preparation of dispersible colloidal systems of a substance in the form of nanoparticles, United States Patent 5118528 (1990).
- [44] H. Fessi, F. Puisieux, J. Devissaguet, N. Ammoury, S. Benita, Nanocapsule formation by interfacial polymer deposition following solvent displacement, *Int J Pharm* 55 (1989) R1-R4.
- [45] J. Finholt, Influence of formulation on dissolution rate, in: L. Leeson, J. Carstensen (Eds.), *Dissolution Technology*, Washington, DC, 1974, pp. 106–146.
- [46] B. Finn, CELEBREX® (celecoxib) capsules, 1998, <http://labeling.pfizer.com/ShowLabeling.aspx?id=793>, accessed 16 April 2013.
- [47] B. Finn, HIGHLIGHTS OF PRESCRIBING INFORMATION, 2013, <http://labeling.pfizer.com/ShowLabeling.aspx?id=793>, accessed 16 January 2013.
- [48] E.J. Fraser, R.H. Leach, J.W. Poston, A.M. Bold, L.S. Culank, A.B. Lipede, Dissolution-rates and bioavailability of digoxin tablets, *Lancet* 1 (1973) 1393.
- [49] C. Freitas, R.H. Müller, Spray-drying of solid lipid nanoparticles (SLN™), *Eur J Pharm Biopharm* 46 (1998) 145–151.
- [50] A. Frick, C. Stern, *DSC-Prüfung in der Anwendung*, Hanser, München, Wien, 2006.
- [51] J. Gajendran, J. Kraemer, P. Langguth, In vivo predictive release methods for medicated chewing gums, *Biopharmaceutics & drug disposition* 33 (2012) 417–424.

- [52] E. Galia, E. Nicolaidis, D. Hörter, R. Löbenberg, C. Reppas, J.B. Dressman, Evaluation of various dissolution media for predicting in vivo performance of class I and II drugs, *Pharmaceutical Research* 15 (1998) 698–705.
- [53] C.V. Garcia, C.S. Paim, M. Steppe, E.E. Schapoval, Development and validation of a dissolution test for rabeprazole sodium in coated tablets, *J Pharmaceut Biomed* 41 (2006) 833–837.
- [54] J. Garside, A. Mersmann, J. Nývlt, Measurement of crystal growth and nucleation rates, 2 ed., IChemE, Rugby, 2002.
- [55] N. Garti, M. Avrahami, A. Aserin, Improved solubilization of Celecoxib in U-type nonionic microemulsions and their structural transitions with progressive aqueous dilution, *J Colloid Interface Sci* 299 (2006) 352–365.
- [56] I. Ghosh, S. Bose, R. Vippagunta, F. Harmon, Nanosuspension for improving the bioavailability of a poorly soluble drug and screening of stabilizing agents to inhibit crystal growth, *Int J Pharm* 409 (2011) 260–268.
- [57] V. Guieu, C. Ravelet, S. Perrier, Z. Zhu, S. Cayez, E. Peyrin, Aptamer enzymatic cleavage protection assay for the gold nanoparticle-based colorimetric sensing of small molecules, *Anal Chim Acta* 706 (2011) 349–353.
- [58] J. Hazarika, A. Kumar, Controllable synthesis and characterization of polypyrrole nanoparticles in sodium dodecylsulphate (SDS) micellar solutions, *Synthetic Met* 175 (2013) 155–162.
- [59] D. Heng, D.J. Cutler, H.-K. Chan, J. Yun, J.A. Raper, What is a suitable dissolution method for drug nanoparticles?, *Pharm Res* 25 (2008) 1696–1701.
- [60] A. Hildebrand, Physikochemische Charakterisierung von Gallensalz-Mischmizellen als Grundlage für innovative Arzneistoffträgersysteme. Ph.D. Thesis, Halle, 2002.
- [61] R. Hill, B. Snider, A widely applicable automated sampling apparatus for dissolution testing, *Int J Pharm* 2-3 (1987) 175–183.
- [62] A. Homayouni, F. Sadeghi, J. Varshosaz, H.A. Garekani, A. Nokhodchi, Comparing various techniques to produce micro/nanoparticles for enhancing the dissolution of celecoxib containing PVP, *Eur J Pharm Biopharm* 88 (2014) 261–274.
- [63] X. Hu, K.L. Tulsieram, Q. Zhou, L. Mu, J. Wen, Polymeric nanoparticle-aptamer bioconjugates can diminish the toxicity of mercury in vivo, *Toxicol Lett* 208 (2012) 69–74.
- [64] D. Jain, R. Athawale, A. Bajaj, S. Shrikhande, P.N. Goel, R.P. Gude, Studies on stabilization mechanism and stealth effect of poloxamer 188 onto PLGA nanoparticles, *Colloid Surface B* 109 (2013) 59–67.
- [65] J. Jaiswal, S.K. Gupta, J. Kreuter, Preparation of biodegradable cyclosporine nanoparticles by high-pressure emulsification-solvent evaporation process, *J Control Release* 96 (2004) 169–178.
- [66] D.M.K. Jensen, D. Cun, M.J. Maltesen, S. Frokjaer, H.M. Nielsen, C. Foged, Spray drying of siRNA-containing PLGA nanoparticles intended for inhalation, *J Control Release* 142 (2010) 138–145.
- [67] J. Johansson, M. Cauchi, M. Sundgren, Multiple fiber-optic dual-beam UV/Vis system with application to dissolution testing, *J Pharm Biomed Anal* 29 (2002) 469–476.

- [68] W.J. Jones, Dependence on curvature of surface of condensed phase, *Ann Phys* (1913) 441–448.
- [69] D. Juenemann, H. Bohets, M. Ozdemir, R. de Maesschalck, K. Vanhoutte, K. Peeters, L. Nagels, J.B. Dressman, Online monitoring of dissolution tests using dedicated potentiometric sensors in biorelevant media, *Eur J Pharm Biopharm* 78 (2011) 158–165.
- [70] J.-U.A.H. Junghanns, R.H. Müller, Nanocrystal technology, drug delivery and clinical applications, *Int J Nanomed* 3 (2008) 295–310.
- [71] M. Kakran, N.G. Sahoo, L. Li, Z. Judeh, Fabrication of quercetin nanoparticles by anti-solvent precipitation method for enhanced dissolution, *Powder Technol* 223 (2012) 59–64.
- [72] M. Kamba, Y. Seta, N. Takeda, T. Hamaura, A. Kusai, H. Nakane, K. Nishimura, Measurement of agitation force in dissolution test and mechanical destructive force in disintegration test, *Int J Pharm* 250 (2003) 99–109.
- [73] N. Khayata, W. Abdelwahed, M. Chehna, C. Charcosset, H. Fessi, Stability study and lyophilization of vitamin E-loaded nanocapsules prepared by membrane contactor, *Int J Pharm* 439 (2012) 254–259.
- [74] P. Khoshakhlagh, R. Johnson, P. Langguth, T. Nawroth, L. Schmueser, N. Hellmann, H. Decker, N.K. Szekely, Fasted-State Simulated Intestinal Fluid "FaSSIF-C", a Cholesterol Containing Intestinal Model Medium for In Vitro Drug Delivery Development, *Journal of Pharmaceutical Sciences* 104 (2015) 2213–2224.
- [75] P. Khoshakhlagh, R. Johnson, T. Nawroth, P. Langguth, L. Schmueser, N. Hellmann, H. Decker, N.K. Szekely, Nanoparticle structure development in the gastro-intestinal model fluid FaSSIF mod6.5 from several phospholipids at various water content relevant for oral drug administration, *Eur. J. Lipid Sci. Technol.* 116 (2014) 1155–1166.
- [76] J. Kiefer, Crossflow-Membranfiltration - Eine verfahrenstechnische Betrachtung, *Getränkeindustrie* (2006) 40–47.
- [77] C. Kindermann, K. Matthée, J. Strohmeyer, F. Sievert, J. Breitzkreutz, Tailor-made release triggering from hot-melt extruded complexes of basic polyelectrolyte and poorly water-soluble drugs, *Eur J Pharm Biopharm* 79 (2011) 372–381.
- [78] L.F. Knapp, The solubility of small particles and the stability of colloids, *T Faraday Soc* (1922) 457–465.
- [79] P. Kocbek, S. Baumgartner, J. Kristl, Preparation and evaluation of nanosuspensions for enhancing the dissolution of poorly soluble drugs, *Int J Pharm* 312 (2006) 179–186.
- [80] D.E. Koppel, Analysis of Macromolecular Polydispersity in Intensity Correlation Spectroscopy: The Method of Cumulants, *J Chem Phys (The Journal of Chemical Physics)* 57 (1972) 4814–4820.
- [81] H.-J. Krause, P. Rohdewald, Preparation of Gelatin Nanocapsules and Their Pharmaceutical Characterization, *Pharm Res* (1985) 239–243.
- [82] H.P. Latscha, U. Kazmaier, H.A. Klein, *Chemie für Pharmazeuten: Unter Berücksichtigung des "GK" Pharmazie mit 57 Tab*, 5 ed., Springer, Berlin [u.a.], 2002.
- [83] P. Lertsutthiwong, K. Noomun, N. Jongaroonngamsang, P. Rojsitthisak, U. Nimmannit, Preparation of alginate nanocapsules containing turmeric oil, *Carbohydr Polym* 74 (2008) 209–214.

- [84] X.-X. Li, Y. Wang, P.-P. Xu, Q.-Z. Zhang, K. Nie, X. Hu, B. Kong, L. Li, J. Chen, Effects of temperature and wavelength choice on in-situ dissolution test of Cimetidine tablets, *J Pharm Anal* 3 (2013) 71–74.
- [85] S.B. Lim, A. Banerjee, H. Önyüksel, Improvement of drug safety by the use of lipid-based nanocarriers, *J Control Release* 163 (2012) 34–45.
- [86] F. Lince, D.L. Marchisio, A.A. Barresi, Strategies to control the particle size distribution of poly-epsilon-caprolactone nanoparticles for pharmaceutical applications, *J Colloid Interface Sci* 322 (2008) 505–515.
- [87] J. Lindenbaum, M.H. Mellow, M.O. Blackstone, V.P. Butler, Variation in biologic availability of digoxin from four preparations, *N Engl J Med* 285 (1971) 1344–1347.
- [88] Y. Liu, C. Sun, Y. Hao, T. Jiang, L. Zheng, S. Wang, Mechanism of dissolution enhancement and bioavailability of poorly water soluble celecoxib by preparing stable amorphous nanoparticles, *J Pharm Pharm Sci* 13 (2010) 589–606.
- [89] S. Lutter, J. Koetz, B. Tiersch, A. Boschetti-de-Fierro, V. Abetz, Formation of gold nanoparticles in triblock terpolymer-modified inverse microemulsions, *Colloid Surface A* 329 (2008) 169–176.
- [90] A.N. Martin, H. Leuenberger, *Physikalische Pharmazie: Pharmazeutisch angewandte physikalisch-chemische Grundlagen ; mit 163 Tabellen*, 4 ed., Wiss. Verl.-Ges., Stuttgart, 2002.
- [91] A. Mihranyan, M. Strømme, Solubility of fractal nanoparticles, *Surf Sci* 601 (2007) 315–319.
- [92] C.E. Mora-Huertas, H. Fessi, A. Elaissari, Polymer-based nanocapsules for drug delivery, *Int J Pharm* 385 (2010) 113–142.
- [93] S.E. Morgan, K. Havelka, R. Lochhead (Eds.), *Cosmetic Nanotechnology*. ACS Symposium Series, 2007.
- [94] M. Mosharraf, C. Nyström, The effect of particle size and shape on the surface specific dissolution rate of microsized practically insoluble drugs, *Int J Pharm* 122 (1995) 35–47.
- [95] D. Mou, H. Chen, J. Wan, H. Xu, X. Yang, Potent dried drug nanosuspensions for oral bioavailability enhancement of poorly soluble drugs with pH-dependent solubility, *Int J Pharm* 413 (2011) 237–244.
- [96] R. Müller, B. Böhm, M. Grau, Nanosuspensions: a formulation approach for poorly soluble and poorly bioavailable drugs, in: D.L. Wise (Ed.), *Handbook of pharmaceutical controlled release technology*, Marcel Dekker, New York, 2000, pp. 345–357.
- [97] R.H. Müller, S. Gohla, C.M. Keck, State of the art of nanocrystals--special features, production, nanotoxicology aspects and intracellular delivery, *Eur J Pharm Biopharm* 78 (2011) 1–9.
- [98] R.H. Müller, C. Jacobs, O. Kayser, Nanosuspensions as particulate drug formulations in therapy. Rationale for development and what we can expect for the future, *Adv Drug Deliv Rev* 47 (2001) 3–19.
- [99] E. Mutschler, *Mutschler Arzneimittelwirkungen: Lehrbuch der Pharmakologie und Toxikologie*, 9 ed., Wiss. Verl.-Ges., Stuttgart, 2008.
- [100] T. Nawroth, P. Buch, K. Buch, P. Langguth, R. Schweins, Liposome formation from bile salt-lipid micelles in the digestion and drug delivery model FaSSIF(mod) estimated by combined time-resolved neutron and dynamic light scattering, *Molecular pharmaceutics* 8 (2011) 2162–2172.
- [101] E. Nelson, Solution rate of theophylline salts and effects from oral administration, *J Am Pharm Assoc* 46 (1957) 607–614.

- [102] J. Ní Mhurchú, G. Foley, Dead-end filtration of yeast suspensions: correlating specific resistance and flux data using artificial neural networks, *J Membr Sci* 281 (2006) 325–333.
- [103] M. Nicklasson, A. Orbe, J. Lindberg, B. Borga, A.-B. Magnusson, G. Nilsson, R. Ahlgren, L. Jacobsen, A collaborative study of the in vitro dissolution of phenacetin crystals comparing the flow through method A collaborative study of the in vitro dissolution of phenacetin crystals, *Int J Pharm* 69 (1991) 255–264.
- [104] A. Noyes, W. Whitney, The rate of solution of solid substances in their own solutions, *J Am Chem Soc* 19 (1897) 930–934.
- [105] W. Ostwald, On the supposed isomerism of red and yellow mercury oxide and the surface tension of solid bodies, *Z Phys Chem* (1900) 495–503.
- [106] J. Park, P.M. Fong, J. Lu, K.S. Russell, C.J. Booth, W.M. Saltzman, T.M. Fahmy, PEGylated PLGA nanoparticles for the improved delivery of doxorubicin, *Nanomed-Nanotechnol* 5 (2009) 410–418.
- [107] S.-H. Park, H.-K. Choi, The effects of surfactants on the dissolution profiles of poorly water-soluble acidic drugs, *Int J Pharm* 321 (2006) 35–41.
- [108] Particle size analysis: Dynamic light scattering (DLS) = Analyse granulométrique: dispersion lumineuse dynamique (DLD), 1 ed., International Organization for Standardization, Geneva, Switzerland, 2008.
- [109] J. Patel, Patel D.J., V. Pandya, An Overview: Nanoparticles, *Int J Pharm Sci Nanotech* 1 (2008) 215–220.
- [110] G. Pearce, Introduction to membranes: Filtration for water and wastewater treatment, *Filtr Separat* 44 (2007) 24–27.
- [111] K. Peeters, R. de Maesschalck, H. Bohets, K. Vanhoutte, L. Nagels, In situ dissolution testing using potentiometric sensors, *Eur J Pharm Biopharm* 34 (2008) 243–249.
- [112] B. Penth, Kontinuierliche Fällung von nanoskaligen Produkten in Mikroreaktoren, Patent DE102005048201A1 20.04.2006 (2005).
- [113] A. Pérez, A.J. Sandoval, A. Cova, A.J. Müller, Glass transitions and physical aging of cassava starch - corn oil blends, *Carbohydr Polym* 105 (2014) 244–252.
- [114] T.-M. Perger, M. Bester-Rogac, Thermodynamics of micelle formation of alkyltrimethylammonium chlorides from high performance electric conductivity measurements, *J Colloid Interface Sci* 313 (2007) 288–295.
- [115] R. Peschka, T. Purmann, R. Schubert, Cross-flow filtration--an improved detergent removal technique for the preparation of liposomes, *Int J Pharm* 162 (1998) 177–183.
- [116] C. Pinto Reis, R.J. Neufeld, A.J. Ribeiro, F. Veiga, Nanoencapsulation I. Methods for preparation of drug-loaded polymeric nanoparticles, *Nanomed-Nanotechnol* 2 (2006) 8–21.
- [117] E.-M. Prinz, Multi-functionalized magnetic nanoparticles as drug-delivery systems. Ph.D. Thesis, Saarbrücken, 2012.
- [118] D. Quintanar-Guerrero, E. Allémann, H. Fessi, Doelker E., Preparation Techniques and Mechanisms of Formation of Biodegradable Nanoparticles from Preformed Polymers, *Drug Dev Ind Pharm* 24 (1998) 11 13-1 128.

- [119] D. Quintanar-Guerrero, D. Tamayo-Esquivel, A. Ganem-Quintanar, E. Allémann, E. Doelker, Adaptation and optimization of the emulsification-diffusion technique to prepare lipidic nanospheres, *Eur J Pharm Sci* 26 (2005) 211–218.
- [120] D.A. Quinteros, V.R. Rigo, A.F.J. Kairuz, M.E. Olivera, R.H. Manzo, D.A. Allemandi, Interaction between a cationic polymethacrylate (Eudragit E100) and anionic drugs, *Eur J Pharm Sci* 33 (2008) 72–79.
- [121] S.A. Qureshi, I.J. McGilveray, Typical variability in drug dissolution testing: study with USP and FDA calibrator tablets and a marketed drug (glibenclamide) product, *Eur J Pharm Sci* 7 (1999) 249–258.
- [122] A. Ravazzini, A. van Nieuwenhuijzen, J. van der Graaf, Direct ultrafiltration of municipal wastewater: comparison between filtration of raw sewage and primary clarifier effluent, *Desalination* 178 (2005) 51–62.
- [123] S.C.P. Rekha M.R., in: C. van der Walle (Ed.), *Peptide and Protein Delivery*, Elsevier Science, Burlington, 2011, pp. 165–194.
- [124] G. Romero, S. Moya, Chapter 4 – Synthesis of Organic Nanoparticles, in: J.M.d.I. Fuente, V. Grazu (Eds.), *Nanobiotechnology: Inorganic nanoparticles vs organic nanoparticles*, Elsevier, [S.I.], 2012, pp. 115–141.
- [125] M.S. Romero-Cano, B. Vincent, Controlled release of 4-nitroanisole from poly(lactic acid) nanoparticles, *J Control Release* 82 (2002) 127–135.
- [126] Rote Liste 2012: Arzneimittelverzeichnis für Deutschland (einschliesslich EU-Zulassungen und bestimmter Medizinprodukte), 52 ed., Rote Liste Service, Frankfurt/Main, 2012.
- [127] J. Salazar, A. Ghanem, R.H. Müller, J.P. Möschwitzer, Nanocrystals: Comparison of the size reduction effectiveness of a novel combinative method with conventional top-down approaches, *Eur J Pharm Biopharm* 81 (2012) 82–90.
- [128] S. Samanman, P. Kanatharana, P. Asawatreratanakul, P. Thavarungkul, Characterization and application of self-assembled layer by layer gold nanoparticles for highly sensitive label-free capacitive immunosensing, *Electrochim Acta* 80 (2012) 202–212.
- [129] R.M. Samstein, K. Perica, F. Balderrama, M. Look, T.M. Fahmy, The use of deoxycholic acid to enhance the oral bioavailability of biodegradable nanoparticles, *Biomaterials* 29 (2008) 703–708.
- [130] M. Sangwai, P. Vavia, Amorphous ternary cyclodextrin nanocomposites of telmisartan for oral drug delivery: Improved solubility and reduced pharmacokinetic variability, *Int J Pharm* 453 (2013) 423–432.
- [131] N.C. Santos, M.A. Castanho, An overview of the biophysical applications of atomic force microscopy, *Biophys Chem* 107 (2004) 133–149.
- [132] A. Sarnes, J. Østergaard, S.S. Jensen, J. Aaltonen, J. Rantanen, J. Hirvonen, L. Peltonen, Dissolution study of nanocrystal powders of a poorly soluble drug by UV imaging and channel flow methods, *Eur J Pharm Sci* 50 (2013) 511–519.
- [133] T. Scheper, *Diplom Chemie Grundoperationen Filtration 1*, 2011, http://www.tci.uni-hannover.de/index.php?elD=tx_nawsecuredl&u=0&file=uploads/media/diplom-chemie-grundoperationen-filtration-

- 1.pdf&t=1373373828&hash=7910faa499098566460d8a57f9276ab628867a4d, accessed 8 July 2013.
- [134] O. Scherzer, Über einige Fehler von Elektronenlinsen, *Zeitschrift für Physik* 9 (1936) 593–603.
- [135] F. Schwertfirm, J. Gradl, H.C. Schwarzer, W. Peukert, M. Manhart, The low Reynolds number turbulent flow and mixing in a confined impinging jet reactor, *Int J Heat Fluid Fl* 28 (2007) 1429–1442.
- [136] C. Selbach, Polymerpartikel zur ektoparasitären Anwendung am Tier. Dissertation, Universitäts- und Landesbibliothek Bonn, Bonn, 2010.
- [137] S. Sethia, E. Squillante, Solid dispersion of carbamazepine in PVP K30 by conventional solvent evaporation and supercritical methods, *Int J Pharm* 272 (2004) 1–10.
- [138] M. Shah, Dissolution Apparatus and Detail As Per USP, 2011, <http://pharmatips.doyouknow.in/>, accessed 13 February 2013.
- [139] Shah V. P., A. Noory, C. Noory, B. McCullough, S. Clarke, R. Everett, H. Naviasky, B.N. Srinivasan, D. Fortman, J.P. Skelly, In vitro dissolution of sparingly water-soluble drug dosage forms, *Int J Pharm* 125 (1995) 99–106.
- [140] P.M.S.L. Shanthi, R.V. Mangalaraja, A.P. Uthirakumar, S. Velmathi, T. Balasubramanian, M. Ashok, Synthesis and characterization of porous shell-like nano hydroxyapatite using cetrimide as template, *J Colloid Interface Sci* 350 (2010) 39–43.
- [141] T.R. Shaw, M.R. Howard, J. Hamer, Recent changes in biological availability of digoxin. Effect of an alteration in 'Lanoxin' tablets, *Br Heart J* 36 (1974) 85–89.
- [142] J. Skelly, Bioavailability of sustained release dosage forms - relationship with in-vitro dissolution, in: A. Yacobi, E. Holperin-Walega (Eds.), *Oral Sustained Release Formulations*, Pergamon, New York, 1988, p. 57.
- [143] D.F. Stamatialis, B.J. Papenburg, M. Gironés, S. Saiful, S.N. Bettahalli, S. Schmitmeier, M. Wessling, Medical applications of membranes: Drug delivery, artificial organs and tissue engineering, *J Membrane Sci* 308 (2008) 1–34.
- [144] T. Sugimoto, Preparation of monodispersed colloidal particles, *Adv Colloid Interfac* 28 (1987) 65–108.
- [145] B. Sun, Y. Yeo, Nanocrystals for the parenteral delivery of poorly water-soluble drugs, *Curr Opin Solid St M* 16 (2012) 295–301.
- [146] A. Sze, D. Erickson, L. Ren, D. Li, Zeta-potential measurement using the Smoluchowski equation and the slope of the current-time relationship in electroosmotic flow, *J Colloid Interface Sci* 261 (2003) 402–410.
- [147] Z. Tan, H. Abe, M. Naito, S. Ohara, Oriented growth behavior of Ag nanoparticles using SDS as a shape director, *J Colloid Interface Sci* 348 (2010) 289–292.
- [148] R. Tantra, P. Schulze, P. Quincey, Effect of nanoparticle concentration on zeta-potential measurement results and reproducibility, *Particuology* 8 (2010) 279–285.
- [149] R.E. Thach, S.S. Thach, Damage to biological samples caused by the electron beam during electron microscopy, *Biophys J (Biophysical Journal)* 11 (1971) 204–210.

- [150] The United States Pharmacopeia 2011: USP 34 ; The national formulary NF 29, United States Pharmacopeial Convention, Rockville, MD, 2010.
- [151] A.A. Thorat, S.V. Dalvi, Liquid antisolvent precipitation and stabilization of nanoparticles of poorly water soluble drugs in aqueous suspensions: Recent developments and future perspective, *Chem Eng J* 181-182 (2012) 1–34.
- [152] A.E. Türeli, Nanoparticle Preparation Process Using Novel Microjet Reactor Technology for Enhancing Dissolution Rates of Poorly Water Soluble Drugs. Ph.D. Thesis, Mainz, 2015.
- [153] U.S. Department of Health and Human Services, Food and Drug Administration, Center for Drug Evaluation and Research (CDER), Guidance for Industry: Dissolution Testing of Immediate Release Solid Oral Dosage Forms, 1997, <http://www.fda.gov/downloads/Drugs/GuidanceComplianceRegulatoryInformation/Guidances/ucm070237.pdf>, accessed 21 February 2013.
- [154] U.S. Food and Drug Administration, Dissolution Methods Database, 2010, http://www.accessdata.fda.gov/scripts/cder/dissolution/dsp_SearchResults_Dissolutions.cfm?PrintAll=1, accessed 25 November 2014.
- [155] C.-M.L. Udo Bakowsky, Nanopartikel als Wirkstoffträger, *Pharmazeutische Zeitung* (2003).
- [156] I. Valente, E. Celasco, D. Marchisio, A. Barresi, Nanoprecipitation in confined impinging jets mixers: Production, characterization and scale-up of pegylated nanospheres and nanocapsules for pharmaceutical use, *Chem Eng Sci* 77 (2012) 217–227.
- [157] S. Verma, R. Gokhale, D.J. Burgess, A comparative study of top-down and bottom-up approaches for the preparation of micro/nanosuspensions, *Int J Pharm* 380 (2009) 216–222.
- [158] E. Verwey, J. Overbeek, Theory of the stability of lyophobic colloids, *J Coll Sci Imp u Tok* 10 (1955) 224–225.
- [159] J.-X. Wang, Q.-X. Zhang, Y. Zhou, L. Shao, J.-F. Chen, Microfluidic synthesis of amorphous cefuroxime axetil nanoparticles with size-dependent and enhanced dissolution rate, *Chem Eng J* 162 (2010) 844–851.
- [160] X.-Q. Wang, Q. Zhang, pH-sensitive polymeric nanoparticles to improve oral bioavailability of peptide/protein drugs and poorly water-soluble drugs, *Eur J Pharm Biopharm* 82 (2012) 219–229.
- [161] C. Weiler, Generierung leicht dispergierbarer Inhalationspulver mittels Sprühtrocknung. Dissertation, 09: Chemie, Pharmazie und Geowissenschaft. 09: Chemie, Pharmazie und Geowissenschaft, Mainz, 2009.
- [162] D.L. Wise (Ed.), Handbook of pharmaceutical controlled release technology, Marcel Dekker, New York, 2000.
- [163] C.-Y. Wu, L.Z. Benet, Predicting Drug Disposition via Application of BCS: Transport/Absorption/ Elimination Interplay and Development of a Biopharmaceutics Drug Disposition Classification System, *Pharm Res* 22 (2005) 11–23.
- [164] L. Wu, J. Zhang, W. Watanabe, Physical and chemical stability of drug nanoparticles, *Adv Drug Deliv Rev* 63 (2011) 456–469.

-
- [165] J.-W. Yoo, N. Giri, C.H. Lee, pH-sensitive Eudragit nanoparticles for mucosal drug delivery, *Int J Pharm* 403 (2011) 262–267.
- [166] S. Zhang, R. Ruiz SR., Fast Bonding Hair/Eyelash Extension Adhesive Compositions Based on Medical Grade High Viscosity Cyanoacrylates Fast Bonding Hair/Eyelash Extension Adhesive Compositions Based on Medical Grade High Viscosity Cyanoacrylates, Patent US20120247497 A1 (2011).
- [167] Z. Zhang, D.W. Grijpma, J. Feijen, Poly(trimethylene carbonate) and monomethoxy poly(ethylene glycol)-block-poly(trimethylene carbonate) nanoparticles for the controlled release of dexamethasone, *J Control Release* 111 (2006) 263–270.
- [168] M.X. Zhou, D. Shoudt, G. Calderon, M. Feng, Application of USP Apparatus 7 to In Vitro Drug Release in Scopolamine Transdermal Systems, *Dissolution Technol.* 14 (2007) 25–29.

List of Tables

Table 1: Advantages of nanoparticulate towards coarsely-dispersed API for oral administration of drugs.	3
Table 2: Classification of electron microscopy techniques according to type of detection and instrument (according to Colliex and Kohl, 2008 [25])......	31
Table 3: Compendial dissolution tests (USP) [138,150]......	37
Table 4: Biopharmaceutics Classification System (BCS) according to Amidon et al. [6]......	38
Table 5: Modes of membrane filtration according to Scheper [133].	45
Table 6: Used equipment. (continued)	50
Table 7: Chemical reagents.	53
Table 8: Dissolution media.....	54
Table 9: Flow rates of MJR assembly – micro annular gear pump at selected rotational speeds (manufacturer specification).	56
Table 10: Technical parameters of MJR preparation of celecoxib-Eudragit E 100-NPs by nanoprecipitation – alternative method (without use of co-stabilizer).	57
Table 11: HPLC method parameters for the determination of celecoxib content in NPs.	59
Table 12: Properties of the used cross-flow filtration modules.....	63
Table 13: Flow-through properties of the cross-flow filtration system (permeate plus retentate and permeate), n=3, values are mean \pm SD.	71
Table 14: Bench-top preparation (emulsification-diffusion) of celecoxib-Eudragit E 100 – NPs with Poloxamer 407 as co-stabilizer. Solvent phase: 25/50/100 mg/mL celecoxib and 50/100/200 mg/mL Eudragit E 100 in 2 mL ethyl acetate, non-solvent phase: 2.5/12.5/25/50 mg/mL Poloxamer 407 in 10 mL of water, 3 x 30 s homogenization at 30000 rpm, removal of ethyl acetate in rotary evaporator (5 min at 40 °C, 220 mbar and 280 rpm followed by 10 min at 40 °C, 180 mbar, and 280 rpm), n=3 (25 mg/mL celecoxib, 50 mg/mL Eudragit E 100 and 12.5 mg/mL Poloxamer 407) and n=1 (other formulations), n=1: Z-Average, PDI and ZP values are mean of three measurements \pm SD, EE values respectively single measurement, n=3: values are mean \pm SD.	82
Table 15: MJR preparation of celecoxib-Eudragit E 100-NPs stabilized with Poloxamer 407, nanoprecipitation technique: Solvent phase: 25 mg/mL celecoxib and 50 mg/mL Eudragit E 100 in methanol, non-solvent phase: 12.5 mg/mL Poloxamer 407 in water, operation temperature: 40 and 60 °C, nitrogen pressure: 0 and 0.5 bar, pump rotational speed (solvent phase : non-solvent phase) 300 : 1500 rpm and 1200 :	

6000 rpm, n=1, Z-Average, PDI and ZP values are mean of three measurements \pm SD, EE values respectively single measurement.	96
Table 16: Z-Average, PDI (DLS), shape and diameter (SEM) of MJR produced celecoxib-Eudragit E 100-NPs (nanoprecipitation and emulsification-diffusion technique), values are mean of three measurements \pm SD.	105
Table 17: Statistical comparison of dissolution profiles of celecoxib-Eudragit E 100-NPs of different size and celecoxib (API) powder: Evaluation performed with model independent approach using a similarity factor according to FDA "Guidance for Industry: Dissolution Testing of Immediate Release Solid Oral Dosage Forms" [153], equivalence is given if $f_1 < 15$ (0–15) and $f_2 > 50$ (50–100).....	126
Table 18: R_{max} - and k-values of the dissolution of the differently-sized NP batches. R_{max} values obtained as y-intercept of a line through the last three sampling points after plotting of the reciprocal of release percentage against the reciprocal of dissolution time. k-values obtained as slope of the regression line through the first three sampling points after plotting of the natural logarithm of release against dissolution time.	128
Table 19: Preparation of celecoxib-Eudragit E 100 – NPs with Poloxamer 407 as co-stabilizer. Solvent phase: 5 mg/mL celecoxib and 5/10 mg/mL Eudragit E 100 in 1/2/5 mL of ethyl acetate, non-solvent phase: 1 mg/mL Poloxamer 407 in 10 mL of water, 3 x 30 s homogenization with the high speed homogenizer at 30,000 rpm, removal of ethyl acetate in the rotary evaporator (5 min at 40 °C, 220 mbar and 280 rpm followed by 10 min at 40 °C, 180 mbar, and 280 rpm), n=1, Z-Average, PDI and ZP values are mean of three measurements \pm SD, EE values respectively single measurement.	159
Table 20: Preparation of celecoxib-Eudragit E 100 – NPs with SDS as co-stabilizer. Solvent phase: 5 mg/mL celecoxib and 5/10 mg/mL Eudragit E 100 in 1/2/5 mL of ethyl acetate, non-solvent phase: 1 mg/mL SDS in 10 mL of water, 3 x 30 s homogenization with the high speed homogenizer at 30,000 rpm, removal of ethyl acetate in the rotary evaporator (5 min at 40 °C, 220 mbar and 280 rpm followed by 10 min at 40 °C, 180 mbar, and 280 rpm), n=1, Z-Average, PDI and ZP values are mean of three measurements \pm SD, EE values respectively single measurement.	160
Table 21: Preparation of celecoxib-Eudragit E 100 – NPs with PVA (MW: 27,000) as co-stabilizer. Solvent phase: 5 mg/mL celecoxib and 5/10 mg/mL Eudragit E 100 in 1/2/5 mL of ethyl acetate, non-solvent phase: 1 mg/mL PVA in 10 mL of water, 3 x 30 s homogenization with the high speed homogenizer at 30,000 rpm, removal of ethyl acetate in the rotary evaporator (5 min at 40 °C, 220 mbar and 280 rpm followed by 1 min at 40 °C, 180 mbar, and 280 rpm), n=1, Z-Average, PDI and	

ZP values are mean of three measurements \pm SD, EE values respectively single measurement.	161
Table 22: Preparation of celecoxib-Eudragit E 100 – NPs with varying amounts of Poloxamer 407. Solvent phase: 5 mg/mL celecoxib and 10 mg/mL Eudragit E 100 in 2 mL of ethyl acetate, non-solvent phase: 0.1/0.5/1/2.5/5/10 mg/mL Poloxamer 407 in 10 mL of water, 3 x 30 s homogenization with the high speed homogenizer at 30,000 rpm, removal of ethyl acetate in the rotary evaporator (5 min at 40 °C, 220 mbar and 280 rpm followed by 10 min at 40 °C, 180 mbar, and 280 rpm), n=3, values are mean \pm SD.....	162
Table 23: Stability study of celecoxib-Eudragit E 100 – NPs stabilized with Poloxamer 407: Solvent phase: 5 mg/mL celecoxib and 10 mg/mL Eudragit E 100 in 2 mL of ethyl acetate, non-solvent phase: 2.5 mg/mL Poloxamer 407 in 10 mL of water, 3 x 30 s homogenization with the high speed homogenizer at 30,000 rpm, removal of ethyl acetate in the rotary evaporator (5 min at 40 °C, 220 mbar and 280 rpm followed by 10 min at 40 °C, 180 mbar, and 280 rpm), stored at room temperature, n=3, values are mean \pm SD.....	163
Table 24: Stability study of celecoxib-Eudragit E 100 – NPs stabilized with Poloxamer 407: Solvent phase: 5 mg/mL celecoxib and 10 mg/mL Eudragit E 100 in 2 mL of ethyl acetate, non-solvent phase: 2.5 mg/mL Poloxamer 407 in 10 mL of water, 3 x 30 s homogenization with the high speed homogenizer at 30,000 rpm, removal of ethyl acetate in the rotary evaporator (5 min at 40 °C, 220 mbar and 280 rpm followed by 10 min at 40 °C, 180 mbar, and 280 rpm), stored at 5 °C, n=3, values are mean \pm SD.	163
Table 25: Stability study of celecoxib-Eudragit E 100 – NPs stabilized with Poloxamer 407: Solvent phase: 25 mg/mL celecoxib and 50 mg/mL Eudragit E 100 in 2 mL of ethyl acetate, non-solvent phase: 12.5 mg/mL Poloxamer 407 in 10 mL of water, 3 x 30 s homogenization with the high speed homogenizer at 30,000 rpm, removal of ethyl acetate in the rotary evaporator (5 min at 40 °C, 220 mbar and 280 rpm followed by 10 min at 40 °C, 180 mbar, and 280 rpm), stored at room temperature, n=3, values are mean \pm SD.....	164
Table 26: Stability study of celecoxib-Eudragit E 100 – NPs stabilized with Poloxamer 407: Solvent phase: 25 mg/mL celecoxib and 50 mg/mL Eudragit E 100 in 2 mL of ethyl acetate, non-solvent phase: 12.5 mg/mL Poloxamer 407 in 10 mL of water, 3 x 30 s homogenization with the high speed homogenizer at 30,000 rpm, removal of ethyl acetate in the rotary evaporator (5 min at 40 °C, 220 mbar and 280 rpm followed by 10 min at 40 °C, 180 mbar, and 280 rpm), stored at 5 °C, n=3, values are mean \pm SD.	164

Table 27: Stability study of celecoxib-Eudragit E 100 – NPs stabilized with Poloxamer 407: t-test for comparison of storage at room temperature versus storage at 5 °C and usage of 5 mg/mL versus 25 mg/mL celecoxib in solvent phase, data rows from days 0 to 14 are respectively compared.	165
Table 28: MJR preparation of celecoxib-Eudragit E 100 – NPs stabilized with Poloxamer 407 using DoE: Solvent phase: 25 mg/mL celecoxib and 50 mg/mL Eudragit E 100 in ethyl acetate, non-solvent phase: 12.5 mg/mL Poloxamer 407 in water, operation temperature: 40-60 °C, nitrogen pressure: 0-0.50 bar, pump rotational speed (solvent phase : non-solvent phase) 300 : 1500 rpm to 1200 : 6000 rpm, removal of remaining ethyl acetate by evaporating for 18 h in the fume hood, values are mean of three measurements.	166
Table 29: MJR preparation of celecoxib-Eudragit E 100 – NPs stabilized with Poloxamer 407, validation of DoE model: Solvent phase: 25 mg/mL celecoxib and 50 mg/mL Eudragit E 100 in ethyl acetate, non-solvent phase: 12.5 mg/mL Poloxamer 407 in water, operation temperature: 55-59 °C, nitrogen pressure: 0.31-0.47 bar, pump rotational speed (solvent phase : non-solvent phase) 300 : 1500 rpm to 719 : 3595 rpm, removal of remaining ethyl acetate by evaporating for 18 h in the fume hood, n=1, Z-Average, PDI and ZP values are mean of three measurements ± SD, EE values respectively single measurement.	167
Table 30: Dissolution of celecoxib-Eudragit E 100-NPs in HCl pH 1.2: NP properties: 80 nm (Z-Average), 0.131 (PDI) and 2.573 mg/mL (celecoxib concentration of the nanosuspension), detection: UV-Vis (248 nm), n=3, values are mean ± SD.	168
Table 31: Dissolution of celecoxib-Eudragit E 100-NPs in diluted HCl pH 1.2 + 0.15 M NaCl: NP properties: 100 nm (Z-Average), 0.100 (PDI) and 2.331 mg/mL (celecoxib concentration of the nanosuspension), detection: UV-Vis (248 nm), n=1.	168
Table 32: Dissolution of celecoxib-Eudragit E 100-NPs in diluted HCl pH 1.2 + 0.001/0.01/0.3/1.0 % cetrimide: NP properties: 80 nm (Z-Average), 0.131 (PDI) and 2.573 mg/mL (celecoxib concentration of the nanosuspension), detection: UV-Vis (248 nm), n=1.	169
Table 33: Dissolution of celecoxib-Eudragit E 100-NPs in diluted HCl pH 1.2 + 0.3 % cetrimide: NP properties: 160 nm (Z-Average), 0.094 (PDI) and 2.388 mg/mL (celecoxib concentration of the nanosuspension), filters: cross-flow filtration modules of 100 and 500 kDa and 0.2 µm syringe filter holders (dead-end), detection: UV-Vis (248 nm), n=3, values are mean ± SD.	169
Table 34: Dissolution of celecoxib-Eudragit E 100-NPs in diluted HCl pH 1.2 + 0.05 % cetrimide: NP properties: 160 nm (Z-Average), 0.094 (PDI) and 2.509 mg/mL (celecoxib concentration of the nanosuspension),	

filters: cross-flow filtration modules of 100 and 500 kDa and 0.2 μm syringe filter holders (dead-end), detection: UV-Vis (248 nm), n=3, values are mean \pm SD.	170
Table 35: Dissolution of celecoxib-Eudragit E 100-NPs in phosphate buffer pH 2.0/2.5/3.5/4.5/5.2+ 0.3 % cetrимide: NP properties: 220 nm (Z-Average), 0.086 (PDI) and 3.666 mg/mL (celecoxib concentration of the nanosuspension), filter: 500 kDa cross-flow filtration module, detection: UV-Vis (248 nm), n=3, values are mean \pm SD.....	170
Table 36: Dissolution of celecoxib-Eudragit E 100-NPs of different size and celecoxib powder in phosphate buffer pH 2.0 + 0.3 % cetrимide: NP properties: 221/255/293/362/497 nm (Z-Average), < 0.25 (PDI) and ~ 2.650–4.850 mg/mL (celecoxib concentration of the nanosuspension), API powder: 2537 $\mu\text{g/mL}$ (celecoxib concentration of the suspension), filter: 500 kDa cross-flow filtration module, detection: UV-Vis (248 nm), n=6, values are mean \pm SD.	171

List of Figures

Figure 1: Classification scheme of NPs. Differentiation between nanospheres and nanocapsules and among them between nanoemulsions and enveloped solid systems (based on [3]).	4
Figure 2: Structure of celecoxib.	6
Figure 3: Structure of Eudragit E.	7
Figure 4: Structure of SDS.	7
Figure 5: Structure of PVA.	8
Figure 6: Structure of Poloxamers (Poloxamer 407: $x=101$ $y=56$ $z=101$ [166]).	8
Figure 7: Schematic of pharmaceutical top-down production techniques. From diminution steps like milling microparticles are obtained. These can either be directly transferred to dosage forms or further diminished (e.g. through wet milling) to yield NPs.	11
Figure 8: Schematic of the production of polymeric NPs with emulsification/solvent-diffusion technique.	13
Figure 9: Schematic of steps of precipitation process.	16
Figure 10: Functional principle of MicroJetReactor. (a) Schematic of MJR (mode of operation): Two opposed high velocity linear jets collide in reactor chamber (shown as original photograph). The left stream carries the non-solvent (alone or with co-stabilizer), the right stream the solvent containing API (nanocrystal production) or API and polymer (polymeric NP production). The third access (on the top) leads inert gas (usually nitrogen N_2) to the reactor chamber. The resulting nanosuspension leaves the outlet (on the bottom). (b) Enlargement (side view) of reactor part (jets collision in the middle). The solvent is evaporated by increased temperature (water bath + pump heaters), while the non-solvent containing the NPs (nanosuspension) leaves the outlet together with the inert gas. (c) Enlargement of jets collision and NP formation process (coaxial view \rightarrow liquid jets come from below and above the visual plane). The red circle exhibits mixing of solvent and non-solvent. NPs grow consistently from the collision point on the way to the edge of the lens. The gas stream limits the liquid jets collision to the center of the reactor.	17
Figure 11: Schematic of zeta potential.	23
Figure 12: Schematic of DSC measuring cell.	26
Figure 13: Schematic of a typical DSC heating-up curve.	27
Figure 14: Schematic of an IR instrument (double-beam system).	28
Figure 15: Schematic of the Airy disc.	29
Figure 16: Beam path in a light microscope (simplified).	29

Figure 17: Schematic of a SEM with secondary electron detection (based on Zeiss Evo Series product in-formation [20]).....	32
Figure 18: Schematic of an AFM including an image detail of the sample scanning operation.	34
Figure 19: Classification of pressure driven filtration techniques according to filtration range.....	46
Figure 20: Schematic of dead-end- and cross-flow filtration.	47
Figure 21: NP preparation procedure (bench top/emulsification-solvent evaporation).	55
Figure 22: Cross-flow filtration module: Schematic of a MicroKros filter module (image derived from http://eu.spectrumlabs.com/filtration/MicroKros.html?xfr=1373374033;) with an enlargement of the hollow fibers (a) and photograph of this module as used in the dissolution apparatus (b).	64
Figure 23: DLS size distribution reports (volume-weighted) of a celecoxib-Eudragit E 100 aqueous nanosuspension; NP-preparation: nanoprecipitation technique–alternative method using HPLC pumps and a non-solvent phase without surfactant (see chapter 2.2.1.2); unfiltered nanosuspension (1 : 20 dilution in water) (a) versus liquid obtained from filtration of this nanosuspension through a 100 kDa CF module (b); NP properties: 143 nm (Z-Average), 0.237 (PDI).	66
Figure 24: DLS size distribution reports (volume-weighted) of a celecoxib-Eudragit E 100 aqueous nanosuspension; NP-preparation: nanoprecipitation technique–alternative method using HPLC pumps and a non-solvent phase without surfactant (see chapter 2.2.1.2); unfiltered nanosuspension (1 : 100 dilution in water) (a) versus liquid obtained from filtration of this nanosuspension through a 500 kDa CF module (b); NP properties: 216 nm (Z-Average), 0.108 (PDI).	67
Figure 25: Photograph of the dissolution test assembly (a), with image details of the filtrate outlet (b) and the sample withdrawal (c).	69
Figure 26: Bench-top preparation (emulsification-diffusion) of celecoxib-Eudragit E 100 – NPs with Poloxamer 407 as co-stabilizer, (a) Z-Average and PDI, (b) ZP and EE: Solvent phase: 5 mg/mL celecoxib and 5/10 mg/mL Eudragit E 100 in 1/2/5 mL of ethyl acetate, non-solvent phase: 1 mg/mL Poloxamer 407 in 10 mL of water, n=1, Z-Average, PDI and ZP values are mean of three measurements, EE values respectively single measurement, red lines represent SD.	75
Figure 27: DLS size distribution report (volume-weighted) of celecoxib-Eudragit E 100 – NPs with Poloxamer 407 as co-stabilizer: Solvent phase: 5 mg/mL celecoxib and 10 mg/mL Eudragit E 100 in 2 mL of ethyl acetate, non-solvent phase: 1 mg/mL Poloxamer 407 in 10 mL of water; Preparation method: Bench-top (emulsification-diffusion).	76

- Figure 28: Bench-top preparation (emulsification-diffusion) of celecoxib Eudragit E 100 – NPs with varying amounts of Poloxamer 407, (a) Z-Average and PDI, (b) ZP and EE: Solvent phase: 5 mg/mL celecoxib and 10 mg/mL Eudragit E 100 in 2 mL of ethyl acetate, non-solvent phase: 0.1/0.5/1/2.5/5/10 mg/mL Poloxamer 407 in 10 mL of water, n=3, red lines represent SD. 79
- Figure 29: DLS size distribution report (volume-weighted) of celecoxib-Eudragit E 100 – NPs with Poloxamer 407 as co-stabilizer: Solvent phase: 5 mg/mL celecoxib and 10 mg/mL Eudragit E 100 in 2 mL of ethyl acetate, non-solvent phase: 2.5 mg/mL Poloxamer 407 in 10 mL of water; Preparation method: Bench-top (emulsification-diffusion). 80
- Figure 30: DLS size distribution report (volume-weighted) of celecoxib-Eudragit E 100 – NPs with Poloxamer 407 as co-stabilizer: Solvent phase: 25 mg/mL celecoxib and 50 mg/mL Eudragit E 100 in 2 mL of ethyl acetate, non-solvent phase: 12.5 mg/mL Poloxamer 407 in 10 mL of water; Preparation method: Bench-top (emulsification-diffusion). 83
- Figure 31: Photographs of celecoxib-Eudragit E 100-NPs stabilized with Poloxamer 407, after preparation (a), 7 d at ambient temperature (b), 7 d at 5 °C (c), 28 d at ambient temperature (d), 28 d at 5 °C (e) and 28 d at 5 °C (top view) (f): C = celecoxib, E = Eudragit E 100, P = Poloxamer 407, RT = room/ambient temperature. 86
- Figure 32: Stability study of celecoxib-Eudragit E 100 – NPs stabilized with Poloxamer 407 (Z-Average and PDI): Solvent phase: 5/25 mg/mL celecoxib and 10/50 mg/mL Eudragit E 100 in 2 mL ethyl acetate, non-solvent phase: 2.5/12.5 mg/mL Poloxamer 407 in 10 mL water, respectively stored at room temperature (RT) and at 5 °C, n=3, values are mean of three measurements, red lines represent SD. 87
- Figure 33: Stability study of celecoxib-Eudragit E 100 – NPs stabilized with Poloxamer 407 (ZP): Solvent phase: 5/25 mg/mL celecoxib and 10/50 mg/mL Eudragit E 100 in 2 mL ethyl acetate, non-solvent phase: 2.5/12.5 mg/mL Poloxamer 407 in 10 mL water, respectively stored at room temperature (RT) and at 5 °C, n=3, values are mean of three measurements, red lines represent SD. 88
- Figure 34: Stability study of celecoxib-Eudragit E 100 – NPs stabilized with Poloxamer 407 (EE), (a) 5 mg/mL celecoxib and (b) 25 mg/mL celecoxib: Solvent phase: 5/25 mg/mL celecoxib and 10/50 mg/mL Eudragit E 100 in 2 mL ethyl acetate, non-solvent phase: 2.5/12.5 mg/mL Poloxamer 407 in 10 mL water, respectively stored at room temperature (RT) and at 5 °C, n=3, single measurements, red lines represent SD. 89
- Figure 35: DLS size distribution reports (volume-weighted) of celecoxib-Eudragit E 100 – NPs with Poloxamer 407 as co-stabilizer: Solvent phase: 25 mg/mL celecoxib and 50 mg/mL Eudragit E 100 in 2 mL of

ethyl acetate, non-solvent phase: 12.5 mg/mL Poloxamer 407 in 10 mL of water; immediately after preparation (day 0) (a) and after two weeks storage at ambient temperature (day 14) (b); Preparation method: Bench-top (emulsification-diffusion).....	90
Figure 36: Design cube (particle size) of the DoE model. Values at the cube edges represent the Z-Average in nm (dependent variable). The x-axis (A) represents the temperature (in °C), the y-axis (C) the flow rate (expressed as pump rotational speed in rpm) and the z-axis (B) the nitrogen pressure (in bar).	92
Figure 37: Design of experiments – validation: Actual Z-Average values of ten approaches in three sizes (300, 350, 400 and 450 nm) plotted against predicted values obtained from DoE equation.	93
Figure 38: DLS size distribution report (volume-weighted) of celecoxib-Eudragit E 100 – NPs stabilized with Poloxamer 407, prepared with MJR (emulsification-diffusion): Solvent phase: 25 mg/mL celecoxib and 50 mg/mL Eudragit E 100 in ethyl acetate, non-solvent phase: 12.5 mg/mL Poloxamer 407 in water, operation temperature: 58.4 °C, nitrogen pressure: 0.40 bar, pump rotational speed (solvent phase : non-solvent phase) 510 : 2550 rpm; predicted Z-Average: 350 nm.	94
Figure 39: DLS size distribution report (volume-weighted) of celecoxib-Eudragit E 100 – NPs stabilized with Poloxamer 407, prepared with MJR (nanoprecipitation): Solvent phase: 25 mg/mL celecoxib and 50 mg/mL Eudragit E 100 in methanol, non-solvent phase: 12.5 mg/mL Poloxamer 407 in water, operation temperature: 50.0 °C, without nitrogen, pump rotational speed (solvent phase : non-solvent phase) 1200 : 6000 rpm.	97
Figure 40: DSC traces of Eudragit E 100, celecoxib, a physical mixture of celecoxib and Eudragit E 100 as well as of celecoxib-Eudragit E 100-NPs prepared by MJR (emulsification-diffusion and nanoprecipitation technique).....	99
Figure 41: FTIR spectra of celecoxib sodium salt (charged) and celecoxib (non-charged).....	101
Figure 42: FTIR spectra of Eudragit E 100 (non-charged) and protonated Eudragit E (charged).	102
Figure 43: FTIR spectra of physical mixtures of celecoxib and Eudragit E 100 and charged celecoxib and Eudragit E 100 as well as celecoxib-of Eudragit E 100-NPs prepared by MJR (emulsification-diffusion and nanoprecipitation technique).	103
Figure 44: SEM image (a) and volume-weighted DLS size distribution report (b) of MJR produced celecoxib-Eudragit E 100-particles (nanoprecipitation technique): NP properties (determined by DLS, mean of three measurements): 1156 nm (Z-Average), 0.144 (PDI).	106

Figure 45: SEM image (a) and volume-weighted DLS size distribution report (b) of MJR produced celecoxib-Eudragit E 100-NPs (nanoprecipitation technique): NP properties (determined by DLS, mean of three measurements): 387 nm (Z-Average), 0.285 (PDI).....	107
Figure 46: SEM image (a) and volume-weighted DLS size distribution report (b) of MJR produced celecoxib-Eudragit E 100-NPs (emulsification-diffusion technique): NP properties (determined by DLS, mean of three measurements): 611 nm (Z-Average), 0.258 (PDI).....	108
Figure 47: SEM image (a) and volume-weighted DLS size distribution report (b) of MJR produced celecoxib-Eudragit E 100-NPs (emulsification-diffusion technique): NP properties (determined by DLS, mean of three measurements): 254 nm (Z-Average), 0.148 (PDI).....	109
Figure 48: SEM image (a) and volume-weighted DLS size distribution report (b) of MJR produced celecoxib-Eudragit E 100-NPs (nanoprecipitation technique–alternative method using HPLC pumps and a non-solvent phase without surfactant, see chapter 2.2.1.2): NP properties (determined by DLS, mean of three measurements): 109 nm (Z-Average), 0.132 (PDI).	110
Figure 49: AFM images (two different enlargements of the same sample) of MJR produced celecoxib-Eudragit E 100-NPs (nanoprecipitation technique–alternative method using HPLC pumps and a non-solvent phase without surfactant, see chapter 2.2.1.2): NP properties (determined by DLS, mean of three measurements): 109 nm (Z-Average), 0.132 (PDI); volume-weighted DLS size distribution report shown in Figure 48 (b).	112
Figure 50: Dissolution of celecoxib-Eudragit E 100-NPs in HCl pH 1.2: NP properties: 80 nm (Z-Average), 0.131 (PDI) and 2.573 mg/mL (celecoxib concentration of the nanosuspension, i.e. a 2.573 mg dose of celecoxib), detection: UV-Vis (248 nm), n=3, red lines represent SD. ...	114
Figure 51: SEM image with precipitations of a 1:100 dilution of celecoxib-Eudragit E 100-NPs in 0.1 M HCl after 24 h storage at ambient temperature; NP preparation parameters: MJR, nanoprecipitation technique-alternative method (without usage of a surfactant).....	115
Figure 52: Dissolution of celecoxib-Eudragit E 100-NPs in HCl pH 1.2 + 0.15 M NaCl: NP properties: 100 nm (Z-Average), 0.100 (PDI) and 2.331 mg/mL (celecoxib concentration of the nanosuspension, i.e. a 2.331 mg dose of celecoxib), detection: UV-Vis (248 nm), n=1.	116
Figure 53: Dissolution of celecoxib-Eudragit E 100-NPs in HCl pH 1.2 + 0.001/0.01/0.3/1.0 % cetrimide: NP properties: 80 nm (Z-Average), 0.131 (PDI) and 2.573 mg/mL (celecoxib concentration of the nanosuspension, i.e. a 2.573 mg dose of celecoxib), detection: UV-Vis (248 nm), n=1.....	118

- Figure 54: Dissolution of celecoxib-Eudragit E 100-NPs in diluted HCl pH 1.2 + 0.3 % cetrимide: NP properties: 160 nm (Z-Average), 0.094 (PDI) and 2.388 mg/mL (celecoxib concentration of the nanosuspension, i.e. a 2.388 mg dose of celecoxib), filters: CF modules of 100 kDa and 500 kDa and 0.2 μ m syringe filter holders (dead-end), detection: UV-Vis (248 nm), n=3, red lines represent SD. 120
- Figure 55: Dissolution of celecoxib-Eudragit E 100-NPs in diluted HCl pH 1.2 + 0.05 % cetrимide: NP properties: 160 nm (Z-Average), 0.094 (PDI) and 2.509 mg/mL (celecoxib concentration of the nanosuspension, i.e. a 2.509 mg dose of celecoxib), filters: cross-flow filtration modules of 100 and 500 kDa and 0.2 μ m syringe filter holders (dead-end), detection: UV-Vis (248 nm), n=3, red lines represent SD. 121
- Figure 56: Dissolution of celecoxib-Eudragit E 100-NPs in phosphate buffer pH 2.0/2.5/3.5/4.5/5.2+ 0.3 % cetrимide: NP properties: 220 nm (Z-Average), 0.086 (PDI) and 3.666 mg/mL (celecoxib concentration of the nanosuspension, i.e. a 3.666 mg dose of celecoxib), filter: 500 kDa cross-flow filtration module, detection: UV-Vis (248 nm), n=3, red lines represent SD. 123
- Figure 57: Dissolution of celecoxib-Eudragit E 100-NPs of different size and celecoxib (API) powder in phosphate buffer pH 2.0 + 0.3 % cetrимide: NP properties: 221/255/293/362/497 nm (Z-Average), < 0.25 (PDI) and ~ 2.650–4.850 mg/mL (celecoxib concentration of the nanosuspension, i.e. 0.663 mg-1.213 mg celecoxib dose), API powder: 2537 μ g/mL (celecoxib concentration of the suspension), filter: 500 kDa cross-flow filtration module, detection: UV-Vis (248 nm), n=6, red lines represent SD. 125
- Figure 58: Plot of the reciprocal of release percentage against the reciprocal of dissolution time for the NP batch of 362 nm diameter. The R_{max} corresponds to the reciprocal of the y-intercept of the red line through the last three sampling points. 129
- Figure 59: Plot of the natural logarithm of release against dissolution time for the NP batch of 362 nm diameter (vertical bars represent the standard deviation). The k-value corresponds to the slope of the red regression line through the first three sampling points. 130
- Figure 60: (a) Schematic of a celecoxib-Eudragit E 100-NP in aqueous suspension co-stabilized by Poloxamer 407: Celecoxib (white spheres) molecular complexes embedded in a matrix of Eudragit E 100 (orange sphere). Surface charge is positive due to protonated Eudragit molecules (orange lines). Poloxamer 407 (blue lines) molecules contribute to stabilization by inclusion between Eudragit molecules. (b) Molecular complex of celecoxib and Eudragit E 100, dotted line shows ionic interaction. (c) Hydrophobic domains (dotted circles) of Eudragit, Poloxamer and celecoxib molecules. 135

Figure 61: Equations of the reaction of celecoxib-Eudragit E complex with NaCl leading to exchange of deprotonated celecoxib by a chloride ion (a) followed by protonation of celecoxib (b) (Cel = celecoxib and EU = Eudragit E).	145
Figure 62: Structure of cetrimide.	146
Figure 63: Schematic of two theoretical degradation pathways of celecoxib-Eudragit E 100-NPs. (a) continuous surface erosion of the NP in the dissolution liquid with release of dissolved celecoxib and Eudragit E 100 and (b) disintegration of the NP in several fragments followed by erosion of these fragments.....	150
Figure 64: SEM image of MJR produced celecoxib-Eudragit E 100-particles (nanoprecipitation technique): NP properties (determined by DLS, mean of three measurements): 1156 nm (Z-Average), 0.144 (PDI).....	172
Figure 65: SEM image of MJR produced celecoxib-Eudragit E 100-NPs (nanoprecipitation technique): NP properties (determined by DLS, mean of three measurements): 387 nm (Z-Average), 0.285 (PDI).....	172
Figure 66: SEM image of MJR produced celecoxib-Eudragit E 100-NPs (emulsification-diffusion technique): NP properties (determined by DLS, mean of three measurements): 611 nm (Z-Average), 0.258 (PDI).....	173
Figure 67: SEM image of MJR produced celecoxib-Eudragit E 100-NPs (emulsification-diffusion technique): NP properties (determined by DLS, mean of three measurements): 254 nm (Z-Average), 0.148 (PDI).....	173
Figure 68: DLS size distribution reports (volume-weighted) of celecoxib-Eudragit E 100-NPs; NP-preparation: nanoprecipitation technique– alternative method, non-solvent phase without surfactant, see chapter 2.2.1.2; unfiltered nanosuspension (a) versus liquid obtained from filtration of this nanosuspension through a 500 kDa CF module (b) and from filtration through a syringe filter holder with 0.2 μm pore size (c); NP properties: 160 nm (Z-Average), 0.094 (PDI).....	174
Figure 69: Simulation of the NP dissolution process in dissolution medium: DLS size distribution reports (volume-weighted) of celecoxib-Eudragit E 100-NPs; same nanosuspension as in Figure 68, but respectively measured at 37 °C (dissolution test temperature); 1:100 aqueous dilution of the nanosuspension (a) versus 1:100 dilution in 0.1 M HCl + 0.3 % cetrimide after 15 min incubation time in the cuvette of the DLS instrument (b).	175
Figure 70: Laser light diffraction size distribution report of unprocessed celecoxib particles; density distribution and cumulative distribution; volume-weighted median diameter (VMD) in red rectangle.	176
Figure 71: DLS size distribution reports (volume-weighted) of two dissolution media: HCl pH 1.2 + 0.05 % cetrimide (a) and HCl pH 1.2 + 0.3 % cetrimide (with micelles) (b).....	177

List of Equations

(1) Nernst-Brunner equation	2
(2) Ostwald-Freundlich equation	2
(3) Nucleation rate	15
(4) Particle growth rate	15
(5) Stokes-Einstein relationship	20
(6) Particle size distribution	20
(7) Calculation of volume-weighted distributions	21
(8) Smoluchowski formula	23
(9) Specific thermal heat capacity (DSC)	24
(10) Specific heat flow (DSC).....	24
(11) Wave number	27
(12) Diameter of the Airy disc (SEM	29
(13) Numeric aperture (SEM).....	30
(14) Resolution (SEM)	30
(15) Noyes-Whitney equation	35
(16) Hagen-Poiseuilles law	47
(17) Entrapment efficiency	59
(18) Difference factor (f1)	73
(19) Similarity factor (f2)	73
(20) DoE model equation	91

Acknowledgement

Curriculum vitae

Personal Information

Name	Julian Schichtel
Date of birth	April 7th 1983
Place of birth	Saarbrücken
Nationality	German
Present address	Elversberger Straße 76e, D-66299 Friedrichsthal

Doctoral Thesis

02/2011 –	Department of Biopharmaceutics and Pharmaceutical Technology, Johannes Gutenberg University, Mainz
-----------	--

Diploma Thesis

05/2009	Department of Pharmaceutical Nanotechnology, Saarland University, Saarbrücken Title: <i>Template-Size-Dependency of the Fluorescence of Polyelectrolyte-modified Gold Nanoparticles</i>
---------	--

Undergraduate Study

12/2008	Certification as a pharmacist
10/2003 – 10/2007	Pharmaceutical studies, Saarland University, Saarbrücken

Military Service

10/2002 – 12/2002	8./Sanitätsregiment 5, Rennerod/Westerwald
01/2003 – 06/2003	Sanitätszentrum Merzig

Internships

06/2015 –	Qualified Person at URSAPHARM Arzneimittel, Saarbrücken
01/2015 – 05/2015	Branch manager of Adler-Apotheke, Zweibrücken
02/2012 – 12/2014	Scientist at MJR PharmJet, Homburg
09/2009 – 12/2011	Junior scientist at PHAST quality standards, Homburg
06/2007 – 11/2007	Practical training for pharmacists at Rochus Apotheke, Spiesen-Elversberg

Publications

03/2015	<i>Partikelmessung von F&E bis GMP; Stand der Technik und Einsatz in Entwicklung und Qualitätskontrolle-Regulatorische Anforderungen.</i> Authors: Julian Schichtel, Akif Emre Türelı, Markus Limberger. Book chapter in „Partikel in der Pharmaproduktion“, Frank Stieneker (Ed.), Editio Cantor Verlag
07/2012	<i>Dissolution testing of orally disintegrating tablets.</i> Authors: Kraemer J., Gajendran J., Guillot A., Schichtel J., Tuereli A., Journal of Pharmacy and Pharmacology 2012 July; 64(7): 911-918

Oral Presentations

03/2015 FAH-Seminar „Pharmaproduktion und Partikel“ (Bonn), Lecture: *Partikelmessung von F&E bis GMP; Stand der Technik und Einsatz in Entwicklung und Qualitätskontrolle.*
Author: Julian Schichtel

09/2014 Annual Meeting of the German Pharmaceutical Society DPhG Trends and Perspectives in Pharmaceutical Sciences,
Short lecture: *Determination of the Dissolution Behaviour of Celecoxib-Eudragit E 100-Nanoparticles using Cross-Flow Filtration.*
Author: Julian Schichtel

Poster Presentations

09/2014 Annual Meeting of the German Pharmaceutical Society DPhG Trends and Perspectives in Pharmaceutical Sciences
Determination of the Dissolution Behaviour of Celecoxib-Eudragit E 100-Nanoparticles using Cross-Flow Filtration
Authors: Julian Schichtel, Eva-Marie Prinz, Akif Emre Türeli, Peter Langguth